

AD-A202 487

R-1181

SPHERICAL GEODETIC TRANSFORMATIONS

VOLUME I OF II

**SPECTRAL THEORY AND
OPTIMAL TEMPLATE DESIGN**

by

William M. Robertson

September 1978

Prepared for:

**Defense Mapping Agency Aerospace Center (STT)
St. Louis Air Force Station, Missouri 63118**

Monitoring Office:

**Space and Missile Systems Organization (MNCA)
Norton Air Force Base, California 92409**

DTIC
ELECTE
S **D**
DEC 19 1988
CS
D



The Charles Stark Draper Laboratory, Inc.

Cambridge, Massachusetts 02139

Approved for public release; distribution unlimited.

88 12 19 05 9

Unclassified

SECURITY CLASSIFICATION OF THIS PAGE (When Data Entered)

REPORT DOCUMENTATION PAGE		READ INSTRUCTIONS BEFORE COMPLETING FORM
1. REPORT NUMBER R-1181	2. GOVT ACCESSION NO.	3. RECIPIENT'S CATALOG NUMBER
4. TITLE (and Subtitle) SPHERICAL GEODETIC TRANSFORMATIONS VOLUME I OF II - SPECTRAL THEORY & OPTIMAL TEMPLATE DESIGN		5. TYPE OF REPORT & PERIOD COVERED FINAL 9/30/77 thru 9/30/78
7. AUTHOR(s) William M. Robertson		6. PERFORMING ORG. REPORT NUMBER
9. PERFORMING ORGANIZATION NAME AND ADDRESS The Charles Stark Draper Laboratory, Inc. Cambridge, Massachusetts 02139		8. CONTRACT OR GRANT NUMBER(s) F04704-78-C-0002
11. CONTROLLING OFFICE NAME AND ADDRESS Defense Mapping Agency Aerospace Center (STT) St. Louis, Missouri 63118		10. PROGRAM ELEMENT, PROJECT, TASK AREA & WORK UNIT NUMBERS Services Line Item 0003; Task 3.12
14. MONITORING AGENCY NAME & ADDRESS (if different from Controlling Office) Space and Missile Systems Organization Air Force Systems Command (MNCA) Norton Air Force Base, California 92409		12. REPORT DATE September 1978
		13. NUMBER OF PAGES 315
		15. SECURITY CLASS. (of this report) Unclassified
		16. DECLASSIFICATION/DOWNGRADING SCHEDULE --
16. DISTRIBUTION STATEMENT (of this Report) Approved for public release; distribution unlimited.		
17. DISTRIBUTION STATEMENT (of the abstract entered in Block 20, if different from Report)		
18. SUPPLEMENTARY NOTES		
19. KEY WORDS (Continue on reverse side if necessary and identify by block number) Geodesy Vening-Meinesz' Integral Spectral Analysis Spherical Digital Filters Stokes' Integral		
20. ABSTRACT (Continue on reverse side if necessary and identify by block number) (see page iii of document)		

DD FORM 1 JAN 73 1473

EDITION OF 1 NOV 65 IS OBSOLETE

Unclassified

SECURITY CLASSIFICATION OF THIS PAGE (When Data Entered)

R-1181

SPHERICAL GEODETIC TRANSFORMATIONS

VOLUME I OF II

SPECTRAL THEORY
AND
OPTIMAL TEMPLATE DESIGN

by

William M. Robertson

September 1978

Approved

Norman E. Sears
Norman E. Sears



The Charles Stark Draper Laboratory, Inc.
Cambridge, Massachusetts 02139

Approved	
DTIC	
DTIC	
DTIC	
DTIC	
By	
Date	
A-1	

ACKNOWLEDGEMENT

This report was prepared by the Charles Stark Draper Laboratory, Inc. for the Defense Mapping Agency Aerospace Center under Task #3.12 (DMA Geodesy Studies), Services Line Item No. 0003 of Contract F04704-78-C-0002 with the Space and Missile Systems Organization of the Air Force Systems Command.

Support for the performance of the work described in this Report has been provided under the following contracts between U.S. Government agencies and The Charles Stark Draper Laboratory, Inc.:

Task #3.12 (DMA Geodesy Studies), Services Line Item No. 0003 of Contract F04704-78-C-0002 with the Space and Missile Systems Organization of the Air Force Systems Command.

Task #3.12 (DMA Geodesy Studies) of Change Order P00073 of Contract F04701-73-C-0277 with the Space and Missile Systems Organization of the Air Force Systems Command.

Task #1150 (4320) (Gravity Model) of Contract N00030-78-C-0100 with the Strategic Systems Project Office of the U.S. Navy.

Task #4300 (Guidance System Initialization) of Contract N00030-77-C-0070 with the Strategic Systems Project Office of the U.S. Navy.

The author especially wishes to acknowledge the support provided by the U.S. Navy under the last contract listed above. This support came at a very early stage in the author's work, and was the enabling force for the subsequent development and application of the theory as described in this document.

Publication of this report does not constitute approval by the Defense Mapping Agency or the U.S. Air Force or the U.S. Navy of the findings or conclusions contained herein. It is published for the exchange and stimulation of ideas.

ABSTRACT

→ A general theory and method is developed by which more accurate and efficient summation approximations can be derived for any of the integral transformations of geodesy. The theory and method are applied to the well-known Stokes' and Vening-Meinesz' Integrals and improved summations are determined which have lower rms discretization errors than the approximations presently in use, even though only rudimentary optimization algorithms are employed. Thus the validity of the theory and the feasibility of the method are numerically demonstrated.

The theory is based upon spherical spectral analysis, a branch of mathematics describing the spectral (or frequency domain) properties of data and linear operators defined over spherical coordinates. It parallels Fourier analysis for cartesian coordinates. The scarcely-known Legendre transform is shown to be the fundamental spectral transform in spherical coordinates, converting the spherical spatial domain into the spherical frequency domain and converting spherical convolution into ordinary multiplication.

→ The integral transformations of geodesy are revealed as two-dimensional spherical convolutions, and their discrete summation approximations are interpreted as spherical digital filters with a number of adjustable parameters determined by the underlying template. The spherical "transfer functions" of the integral transformations and of their discrete summation approximations are derived and shown to be close but not exactly equal to each other, as expected. An analytic expression for the partial derivative of the discrete summation transfer function with respect to its parameters is derived and used in a Gauss-Newton optimization process, which adjusts the parameters incrementally so that the approximating transfer function of the summation matches the ideal transfer function of the integral as well as possible in a least-squares sense. This is equivalent to minimizing the rms discretization error of the approximation, and may be interpreted as spherical digital filter design for geodetic transformations.

FOREWORD

This document is not, and is not intended to be, a treatise of mathematics nor of geodesy nor of signal processing. Rather it is meant as a readable and understandable survey of the application of a branch of mathematics to an important part of geodesy using signal processing concepts, and as a demonstration of the possibility of obtaining useful practical results from such cross-fertilization. In point of fact, it was the desire for practical results which led to the realization that the underlying problem had to be attacked from a combined mathematical, geodetic, and signal-processing viewpoint.

Although many subjects are covered in the document, an attempt was made to present sufficient detail (especially for the classical transformations) so as to provide the reader with an appreciation of the texture and richness of the material.

PERSONAL ACKNOWLEDGEMENT

The author wishes to acknowledge his intellectual debt to Dr. Peter Meissl through the report "A Study of Covariance Functions Related to the Earth's Disturbing Potential" (Meissl, 1971). It was a reading of this report which enlightened the author with the fundamental ideas of the spectral theory of classical geodetic integrals and which led to the elaboration and extension of the theory presented herein.

The author also wishes to recognize Mr. A.R. DiDonato for his development of simple recurrence relations for the indefinite integrals of the associated Legendre functions (DiDonato, 1977). These formulae were essential in the numerical implementation of the author's theory, permitting the spectrum of discrete summation transformations to be rather easily computed for higher frequencies.

The author especially wishes to express his gratitude and appreciation to Ruth Erickson for her talent and care in the typing and physical preparation of both volumes of this document.

TABLE OF CONTENTS

<u>Section</u>	<u>Page</u>
1 INTRODUCTION AND SUMMARY OF RELATED WORK	1-1
2 SPECTRAL THEORY OF DATA AND OPERATORS	2-1
2.1 Introduction	2-1
2.2 Spectral Analysis of Data and Operators	2-1
2.3 Cartesian Spectral Transforms	2-5
2.4 Spherical Spectral Transforms	2-8
2.5 Convolution Expressions	2-11
3 SPECTRAL THEORY OF THE INTEGRAL TRANSFORMATIONS OF GEODESY	3-1
3.1 Introduction	3-1
3.2 Isotropic Geodetic Transformations	3-1
3.3 Anisotropic Geodetic Transformations	3-31
3.4 Transformations Involving Outward Surface Partial Derivatives	3-41
4 SPECTRAL THEORY OF THE DISCRETE SUMMATION TRANSFORMATIONS OF GEODESY	4-1
4.1 Introduction	4-1
4.2 Bull's-Eye Templates and Discrete Summation transformations	4-2
4.3 Stokes' Discrete Summation Transformations	4-3
4.4 Vening-Meinesz' Discrete Summation Transformations	4-18
4.5 Inner Zone Operators and Their Spectra for First Order Geodetic Transformations	4-29
5 SPECIFIC TEMPLATES AND EXAMPLES OF SPECTRA	5-1
5.1 Specific Templates	5-1
5.2 Examples of Spectra	5-14

(TABLE OF CONTENTS continued)

<u>Section</u>		<u>Page</u>
6	TEMPLATE OPTIMIZATION METHODS AND DISCRETE SUMMATION TRANSFORMATIONS	6-1
6.1	Introduction	6-1
6.2	Global RMS Discretization Error	6-3
6.3	Optimization Algorithm	6-6
7	TEMPLATE OPTIMIZATION RESULTS	7-1
7.1	Summary	7-1
7.2	Results for the Stokes' Transformation	7-3
7.3	Results for the Vening-Meinesz' Transformation.	7-11
7.4	Results Using Variations in the Optimization Algorithm	7-21
8	SUMMARY AND CONCLUSIONS	8-1
9	RECOMMENDATIONS FOR FURTHER INVESTIGATION	9-1
 <u>Appendix</u>		
A	DEFINITIONS AND NOTATIONS FOR THE ASSOCIATED LEGENDRE FUNCTIONS	A-1
B	RECURSION RELATIONS FOR THE INDEFINITE INTEGRALS OF THE ASSOCIATED LEGENDRE FUNCTIONS	B-1
B.1	Shepperd-Robertson Recursion	B-1
B.2	Robertson-Clenshaw Recursion	B-9
B.3	DiDonato Recursion	B-12
B.4	Paul Recursion	B-13
C	LISTINGS OF THE COMPREHENSIVE FILTER DESIGN COMPUTER PROGRAM	C-1
D	EXPLANATION OF THE COMPREHENSIVE FILTER DESIGN COMPUTER PROGRAM	D-1
E	DISCUSSION OF THE EXCLUSION OF SMALL RING RADII FROM THE DIFFERENTIAL ADJUSTMENT PROCEDURE	E-1
F	DERIVATION OF ALGORITHM FOR CALCULATING THE STOKES' EQUAL RING CONTRIBUTION TEMPLATE	F-1
LIST OF REFERENCES		R-1

LIST OF FIGURES

<u>Figure</u>	<u>Page</u>
2.5-1 Relationship of Points on a Spherical Surface for Interpretation of Spherical Convolution	2-14
3.2-1 Summary of Mathematical Relationships for the Classic Stokes' Integral Transformation	3-9
3.2-2 Summary of Mathematical Relationships of the Analog of the Stokes' Integral Transformation for Surface Layer Density	3-10
3.2-3 Summary of Mathematical Relationships for the Molodenskii Integral Transformation	3-11
3.2-4 Summary of Mathematical Relationships for the Truncated Stokes' Integral Transformation	3-12
3.2-5 Summary of Mathematical Relationships for the Cap-Averaging Integral Transformation	3-13
3.2-6 Schematic Diagram for the Interpretation of the Generalized Anomaly of Type "k"	3-15
3.2-7 Closed Form Expressions for the Generalized Stokes' Function	3-17
3.2-8 Summary of Mathematical Relationships for the Generalized Stokes' Integral Transformation	3-19
3.2.3-1 Flow Diagram of Basic Geodetic Transformations and Their Spectra	3-20
3.2.4-1 Summary of Mathematical Relationships for the Identity and Upward Continuation Integral Transformation	3-23
3.2.5-1 Summary of Mathematical Relationships for the Gravity Anomaly Vertical Gradient Integral Transformation	3-26
3.2.5-2 Flow Diagram of Eigenvalues of Vertical Gradient Geodetic Transformations	3-28

<u>Figure</u>		<u>Page</u>
3.2.5-3	Summary of Mathematical Relationships for the Vertical Stress Gradient Integral Transformation . .	3-30
3.3.1-1	Summary of Mathematical Relationships for the Classic Vening-Meinesz' Integral Transformation. . .	3-34
3.3.1-2	Summary of Mathematical Relationships for the Vertical Shear Gradient Integral Transformation. . .	3-36
3.3.1-3	Summary of Mathematical Relationships for the Horizontal Stress and Shear Gradient Integral Transformations	3-39
3.3.2-1	Flow Diagrams of Spectra of Various Other Geodetic Transformations	3-40
3.4-1	Geometry of the Outward Surface Partial Derivative	3-42
3.4-2	Summary of Mathematical Relationships for Malkin's Integral Transformation	3-44
3.4-3	Summary of Mathematical Relationships for the Second Molodenskii Integral Transformation	3-45
3.4-4	Values of Some Wallis Coefficients	3-48
4.2-1	Bull's-Eye Template	4-3
4.3.1-1	Stokes' Midpoint Averaging Function $\bar{S}(\psi)$	4-6
4.3.2-1	Stokes' Integrated-Mean Averaging Function $\hat{S}(\psi)$. . .	4-10
4.3.3-1	Stokes' Comb Function $\hat{\bar{S}}(\psi)$	4-13
4.3.4-1	Summary of Relationships for the Discrete Stokes' Summation Trnasformation Using Midpoint Weighting	4-15
4.3.4-2	Summary of Relationships for the Discrete Stokes' Summation Using Integrated-Mean Weighting	4-16
4.3.4-3	Summary of Relationships for the Discrete Stokes' Summation Transformation on Point Gravity Anomalies	4-17
4.4.1-1	Vening-Meinesz' Midpoint Averaging Function $\bar{V}_M(\psi)$	4-20
4.4.2-1	Vening-Meinesz' Integrated-Mean Averaging Function $\hat{V}_M(\psi)$	4-22
4.4.3-1	Summary of Relationships for the Discrete Vening-Meinesz' Summation Using Midpoint Summation	4-27

<u>Figure</u>		<u>Page</u>
4.4.3-2	Summary of Relationships for the Discrete Vening-Meinesz' Summation Using Integrated-Mean Weighting .	4-28
4.5-1	Summary of Mathematical Relationships for the Single Dipole Finite Difference Operator	4-30
4.5-2	Summary of Mathematical Relationships for the Double Dipole Finite Difference Operator	4-31
4.5-3	Summary of Mathematical Relationships for the Rice Weighted Quadruple Dipole Operator	4-32
4.5-4	Summary of Mathematical Relationships for the Truncated Vening-Meinesz' Transformation	4-35
5.2.1-1	Spectra of Stokes' Transformation (34-Ring Pick-Picha-Vyskocil Template)	5-16
5.2.1-2	Spectra of Stokes' Transformation (101-Ring Circularized AGEMIT Template)	5-20
5.2.2-1	Spectra of Vening-Meinesz' Transformation (23-Ring Equal Contribution Template).	5-26
5.2.2-2	Spectra of Vening-Meinesz' Transformation (125-Ring Equal Contribution Template)	5-27
6.1-1	Example of Iterative Decrease of the Discretization Error	6-2
6.3.4-1	Example of Output Weighting	6-16
7.1-1	Summary of Basic Optimization Results	7-2
7.2.1-1	Summary of 34-Ring Template Optimization for the Classic Stokes' Transformation	7-5
7.2.1-2	Summary of 66-Ring Template Optimization for the Classic Stokes' Transformation Beginning with an Equal Ring Contribution Template	7-6
7.2.1-3	Summary of 101-Ring Template Optimization for the Classic Stokes' Transformation	7-7
7.2.2-1	Summary of 34-Ring Template Optimization for the Stokes' Transformation Analog	7-10
7.3.1-1	Summary of 23-Ring Template Optimization for the Vening-Meinesz' Analog Transformation, Beginning from an Equal Ring Contribution Template	7-12
7.3.1-2	Summary of 23-Ring Template Optimization for the Vening-Meinesz' Analog Transformation, Beginning from the Pick-Picha-Vyskocil Template	7-12

<u>Figure</u>		<u>Page</u>
7.3.2-1	Summary of 125-Ring Template Optimization for the Vening-Meinesz' Analog Transformation, Beginning from an Equal Ring Contribution Template. (Damping = 0.5)	7-14
7.3.2-2	Summary of 125-Ring Template Optimization for the Vening-Meinesz' Analog Transformation, Beginning from an Equal Ring Contribution Template. (Damping = 0.25)	7-16
7.3.2-3	Summary of 125-Ring Template Optimization for the Vening-Meinesz' Analog Transformation, Beginning from Circularized AGEMIT Template	7-18
7.4.1-1	Comparison of Vening-Meinesz' Optimization Using Increment Damping Variation	7-22
7.4.1-2	Comparison of Vening-Meinesz' Optimization Using Increment Damping Variation	7-24
7.4.1-3	Comparison of Vening-Meinesz' Optimization Using Increment Damping Variation	7-26
7.4.2-1	Iterations of a Stokes' Optimization Run Using Output Weighting	7-30
E-1	Example of Large Increments (Vening-Meinesz, 23 rings, maximum degree 50)	E-2
E-2	Example of Large Increments (Stokes, 34 rings, maximum degree 50)	E-3
E-3	Example of Large Increments (Stokes, 34 rings, maximum degree 500).	E-3
E-4	Example of Large Increments (Stokes, 101 rings, maximum degree 1000)	E-4
E-5	Example of Large Increments (Vening-Meinesz, 23 rings, maximum degree 1440)	E-5
E-6	Example of Large Increments (Vening-Meinesz, 125 rings, maximum degree 1440).	E-5
E-7	Example of Large Increments (Vening-Meinesz, 125 rings, maximum degree 1440)	E-6
E-8	Summary of Cases for Small Ring Radii Exclusion	E-7
F-1	Sub-areas Under the Curve $S(\psi)\sin\psi$	F-2
F-2	Dead-bands around the Zeros of $S(\psi)\sin\psi$	F-2
F-3	Nature of Solution	F-4
F-4	Solution for $\Delta b = 0$	F-5
F-5	Solution for $\Delta a = 0$	F-6

LIST OF TABLES

<u>Table</u>		<u>Page</u>
5.1.1-1	Pick-Picha-Vyskocil Template Parameters for the Stokes' Transformation	5-4
5.1.1-2	Pick-Picha-Vyskocil Template Parameters for the Vening-Meinesz' Transformation	5-5
5.1.1-3	The Original Rice Inner Zone Template Parameters . .	5-6
5.1.1-4	Kazansky Inner Zone Template Parameters	5-6
5.1.2-1	Template Parameters for the 23-Ring Equal Contribution Template with ψ_0 = the initial radius of Pick-Picha-Vyskocil	5-12
5.1.2-2	Template Parameters for the 125-Ring Equal Contribution Template with $\psi_0 R = 235$ meters	5-12
5.1.3-1	Template Parameters for the Circularized AGE MIT Template	5-13
5.1.3-2	Template Parameters for the 125-Ring "Rice-DMAAC" Template	5-15
6.2-1	Discretization Error of Various Templates for Stokes' Transformation	6-5
6.2-2	Discretization Error of Various Templates for Vening-Meinesz' Transformation	6-6
B-1	The $b_{n,k}$ coefficients	B-4
B-2	The $c_{n,k}$ coefficients	B-6
B-3	The d_k coefficients	B-7
B-4	Estimates of certain $b_{n,k}$ coefficients	B-8
B-5	The $\beta_{j,l}$ coefficients	B-10
B-6	The $h_{n,k}$ coefficients	B-11
D-1	Major Inputs to FITFILT	D-3

GLOSSARY OF SYMBOLS

<u>Symbol</u>		<u>Section</u>	<u>Page</u>
A_{ij}	Surface area of the (i,j)th compartment on the unit sphere	4.3 4.4	
$\bar{C}_{ij}, \bar{S}_{ij}$	Integrated-mean values of the cosine and sine functions in the (i,j)th compartment	4.4.2	4-23
dg	Gravity variation ($dg = d_0g$)	3.2.2	3-14
$d\sigma$	Element of surface area on unit sphere ($d\sigma = \sin \psi d\psi d\alpha$)	3.2	3-2
d_kg	Generalized gravity anomaly of type "k"	3.2.2	3-14
$f(\psi, \alpha),$ $f_{IN}(\psi, \alpha)$	Input geodetic quantity to an integral transformation	3.2 3.3	3-2 3-31
$f_{OUT},$ $f_{OUT}(\psi, 0)$	Output of integral transformation corresponding to input $f(\psi, \alpha)$ or $f_{IN}(\psi, \alpha)$	3.2 3.3	3-2 3-31
$F_n, F_{nm},$ F_n^m, F_n^m	Fourier or Legendre coefficients of the function "f"	2.3 2.4	2-4 2-8
$F_{2D}[\],$ $F_{2D}^{-1}[\]$	Two-dimensional Fourier transform and Inverse Fourier transform of quantity in brackets	2.3	2-5
G	Nominal value of earth's gravity	3.2	3-3
$H[\],$ $H^{-1}[\]$	Hankel transform and Inverse Hankel transform of quantity in brackets	2.3	2-6
$k(\cos \psi),$ $K(\cos \psi)$	Kernel of an isotropic geodetic transformation	3.2	3-2

<u>Symbol</u>		<u>Section</u>	<u>Page</u>
$L\{ \},$ $L[]$	Legendre transform of quantity in braces or brackets	2.4	2-8
$L^{-1}\{ \},$ $L^{-1}[]$	Inverse Legendre transform of quantity in braces or brackets	2.4	2-8
m	Spherical harmonic order	2.4	2-8
$M(\psi)$	Specific kernel function related to Molo- denskii transformation	3.2.1.3	3-6
n	Spherical harmonic degree	2.4	2-8
(n) or n [subscript]	the n^{th} spherical harmonic of the main- line quantity	3.2.5	3-24
$P_{nm}(\cos \psi)$	Associated Legendre function (Ferrers' convention)	Appendix A	A-2
$P_n^m(\cos \psi)$	Associated Legendre function (Hobson convention)	Appendix A	A-1
$\hat{P}_{n(k)}$	Integrated-mean value of the Legendre polynomial $P_n(\cos \psi)$ in the k^{th} ring	4.3.2	4-11 4-11
$\hat{P}_{n,i}^m$	Integrated-mean value of the Hobson associated Legendre function over the i^{th} ring	4.4.2	4-25
$q_n(\psi_0)$	Cook coefficients	4.5.3 6.3.3	4-34 6-12
$Q_n(\psi_0)$	Molodenskii coefficients	3.2.1.4 6.3.3	3-7 6-12
R	Nominal value of earth's radius	3.2	3-3
s	Linear distance from point of evaluation [$s = R\psi$]	4.5.2	4-33
$S(\psi),$ $S(\cos \psi)$	Stokes' function	3.2.1.1	3-3

<u>Symbol</u>		<u>Section</u>	<u>Page</u>
$\bar{S}(\psi)$	Residual Stokes' function ($=S(\psi)$ for $\psi_0 < \psi \leq \pi$, otherwise 0)	3.2.1.4	3-7
$\tilde{S}(\psi)$	Truncated Stokes' function ($=S(\psi)$ for $0 \leq \psi < \psi_0$, otherwise 0)	3.2.1.4	3-7
$\hat{S}(\psi)$	Stokes' Midpoint Weighting function	4.3.1	4-5
$\dot{S}(\psi)$	Stokes' Integrated-Mean Averaging function	4.3.2	4-8
$S_k(\psi)$	Generalized Stokes' function of type "k"	3.2.2	3-16
S_n	Sequence like Wallis coefficients [$S_n = 1/\sqrt{n(n+1)}$]	3.4.1 3.4.2	3-41 3-50
$\dot{S}_{(i)}$	Integrated-Mean Value of Stokes' function in the i th ring	4.3.2	4-8
$S\{ \},$ $S[]$	Spectral transform of quantity in braces or brackets	2.2	2-3
$S^{-1}\{ \},$ $S^{-1}[]$	Inverse spectral transform of quantity in braces or brackets	2.2	2-3
t	Sine of <u>half</u> the spherical arc distance ψ	5.1.2	5-8
T	Anomalous potential	3.2.2	3-32
$T_{zx}, T_{zy},$ $T_{yy}, T_{xx},$ T_{xy}	Partial derivatives of the anomalous potential with respect to subscript variables	3.3.1.2 3.3.1.3	3-35 3-37
$VM(\psi),$ $VM(\cos \psi)$	Classical Vening-Meinesz function [$VM(\psi) = \partial S(\psi) / \partial \psi$]	3.3	3-32
$\hat{VM}(\psi)$	Vening-Meinesz' midpoint averaging function	4.4.1	4-18
$\dot{VM}(\psi)$	Vening-Meinesz integrated-mean averaging function	4.4.2	4-21

<u>Symbol</u>		<u>Section</u>	<u>Page</u>
$\hat{V}M_i$	Integrated-mean value of Vening-Meinesz function in the i th ring	4.4.2	4-21
W_n	Wallis coefficient	3.4	3-43
x, x_i	Cosine of spherical arc distance ψ or spherical ring boundary radius ψ_i		
$\underline{x}, \underline{\hat{x}}, \underline{\hat{\hat{x}}}$	Sets of template parameters considered as a parameter vector	6.3.1	6-7
α	Spherical azimuth angle from local north to generic point measured at point of evaluation	2.5	2-13
α_{ij}	Spherical compartment boundary azimuth in the i th ring	4.2	4-3
$\delta_{2D}(\psi)$	Two-dimensional Dirac Delta Function	3.2.1.3	3-6
$\overline{\Delta g}_{ij}$	Mean gravity anomaly in the (i,j) th compartment	4.3 4.4	4-7 4-19
Δx	Increment in template parameters \underline{x}	6.3.1	6-8
$\Delta \lambda(\underline{x})$	Residual Spectrum considered as a function of the template parameters \underline{x}	6.3.1	6-7
$\vec{\epsilon}, \underline{\epsilon}$	Vertical Deflection vector [$\vec{\epsilon} = (\xi, \eta)$]	3.4	3-4
ϵ_k	Neumann factor ($\epsilon_0 = 1, \epsilon_k = 2$ for $k \neq 0$)	2.3.2	2-7
θ	Colatitude ($90^\circ - \text{latitude}$)	2.5	2-13
$\lambda_n\{ \}, \lambda_n[], \lambda_n$	Spectrum of the isotropic kernel included in braces or brackets or not specified explicitly	3.2	3-2
$\lambda_n^m\{ \}, \lambda_n^m[], \lambda_n^m$	Spectrum of the anisotropic kernel included in braces or brackets or not specified explicitly	3.3	3-31

<u>Symbol</u>		<u>Section</u>	<u>Page</u>
$\lambda_{-n}^m\{f_{IN} + f_{OUT}\},$ $\lambda_{-n}^m\{K:f_{IN} + f_{OUT}\}$	Spectrum of the transformation converting the input f_{IN} into the output f_{OUT} , and having kernel K.		
$\lambda(\underline{x})$	Spectrum of a discrete summation transformation with template parameters \underline{x}	6.3.1	6-7
$\sigma_n^2\{ \}$	Degree variances of quantity in braces	6.3.1.1	6-9
$\mu(\psi, \alpha)$	Surface layer density (single layer)	3.2.1.2	3-4
ψ	Spherical arc distance on a unit sphere from the point of evaluation. "Spherical radius".	2.5	2-13
ψ_0	Spherical radius of small spherical cap around point of evaluation	3.2.1.4 4.2	3-7 4-3
ψ_i	Spherical ring boundary radius	4.2	4-3
ψ_{LIMIT}	Spherical radius for exclusion of small ring radii adjustment	6.3.3	6-13
$()!!!$	Schuster's Factorial $(2n)!!! = 2 \cdot 4 \cdot 6 \cdots (2n)$ $(2n-1)!!! = 1 \cdot 3 \cdot 5 \cdots (2n-1)$	3.4.2	3-46
$\{ \}_{rms}$	Global root-mean-square value of quantity in braces	6.2	6-3
*	Convolution operator	2.2 2.5	2-3 2-11

SECTION 1

INTRODUCTION AND SUMMARY OF RELATED WORK

1.1 Introduction

The numerical evaluation of certain spherical geodetic transformations, such as the Stokes', Vening-Meinesz', and Molodenskii Integrals, is performed frequently and repeatedly in various research facilities which desire a knowledge of the earth's external gravitational field. The computation is required in order to convert known geodetic/gravimetric quantities, such as surface gravity anomaly measurements, into other geodetic/gravimetric quantities, such as geoid height or gravity disturbance vectors at altitude. The computer algorithms carrying out the computation are by necessity finite summations which only approximate the mathematically rigorous integral transformations of geodetic theory to various degrees of accuracy.

Due to the computational burden involved, it is highly desirable to make the algorithms as efficient as possible, with the highest accuracy attainable for the smallest amount of computer time. Geodesists have long known that it is inefficient to sum these integrals over grid patterns or templates whose compartments are equally-spaced over the whole earth. Various non-equally-dimensioned grids or templates have therefore been empirically devised which provide more efficient approximations of the theoretical transformations. However, no research has been carried out to derive optimum summation schemes or grids from fundamental mathematical principles.

Besides reducing the computation time, it is even more important that the summation approximations preserve as well as possible the spectral (frequency domain) properties of the integral transformations, since it is only in this manner that output quantities can be obtained from the summations with nearly correct frequency characteristics. Otherwise results might be obtained in which certain spatial frequencies had been unknowingly eliminated or distorted.

To achieve these objectives, it is natural to expect that the mathematical techniques involved would include modern signal-processing and filtering theory, appropriately adapted to spherical geometry.

The present data-processing situation for spherical geodetic transformations is rather analogous to that for planar gravimetric and magnetic transformations during the 1930's and 1940's in the early years of scientific geophysical exploration for oil and gas. During that period, a number of summation approximations were developed and applied,* especially for calculating the second vertical derivative of the anomalous potential (which emphasizes local features and removes some regional trends) and the downward continuation of anomalies (which yields estimates of subterranean masses). However, as Nettleton remarks:** "For the first 20 years or so of their use, second derivatives and the related upward and downward continuation were treated as mathematical operations in themselves and not as filtering functions. Millions of square miles were mapped with second derivative contours ... apparently without realizing that the systems used did not come close to actually determining the mathematical quantity implied."

At about the same time, Norbert Wiener of M.I.T. was developing the theory of prediction and filtering of stationary time series on a highly rigorous level. The possibility of the practical application of this theory in seismic analysis led to the formation of the M.I.T. Geophysical Analysis Group in 1952, and in particular to the thesis of Enders A. Robinson (1954) which "could serve as the framework for a logical development of the entire subject of digital processing."*** As a result of these mathematical advances, the various gravimetric and magnetic summations in use were analyzed in the late 1950's and early 1960's from the signal processing or filtering point of view. It was quickly realized why they possessed certain inherent qualities and how desired qualities could be designed into new summation operators. Nettleton (1976, pp. 158-170) provides a nice review of these developments.

While the spherical geodetic summations of today are presumably determining much more accurate approximations of the mathematical quantities involved than the early planar summations mentioned by Nettleton, the present transformations are still largely conceived of

* Nettleton (1976, pg. 140) gives some early references.

** Op. cit., pg. 137.

*** As Flinn (1967, pg. 412) has observed.

as mathematical procedures in themselves (i.e. computer subroutines) and not as filtering operations.

It is the purpose of the present study to change this viewpoint. The concepts and techniques of spectral analysis and signal processing are modified and adapted for the underlying spherical geometry. The integral transformations of geodesy are shown to be two-dimensional convolution operators, and their associated summation approximations are interpreted as linear shift-invariant transformations on the input data, i.e. as spherical digital filters. The characteristics of the transformations in the frequency domain are investigated through the determination of their spectra (transfer functions, frequency responses). And an attempt is made to design optimum spherical summation approximations to the Stokes' and Vening-Meinesz' Integrals by mathematically adjusting the grid or template parameters in the summation so that its resulting spectrum will match as well as possible the ideal spectrum of the corresponding theoretical integral transformations.

In particular, a brief review of the spectral theory of data and operators over both two-dimensional cartesian and two-dimensional spherical coordinates is presented in Chapter 2 so as to summarize the results and emphasize their analogies. Chapter 3 develops the spectral theory of the theoretical spherical integral transformations of geodesy, providing many examples of the "ideal" transfer functions of these transformations. A similar theory for the discrete summation approximations of the Stokes' and Vening-Meinesz' Integrals is carried out in Chapter 4. The details of a number of specific templates are described in Chapter 5, and plots are presented to illustrate the small but significant differences between the ideal transfer functions and those of the approximating summations. In Chapter 6, a description is given of the constrained optimization algorithm and certain variations thereof which were used to incrementally adjust template parameters to reduce the rms discretization error, and the improved results which were obtained are presented in Chapter 7. The conclusions of the study are given in Chapter 8, and recommendations for further investigation in Chapter 9. The six appendices provide mathematical details of the associated Legendre functions, a listing and explanation of the comprehensive filter design computer program, and discussions of other particulars too lengthy to be included in the text. Volume II is a catalog of the spatial and frequency domain representations of approximately 100 spherical integral transformations, of which about 85 have an explicitly geodetic interpretation.

1.2 Related Work

The author is aware of only a few other people who are studying or who have published papers on the spectral theory of spherical geodetic transformations. Only one of these has (indirectly) investigated the effect of the discretization of an integral transformation to a finite summation transformation, although summations are always used in practice.

A brief review of the published work of these authors is given in the following paragraphs.

Meissl (1971) has unquestionably laid the foundation for the application of functional analysis and spectral theory to spherical geodetic transformations. In his report, the fundamental definitions and formulae for the spectrum of a transformation are given, with a number of specific examples. However, Meissl's developments are primarily oriented toward isotropic (zeroth-order) operators, and no discrete summation transformations are discussed. Nevertheless the fundamental relationships all appear (in a Hilbert space setting), and the present author has benefited greatly from Meissl's ideas.

Neyman (1974) has also approached the study of spherical geodetic transformations from the functional-analytic or spectral-theoretic point of view. He has given definitions of the spectrum of such transformations which are equivalent to Meissl's and to those of the present document (exclusive of a normalizing factor). Moreover, he has briefly considered anisotropic transformations and their spectra, and has sketched in a few paragraphs the idea of approximating transfer functions over subregions of a sphere. Neyman's paper was brought to the attention of the present author by Louis Decker of the Defense Mapping Agency in January 1978 after the present theory was well developed (Robertson, 1977a, 1977b). It is very likely that Neyman has further results which have not yet appeared outside the original Russian literature.

Molodenskii (1962) has extensively investigated the mathematical properties of the Stokes' and Vening-Meinesz' transformations, especially the truncated versions of these transformations and the effect of the regions remote from the point of evaluation. Clearly he is aware of the spectral properties of these transformations, although his mathematics is not formally cast in spectral analysis terminology. While he has derived more rapidly convergent expressions for the classic geodetic

integral transformations, he does not consider discrete summation approximations. Molodenskii's work is pioneering and contains many ideas whose consequences have not yet been fully explored or appreciated.

Colombo (1977) has attacked a very specific problem in geodetic computations, namely how to adjust the kernel function of a spherical geodetic transformation when the integral is to be carried out only over a spherical cap rather than the entire sphere, in order that the mean square error of such an approximation may be minimized. While Colombo does not explicitly define spectra of operators or develop a general theory, it is obvious that he is aware of the frequency domain interpretation of spherical geodetic transformations. As he says in his abstract, "The technique can be regarded as a method of designing two-dimensional filters to transform signals distributed on the surface of a sphere." All of Colombo's results are for the isotropic Stokes' and Molodenskii Integrals. The present author became aware of Colombo's work from the abstract appearing in EOS in December 1977, and received Colombo's paper in June 1978.

Zondek (1977) is the only other researcher who has (indirectly) investigated the effect of the discretization of a spherical geodetic integral transformation. Specifically he has studied the effect of compartmentally averaging the output of the Stokes' Integral rather than the input. Since the compartmental averaging operator and the Stokes' Integral operator are commutative, Zondek's results may be immediately interpreted in terms of a discretization of the Stokes' Integral. To carry out the numerical calculations, Zondek uses DiDonato's (1977) algorithm which was specifically developed for this purpose. The present author also uses DiDonato's algorithm and became aware of it through reading Zondek's paper in early 1978.

Potter and Frey (1967) have examined the mathematical and statistical properties of spherical "rotation-invariant" linear operators and probability distributions, defining their spectra, exhibiting the one-dimensional convolution theorem, and proving that the power spectrum is positive. In particular, they have applied their approach to the Poisson kernel, and shown that the spherical upward continuation convolution may be represented by a single integral involving a complete elliptic integral. While their results are limited to isotropic kernels, Potter and Frey have developed many fundamental ideas in their short terse paper. The present author became aware of their work just before this document was finished.

General expositions of the spectral theory of linear operators are given by Liusternik and Sobolev (1961), Kato (1966), and Dunford and Schwartz (1958 and 1963). The geodetically-oriented reader is likely to find these treatises rather formidable. Nevertheless they show how far and how deeply the mathematics of this theory has been developed. The symbol " λ " for the spectrum of an operator is inherited from such treatises.

SECTION 2

SPECTRAL THEORY OF DATA AND OPERATORS

2.1 Introduction

A brief summary of the most important concepts and formulae of spectral theory for data and for operators in both two-dimensional cartesian spaces and two-dimensional spherical spaces is presented in this chapter. The analogies of the ideas and the results for both types of "inputs" and for both types of spaces are stressed in order to show the fundamental unity and generality of the theory. It is assumed that most readers will be familiar with at least the spectral theory of data in one or two dimensional cartesian spaces, but may never have considered the continuation of the theory to operators or to spherical spaces. The engineering reader, however, may actually have knowledge of some of the results of the spectral theory of operators in one-dimensional cartesian space, namely the use of transfer functions, without realizing that this is a part of a more general theory.

2.2 Spectral Analysis of Data and Operators

Of fundamental importance in the spectral theory is the concept of the spectrum, which has a meaning both for data and for linear operators.

Data, or "signals" as data is often called in electrical engineering, are values of one or more dependent variables associated with each value of one or more independent variables such as time or position. Thus data are functions in the ordinary sense having individual numbers as input and as output.

Linear operators are mathematical transformations which linearly transform sets of input data into sets of output data. Thus they are "functions of functions", having functions as input and as output. They are called "operators" by mathematicians to distinguish them from functions. An example is the operator which yields the derivative of any (arbitrary) input function.

The spectrum of a set of data is a mathematical description of the strengths and phases of the frequencies or periodicities present in the data. The data may be distributed in time or in single or multi-dimensional space; the spectrum will then represent the time or spatial frequencies respectively. The values of the spectrum are obtained by performing a "spectral transform" on the data. In the case when the independent variables of the data are cartesian, the spectral transform is the well-known Fourier transform, and the spectrum is sometimes called the set of Fourier coefficients of the data. When the independent variables form a spherical coordinate system, the spectral transform is the scarcely-known Legendre transform. The explicit mathematical expressions for the spectral transform in two-dimensional cartesian and spherical spaces will be exhibited in later sections of this chapter.

The spectrum of a linear operator or transformation is a mathematical description of the (multiplicative) strengths and the (additive) phases by which the operator respectively amplifies/attenuates and shifts the frequencies present in the input data as the operator transforms this data into output data. In other words, the spectrum describes the ratios of the strengths, and the differences of the phases, of the output frequencies to the input frequencies. Individual values of the spectrum are called eigenvalues. The spectrum of a very wide and important class of linear operators, namely convolution operators, may be obtained by performing a spectral transform on the kernel function of the integral representing the convolution. This is in direct analogy to the case of data. Again in the operator case, the spectral transform is the Fourier transform when the independent variables are cartesian and the Legendre transform when the independent variables are spherical. In electrical engineering terminology, the spectrum of an operator is called its frequency response or transfer function and the kernel of a convolution operator is called its impulse response.

It is common to speak of examining data or operators in both the "time or spatial domain" and the "frequency domain". The former refers to the original data or operator explicitly expressed in terms of time or spatial parameters, while the latter refers to the spectrum of the data or the operator and is therefore expressed as a function of (time or spatial) frequency.

Just as the data or the operator may be decomposed (or expanded) into its constituent frequencies or spectrum by a spectral transform, so may the original data or convolution operator kernel be recovered from

its spectrum by an inverse spectral transform on the spectrum. The actual formulae exhibiting the reciprocal relationships will soon be presented.

The process of convolution and the spectral transform are intimately related by the fact that the spectral transform converts convolution in the spatial domain into (ordinary) multiplication in the frequency domain. It is this fundamental property, plus the fact that so many linear operators may be represented by a convolution transformation, which is at the base of the theory and its applicability.

Of particular importance for geodetic theory is the fact that all of the classical (and non-classical) geodetic integral transformations are convolutions in one- or two-dimensional spherical space. For example, the Stokes' Integral is the convolution of the Stokes' function $S(\psi)$ with the gravity anomalies $\Delta g(\psi, \alpha)$.

To be more specific, let "k" and "f" represent functions, let "k*f" represent their convolution, and let $S\{ \}$ represent the spectral transform of the function within the braces. Then the fundamental relationship is expressed as

$$S\{k*f\} = S\{k\} \cdot S\{f\}.$$

It can also be shown (Bracewell, 1965, pg. 110) that

$$S\{k f\} = S\{k\} * S\{f\}$$

and from these relations it is deducible that if K and F are functions in the frequency domain and $S^{-1}\{ \}$ is the inverse spectral transform, then

$$S^{-1}\{K*F\} = S^{-1}\{K\} \cdot S^{-1}\{F\}$$

and

$$S^{-1}\{K F\} = S^{-1}\{K\} * S^{-1}\{F\}$$

However, the last three relations are not of interest here.

Several properties of the spectrum are:

- a) The spectrum of the sum of two (or more) linear convolution transformations is equal to the sum of the spectra of the transformations. This is due to the linearity of the transformations and of the spectral transform.

- b) The spectra of a composite transformation formed by the sequential application of one transformation on the output of another transformation is the product of the spectra of the individual transformations. This may be seen as follows. Let $k_1(x)$ and $k_2(x)$ be the kernels of the two transformations. Suppose $g_2(x) = k_2 * f_2 = k_2 * (k_1 * f_1)$. Then

$$\begin{aligned} S\{g_2\} &= S\{k_2\} S\{k_1 * f_1\} = \\ &= S\{k_2\} S\{k_1\} S\{f_1\} \end{aligned}$$

- c) The elements of the spectrum of an inverse transformation are the reciprocals of the elements of the forward transformation. This follows immediately from the above property.
- d) An element of the spectrum of a transformation is zero if and only if the transformation eliminates the corresponding input frequency while generating the output. This is a direct consequence of the fundamental property.
- e) The magnitudes* of the elements of the spectrum equal the amplification/attenuation factors of the transformation on the global root-mean-square values of the corresponding frequencies of the input:

$$\{g_n\}_{rms} = S_n\{k\} \cdot \{f_n\}_{rms}$$

where the subscript "n" indicates the n^{th} frequency or harmonic. This is a direct consequence of the fact that the global mean-square value of data of a single frequency is equal to the global mean-square value of the spectrum of the data at that frequency.

* also known as the gain function

2.3 Cartesian Spectral Transforms

In the case when the independent variables form a cartesian coordinate system, the spectral transform is the standard Fourier transform. The Fourier transform and its inverse assume several slightly different forms depending upon whether the data or the operator is periodic or non-periodic over the infinite line or plane. For simplification, only the two-dimensional case and the one-dimensional specialization when the data or the operator kernels are radially symmetric (isotropic about the origin) will be considered. The extension to a higher number of dimensions is relatively straightforward, but in this document there will be no need for this generality.

The following notational conventions will be used in the expressions for cartesian spectral transforms:

- Lower-case letters denoting functions [especially $f(x,y)$ and $f(r)$] represent data or operator kernels in the spatial domain.
- Upper-case letters denoting functions [especially $F(u,v)$ and $F(q)$] represent the corresponding data or operator kernels in the frequency domain.
- The independent variables x and y , and $r = \sqrt{x^2 + y^2}$ are spatial distance parameters and hence have units of length, while the variables u and v , $q = \sqrt{u^2 + v^2}$ are spatial frequency parameters and have units of inverse length or more intuitively cycles per unit length.

2.3.1 Infinite (Non-Periodic) Case

When the data or the operator kernel $f(x,y)$ extends infinitely in both dimensions, the (two-dimensional) spectral transform is the infinite two-dimensional Fourier transform:

$$F_{2D}[f(x,y)] = \int_{-\infty}^{\infty} \int_{-\infty}^{\infty} e^{-i2\pi(ux + vy)} f(x,y) dx dy = F(u,v)$$

and the (two-dimensional) inverse spectral transform is the infinite two-dimensional inverse Fourier transform:

$$F_{2D}^{-1}[F(u,v)] = \int_{-\infty}^{\infty} \int_{-\infty}^{\infty} e^{+i2\pi(ux + vy)} F(u,v) du dv = f(x,y)$$

That the inversion formula is correct, or in other words that the original function $f(x,y)$ is regained from the spectrum $F(u,v)$ through the application of the inverse transform is shown in most classical texts on the Fourier Transform, e.g. Titchmarsh (1948), where the precise restrictions on the function $f(x,y)$ are also stated.

When the data or operator kernel $f(x,y)$ is radially symmetric about the origin, in other words when $f(x,y)$ may be written as a function $f(r)$ of the single radius variable $r = \sqrt{x^2 + y^2}$, then it may be shown (Bracewell, 1965, pg. 247) that the spectrum F of $f(r)$ is also radially symmetric having the form $F(q)$ where $q = \sqrt{u^2 + v^2}$ and is given by the Hankel transform (or zeroth order) of $f(r)$:

$$F_{2D}[f(x,y)] = H[f(r)] = 2\pi \int_0^{\infty} r J_0(2\pi r q) f(r) dr = F(q)$$

and the inverse spectral transform is likewise the inverse Hankel transform of $F(q)$:

$$F_{2D}^{-1}[F(u,v)] = H^{-1}[f(q)] = 2\pi \int_0^{\infty} q J_0(2\pi q r) F(q) dq = f(r)$$

From the above relationships, it is evident that the spectrum may be continuous as opposed to discrete, in that it may assume values for every frequency u and v or q .

2.3.2 Finite (Periodic) Case

When the data or the operator kernel $f(x,y)$ is doubly periodic with periods $2X$ and $2Y$ in the x and y directions respectively, then the (two-dimensional) spectral transform is the two-dimensional finite Fourier transform (Rektorys, 1969, pg. 703).

$$F_{2D}[f(x,y)] = \epsilon_n \epsilon_m \int_{-X}^{+X} \int_{-Y}^{+Y} e^{-i2\pi(n\frac{x}{2X} + m\frac{y}{2Y})} f(x,y) \frac{dx}{2X} \frac{dy}{2Y} = F_{nm}$$

and the inverse spectral transform is the two-dimensional inverse Fourier transform summation:

$$F_{2D}^{-1}[F_{nm}] = \sum_{n=0}^{\infty} \sum_{m=0}^{\infty} F_{nm} e^{i2\pi(n\frac{x}{2X} + m\frac{y}{2Y})} = f(x,y)$$

where

$$\varepsilon_k = \begin{cases} 1 & \text{when } k = 0 \\ 2 & \text{when } k \neq 0 \end{cases}$$

and is called the Neumann factor (Magnus-Oberhettinger, 1949, pg. 64; Morse-Feshbach, 1953, Vol. I, pg. 774).

When the data or operator kernel $f(x,y)$ is radially symmetric about the origin,* or in other words when $f(x,y)$ may be written as a function $f(r)$ of a single radius variable $r = \sqrt{x^2 + y^2}$, then it may be shown (Rektorys, 1969, pg. 720) that the spectrum of $f(r)$ is also radially symmetric having the form $F(q)$ where $q = \sqrt{u^2 + v^2}$ and is given by the finite Hankel transform (or zeroth order) of $f(r)$:

$$F_{2D}[f(x,y)] = H[f(r)] = 2\pi \int_0^R r \left(\frac{J_0(2\pi q_n r)}{J_1(2\pi q_n R)} \right) f(r) \frac{dr}{\pi R^2} = F_n$$

and the inverse spectral transform is likewise the inverse Hankel transform of $F(q)$:

$$F_{2D}^{-1}[F_{nm}] = H^{-1}[F_n] = \sum_{n=0}^{\infty} F_n \left(\frac{J_0(2\pi q_n r)}{J_1(2\pi q_n R)} \right) = f(r)$$

where the q_n are the roots of $J_0(2\pi q R) = 0$ and J_0 and J_1 are Bessel functions.

From all the above relationships it may be seen that in the finite case the spectrum is discrete as opposed to continuous, in that it has values only for certain discrete frequencies. This is a direct consequence of the fact that the fundamental wavelengths $2X$ and $2Y$ are finite. Only integral multiples of the fundamental frequencies corresponding to these wavelengths can be present.

In the formulae, the normalization factors $2X$ and $2Y$, corresponding to the total lengths of the intervals over which integration is performed, have been grouped with the differential elements dx and dy . The author has found that this convention brings out essential characteristics of the relationships by removing "extraneous" factors. In particular, the Neumann factor(s) naturally appear(s) before the forward transform expression. This convention is rarely adhered to in the literature.

* as well as doubly periodic and hence radially symmetric about the center of each repetitive block.

2.4 Spherical Spectral Transforms

In the case when the independent variables form a spherical coordinate system, the spectral transform is the Legendre transform. Since a sphere is finite and a function defined on the sphere may be considered doubly periodic with period 2π in the "longitude" variable and period π in the "latitude" or "co-latitude" variable, the spherical spectral transform has only one type, namely the finite periodic type, and consequently the spectrum is discrete.

The following notational conventions will be used in the expressions for spherical geodetic transforms:

- In agreement with traditional geodetic symbolism,* the variables ψ and α denote "spherical arc distance" or "spherical radius" and "spherical azimuth of an arbitrary point on the sphere" from "origin", also on the sphere. For geodetic transformations, the origin is the point at which the value of the output is desired. When the origin is the North Pole, then the spherical radius ψ is identical to colatitude and the spherical azimuth α is identical to west longitude.

The two-dimensional Legendre transform is defined by:

$$L_{2D}[f(\psi, \alpha)] = \epsilon_m \sqrt{\frac{(n-m)!}{(n+m)!}} \int_0^{2\pi} \int_0^\pi f(\psi, \alpha) \begin{pmatrix} \cos m\alpha \\ \sin m\alpha \end{pmatrix} P_n^m(\cos \psi) \frac{\sin \psi d\psi d\alpha}{4\pi} = \begin{cases} F_n^m \\ F_n^m \end{cases}$$

and the inverse two-dimensional Legendre transform by:

$$L_{2D}^{-1}[F_n^m, F_n^m] = \sum_{n=0}^{\infty} \sum_{m=0}^n (F_n^m \cos m\alpha + F_n^m \sin m\alpha) (2n+1) \sqrt{\frac{(n-m)!}{(n+m)!}} P_n^m(\cos \psi) = f(\psi, \alpha)$$

That the inversion formula is correct, or in other words that the original function $f(\psi, \alpha)$ is regained from the spectrum (F_n^m and F_n^m) through the inverse Legendre transform is shown in Heiskanen-Moritz (1969, pp. 29-30).

When the data or operator kernel $f(\psi, \alpha)$ is radially symmetric ("isotropic") about the origin, or in other words when $f(\psi, \alpha)$ is a

* Heiskanen-Moritz, 1967, pg. 95.

function of the spherical radius ψ only, then all of the discrete eigenvalues F_n^m and F_n^m vanish except for the F_n^0 , and the spectral transform expression and its inverse simplify to single integrals:

$$\begin{aligned} L[f(\psi)] &= \int_0^\pi f(\psi) P_n(\cos \psi) \frac{\sin \psi d\psi}{2} = F_n \\ &= \int_{-1}^{+1} f(\cos \psi) P_n(\cos \psi) \frac{d(\cos \psi)}{2} \\ L^{-1}[F_n] &= \sum_{n=0}^{\infty} F_n (2n+1) P_n(\cos \psi) = f(\psi) \end{aligned}$$

where the standard notational simplifications

$$P_n^0(\cos \psi) \equiv P_n(\cos \psi); F_n^0 \equiv F_n$$

have been used. In the above equation no distinction has been made between $f(\psi)$ and $f(\cos \psi)$ as functions of ψ , although strictly they are not the same function "f" of a single argument.

The definitions given above for the two-dimensional Legendre transform and its inverse utilize the associated Legendre functions $P_n^m(\cos \psi)$ of n^{th} degree and m^{th} order, which are defined in Appendix A.

Very little seems to have been published about Legendre transforms and "Legendre analysis" explicitly, in contrast to the plethora of results and publications about the Fourier transform and Fourier analysis. In fact, the very words "Legendre transform" may be unknown to many readers. Apparently the earliest paper in which the idea of the Legendre transform as used in this document was defined and utilized was that of Tranter (1950). The convolution theorem in one-dimensional spherical space was developed by Churchill and Dolph (1954), and the basic results of the operational calculus of Legendre transforms were published by Churchill (1954).

It should be noted that the forward and inverse Legendre transform relations given above differ slightly from those customarily given in the literature, specifically in the placement of the factor $(2n+1)$. This difference is a consequence of the author's choice

between two desirable but conflicting properties: the use of truly orthonormalized basis functions versus the spectrum of the identity transformation equaling unity. Most other authors have selected the former, while this document has chosen the latter.

The motivation in the former case is very strong. By defining normalized associated Legendre functions $\bar{P}_n^m(\cos \psi)$ by

$$\bar{P}_n^m(\cos \psi) = \sqrt{\epsilon_m (2n+1) \frac{(n-m)!}{(n+m)!}} P_n^m(\cos \psi),$$

it follows that

$$\int_0^\pi [\bar{P}_n^m(\cos \psi)]^2 \frac{\sin \psi d\psi}{2} = \epsilon_m$$

and

$$\int_0^{2\pi} \int_0^\pi [\bar{P}_n^m(\cos \psi) \cos m\alpha]^2 \frac{d\sigma}{4\pi} = 1$$

$$\int_0^{2\pi} \int_0^\pi [\bar{P}_n^m(\cos \psi) \sin m\alpha]^2 \frac{d\sigma}{4\pi} = 1$$

which results in the following beautifully symmetric forward and inverse transform formulae:

$$T_{2D}[f(\psi, \alpha)] = \iint f(\psi, \alpha) \bar{P}_n^m(\cos \psi) \begin{cases} \cos m\alpha \\ \sin m\alpha \end{cases} \frac{d\sigma}{4\pi} = \begin{cases} \bar{F}_n^m \\ \bar{F}_n^m \end{cases}$$

$$T_{2D}^{-1}[\bar{F}_n^m, \bar{F}_n^m] = \sum_{n=0}^{\infty} \sum_{m=0}^{\infty} [\bar{F}_n^m \cos m\alpha + \bar{F}_n^m \sin m\alpha] \bar{P}_n^m(\cos \psi) = f(\psi, \alpha)$$

In these formulae no extraneous constant factors appear since they have all been embedded in the normalized associated Legendre function \bar{P}_n^m . However under this convention, the "Legendre transform" of the Dirac Delta kernel (which corresponds to the identity operator) is

$$\begin{aligned} \bar{F}_n^0 &= \sqrt{2n+1} & \bar{F}_n^0 &= 0 \\ \bar{F}_n^m &= 0 & \bar{F}_n^m &= 0 \end{aligned}$$

This would imply, under a signal processing interpretation, that the strengths of zonal* harmonics of the input are amplified by the factor $\sqrt{2n+1}$ by the identity transformation - a patently erroneous result.

To preclude this problem, this document has chosen the property that the spectrum of the identity transformation is unity as a fundamental assumption. The somewhat unsymmetrical forward and inverse Legendre transform relations first given above then result, with the factor of $(2n+1)$ appearing only in the inverse transform relation.

2.5 Convolution Expressions

There are different expressions for the convolution operation, as well as for the spectral transform, depending upon the dimensionality of the space and the type of coordinate system.

In one-dimensional cartesian space, the convolution $k*f$ of two functions $k(x)$ and $f(x)$ is given by

$$\begin{aligned} g(x) = k*f &= \int_{-\infty}^{\infty} k(x') f(x-x') dx' \\ &= \int_{-\infty}^{\infty} k(x-x') f(x') dx' \end{aligned}$$

The convolutional linear operator represented by this integral has the kernel $k(x)$ and maps the input data function $f(x)$ into the output data function $g(x)$. The spectral transform of the output will thus be

$$S\{g\} = S\{k\} \cdot S\{f\}$$

In the two-dimensional cartesian space, the convolution $k*f$ of two functions $k(x,y)$ and $f(x,y)$ is given by

$$\begin{aligned} g(x,y) = k*f &= \int_{-\infty}^{\infty} \int_{-\infty}^{\infty} k(x',y') f(x-x',y-y') dx' dy' \\ &= \int_{-\infty}^{\infty} \int_{-\infty}^{\infty} k(x-x',y-y') f(x',y') dx' dy' \end{aligned}$$

* those for which $m=0$

In one-dimensional spherical space, the convolution of two functions $k(\cos \theta)$ and $f(\cos \theta)$ is given by*

$$g(\cos \theta) = k * f = \int_0^{2\pi} \int_0^{\pi} k(\cos \psi) f(\cos \theta') \frac{\sin \theta' d\theta' d\lambda'}{4\pi}$$

where

$$\cos \psi = \cos \theta \cos \theta' + \sin \theta \sin \theta' \cos(\lambda - \lambda')$$

or by

$$g(\cos \theta) = k * f = \int_0^{2\pi} \int_0^{\pi} k(\cos \psi) f(\cos \theta') \frac{\sin \psi d\psi d\alpha}{4\pi}$$

where $\cos \theta' = \cos \theta \cos \psi + \sin \theta \sin \psi \cos \alpha$

In two-dimensional spherical space, the convolution of two functions $k(\cos \theta, \lambda)$ and $f(\cos \theta, \lambda)$ is given by the following equation in "geographic" coordinates.

$$g(\cos \theta, \lambda) = k(\cos \theta, \lambda) * f(\cos \theta, \lambda) = \int_0^{2\pi} \int_0^{\pi} k(\cos \psi, \alpha) f(\cos \theta', \lambda') \frac{\sin \theta' d\theta' d\lambda'}{4\pi}$$

where

$$\cos \psi = \cos \theta \cos \theta' + \sin \theta \sin \theta' \cos(\lambda - \lambda')$$

$$\cos \alpha \sin \psi = \sin \theta \cos \theta' - \cos \theta \sin \theta' \cos(\lambda - \lambda')$$

$$\sin \alpha \sin \psi = \sin \theta' \sin(\lambda - \lambda')$$

or by the following equation in "local spherical polar" coordinates

$$g(\cos \theta, \lambda) = k(\cos \theta, \lambda) * f(\cos \theta, \lambda) = \int_0^{2\pi} \int_0^{\pi} k(\cos \psi, \alpha) f(\cos \theta', \lambda') \frac{\sin \psi d\psi d\alpha}{4\pi}$$

where

$$\cos \theta' = \cos \theta \cos \psi + \sin \theta \sin \psi \cos \alpha$$

$$\cos(\lambda - \lambda') \sin \theta' = \sin \theta \cos \psi - \cos \theta \sin \psi \cos \alpha$$

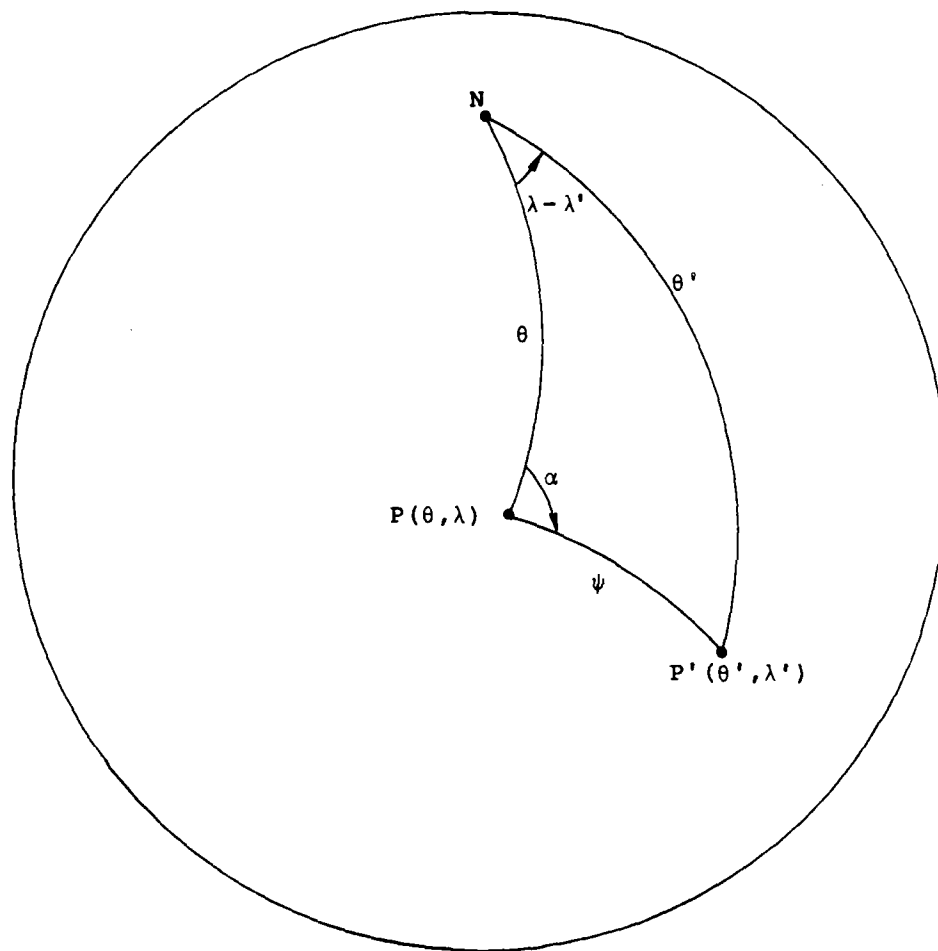
$$\sin(\lambda - \lambda') \sin \theta' = \sin \psi \sin \alpha$$

* See Churchill and Dolph (1954)

While the spherical convolution formulae appear complicated, they are rather simple when visualized. See Figure 2.5-1. The spherical convolution of two functions is the integral of the product of the two functions evaluated over all constant "spherical shifts" of the independent parameters, just as the cartesian convolution is the same integral of a product evaluated over all constant "linear shifts" of the independent parameters. The trigonometric expressions in the spherical formulae merely relate the shifted values of the coordinates of two points on a sphere.

In traditional geodetic notation, the convolution integrals are written slightly differently, but the meaning is exactly the same. Specifically the function values $f(\cos \theta')$ or $f(\cos \theta', \lambda')$ are denoted by $f(\psi)$ or $f(\psi, \alpha)$. Both expressions refer to the value of the function "f" at the generic point P' on the sphere, the difference being in whether the actual functional form of "f" is given in geographic coordinates or local spherical polar coordinates. Throughout the rest of this document, the traditional geodetic notation will be used.

As has been mentioned, the validity of the one-dimensional spherical convolution theorem was established by Churchill and Dolph (1954). Their proof is based upon the addition theorem for the Legendre polynomials. In the two-dimensional spherical case, the author is not aware of an explicit proof of the convolution theorem but is convinced that the proof will be based on the addition theorem of the associated Legendre functions. As pointed out by Kaula (1967, pg. 90), this area of knowledge seems to be studied principally by quantum physicists, such as Wigner (1959) and Edmonds (1957).



N = North Pole
 $P(\theta, \lambda)$ = Point P with colatitude θ and longitude λ
 $P'(\theta', \lambda')$ = Point P' with colatitude θ' and longitude λ'
 ψ = Spherical Arc length from P to P'
 α = Spherical Angle NPP'

Figure 2.5-1. Relationship of Points on a Spherical Surface for Interpretation of Spherical Convolution.

SECTION 3

SPECTRAL THEORY OF THE INTEGRAL TRANSFORMATIONS OF GEODESY

3.1 Introduction

In this chapter, the theoretical "continuous" integral transformations of geodesy and their spectra will be examined. The term "continuous" here implies that the input data to the transformation is assumed to exist at every point on the surface of the sphere and hence to be continuously or densely distributed over the sphere as opposed to a discrete distribution. Thus an integral expression is truly required in the description of the transformation in order to take into account "every" piece of data.

The theoretical Stokes' and Vening-Meinesz' Integrals are precisely of this type. Mathematically they require that point gravity anomalies must be known continuously or densely over the entire surface of the earth. In reality of course this is not possible. Moreover in practical computations, the integral must be approximated by a summation.

However, since only the theoretical "continuous" integral transformations of geodesy are rigorously correct,* the spectral theory of these transformations will be developed to provide an idealized standard against which any approximations may be compared.

3.2 Isotropic Geodetic Transformations

Isotropic geodetic transformations are geodetic transformations whose kernel is independent of the azimuth α . The classical example is Stokes' Integral. They are more properly called "zeroth-order" geodetic transformations, which distinguishes them from the "first-order" geodetic transformations whose kernel contains the two-dimensional vector $(\cos \alpha, \sin \alpha)$, such as the Vening-Meinesz' Integral, and in general from "m'th-order" geodetic transformations whose kernels contain the vector $(\cos m\alpha, \sin m\alpha)$.

* neglecting ellipsoidal effects

The general form for an isotropic geodetic transformation is

$$\begin{aligned}
 f_{\text{OUT}}(0,0) &= \iint K(\cos \psi) f(\psi, \alpha) \frac{d\sigma}{4\pi} \\
 &= \int_0^{\pi} \int_0^{2\pi} K(\cos \psi) f(\psi, \alpha) \frac{\sin \psi d\alpha d\psi}{4\pi} \\
 &= \int_{-1}^{+1} \int_0^{2\pi} K(\cos \psi) f(\psi, \alpha) \frac{d\alpha}{2\pi} \frac{d(\cos \psi)}{2}
 \end{aligned}$$

Since the kernel is independent of the azimuth α , the double integral may be simplified to a single integral on the mean value $\bar{f}(\psi)$ of the input $f(\psi, \alpha)$ around the spherical radius ψ :

$$\begin{aligned}
 f_{\text{OUT}}(0,0) &= \int_0^{\pi} K(\cos \psi) \bar{f}(\psi) \frac{\sin \psi d\psi}{2} \\
 &= \int_{-1}^{+1} K(\cos \psi) \bar{f}(\cos \psi) \frac{d(\cos \psi)}{2}
 \end{aligned}$$

where

$$\bar{f}(\psi) = \int_0^{2\pi} f(\psi, \alpha) \frac{d\alpha}{2\pi}$$

In other words, the output of an isotropic geodetic transformation is directly dependent only on the mean value of the input around each (infinitesimally wide) spherical radius ψ and not on the explicit value of the input at each point on each of the spherical radii.

From the fundamental Legendre transform relations, it follows as a special case that the spectrum of an isotropic geodetic transformation is given by

$$L\{K(\cos \psi)\} = \int_{-1}^{+1} K(\cos \psi) P_n(\cos \psi) \frac{d(\cos \psi)}{2} = \lambda_n[K]$$

where $P_n(\cos \psi)$ are the Legendre polynomials, n is a non-negative integer, and $K(\cos \psi)$ is the kernel of the transformation.

Conversely, the kernel of the geodetic transformation is expressed in terms of the spectrum λ_n by

$$L^{-1}\{\lambda_n[K]\} = K(\cos \psi) = \sum_{n=0}^{\infty} \lambda_n (2n+1) P_n(\cos \psi)$$

Since the output $f_{OUT}(0,0)$ is the spherical convolution $K*f$, of the kernel $K(\cos \psi)$ with the input data function $f(\psi, \alpha)$

$$f_{OUT} = K * f$$

it follows from the convolution theorem

$$L\{f_{OUT}\} = L\{K\} \cdot L\{f\}$$

and the global mean-square value property for individual frequencies or harmonics that the global mean-square value of the output is

$$\left|f_{OUT}\right|_{rms}^2 = \sum_{n=0}^{\infty} \left|f_{OUT(n)}\right|_{rms}^2 = \sum_{n=0}^{\infty} |\lambda_n\{K\}|^2 \left|f_{(n)}\right|_{rms}^2$$

in terms of the spectral coefficients and the global mean-square values of the input data function frequencies.

3.2.1 Some Examples of Isotropic Geodetic Transformations

A number of examples will now be given of the foregoing theory to illustrate its application to common transformations. A rather extensive catalog of spherical geodetic transformations and spectra is given in Volume II of this document.

3.2.1.1 Stokes' Integral

The classical Stokes' Integral is an isotropic geodetic transformation having the gravity anomaly Δg as input and the geoid height N as output:

$$N = \frac{R}{G} \iint S(\psi) \Delta g(\psi, \alpha) \frac{d\sigma}{4\pi}$$

where R and G are nominal values of the earth's radius and gravity, and $S(\psi)$ is the Stokes' function

$$S(\psi) = \frac{1}{\sin \psi/2} - 6 \sin \frac{\psi}{2} + 1 - 5 \cos \psi + 3 \cos \psi \ln(\sin \frac{\psi}{2} + \sin^2 \frac{\psi}{2})$$

The kernel of this transformation is

$$\frac{R}{G} S(\psi).$$

Following the convention of this document, the normalizing factor 4π has been grouped with the differential element $d\sigma$ of spherical surface area since it is the total surface area of the unit sphere. Some authors, such as Pick-Picha-Vyskocil (1973), write Stokes' Integral over the surface of a sphere having the earth's radius. In this case, the differential surface area element $dS = R^2 d\sigma$, and the normalizing factor is $4\pi R^2$, so it is immediately obvious that the R^2 factors cancel when the normalizing convention is followed.

The spectrum of the Stokes' integral transformation is:

$$L\left\{\frac{R}{G} S(\cos \psi)\right\} = \frac{R}{G} \lambda_n\{S\} = \frac{R}{G} \begin{cases} 0 & \text{for } n = 0, 1 \\ \frac{1}{n-1} & \text{for } n \geq 2 \end{cases}$$

and the Stokes' kernel has the well-known expansion

$$\frac{R}{G} L^{-1}\left\{\lambda_n[S]\right\} = \frac{R}{G} S(\psi) = \frac{R}{G} \sum_{n=2}^{\infty} \frac{2n+1}{n-1} P_n(\cos \psi).$$

Since the magnitudes of the spectral coefficients decrease in value with increasing spherical harmonic degree n , the higher frequencies present in the input become more damped than the lower frequencies during the transformation of the input into the output. Hence the Stokes' Integral is a "smoothing" transformation. This corresponds to our physical intuition that the geoid height has smoother characteristics than gravity anomalies.

3.2.1.2 Stokes Integral Analog for Surface Layer Density

Analogous to the classical Stokes' Integral is an isotropic geodetic transformation having the surface layer density μ as input and the geoid height N as output:*

*Heiskanen-Moritz (1967, pg. 237, eqn. 6-58)

$$N = \frac{R}{G} \iint \frac{2 \mu(\psi, \alpha)}{(2 \sin \frac{\psi}{2})^3} \frac{d\sigma}{4\pi}$$

The factor $2 \sin \psi/2$ in the denominator has been emphasized to remind the reader that it is the linear distance (through the sphere) from the point of evaluation to the generic point (ψ, α) of integration at a spherical arc distance ψ .

The spectrum of this integral transformation is:

$$L \left\{ \frac{R}{G} \frac{1}{\sin \frac{\psi}{2}} \right\} = \frac{R}{G} \lambda_n \left\{ \frac{1}{\sin \frac{\psi}{2}} \right\} = \frac{R}{G} \frac{1}{n + \frac{1}{2}} = \frac{R}{G} \frac{2}{2n+1}$$

as may be deduced from the spectral expansion of the kernel:*

$$L^{-1} \left\{ \frac{R}{G} \lambda_n \right\} = \frac{R}{G} \frac{2}{(2 \sin \frac{\psi}{2})^3} = \frac{R}{G} \sum_{n=0}^{\infty} 2 P_n(\cos \psi) = \frac{R}{G} \sum_{n=0}^{\infty} \frac{2}{2n+1} (2n+1) P_n(\cos \psi)$$

3.2.1.3 Molodenskii's Integral

Molodenskii's Integral** is an isotropic geodetic transformation which converts geoid height N into gravity anomaly Δg :

$$\Delta g_0 = -\frac{G}{R} N_0 - 2 \frac{G}{R} \iint \frac{(N - N_0)}{(2 \sin \frac{\psi}{2})^3} \frac{d\sigma}{4\pi}$$

where the zero subscripts indicate quantities at the point of evaluation (origin). Thus this transformation has the reverse inputs and outputs of Stokes' Integral, and may be considered to be the inverse of Stokes' Integral. Consequently it will have reciprocal values for its spectral coefficients to those of Stokes' Integral, namely:

$$\lambda_n = \frac{G}{R} \begin{cases} ? & \text{for } n = 0, 1 \\ (n-1) & \text{for } n \geq 2 \end{cases}$$

*Pick-Picha-Vyskocil (1973, pg. 476, eqn. 1545)

**Molodenskii (1962, pg. 50, eqn. III.2.4). Also Pick-Picha-Vyskocil (1973, pg. 243, eqn. 697)

The spectral coefficients for the zeroth and first degree harmonics must be investigated separately. Stokes' Integral is known (Heiskanen-Moritz, 1967, pg. 92) to automatically remove the zeroth and first degree harmonics while calculating the output from the input. Therefore its zeroth and first-degree spectral coefficients λ_0 and λ_1 must be zero. However in Molodenskii's Integral if the input geoid height is chosen to be a pure zeroth harmonic ($N=N_0$) or a pure first harmonic ($N=N_0 \cos \psi$), the respective outputs will be

$$\Delta g_0 = -\frac{G}{R} N_0 \quad \text{and} \quad \Delta g_1 = 0$$

implying respectively that

$$\lambda_0 = -\frac{G}{R} \quad \text{and} \quad \lambda_1 = 0$$

so that the spectral coefficients of Molodenskii's Integral are

$$\lambda_n = \frac{G}{R}(n-1) \quad n=0,1,2,\dots$$

and the expansion of the Molodenskii kernel is formally

$$\frac{G}{R} \sum_{n=0}^{\infty} (n-1)(2n+1) P_n(\cos \psi).$$

The Molodenskii kernel may be written symbolically as

$$\frac{G}{R} [-\delta_{2D}(\psi) + M(\psi)]$$

where $\delta_{2D}(\psi)$ is the two-dimensional spherical Dirac Delta function having the property that

$$\iint \delta_{2D}(\psi) f(\psi, \alpha) \frac{d\sigma}{4\pi} = f(0,0)$$

and where $M(\psi)$ is a "function" with the property that

$$\iint M(\psi) f(\psi, \alpha) \frac{d\sigma}{4\pi} = \iint \frac{-2[f(\psi, \alpha) - f(0,0)]}{(2 \sin \frac{\psi}{2})^3} \frac{d\sigma}{4\pi}$$

The $M(\psi)$ transformation will be useful in other contexts.

3.2.1.4 Truncated Stokes' Integral

The truncated Stokes' Integral is an isotropic geodetic transformation identical to the classical Stokes' Integral except that the integration is carried out only over a spherical cap of spherical radius ψ_0 rather than over the entire sphere:

$$N(\psi_0) = \frac{R}{G} \int_0^{2\pi} \int_0^{\psi_0} S(\psi) \Delta g(\psi, \alpha) \frac{\sin \psi \, d\psi \, d\alpha}{4\pi}$$

If the truncated Stokes' function $\tilde{S}(\psi)$ is defined by*

$$\tilde{S}(\psi) = \begin{cases} S(\psi) & \text{for } 0 \leq \psi \leq \psi_0 \\ 0 & \text{for } \psi_0 < \psi \leq \pi \end{cases}$$

then the transformation may also be written

$$N(\psi_0) = \frac{R}{G} \iint \tilde{S}(\psi) \Delta g(\psi, \alpha) \frac{d\sigma}{4\pi}$$

The spectrum of this transformation is

$$L\left\{\frac{R}{G} \tilde{S}\right\} = \lambda_n \left\{\frac{R}{G} \tilde{S}\right\} = \frac{R}{G} \begin{cases} 0 - \frac{1}{2} Q_n(\psi_0) & \text{for } n = 0, 1 \\ \frac{1}{n-1} - \frac{1}{2} Q_n(\psi_0) & \text{for } n \geq 2 \end{cases}$$

where the $Q_n(\psi_0)$ are the Molodenskii functions, defined in Molodenskii (1962, pg. 147) or Heiskanen-Moritz (1967, pg. 260-263). The proof of this spectral relationship is straight-forward using the definitions of the Legendre transform and the Molodenskii functions. From the relationship it is seen that the Molodenskii functions have a very elegant spectral-theoretic interpretation. The factor of one half appears due to the normalization convention used in this document for the Legendre transform. Following this convention the normalized Molodenskii functions $\hat{Q}(\psi_0) = \frac{1}{2} Q_n(\psi_0)$ would be a more natural choice

* The tilde notation is used so that there will be some similarity but especially no conflict with the bar notation of Molodenskii and Heiskanen-Moritz (1967, pg. 260). Thus $S(\psi) = \bar{S}(\psi) + \tilde{S}(\psi)$.

of fundamental function, but the unnormalized ones have become established in the literature.

3.2.1.5 Averaging Over a Spherical Cap

The transformation which calculates the integrated-mean value of a quantity over a spherical cap is an isotropic transformation having the form

$$\begin{aligned}\bar{f}(\psi_0) &= \int_0^{2\pi} \int_0^{\psi_0} \frac{2}{1 - \cos \psi_0} f(\psi, \alpha) \frac{d\sigma}{4\pi} \\ &= \int_0^{2\pi} \int_0^{\psi_0} \frac{1}{\sin^2 \frac{\psi_0}{2}} f(\psi, \alpha) \frac{d\sigma}{4\pi}\end{aligned}$$

where $f(\psi, \alpha)$ is the input data function and $\bar{f}(\psi_0)$ is mean value of the data over the cap of spherical radius ψ_0 . For example, the input data might be point gravity anomalies; then the output would be mean gravity anomalies. The transformation has this explicit representation because the surface area of the spherical cap of radius ψ_0 on a unit sphere is

$$\frac{1 - \cos \psi_0}{2} 4\pi = \sin^2 \frac{\psi_0}{2} 4\pi.$$

The spectrum of this transformation is

$$\begin{aligned}\lambda_n &= \frac{1}{1 - \cos \psi_0} \int_{\cos \psi_0}^1 P_n(x) dx \\ &= \frac{P_{n-1}(\cos \psi_0) - P_{n+1}(\cos \psi_0)}{(1 - \cos \psi_0)(2n+1)}\end{aligned}$$

where $P_{-1}(\cos \psi_0) \equiv 1$.

This quantity can be shown* to be of the order of $n^{-3/2}$. In other words the transformation is a smoothing operator (as expected!) but with stronger smoothing than the Stokes' transformation.

* Meissl (1971, pg. 24)

3.2.1.6 Summary of Isotropic Examples

The mathematical relationships for the examples of isotropic geodetic transformations which have just been described are summarized in Figures 3.2-1 through 3.2-5.

- **TRANSFORMATION: STOKES INTEGRAL**

INPUT: Δg (GRAVITY ANOMALY)

OUTPUT: N (GEOID HEIGHT)

- **EXPLICIT FORM**

$$N = \frac{T}{G} = \frac{R}{G} \iint S(\psi) \Delta g \frac{d\sigma}{4\pi}$$

- **EIGENVALUES**

$$\lambda_n = \frac{R}{G} \begin{cases} 0 & \text{FOR } n = 0, 1 \\ \frac{1}{n-1} & \text{FOR } n \geq 2 \end{cases}$$

- **SPECTRAL EXPANSION OF KERNEL**

$$K(\cos \psi) = \frac{R}{G} S(\psi) = \frac{R}{G} \sum_{n=2}^{\infty} \frac{2n+1}{n-1} P_n(\cos \psi)$$

Figure 3.2-1. Summary of Mathematical Relationships for the Classic Stokes' Integral Transformation.

- TRANSFORMATION:

ANALOG OF STOKES FOR SURFACE LAYER DENSITY

INPUT: μ (SINGLE LAYER SURFACE DENSITY)

OUTPUT: N (GEOID HEIGHT)

- EXPLICIT FORM

$$N = \frac{R}{G} \int_0^{2\pi} \int_0^\pi \frac{2\mu}{(2 \sin \frac{\psi}{2})} \frac{d\sigma}{4\pi}$$

- EIGENVALUES

$$\lambda_n = \frac{R}{G} \frac{2}{2n+1} = \frac{R}{G} \frac{1}{n + \frac{1}{2}}$$

- SPECTRAL EXPANSION OF KERNEL

$$K(\cos \psi) = \frac{R}{G} \frac{2}{(2 \sin \frac{\psi}{2})} = \frac{2R}{G} \sum_{n=0}^{\infty} P_n(\cos \psi)$$

Figure 3.2-2. Summary of Mathematical Relationships of the Analog of the Stokes' Integral Transformation for Surface Layer Density.

- TRANSFORMATION: MOLODENSKII (INVERSE STOKES)

INPUT: N (GEOID HEIGHT)

OUTPUT: Δg (GRAVITY ANOMALY)

- EXPLICIT FORM

$$\Delta g_o = -\frac{G}{R} N_o - 2\frac{G}{R} \iint \frac{(N - N_o)}{(2 \sin \frac{\psi}{2})^3} \frac{d\sigma}{4\pi}$$

- EIGENVALUES

$$\lambda_n = \frac{G}{R} \begin{cases} -1 & \text{FOR } n = 0 \\ 0 & \text{FOR } n = 1 \\ n-1 & \text{FOR } n \geq 2 \end{cases}$$

- SPECTRAL EXPANSION OR DECOMPOSITION OF KERNEL

$$K(\cos \psi) = \frac{G}{R} [-\delta(\psi) + M(\psi)] = \frac{G}{R} \sum_{n=0}^{\infty} (n-1)(2n+1) P_n(\cos \psi)$$

FORMALLY

Figure 3.2-3. Summary of Mathematical Relationships for the Molodenskii Integral Transformations.

• TRANSFORMATION: TRUNCATED STOKES

(CLASSICAL STOKES INTEGRATED ONLY
OVER A CAP OF SPHERICAL RADIUS ψ_0)

INPUT: Δg

OUTPUT: $N(\psi_0)$

• EXPLICIT FORM

$$\begin{aligned} N(\psi_0) &= \frac{R}{G} \int_0^{2\pi} \int_0^{\psi_0} S(\psi) \Delta g \frac{d\sigma}{4\pi} \\ &= \frac{R}{G} \int_0^{2\pi} \int_0^{\pi} \tilde{S}(\psi) \Delta g \frac{d\sigma}{4\pi} \end{aligned}$$

$$\text{WHERE } \tilde{S}(\psi) = \begin{cases} S(\psi) & \text{FOR } 0 \leq \psi \leq \psi_0 \\ 0 & \text{FOR } \psi_0 < \psi \leq \pi \end{cases}$$

• EIGENVALUES

$$\lambda_n = \frac{R}{G} \begin{cases} 0 - \frac{1}{2} Q_n(\psi_0) & \text{FOR } n = 0, 1 \\ \frac{1}{n-1} - \frac{1}{2} Q_n(\psi_0) & \text{FOR } n \geq 2 \end{cases}$$

WHERE $Q_n(\psi_0)$ ARE MOLODENSKIY'S FUNCTIONS
(HEISKANEN-MORITZ, PAGES 259-263)

• SPECTRAL EXPANSION OF KERNEL

$$\frac{R}{G} \tilde{S}(\psi) = \sum_{n=0}^{\infty} \lambda_n (2n+1) P_n(\cos \psi)$$

Figure 3.2-4. Summary of Mathematical Relationships for the Truncated Stokes' Integral Transformation.

• **TRANSFORMATION: AVERAGING OVER CAP**

INPUT: f (ANY QUANTITY)

OUTPUT: $\bar{f}(\psi_0)$ (AVERAGE OF THE QUANTITY
OVER CAP OF
SPHERICAL RADIUS ψ_0)

• **EXPLICIT FORM**

$$\bar{f}(\psi_0) = \int_0^{2\pi} \int_0^{\psi_0} \frac{2}{1 - \cos \psi_0} f(\psi, \alpha) \frac{d\sigma}{4\pi}$$

• **EIGENVALUES**

$$\lambda_n = \frac{1}{1 - \cos \psi_0} \int_{\cos \psi_0}^1 P_n(t) dt$$

$$= \frac{P_{n-1}(\cos \psi_0) - P_{n+1}(\cos \psi_0)}{(1 - \cos \psi_0)(2n+1)} = O\left(\frac{1}{n^{3/2}}\right)$$

WHERE $P_{-1} = 1$

• **SPECTRAL EXPANSION OF KERNEL**

$$K(\psi) = \begin{cases} \frac{2}{1 - \cos \psi_0} & \text{FOR } 0 \leq \psi \leq \psi_0 \\ 0 & \text{FOR } \psi_0 < \psi \leq \pi \end{cases}$$

$$= \sum_{n=0}^{\infty} \lambda_n (2n+1) P_n(\cos \psi)$$

Figure 3.2-5. Summary of Mathematical Relationships for the Cap-Averaging Integral Transformation.

3.2.2 Generalized Gravity Anomalies

A large number of formulas may be simplified and consolidated through the concept of the "generalized gravity anomaly of type 'k'". This concept embraces the traditional gravity anomaly Δg , the gravity disturbance δg , and the surface layer density μ , as special cases.

The generalized gravity anomaly of type "k" is defined by:

$$d_k g = -\frac{\partial T}{\partial r} + (k-1) \frac{T}{r}$$

where T is the traditional disturbing potential, r is the radius (from the center of the earth), and k is any real number.

By comparing this formula with those for Δg (Heiskanen-Moritz, pg. 89, eqn. 2-154), for δg (Heiskanen-Moritz, pg. 85, eqn. 2-146'), and for μ (Heiskanen-Moritz, pg. 237, eqn. 6-55), and by defining the "gravity variation dg " as

$$dg = -\frac{\partial T}{\partial r} - \frac{T}{r},$$

it is immediately seen that

$$\Delta g = d_{(-1)} g = \text{gravity anomaly}$$

$$dg = d_0 g = \text{gravity variation (new)}$$

$$\mu = d_{1/2} g = \text{surface layer density}$$

$$\delta g = d_1 g = \text{gravity disturbance}$$

These relations may be represented schematically as shown in Figure 3.2-6.

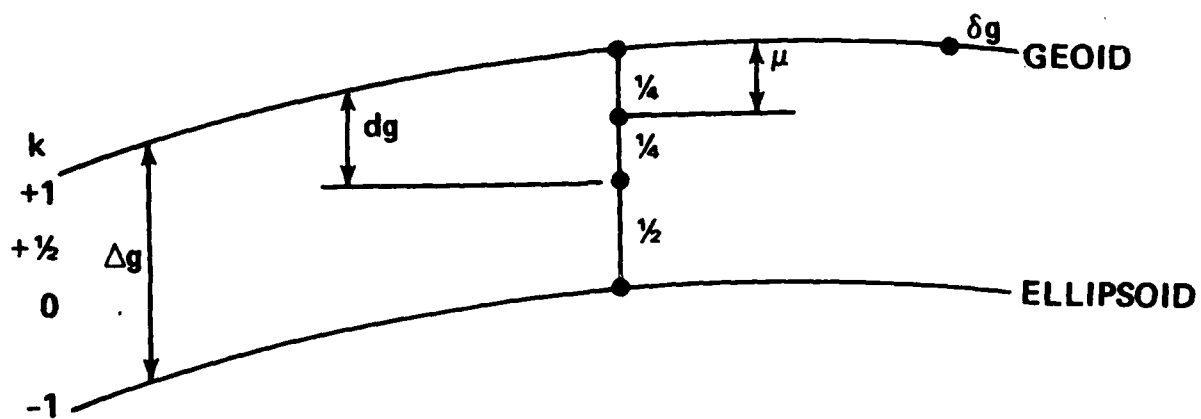


Figure 3.2-6. Schematic Diagram for the Interpretation of the Generalized Anomaly of Type "k".

This figure indicates by how much the gravity disturbance at a point must be "reduced" to convert it to the other gravimetric quantities, or equivalently by what distance the points P and Q are separated when the generalized gravity anomaly is calculated by differencing actual gravity at point P and reference gravity at point Q. For the traditional gravity anomaly P and Q are separated by the geoid height, while for surface layer density they are separated by only one quarter of the geoid height.

Consider now the analog of Stokes' Integral when the input to the integral is the generalized gravity anomaly $d_k g$ of type "k". Let $S_k(\psi)$ denote the generalized Stokes' function which will be the kernel of this integral:

$$N = \frac{T}{G} = \frac{R}{G} \iint S_k(\psi) d_k g(\psi, \alpha) \frac{d\sigma}{4\pi}$$

It may be shown that $S_k(\psi)$ has the following spectral expansion:

$$S_k(\psi) = \sum_{n=n_{\min}}^{\infty} \frac{(2n+1)}{n+k} P_n(\cos \psi)$$

where n_{\min} is zero or the first positive integer such that the denominator $(n+k)$ is always positive. This result implies that the spectrum of the generalized Stokes' transformation is

$$\lambda_n \left(\frac{R}{G} S_k(\psi) \right) = \frac{R}{G} \begin{cases} 0 & n < n_{\min} \\ \frac{1}{n+k} & n \geq n_{\min} \end{cases}$$

Explicit expressions for these functions are given in Figure 3.2-7. The expressions have been obtained from the rather complete table in Pick-Picha-Vyskocil (1973, pg. 476ff). In an effort to achieve clearer notation, the following symbology has also been used for the generalized Stokes' functions in the catalog (Volume II of this document).

$$S_{-1}(\psi) \equiv S(\psi)$$

$$S_0(\psi) \equiv S_{dg}(\psi)$$

$$S_{1/2}(\psi) \equiv S_{\mu}(\psi)$$

$$S_{+1}(\psi) \equiv S_{\delta g}(\psi)$$

A summary of the explicit mathematical relationships of the generalized Stokes' transformation is given in Figure 3.2-8.

$$\bullet \Delta g: S_{-1}(\psi) = \frac{1}{\sin \frac{\psi}{2}} - 6 \sin \frac{\psi}{2} + 1 - 5 \cos \psi - 3 \cos \psi \ln \left(\sin \frac{\psi}{2} + \sin^2 \frac{\psi}{2} \right)$$

$$\bullet dg: S_0(\psi) = \frac{1}{\sin \frac{\psi}{2}} - 2 - 3 \cos \psi - \ln \left(\sin \frac{\psi}{2} + \sin^2 \frac{\psi}{2} \right)$$

$$\bullet \mu: S_{1/2}(\psi) = \frac{1}{\sin \frac{\psi}{2}}$$

$$\bullet \delta g: S_1(\psi) = \frac{1}{\sin \frac{\psi}{2}} - \ln \left(1 + \frac{1}{\sin \frac{\psi}{2}} \right)$$

Figure 3.2-7. Closed Form Expressions for the Generalized Stokes' Function.

- **TRANSFORMATION: GENERALIZED STOKES**

INPUT: $d_k g$ (GENERALIZED GRAVITY ANOMALY)
 OUTPUT: N (GEOID HEIGHT)

- **EXPLICIT FORM**

$$N = \frac{T}{G} = \frac{R}{G} \iint S_k(\psi) d_k g(\psi, \alpha) \frac{d\sigma}{4\pi}$$

WHERE S_k = STOKES' FUNCTION ANALOG FOR
 THE GENERALIZED GRAVITY
 ANOMALY OF TYPE k

- **EIGENVALUES**

$$\lambda_n = \frac{R}{G} \frac{1}{n+k}$$

- **SPECTRAL EXPANSION OR DECOMPOSITION OF KERNEL**

$$K(\cos \psi) = \frac{R}{G} S_k(\psi) = \frac{R}{G} \sum_{n=0}^{\infty} \frac{2n+1}{n+k} P_n(\cos \psi)$$

Figure 3.2-8. Summary of Mathematical Relationships for the Generalized Stokes' Integral Transformation.

3.2.3 Flow Diagrams of Transformations

It is very enlightening conceptually to represent the spectra of geodetic transformations in a flow diagram such as Figure 3.2.3-1. The nodes of the flow diagram are geodetic quantities, and the lines between the nodes represent the transformation (in either direction) between the pair of quantities which a line connects. A direction is arbitrarily specified for each line, and the spectrum of the transformation corresponding to this direction is written beside the line. The spectrum of the inverse transformation is the reciprocal of the spectrum of the forward transformation.

For example, at the extreme left of Figure 3.2.3-1, the transformation from geoid height N to gravity anomalies Δg in the direction of the arrow is Molodenskii's transformation which has the spectrum $(G/R)(n-1)$. Its inverse is the traditional Stokes' Integral with the spectrum* $R/G(n-1)$.

Since the transformation from geoid N to gravity disturbances δg has the spectrum $\lambda_n = (G/R)(n+1)$, it may be inferred using the sequential transformation spectrum multiplication rule that the transformation converting gravity anomalies Δg into gravity disturbances δg has the spectrum

$$\lambda_n \{\Delta g \rightarrow \delta g\} = \frac{n+1}{n-1}$$

Quantities of approximately equal "smoothness" have been positioned on the same horizontal line in the flow diagram. The geoid height is the smoothest quantity and is placed at the top. The gravity anomalies, disturbances, and surface layer densities are "rougher" in the sense that for a specified spectrum of the geoid height these quantities will have spectra whose higher frequencies have been amplified since the transformations from geoid height to these quantities all have spectra of the order of the spherical harmonic degree n , i.e., the n^{th} harmonic of the input is multiplied by (approximately) n to form the n^{th} harmonic of the output. However the transformation between any pair of generalized gravity anomaly quantities has a spectrum of the order of 1, so that the strengths of the higher frequencies are neither amplified nor attenuated, implying that these quantities have approximately equal smoothness.

*For simplicity, the zeroth and first degree spectral coefficients, λ_0 and λ_1 , are neglected.

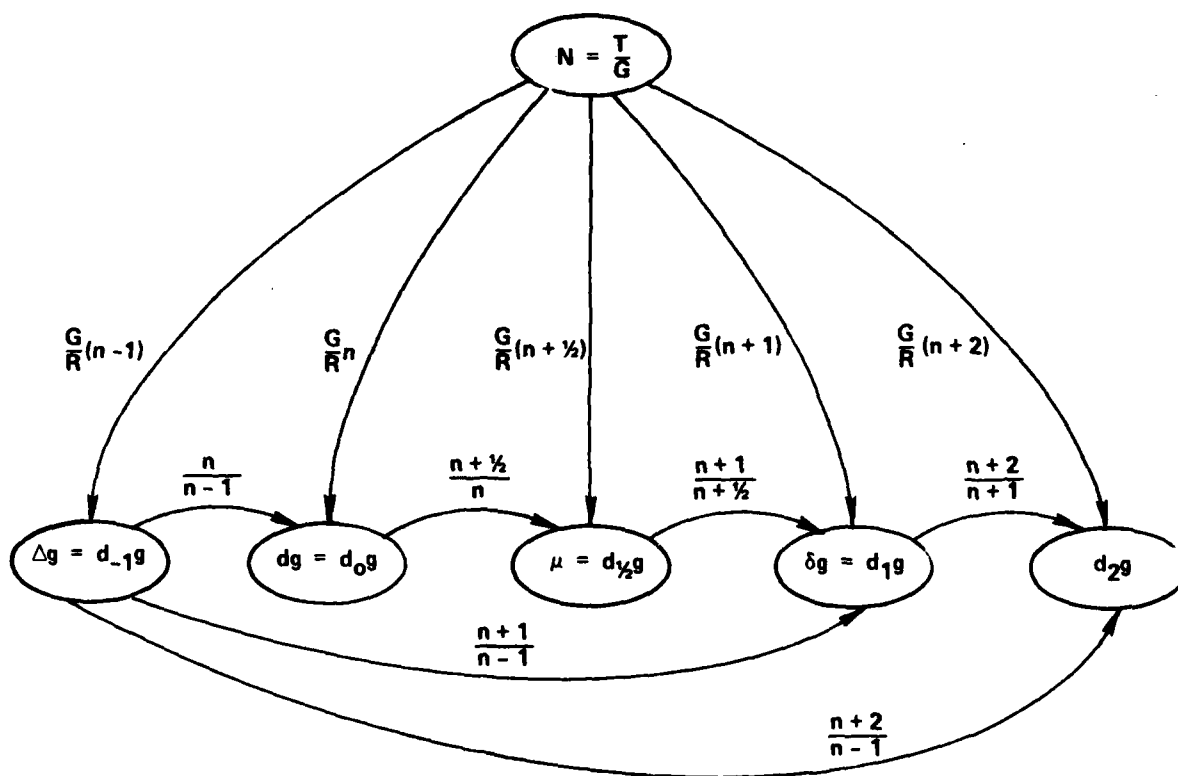


Figure 3.2.3-1. Flow Diagram of Basic Geodetic Transformations and Their Spectra.

3.2.4 Spectra of Spherical Geodetic Transformations with Upward Continuation

It is desired to obtain an expression for the spectrum of an "extended" geodetic transformation, that is, a transformation whose output is a geodetic quantity at an altitude above the surface of the reference sphere and whose input are geodetic quantities on the sphere.

It may be shown (Heiskanen-Moritz, 1967, pg. 20) that any harmonic function* $h(r, \psi, \alpha)$ in the space outside of a reference sphere may be expressed in terms of its "boundary" values $h(R, \psi, \alpha)$ on the surface of the sphere by the relation

$$h(r, \psi, \alpha) = \sum_{n=0}^{\infty} \left(\frac{R}{r} \right)^{n+1} h_n(\psi, \alpha)$$

where $h_n(\psi, \alpha)$ is the n^{th} degree surface spherical harmonic term

$$h_n(\psi, \alpha) = \sum_{m=0}^n \left(H_n^m \cos m \alpha + H_n^m \sin m \alpha \right) (2n+1) \sqrt{\frac{(n-m)!}{(n+m)!}} P_n^m(\cos \psi)$$

and where

$$\begin{Bmatrix} H_n^m \\ H_n^m \end{Bmatrix} = \epsilon_n \sqrt{\frac{(n-m)!}{(n+m)!}} \iint h(R, \psi, \alpha) \begin{Bmatrix} \cos \alpha \\ \sin \alpha \end{Bmatrix} P_n^m(\cos \psi) \frac{d\sigma}{4\pi}$$

By forming the two-dimensional Legendre transform at altitude, namely on an "outer" sphere of radius r , to derive the spectrum of the function $h(r, \psi, \alpha)$ at altitude, it is found that

$$L_{2D}\{h(r, \psi, \alpha)\} = \left(\frac{R}{r} \right)^{n+1} L_{2D}\{h(R, \psi, \alpha)\}$$

Thus the spherical upward continuation operator of a harmonic geodetic quantity has the spectrum

$$\lambda_n\{h(R, \psi, \alpha) + h(r, 0, 0)\} = \left(\frac{R}{r} \right)^{n+1}$$

* a harmonic function is by definition a solution of Laplace's equation

For example, the geoid height N is harmonic, since it is proportional to the disturbing potential T by Brun's Theorem. The gravity anomaly Δg and gravity disturbance δg are not harmonic; however the quantities $(r \Delta g)$ and $(r \delta g)$ are harmonic.* Hence, the operator which upward-continues Δg or δg to altitude from surface values of these same quantities has the spectrum

$$\lambda_n \{ \Delta g(R, \psi, \alpha) \rightarrow \Delta g(r, 0, 0) \} = \left(\frac{R}{r} \right)^{n+2}$$

which may be derived by applying the preceeding relation to the harmonic quantities $(r \Delta g)$ and $(r \delta g)$ and collecting the radius factors.

A summary of the mathematical relations for the upward continuation transformation of harmonic functions is given in Figure 3.2.4-1. When the output radius r equals the input radius R , the identity transformation occurs. This has the spectrum of unity.

In this document, the spectra of surface transformations have generally been investigated since the spectra of corresponding transformations with upward continuation can be obtained trivially by multiplying the surface spectra by the appropriate radius ratio factor (provided the harmonicity condition is satisfied). An important exception to this technique is the class of truncated geodetic transformations.

* Heiskanen-Moritz (1967, pg. 88). In particular, equations 2-155 and 2-153 show that these two quantities may be expanded in a spherical harmonic series.

- **TRANSFORMATION: IDENTITY, UPWARD CONTINUATION**

INPUT: $h(R, \psi, \alpha)$ ON SURFACE OF RADIUS R

OUTPUT: $h(r, 0, 0)$ AT RADIUS r

WHERE h IS ANY HARMONIC FUNCTION (e.g., $r \Delta g$)

- **EXPLICIT FORM**

$$h(r, 0, 0) = \iint \frac{R(r^2 - R^2)}{(r^2 - 2Rr \cos \psi + R^2)^{3/2}} h(R, \psi, \alpha) \frac{d\sigma}{4\pi}$$

- **EIGENVALUES**

$$\lambda_n = \left(\frac{R}{r}\right)^{n+1}, \text{ HENCE } \lambda_n = 1 \text{ WHEN } r = R$$

- **SPECTRAL EXPANSION OR DECOMPOSITION OF KERNEL**

$$\begin{aligned} K(\cos \psi, r, R) &= \frac{R(r^2 - R^2)}{(r^2 - 2Rr \cos \psi + R^2)^{3/2}} \\ &= \sum_{n=0}^{\infty} \left(\frac{R}{r}\right)^{n+1} (2n+1) P_n(\cos \psi) \end{aligned}$$

HENCE

$$\delta(\psi) = \lim_{r \rightarrow R} \frac{R(r^2 - R^2)}{(r^2 - 2Rr \cos \psi + R^2)^{3/2}} = \sum_{n=0}^{\infty} (2n+1) P_n(\cos \psi)$$

Figure 3.2.4-1. Summary of Mathematical Relationships for the Identity and Upward Continuation Integral Transformation.

3.2.5 Vertical Gradients of Geodetic Quantities

Heiskanen and Moritz (1967, pg. 115, eqn. 2-216) have shown that the vertical gradient of gravity anomalies at the surface may be expressed as

$$\frac{\partial \Delta g}{\partial r} = -\frac{1}{R} \sum_{n=0}^{\infty} (n+2) \Delta g_n$$

where Δg_n are the gravity anomaly harmonics (Heiskanen-Moritz, pg. 97)*

$$\Delta g_n = \iint \Delta g(\psi, \alpha) P_n(\cos \psi) \frac{d\sigma}{4\pi} = L_n\{\Delta g\}$$

Hence the spectrum of the transformation from gravity anomalies Δg to their vertical gradient at the surface is

$$\lambda_n \left\{ \Delta g + \frac{\partial \Delta g}{\partial r} \right\} = -\frac{1}{R}(n+2)$$

An explicit expression for the calculation of the vertical gradient of the gravity anomaly has been derived by Heiskanen-Moritz (1967, pg. 115, eqn. 2-217):

$$\frac{\partial \Delta g}{\partial r} = -\frac{2}{R} \Delta g_0 + \frac{2}{R} \iint \frac{(\Delta g - \Delta g_0)}{\left(2 \sin \frac{\psi}{2}\right)^3} \frac{d\sigma}{4\pi}$$

The kernel of this transformation may be represented symbolically by

$$-\frac{1}{R} \left[2\delta_{2D}(\psi) + M(\psi) \right]$$

where the two-dimensional Dirac Delta function $\delta_{2D}(\psi)$ and the function $M(\psi)$ have the properties

$$\iint \delta_{2D}(\psi) f(\psi, \alpha) \frac{d\sigma}{4\pi} = f(0, 0)$$

$$\iint M(\psi) f(\psi, \alpha) \frac{d\sigma}{4\pi} = \iint \frac{-2[f(\psi, \alpha) - f(0, 0)]}{(2 \sin \frac{\psi}{2})^3} \frac{d\sigma}{4\pi}$$

* Note that Heiskanen-Moritz use a different definition of the spectral coefficients, specifically grouping the term $(2n+1)$ differently.

The mathematical relationships for the gravity anomaly vertical gradient transformation are summarized in Figure 3.2.5-1.

From the above spectrum and the spectrum of the Molodenskii Integral, it is easy to see that the spectrum of the transformation having the kernel $M(\psi)$ is

$$\lambda_n \{M(\psi)\} = n$$

since

$$\lambda_n \{\delta_{2D}(\psi)\} = 1$$

This result about $\lambda_n \{M(\psi)\}$ is due to Meissl (1971, pg. 22, eqn. 3-11).

It will now be shown that the transformation from any generalized gravity anomaly to its vertical gradient at the surface has the same spectrum

$$\lambda_n \left\{ d_k g + \frac{\partial d_k g}{\partial r} \right\} = -\frac{1}{R} (n+2)$$

The quantity $(r d_k g)$ is harmonic. Hence

$$[r d_k g(r)] = \sum_{n=0}^{\infty} \left(\frac{R}{r}\right)^{n+1} [R d_k g(R)]_{(n)}$$

or

$$d_k g(r) = \sum_{n=0}^{\infty} \left(\frac{R}{r}\right)^{n+2} [d_k g(R)]_{(n)}$$

Differentiating with respect to r :

$$\begin{aligned} \frac{\partial d_k g(r)}{\partial r} &= \sum_{n=0}^{\infty} (n+2) \left(\frac{R}{r}\right)^{n+1} \left(\frac{-R}{r^2}\right) [d_k g(R)]_{(n)} \\ &= \sum_{n=0}^{\infty} \left(-\frac{n+2}{r}\right) \left(\frac{R}{r}\right)^{n+2} [d_k g(R)]_{(n)} \end{aligned}$$

The last line is the spectral representation of the vertical gradient in terms of the (input) generalized gravity anomaly. It is seen that the strengths of the constituent frequencies of the input are multiplied

- TRANSFORMATION:

VERTICAL GRADIENT OF GRAVITY ANOMALIES (AT SURFACE)

INPUT: Δg
 OUTPUT: $\left. \frac{\partial \Delta g}{\partial r} \right|_{r=R}$

- EXPLICIT FORM

$$\frac{\partial \Delta g}{\partial r} = -\frac{2}{R} \Delta g_0 + \frac{2}{R} \iint \frac{(\Delta g - \Delta g_0)}{(2 \sin \frac{\psi}{2})^3} \frac{d\sigma}{4\pi}$$

- EIGENVALUES

$$\lambda_n = -\frac{1}{R} (n+2)$$

- SPECTRAL EXPANSION OF KERNEL

$$K(\psi) = -\frac{1}{R} [2 \delta(\psi) + M(\psi)] = -\frac{1}{R} \sum (n+2)(2n+1) P_n(\cos \psi)$$

FORMALLY

Figure 3.2.5-1. Summary of Mathematical Relationships for the Gravity Anomaly Vertical Gradient Integral Transformation.

by the factor $-(n+2)/R$; hence, this quantity is the spectrum of this transformation.

A flow diagram of the spectra of the vertical gradient transformations is given in Figure 3.2.5-2, from which a very interesting result may be inferred: The spectrum of the transformation from the generalized gravity anomaly of type 2

$$d_2g = -\frac{\partial T}{\partial r} + \frac{T}{r}$$

to the vertical gradient $\frac{\partial}{\partial r} d_kg$ of the generalized gravity anomaly of type k is equal (within a constant) to the spectrum of the transformation from the geoid height to the generalized gravity anomaly of type k. Hence, the transformations themselves are identical (within the same constant): If the generalized Stokes' transformation L maps geoid height N to the generalized gravity anomaly d_kg :

$$L : N \rightarrow d_kg$$

then the negative of this transformation divided by the nominal value G of gravity maps the generalized gravity anomaly d_2g into the vertical gradient $\partial d_kg / \partial r$:

$$\left(-\frac{1}{G}\right)L : d_2g \rightarrow \frac{\partial d_kg}{\partial r}$$

3.2.6 Vertical Stress Gradient Spectrum

The "extended" Stokes' Integral, which expresses the disturbing potential $T(r)$ at altitude in terms of the surface gravity anomalies, may be differentiated with respect to the radial direction parameter (the radius r) to obtain the gravity disturbance $\delta g(r)$ at altitude. This is carried out by Heiskanen-Moritz (1967, pg. 233ff). The resulting transformation has the kernel

$$-R \frac{\partial S(r, \psi)}{\partial r}$$

where $S(r, \psi)$ is the "extended" Stokes' function. The analytic expression for this transformation may again be differentiated with respect to the radial direction parameter to obtain the vertical stress gradient quantity:

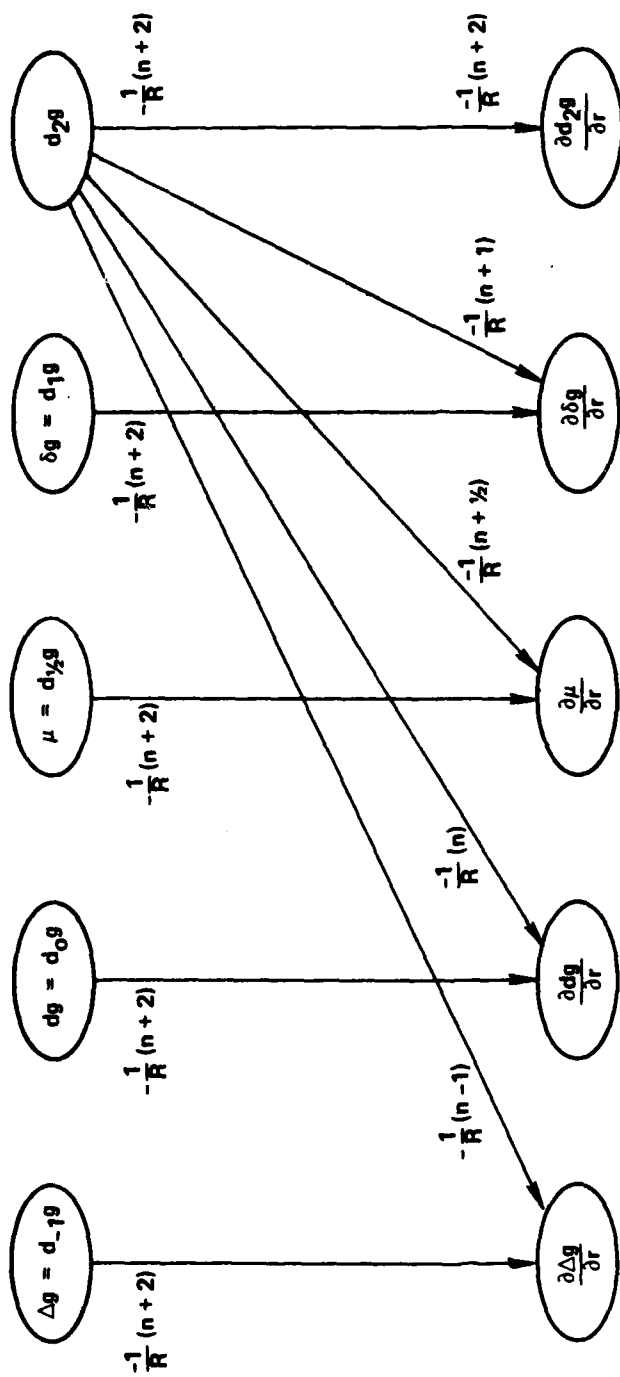


Figure 3.2.5-2. Flow Diagram of Eigenvalues of Vertical Gradient Geodetic Transforms.

$$-\frac{\partial^2 T}{\partial r^2} = \frac{\partial \delta g}{\partial r}$$

which is one of the components of the gravity gradient tensor. This transformation is isotropic and has the kernel

$$-R \frac{\partial^2 S(r, \psi)}{\partial r^2}$$

The analytic expression for this second partial derivative is given by Reed (1973, pg. 71). From the flow diagram of spectra for vertical gradient transformations, it can be determined that the spectrum of this transformation at the surface is

$$\lambda_n \left\{ \Delta g + \frac{\partial \delta g}{\partial r} \right\} = - \frac{(n+2)(n+1)}{R(n-1)} .$$

The mathematical relations for this transformation are summarized in Figure 3.2.5-3. The other components of the gravity gradient tensor are generated by anisotropic transformations and their spectra will be derived in the section pertaining to such transformations.

- TRANSFORMATION: VERTICAL STRESS GRADIENT (AT SURFACE)

INPUT: Δg

OUTPUT: $-T_{zz} = \frac{\partial \delta g}{\partial r}$

- EXPLICIT FORM

$$-T_{zz} = -R \iint \frac{\partial^2 S(r, \psi)}{\partial r^2} \Delta g \frac{d\sigma}{4\pi}$$

- EIGENVALUES

$$\lambda_n = -\frac{1}{R} \begin{cases} 0 & \text{FOR } n = 0, 1 \\ \frac{(n+2)(n+1)}{(n-1)} & \text{FOR } n \geq 2 \end{cases}$$

- SPECTRAL EXPANSION OF KERNEL

$$-R \left. \frac{\partial^2 S(r, \psi)}{\partial r^2} \right|_{r=R} = -\frac{1}{R} \sum_{n=2}^{\infty} \frac{(n+2)(n+1)}{(n-1)} (2n+1) P_n(\cos \psi)$$

Figure 3.2.5-3. Summary of Mathematical Relationships for the Vertical Stress Gradient Integral Transformation.

3.3 Anisotropic Geodetic Transformations

Anisotropic geodetic transformations are geodetic transformations whose kernels depend on the local azimuth α . The classic example is the Vening-Meinesz' Integral which provides the two components of the deflection of the vertical from a knowledge of the gravity anomaly. Each vertical deflection component depends upon the spatial distribution of the gravity anomaly values in azimuth around each spherical radius rather than merely on their mean value.

Anisotropic geodetic transformations are more properly but less intuitively called "non-zeroth-order" geodetic transformations.

The general form of an anisotropic geodetic integral transformation is

$$\begin{aligned} f_{\text{OUT}}(0,0) &= \iint K(\cos \psi) \begin{Bmatrix} \cos M\alpha \\ \sin M\alpha \end{Bmatrix} f(\psi, \alpha) \frac{d\sigma}{4\pi} \\ &= \int_0^{2\pi} \int_0^{\pi} K(\cos \psi) \begin{Bmatrix} \cos M\alpha \\ \sin M\alpha \end{Bmatrix} f(\psi, \alpha) \frac{\sin \psi \, d\psi \, d\alpha}{4\pi} \\ &= \int_0^{2\pi} \int_{-1}^{+1} K(\cos \psi) \begin{Bmatrix} \cos M\alpha \\ \sin M\alpha \end{Bmatrix} f(\psi, \alpha) \frac{d(\cos \psi)}{2} \frac{d\alpha}{2\pi} \end{aligned}$$

From the fundamental Legendre transform relations it follows that the spectrum λ_n^m of an anisotropic integral transformation is given by

$$\begin{aligned} L_{2D} \left\{ K(\cos \psi) \begin{Bmatrix} \cos M\alpha \\ \sin M\alpha \end{Bmatrix} \right\} &= \lambda_n^m \\ &= \epsilon_m \sqrt{\frac{(n-m)!}{(n+m)!}} \iint K(\cos \psi) \begin{Bmatrix} \cos M\alpha \\ \sin M\alpha \end{Bmatrix} \begin{Bmatrix} \cos m\alpha \\ \sin m\alpha \end{Bmatrix} P_n^m(\cos \psi) \frac{d\sigma}{4\pi} \end{aligned}$$

where $K(\cos \psi) \begin{Bmatrix} \cos M\alpha \\ \sin M\alpha \end{Bmatrix}$ is the kernel of the transformation.

Conversely, the kernel of the anisotropic geodetic transformation is expressed in terms of the spectrum by:

$$K(\cos \psi) \begin{Bmatrix} \cos M\alpha \\ \sin M\alpha \end{Bmatrix} = L^{-1} \begin{Bmatrix} \lambda^M \\ -n \end{Bmatrix} = \sum_{n=0}^{\infty} \lambda_n^M (2n+1) \sqrt{\frac{(n-M)!}{(n+M)!}} P_n^M(\cos \psi) \begin{Bmatrix} \cos M\alpha \\ \sin M\alpha \end{Bmatrix}$$

3.3.1 Some Examples of Anisotropic Geodetic Transformations

A few examples will now be given of anisotropic geodetic transformations and their spectra. A rather extensive catalog of spherical geodetic transformations and spectra is given in Volume II of this document.

3.3.1.1 Vening-Meinesz' Integral

The Vening-Meinesz' Integral is an anisotropic geodetic transformation having the gravity anomaly Δg as input and the deflections of the vertical (or equivalently the two horizontal gravity disturbance components) as output. The kernel of the transformation is

$$\frac{\partial S(\psi)}{\partial \psi} \begin{Bmatrix} \cos \alpha \\ \sin \alpha \end{Bmatrix}$$

which is separable into local "radial" and azimuthal parts. By differentiating the spectral expansion of Stokes' kernel

$$S(\psi) = \sum_{n=2}^{\infty} \frac{2n+1}{n-1} P_n(\cos \psi)$$

and making use of the fact that

$$\frac{\partial P_n(\cos \psi)}{\partial \psi} = \frac{\partial P_n(x)}{\partial x} (-1) \sin \psi = P_n^1(\cos \psi)$$

it follows that

$$VM(\psi) \equiv \frac{\partial S(\psi)}{\partial \psi} = \sum_{n=2}^{\infty} \frac{2n+1}{n-1} P_n^1(\cos \psi)$$

or

$$\frac{\partial S(\psi)}{\partial \psi} = \sum_{n=2}^{\infty} \frac{\sqrt{n(n+1)}}{n-1} \frac{2n+1}{\sqrt{n(n+1)}} P_n^1(\cos \psi),$$

Recalling the definition of the spectrum of anisotropic geodetic transformations and noting that

$$\frac{1}{\sqrt{n(n+1)}} = \sqrt{\frac{(n-1)!}{(n+1)!}}$$

we see that the spectrum λ_{-n}^1 of the traditional Vening-Meinesz' transformation* is:

$$\lambda_{-n}^1 \left\{ \begin{array}{c} G\xi \\ \Delta g + \\ G\eta \end{array} \right\} = \lambda_n^1 \left\{ \begin{array}{c} \left\{ \begin{array}{c} 1 \\ 0 \end{array} \right\} \\ \left\{ \begin{array}{c} 0 \\ 1 \end{array} \right\} \end{array} \right. \begin{array}{l} \text{for } G\xi \\ \text{for } G\eta \end{array}$$

where the "gain" is

$$\lambda_n^1 = \frac{\sqrt{n(n+1)}}{n-1}$$

The mathematical relations for this transformation are summarized in Figure 3.3.1-1.

* expressed in terms of horizontal gravity disturbances rather than deflections

• **TRANSFORMATION: VENING-MEINESZ**

INPUT: Δg

OUTPUT: $G\vec{e} = (G\xi, G\eta)$

= HORIZONTAL GRAVITY DISTURBANCE VECTOR

• **EXPLICIT FORM**

$$\begin{Bmatrix} G\xi \\ G\eta \end{Bmatrix} = \iint \frac{\partial S(\psi)}{\partial \psi} \begin{Bmatrix} \cos \alpha \\ \sin \alpha \end{Bmatrix} \Delta g \frac{d\sigma}{4\pi}$$

• **EIGENVALUES**

$$\lambda_n^1 = \begin{cases} 0 & \text{FOR } n = 0, 1 \\ \frac{\sqrt{n(n+1)}}{n-1} & \text{FOR } n \geq 2 \end{cases}$$

• **SPECTRAL EXPANSION OF KERNEL**

$$\begin{aligned} \frac{\partial S}{\partial \psi} \begin{Bmatrix} \cos \alpha \\ \sin \alpha \end{Bmatrix} &= \sum_{n=2}^{\infty} \frac{\sqrt{n(n+1)}}{n-1} \frac{(2n+1)}{\sqrt{n(n+1)}} P_n^1(\cos \psi) \begin{Bmatrix} \cos \alpha \\ \sin \alpha \end{Bmatrix} \\ &= \sum_{n=2}^{\infty} \frac{2n+1}{n-1} P_n^1(\cos \psi) \begin{Bmatrix} \cos \alpha \\ \sin \alpha \end{Bmatrix} \end{aligned}$$

Figure 3.3.1-1. Summary of Mathematical Relationships for the Classic Vening-Meinesz' Integral Transformation

3.3.1.2 Vertical Shear Gravity Gradient

The transformation by which the vertical "shear" gradients are generated from gravity anomalies is a second example of an anisotropic geodetic transformation. The vertical shear gradients are two components of the gravity gradient tensor* and are defined to be the spatial partial derivatives (gradients) of the gravity disturbance in the local north ($\alpha=0$) and local east ($\alpha=90^\circ$) directions. In the local cartesian osculating coordinate system (x =local north, y =local east, z =local down), the vertical "shear" gradients would be represented by $+T_{zx}$ and $+T_{zy}$ using the traditional notation with subscripts denoting partial derivatives with respect to the indicated variables.

Thus

$$+T_{zx} = \frac{\partial \delta g}{R \partial \psi}_{\alpha=0} ; +T_{zy} = \frac{\partial \delta g}{R \partial \psi}_{\alpha=90^\circ}$$

The explicit form of the integral transformation is derived by differentiating the extended Stokes' Integral with respect to the radius r and with respect to spherical radius ψ . Thus the kernel of the transformation is

$$\frac{\partial^2 S(r, \psi)}{\partial r \partial \psi} \begin{Bmatrix} \cos \alpha \\ \sin \alpha \end{Bmatrix}$$

An explicit expression for this kernel has been derived in Reed (1971, pg. 71).

By using the sequential transformation spectral multiplication rule on the Vening-Meinesz' and vertical gradient transformations, it is easily derived that the spectrum of the transformation converting gravity anomalies into vertical shear gravity gradients is the product of

$$-\frac{1}{R}(n+2) \quad \text{and} \quad \begin{cases} 0 & \text{for } n = 0, 1 \\ \frac{\sqrt{n(n+1)}}{n-1} & \text{for } n \geq 2 \end{cases}$$

* when the tensor is represented in a local vertical coordinate system

The mathematical relations for this transformation are summarized in Figure 3.3.1-2.

• TRANSFORMATION: VERTICAL SHEAR GRADIENTS

INPUT: Δg

OUTPUT: $T_{zx} = \frac{\partial \delta g}{R \partial \psi_{(\alpha=0)}}$ AND $T_{zy} = \frac{\partial \delta g}{R \partial \psi_{(\alpha=90^\circ)}}$

• EXPLICIT FORM

$$\begin{Bmatrix} +T_{zx} \\ +T_{zy} \end{Bmatrix} = \iint \frac{\partial^2 S(r, \psi)}{\partial r \partial \psi} \Delta g \begin{Bmatrix} \cos \alpha \\ \sin \alpha \end{Bmatrix} \frac{d\sigma}{4\pi}$$

• EIGENVALUES

$$\lambda_n^1 = -\frac{1}{R} \begin{cases} 0 & \text{FOR } n = 0, 1 \\ \frac{n+2}{n-1} \sqrt{n(n+1)} & \text{FOR } n \geq 2 \end{cases}$$

• SPECTRAL EXPANSION OF KERNEL

$$\left. \frac{\partial^2 S(r, \psi)}{\partial r \partial \psi} \right|_{r=R} \begin{Bmatrix} \cos \alpha \\ \sin \alpha \end{Bmatrix} = \frac{1}{R} \sum_{n=2}^{\infty} \frac{-(n+2)}{(n-1)} (2n+1) P_n^1(\cos \psi) \begin{Bmatrix} \cos \alpha \\ \sin \alpha \end{Bmatrix}$$

Figure 3.3.1-2. Summary of Mathematical Relationships for the Vertical Shear Gradient Integral Transformation.

3.3.1.3 Horizontal Differential Stress and Horizontal Shear Gradients

The transformation by which the horizontal differential stress gradient and horizontal shear gradient are generated from the gravity anomalies is a third example of an anisotropic geodetic transformation and the first example of a second-order transformation.

The explicit form of the transformation may be obtained by differentiating the Vening-Meinesz' Integral with respect to the spherical radius ψ , evaluating the results along the azimuths $\alpha = 0^\circ$ or $\alpha = 90^\circ$, and calculating

$$-(T_{YY} - T_{XX}) = \frac{-G}{R} \left(\left. \frac{\partial \eta}{\partial \psi} \right|_{\alpha=90^\circ} - \left. \frac{\partial \xi}{\partial \psi} \right|_{\alpha=0^\circ} \right)$$

$$2T_{XY} = 2 \frac{G}{R} \left(\left. \frac{\partial \xi}{\partial \psi} \right|_{\alpha=90^\circ} \text{ or } \left. \frac{\partial \eta}{\partial \psi} \right|_{\alpha=0^\circ} \right)$$

The kernel of the transformation will be found to be [Malkin (1933, pg.56)]:

$$\frac{1}{R} \left(\frac{\partial^2 S(\psi)}{\partial \psi^2} - \cot \psi \frac{\partial S(\psi)}{\partial \psi} \right) \begin{Bmatrix} \cos 2\alpha \\ \sin 2\alpha \end{Bmatrix}$$

The easiest way to derive the spectrum of the transformation is to find the spectral expansion of the kernel directly and then identify the spectral coefficients in the expansion. By differentiating the spectral expansion of the Stokes' Integral kernel twice with respect to ψ ,

$$\left(\frac{\partial^2 S(\psi)}{\partial \psi^2} - \cot \psi \frac{\partial S(\psi)}{\partial \psi} \right) = \sum_{n=2}^{\infty} \frac{2n+1}{n-1} \left(\frac{\partial^2 P_n(\cos \psi)}{\partial \psi^2} - \cot \psi \frac{\partial P_n(\cos \psi)}{\partial \psi} \right)$$

and using the relation that

$$\frac{\partial^2 P_n(\cos \psi)}{\partial \psi^2} - \cot \psi \frac{\partial P_n(\cos \psi)}{\partial \psi} = P_n^2(\cos \psi),$$

it is seen that the kernel of the transformation has the expansion:

$$-\frac{1}{R} \left(\frac{\partial^2 S(\psi)}{\partial \psi^2} - \cot \psi \frac{\partial S(\psi)}{\partial \psi} \right) \begin{Bmatrix} \cos 2\alpha \\ \sin 2\alpha \end{Bmatrix} = -\frac{1}{R} \sum_{n=2}^{\infty} \frac{2n+1}{n-1} P_n^2(\cos \psi) \begin{Bmatrix} \cos 2\alpha \\ \sin 2\alpha \end{Bmatrix}$$

By comparing this result with the general kernel expansion formula, it is immediately deduced that the spectral coefficients are

$$\lambda_n^2 = -\frac{1}{R} \begin{cases} 0 & \text{for } n = 0, 1 \\ \frac{\sqrt{(n+2)(n+1)n(n-1)}}{n-1} & \text{for } n \geq 2 \end{cases}$$

The mathematical relations for this transformation are summarized in Figure 3.3.1-3.

3.3.2 Flow Diagram of Spectra

A flow diagram of the spectra of some of the anisotropic transformations discussed in the preceding sections is given in Figure 3.3.2-1. As in the previous flow diagrams, geodetic quantities of approximately equal "smoothness" are drawn on the same horizontal line.

• TRANSFORMATION: HORIZONTAL STRESS AND SHEAR GRADIENTS

INPUT: Δg

OUTPUT: $(T_{yy} - T_{xx})$ AND T_{xy}

• EXPLICIT FORM

$$\left. \begin{aligned} -(T_{yy} - T_{xx}) &= \frac{-G}{R} \left(\frac{\partial \eta}{\partial \psi_{\alpha=90^\circ}} - \frac{\partial \xi}{\partial \psi_{\alpha=0^\circ}} \right) \\ 2T_{xy} &= \frac{G}{R} 2 \left(\frac{\partial \xi}{\partial \psi_{\alpha=90^\circ}} \text{ OR } \frac{\partial \eta}{\partial \psi_{\alpha=0^\circ}} \right) \end{aligned} \right\} = \frac{-1}{R} \iint K(\psi) \Delta g \begin{Bmatrix} \cos 2\alpha \\ \sin 2\alpha \end{Bmatrix} \frac{d\sigma}{4\pi}$$

• EIGENVALUES

$$\lambda_n^2 = \frac{-1}{R} \begin{cases} 0 & \text{FOR } n = 0, 1 \\ \sqrt{\frac{(n+2)(n+1)n(n-1)}{n-1}} & \text{FOR } n \geq 2 \end{cases}$$

• SPECTRAL EXPANSION OF KERNEL

$$K(\psi) \begin{Bmatrix} \cos 2\alpha \\ \sin 2\alpha \end{Bmatrix} = \sum_{n=2}^{\infty} \frac{(2n+1)}{(n-1)} P_n^2(\cos \psi) \begin{Bmatrix} \cos 2\alpha \\ \sin 2\alpha \end{Bmatrix}$$

Figure 3.3.1-3. Summary of Mathematical Relationships for the Horizontal Stress and Shear Gradient Integral Transformation.

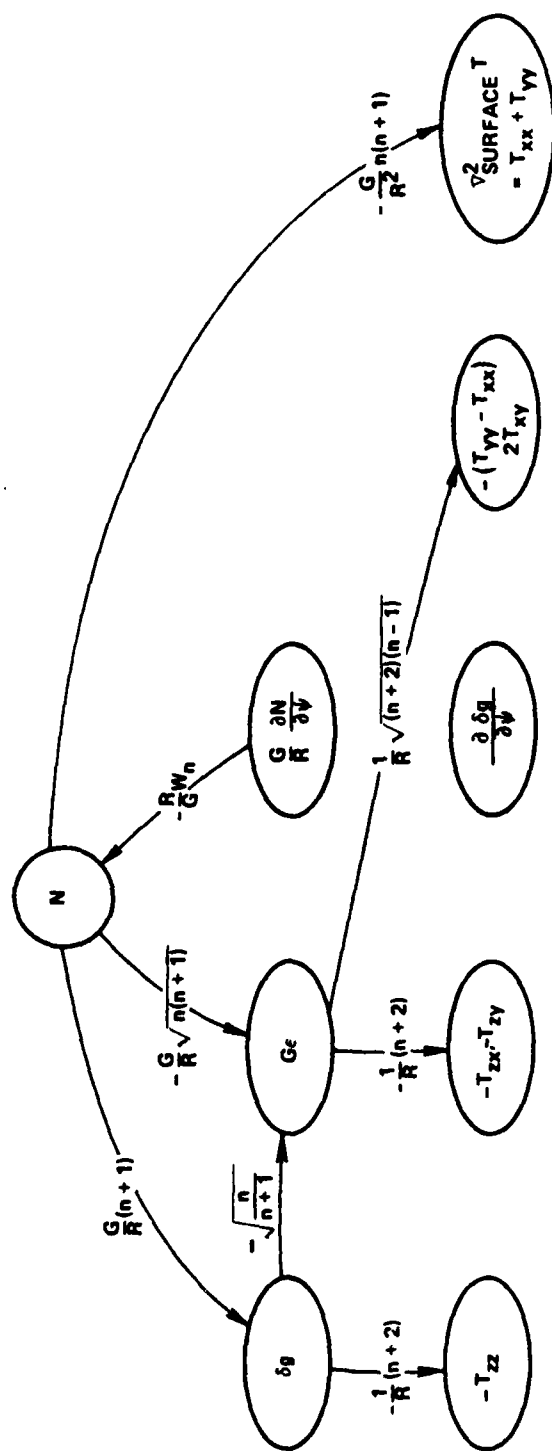


Figure 3.3.2-1. Flow Diagram of Spectra of Various Other Geodetic Transformations.

3.4 Transformations Involving the Outward Surface Partial Derivative

A number of transformations have appeared in the literature which have as input the outward surface partial derivative of various geodetic quantities from the point of evaluation. For example, Malkin's transformation converts the outward surface partial of the geoid height, usually denoted by $\partial N / \partial \psi$, into geoid height N .

These transformations have limited practical use due to the complicated nature of their input and its dependence on the point of evaluation. Nevertheless they are of theoretical interest and in this section they and their spectra will be examined briefly. It will turn out that their spectra all involve a sequence of numbers which had been studied by the English mathematician John Wallis (1616-1703) in his book "Arithmetica Infinitorum" which appeared in 1655. For this reason the author has called these numbers "Wallis coefficients" and denoted them by W_n . A relationship involving the even Wallis coefficients has been called the "Wallis formula" in Abramowitz and Stegun (1964).

3.4.1 The Outward Surface Partial Derivative - Malkin's and Molodenskii's Transformations

The geometry involved in the definition of the outward surface partial derivative is illustrated in Figure 3.4-1. The partial derivative is evaluated along the surface of the (unit) sphere in the radially outward direction from the point of evaluation (the origin of the ψ and α coordinate system). The outward surface partial derivative of the geoid height is equivalent to the component of the deflection of the vertical which lies in the outward direction. In the figure, the symbol ξ represents the vector vertical deflection at the generic point (ψ, α) , while its outward component is $\frac{1}{R} \frac{\partial N}{\partial \psi}$.

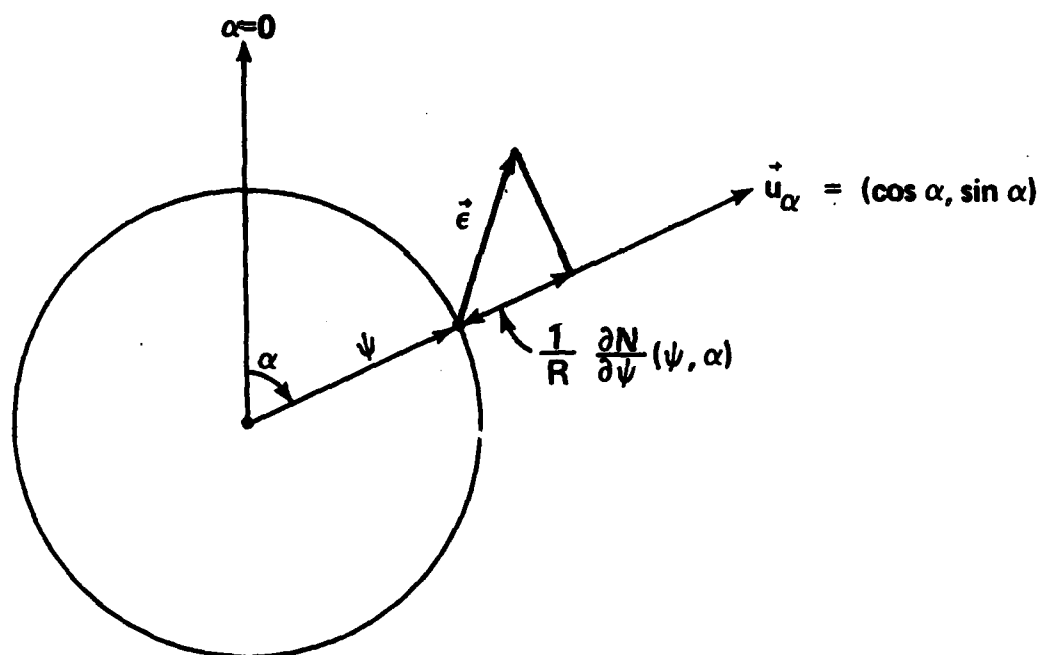
Malkin's transformation is the primary example of the use of outward surface partial derivative data. This transformation is isotropic and has $\partial N / \partial \psi$ as input and the geoid height N as output:

$$N = \iint (-\cot \frac{\psi}{2}) \frac{\partial N}{\partial \psi}(\psi, \alpha) \frac{d\sigma}{4\pi}$$

This was originally derived by Malkin (1933) and may also be found in Pick-Picha-Vyskocil (1973, pg. 245, eqn. 713).

The same transformation also converts the outward surface partial derivative of gravity anomalies into the gravity anomaly at the point of evaluation:

OUTWARD SURFACE PARTIAL DERIVATIVE



EXAMPLE:

$$\frac{\partial N}{\partial \psi}(\psi, \alpha) = R \vec{e}_r \cdot \vec{u}_\alpha = R(\xi \cos \alpha + \eta \sin \alpha)$$

Figure 3.4-1. Geometry of the Outward Surface Partial Derivative.

3.3.1.3 Horizontal Differential Stress and Horizontal Shear Gradients

The transformation by which the horizontal differential stress gradient and horizontal shear gradient are generated from the gravity anomalies is a third example of an anisotropic geodetic transformation and the first example of a second-order transformation.

The explicit form of the transformation may be obtained by differentiating the Vening-Meinesz' Integral with respect to the spherical radius ψ , evaluating the results along the azimuths $\alpha = 0^\circ$ or $\alpha = 90^\circ$, and calculating

$$-(T_{yy} - T_{xx}) = \frac{-G}{R} \left(\frac{\partial \eta}{\partial \psi} \Big|_{\alpha=90^\circ} - \frac{\partial \xi}{\partial \psi} \Big|_{\alpha=0^\circ} \right)$$

$$2T_{xy} = 2 \frac{G}{R} \left(\frac{\partial \xi}{\partial \psi} \Big|_{\alpha=90^\circ} \text{ or } \frac{\partial \eta}{\partial \psi} \Big|_{\alpha=0^\circ} \right)$$

The kernel of the transformation will be found to be [Malkin (1933, pg.56)]:

$$\frac{1}{R} \left(\frac{\partial^2 S(\psi)}{\partial \psi^2} - \cot \psi \frac{\partial S(\psi)}{\partial \psi} \right) \begin{Bmatrix} \cos 2\alpha \\ \sin 2\alpha \end{Bmatrix}$$

The easiest way to derive the spectrum of the transformation is to find the spectral expansion of the kernel directly and then identify the spectral coefficients in the expansion. By differentiating the spectral expansion of the Stokes' Integral kernel twice with respect to ψ ,

$$\left(\frac{\partial^2 S(\psi)}{\partial \psi^2} - \cot \psi \frac{\partial S(\psi)}{\partial \psi} \right) = \sum_{n=2}^{\infty} \frac{2n+1}{n-1} \left(\frac{\partial^2 P_n(\cos \psi)}{\partial \psi^2} - \cot \psi \frac{\partial P_n(\cos \psi)}{\partial \psi} \right)$$

and using the relation that

$$\frac{\partial^2 P_n(\cos \psi)}{\partial \psi^2} - \cot \psi \frac{\partial P_n(\cos \psi)}{\partial \psi} = P_n^2(\cos \psi),$$

it is seen that the kernel of the transformation has the expansion:

$$-\frac{1}{R} \left(\frac{\partial^2 S(\psi)}{\partial \psi^2} - \cot \psi \frac{\partial S(\psi)}{\partial \psi} \right) \begin{Bmatrix} \cos 2\alpha \\ \sin 2\alpha \end{Bmatrix} = -\frac{1}{R} \sum_{n=2}^{\infty} \frac{2n+1}{n-1} P_n^2(\cos \psi) \begin{Bmatrix} \cos 2\alpha \\ \sin 2\alpha \end{Bmatrix}$$

By comparing this result with the general kernel expansion formula, it is immediately deduced that the spectral coefficients are

$$\lambda_n^2 = -\frac{1}{R} \begin{cases} 0 & \text{for } n = 0, 1 \\ \frac{\sqrt{(n+2)(n+1)n(n-1)}}{n-1} & \text{for } n \geq 2 \end{cases}$$

The mathematical relations for this transformation are summarized in Figure 3.3.1-3.

3.3.2 Flow Diagram of Spectra

A flow diagram of the spectra of some of the anisotropic transformations discussed in the preceding sections is given in Figure 3.3.2-1. As in the previous flow diagrams, geodetic quantities of approximately equal "smoothness" are drawn on the same horizontal line.

- **TRANSFORMATION: MOLODENSKII #2**

INPUT: $\partial \Delta g / \partial \psi$

OUTPUT: Δg

- **EXPLICIT FORM**

$$\Delta g = \iint (-\cot \frac{\psi}{2}) \frac{\partial \Delta g}{\partial \psi} \frac{d\sigma}{4\pi}$$

- **EIGENVALUES**

$\lambda_n = -W_n$ WHERE W_n ARE THE WALLIS COEFFICIENTS

- **SPECTRAL EXPANSION OF KERNEL**

$$-\cot \frac{\psi}{2} = -\sum_{n=0}^{\infty} W_n (2n+1) P_n (\cos \psi)$$

Figure 3.4-3. Summary of Mathematical Relationships for the Second Molodenskii Integral Transformation.

in a rather tight manner from above and from below respectively. This may be seen numerically in Figure 3.4-4 of the next section. The sequence S_n is the set of reciprocals of the spectrum of the transformation which converts geoid height into deflections

$$\lambda_n^1 \left\{ \frac{N}{R} + \xi \text{ or } \eta \right\} = \sqrt{n(n+1)} = \frac{1}{S_n}$$

Hence the inverse transformation has the spectrum

$$\lambda_n \left\{ \xi \text{ or } \eta \rightarrow \frac{N}{R} \right\} = \frac{1}{\sqrt{n(n+1)}} = S_n$$

But the magnitudes of the spectrum of Malkin's transformation

$$\left| \lambda_n \left\{ -\cot \frac{\psi}{2} \right\} \right| = W_n$$

approximately equal S_n , implying that Malkin's transformation and the transformation converting deflections to geoid height are approximately the same. This result agrees with intuition since the input to Malkin's transformation is the outward deflection.

3.4.2 Mathematical Properties of the Wallis Coefficients

The even and odd Wallis coefficients have the closed-form expressions:*

$$W_n = \begin{cases} \left[\frac{\pi}{2} \left[\frac{1 \cdot 3 \cdot 5 \cdots (n-1)}{2 \cdot 4 \cdot 6 \cdots (n)} \right]^2 \right. & = \frac{\pi}{2} \left[\frac{(n-1)!!}{n!!} \right]^2 & \left[\begin{matrix} n \\ \text{EVEN} \end{matrix} \right] \\ \left. \frac{\pi}{2} \left[\frac{1 \cdot 3 \cdot 5 \cdots (n)}{2 \cdot 4 \cdot 6 \cdots (n+1)} \right]^2 \frac{n+1}{n} \right. & = \frac{\pi}{2} \left[\frac{n!!}{(n+1)!!} \right]^2 \frac{n+1}{n} & \left[\begin{matrix} n \\ \text{ODD} \end{matrix} \right] \end{cases}$$

where the double factorial indicates a factorial with alternate numbers deleted.

Using the binomial coefficient notation, the even and odd Wallis coefficients may also be expressed (elegantly!) as:

* Gradshteyn-Ryzhik (1965, pg. 822, equations 7.226.1 and 7.226.2)

$$W_n = \begin{cases} \frac{\pi}{2} \frac{1}{4^n} \begin{pmatrix} n \\ \frac{n}{2} \end{pmatrix} \begin{pmatrix} n \\ \frac{n}{2} \end{pmatrix} & [n \text{ even}] \\ \frac{\pi}{2} \frac{1}{4^n} \begin{pmatrix} n-1 \\ \frac{n-1}{2} \end{pmatrix} \begin{pmatrix} n+1 \\ \frac{n+1}{2} \end{pmatrix} & [n \text{ odd}] \end{cases}$$

Finally using Pochhammer's symbol

$$(a)_m = \frac{\Gamma(a+m)}{\Gamma(a)}$$

the even and odd Wallis coefficients have the representation:

$$W_{2m} = \frac{\pi}{2} \frac{\left[\begin{pmatrix} 1 \\ 2 \end{pmatrix}_m \begin{pmatrix} 1 \\ 2 \end{pmatrix}_m \right]}{m! m!} \quad [m = 0, 1, 2, \dots]$$

$$W_{2m+1} = \frac{\pi}{2} \frac{\left[\begin{pmatrix} 1 \\ 2 \end{pmatrix}_m \begin{pmatrix} 1 \\ 2 \end{pmatrix}_{m+1} \right]}{m! (m+1)!}$$

Here the index m has been used to emphasize the distinction between this form (where W_{2m} and W_{2m+1} are given) and the previous form (where W_n is given).

Explicit expressions and numerical values for the first six Wallis coefficients are presented in Figure 3.4-4. The circled numbers indicate by what fraction the current coefficient is multiplied to obtain the next coefficient.

Several integral expressions for the general Wallis coefficients W_n were given in the last section. Several more for the even and odd coefficients are (Erdélyi, 1954, Vol. II, pg. 276):

$$W_{2m} = \int_{-1}^{+1} \frac{1}{\sqrt{1-x^2}} P_{2m}(x) \frac{dx}{2} = \int_0^\pi P_{2m}(\cos \psi) \frac{d\psi}{2}$$

$$W_{2m+1} = \int_{-1}^{+1} \frac{x}{\sqrt{1-x^2}} P_{2m+1}(x) \frac{dx}{2} = \int_0^\pi \cos \psi P_{2m+1}(\cos \psi) \frac{d\psi}{2}$$

n	W_n (n even)	W_n (n odd)	$\frac{1}{\sqrt{n(n+1)}}$
0	$\frac{\pi}{2} = 1.570796$	$\frac{1}{2}$	∞
1	$\frac{1}{2}$	$\frac{\pi}{2} = 1.570796$	0.707107
2	$\frac{\pi}{2} \left(\frac{1}{2}\right)^2 = 0.392699$	$\frac{3}{4}$	0.408248
3	$\frac{3}{4}$	$\frac{\pi}{2} \left(\frac{1}{2}\right)^2 = 0.392699$	0.288675
4	$\frac{\pi}{2} \left(\frac{1 \cdot 3}{2 \cdot 4}\right)^2 = 0.220893$	$\frac{5}{6}$	0.223607
5	$\frac{5}{6}$	$\frac{\pi}{2} \left(\frac{1 \cdot 3}{2 \cdot 4}\right)^2 = 0.220893$	0.182574
6	$\frac{\pi}{2} \left(\frac{1 \cdot 3 \cdot 5}{2 \cdot 4 \cdot 6}\right)^2 = 0.153398$	$\frac{7}{8}$	0.154303

Figure 3.4-4. Values of Some Wallis Coefficients.

The even Wallis coefficients have a number of special properties.
In particular*

$$\begin{aligned}\sqrt{\frac{2}{\pi}} w_{2m} &= (-1)^m P_{2m}(0) = (-1)^m \frac{P'_{2m+1}(0)}{2m+1} \\ &= \frac{2}{\pi} \int_0^{\pi/2} \sin^{2m} x dx = \frac{2}{\pi} \int_0^{\pi/2} \cos^{2m} x dx\end{aligned}$$

And they are closely related to Erdélyi's "g_n" quantities

$$\frac{2}{\pi} w_{2m} = (g_m)^2$$

which figure in trigonometric expansions of the Legendre polynomials:**

$$P_n(\cos \psi) = \sum_{k=0}^n g_k g_{n-k} \cos(n-2k)\psi$$

The author is not yet aware of any analogs of the above properties for the odd Wallis coefficients.

From the integral expression previously stated and the orthogonality of the Legendre polynomials, the following expansions may also be deduced:

$$\frac{1}{\sqrt{1-x^2}} = \sum_{k=0}^{\infty} \{2(2k)+1\} w_{2k} P_{2k}(x)$$

$$\frac{x}{\sqrt{1-x^2}} = \sum_{k=0}^{\infty} \{2(2k+1)+1\} w_{2k+1} P_{2k+1}(x)$$

$$\frac{1+x}{\sqrt{1-x^2}} = \frac{\sqrt{1-x^2}}{1-x} = \sqrt{\frac{1+x}{1-x}} = \sum_{k=0}^{\infty} (2k+1) w_k P_k(x)$$

$$\text{ARCSIN } x = \sum_{k=0}^{\infty} w_{2k} \{P_{2k+1}(x) - P_{2k-1}(x)\}$$

* Erdélyi (1953, Vol. II, pg. 180); Dwight (1961, pg. 215).

** Erdélyi, loc. cit.; also see Frank and von Mises (1961, pg. 434ff).

The relationship of the Wallis coefficients W_n to coefficients S_n of the sequence

$$S_n = \frac{1}{\sqrt{n(n+1)}}$$

will now be described. It is easily deduced that:

$$\sqrt{\underbrace{\left(\frac{W_n}{W_{n-2}}\right)}_{n \text{ EVEN}} \underbrace{\left(\frac{W_n}{W_{n-2}}\right)}_{n \text{ ODD}}} = \sqrt{\frac{n-2}{n} \frac{n-1}{n+1}} = \frac{S_n}{S_{n-2}}$$

This may be interpreted in words as: the factor by which the harmonic mean of odd and even Wallis coefficients decreases over a double step is equal to the factor by which the coefficients in the sequence $1/\sqrt{n(n+1)}$ decrease over the same double step. Less precisely but more intuitively, this may be rephrased as: the sequences W_n and S_n are decreasing at the same rate in the harmonic mean over double steps.

It is known* that

$$\sqrt{W_{2m}} \sim \frac{1}{\sqrt{2m}} \left[1 - \frac{1}{4(2m)} + \frac{1}{32(2m)^2} - \dots \right]$$

Hence, for even n

$$W_n \sim \frac{1}{n} \left[1 - \frac{1}{2n} + \frac{1}{8n^2} - \dots \right]$$

From this it is immediately deduced that

$$\frac{\pi}{2} = \frac{2 \cdot 2 \cdot 4 \cdot 4 \cdot 6 \cdot 6 \cdot 8 \cdot 8 \cdot \dots}{1 \cdot 3 \cdot 3 \cdot 5 \cdot 5 \cdot 7 \cdot 7 \cdot 9 \cdot \dots}$$

which was stated by Wallis in 1655.

* Abramowitz-Stegun (1965, pg. 258, eqn. 6.1.49)

SECTION 4

SPECTRAL THEORY OF THE DISCRETE SUMMATION TRANSFORMATIONS OF GEODESY

4.1 Introduction

In the previous chapter, the spectral theory of the theoretical "continuous" integral transformations of geodesy has been described. In the present chapter, the approximate "discrete" summation transformations of geodesy and their spectra will be examined. Here the term "discrete" implies that the input data to the transformation consists only of a finite set of individual pieces of data over which the summation is made, and that these data are not continuously or densely distributed.

The computer algorithms for the actual evaluation (strictly, approximation) of the Stokes' and Vening-Meinesz' Integrals over mean gravity anomalies are examples of discrete summation transformations.

The conversion of a theoretical "continuous" integral transformation into a discrete summation transformation will be called "discretization". Discretization always introduces some error since some form of approximation must be made to convert the rigorously correct integral expression into a practically implementable summation. If the discretization is made "judiciously", the error introduced thereby will be negligible. One of the main purposes of this entire study is to develop a mathematical theory by which judicious discretizations can be derived from basic principles for any spherical geodetic transformation.

In the present chapter, the spectral theory of discretized geodetic transformations will be developed. Mathematical expressions for the spectra of such transformations will be derived. As may be expected, it will turn out that the numerical values of such spectra will approximate, but not exactly equal, those of the spectra of the corresponding theoretical integral transformation. The difference between the true

and approximate spectra will provide a means of determining the global rms error due to discretization, and of calculating improved discrete summation approximations for which the discretization error is smaller. This will be accomplished by making the approximate spectrum agree as well as possible with the true spectrum, which is equivalent to making the discrete summation transformation agree as well as possible with the true integral transformation in the frequency domain. In this way, even though the transformations may have very different representations in the spatial domain, they will have approximately the same effect in the frequency domain, attenuating and amplifying the appropriate frequencies present in the input data while converting them into output data.

4.2 Bull's-Eye Templates and Discrete Summation Transformations

Let a point be selected on the sphere at which it is desired to calculate the output of a transformation. This point will be called the point of evaluation. Let the surface of the sphere then be partitioned into rings centered around the point of evaluation, and let each ring be further partitioned into compartments. If the point of evaluation were the North Pole of the sphere, then the compartments would be blocks bounded by parallels of latitude and meridians of longitude. In the general case however, the boundaries of the compartments will be lines on the sphere for which spherical radius ψ and the local azimuth α from the point of evaluation assume various constant values ψ_i and α_{ij} respectively. The index "i" will be associated exclusively with spherical radii or spherical rings, and the index "j" with spherical azimuths or spherical sectors. The double indexing of the compartment boundary azimuths α_{ij} will permit full generality in allowing different numbers of compartments in different rings.

In the neighborhood of the point of evaluation, the partition of the spherical surface into rings and compartments resembles a bull's-eye target, as shown in Figure 4.2-1. Hence this type of (spherical) partition will be called a bull's-eye template.

The values of the compartment boundary parameters for a number of bull's-eye templates will be given in Chapter 5.

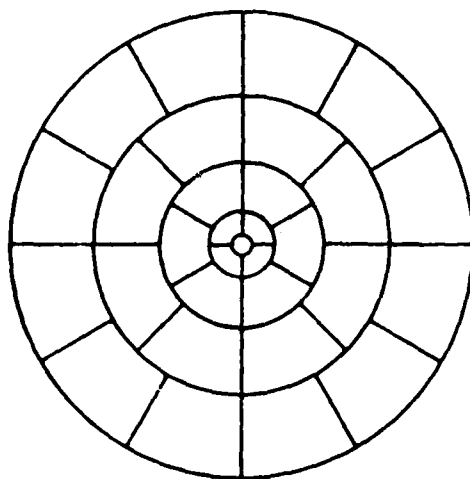


Figure 4.2-1. Bull's-Eye Template.

The following conventions on the spherical radii and azimuth numbering and the spherical ring and compartment numbering will be used in this document:

- a) The initial spherical radius will be represented by ψ_0 . When there is no inner zone, such as in a Stokes' summation, ψ_0 equals zero and is equivalent to the point of evaluation. When there is an inner zone, such as in a Vening-Meinesz' summation, ψ_0 is the truncation radius in accordance with traditional geodetic symbology (Heiskanen-Moritz, 1967, pp. 121 and 259).
- b) The ring bounded by the inner radius ψ_0 and the outer radius ψ_1 will be indexed as ring number 1, and similarly for successive rings. Hence the ring number index will always equal the index of the outer spherical boundary radius of the ring, and the number of rings equals the maximum value of the spherical radius index, although physically there is one more spherical radius, namely ψ_0 .

- c) The initial spherical azimuth α_{i0} of each ring equals zero, and the final spherical azimuth $\alpha_{ij_{\max}}$ of each ring equals 2π or 360° .
- d) The compartment bounded by the lower azimuth α_{i0} and the upper azimuth α_{i1} will be indexed as compartment $(i,1)$ and similarly for successive compartments.

A discrete summation geodetic transformation over a bull's-eye template has the explicit form

$$f_{\text{OUT}} = \sum_i \sum_j w_{ij} f_{ij}$$

where

- f_{ij} is the value of the input geodetic quantity in the (i,j) th compartment,
- w_{ij} is the transformation weight associated with the (i,j) th compartment,
- f_{OUT} is the output geodetic quantity at the template origin (point of evaluation).

The summation is to be carried out conceptually over a set of indices corresponding to compartments which cover the entire sphere. In practice, some of the weights w_{ij} may be zero and can be omitted from the computed implementation of the summation.

Such a transformation is a linear shift-invariant transformation, i.e., a digital filter. The shift invariance property results from the fact that the template and its associated weights shift without change when the point of evaluation is shifted.

Discrete summation transformations may be derived from continuous integral transformations by choosing the kernel $K(\psi, \alpha)$:

- constant in each compartment, for compartmental averaging of the point input data to the integral transformation,
- with a Dirac Delta spike in each compartment for direct sampling of point input data to the integral transformation,
- with other mathematical properties, for other types of compartmental preprocessing of the point input data to the integral transformation.

In most of what follows the kernel $K(\psi, \alpha)$ will be chosen constant in each compartment in order to obtain transformations whose inputs are mean geodetic quantities.

4.3 Stokes' Discrete Summation Transformations

As indicated in the preceeding section, discrete summation transformations may be derived from their continuous integral counterparts in several ways. Moreover even when the kernel is held constant in each compartment, the value to which the kernel is set in each compartment may itself be selected in many ways. Two ways are presented in some detail in the following paragraphs, followed by a short description of choosing the kernel as a Dirac Delta spike.

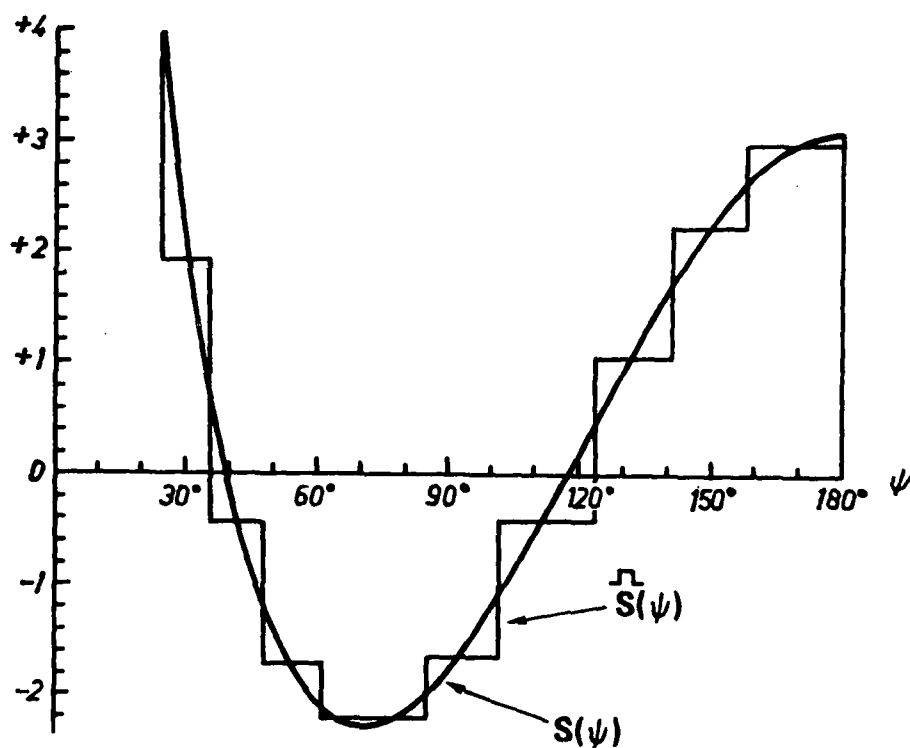
4.3.1 Midpoint Weighting

Let the Stokes' midpoint averaging function $\bar{S}(\psi)$ be the staircase-like (piecewise constant) function which assumes the constant value over each ring of the actual Stokes' function evaluated at the mid-point of that ring measured in spherical distance. Thus,

$$\bar{S}(\psi) = \begin{cases} S\left(\frac{\psi_0 + \psi_1}{2}\right) & \text{for } \psi_0 \leq \psi < \psi_1 \\ S\left(\frac{\psi_1 + \psi_2}{2}\right) & \text{for } \psi_1 \leq \psi < \psi_2 \\ S\left(\frac{\psi_2 + \psi_3}{2}\right) & \text{for } \psi_2 \leq \psi < \psi_3 \\ \text{etc.} \end{cases}$$

The value of the function $\bar{S}(\psi)$ at any particular spherical radius ψ will of course depend in general upon the choice of the spherical ring radii ψ_i ; however, these are assumed to be chosen a priori (or are assumed to be parameters) so the dependence is not explicitly shown in the notation. A typical graph of $\bar{S}(\psi)$ is provided in Figure 4.3.1-1 for a particular choice of spherical ring radii. It will be noticed* that the smooth curve of the Stokes' function $S(\psi)$ passes through the midpoint

*In the figure there are actually two rings between $\psi \approx 62^\circ$ and $\psi \approx 85^\circ$ although it appears that these angles subtend only one ring. The intermediate spherical radius separating these rings falls at $\psi \approx 73^\circ$. To the precision shown in the graph the Stokes' function has the same mid-point value in each of these rings.



$\tilde{S}(\psi)$: STOKES' MIDPOINT AVERAGING FUNCTION
 $S(\psi)$: CLASSICAL STOKES' FUNCTION

Figure 4.3.1-1. Stokes' Midpoint Averaging Function $\tilde{S}(\psi)$.

of each constant "piece" of the Stokes' midpoint averaging function $\bar{S}(\psi)$. This is precisely this function's characterizing property (since the graph is plotted uniformly in the variable ψ).

When the Stokes' midpoint averaging function $\bar{S}(\psi)$ is substituted for the classical Stokes' function $S(\psi)$ in the explicit integral form of the Stokes transformation, the double integral on the (densely-distributed) point gravity anomalies $\Delta g(\psi, \alpha)$ simplifies to a double summation on a finite number of discrete mean gravity anomalies $\bar{\Delta g}_{ij}$

$$N = \frac{R}{G} \iint \bar{S}(\psi) \Delta g(\psi, \alpha) \frac{d\sigma}{4\pi} = \frac{R}{G} \sum_i s\left(\frac{\psi_{i-1} + \psi_i}{2}\right) \sum_j \frac{A_{ij}}{4\pi} \bar{\Delta g}_{ij}$$

where A_{ij} is the surface area of the (i,j)th compartment. This is precisely the formula sought.

Hence the digital filter representation of this transformation may be written

$$N = \frac{R}{G} \sum_i \sum_j \bar{w}_{ij} \bar{\Delta g}_{ij}$$

where the weights are

$$\bar{w}_{ij} = s\left(\frac{\psi_{i-1} + \psi_i}{2}\right) \frac{A_{ij}}{4\pi}$$

The spectrum of this transformation may also easily be derived by again substituting $\bar{S}(\psi)$ for $S(\psi)$, this time in the spectral equation which again reduces to a summation:

$$\lambda_n \{ \bar{S}: \bar{\Delta g} \rightarrow N \} = \frac{R}{G} \int_{-1}^{+1} \bar{S}(\cos \psi) P_n(\cos \psi) \frac{d(\cos \psi)}{2} = \frac{R}{G} \sum_i \left[s\left(\frac{\psi_{i-1} + \psi_i}{2}\right) \int_{x_i}^{x_{i-1}} P_n(x) \frac{dx}{2} \right]$$

where $x \equiv \cos \psi$, $x_i \equiv \cos \psi_i$

The partial derivatives $\partial \lambda_n / \partial x_k$ of the elements of the spectrum with respect to each of the template spherical ring boundary radii (or rather with respect to their cosines) may also be derived. These quantities will be necessary in the implementation of at least squares optimization algorithm which will "adjust" the ring radii to minimize the total rms

error between the spectrum of the Stokes' integral transformation and that of the discrete summation approximation. The partial derivatives $\partial \lambda_n / \partial x_k$ are obtained directly by differentiating the equation for the spectrum, yielding

$$\frac{\partial \lambda_n \{\bar{S}\}}{\partial x_k} = \frac{R}{2G} \left[\frac{\partial S(x)}{\partial x} \right]_{\left(\frac{x_k + x_{k-1}}{2}\right)}^{x_k} \int_{x_{k-1}}^{x_k} P_n(x) \frac{dx}{2} + \frac{\partial S(x)}{\partial x} \left[\left(\frac{x_{k+1} + x_k}{2}\right) \right]^{x_{k+1}} \int_{x_k}^{x_{k+1}} P_n(x) \frac{dx}{2} + S\left(\frac{x_k + x_{k-1}}{2}\right) P_n(x_k) - S\left(\frac{x_{k+1} + x_k}{2}\right) P_n(x_k) \right]$$

Since the initial radius ψ_0 and the final radius $\psi_{i_{\max}}$ are not adjustable, the index k assumes values only between (and including) one and $(i_{\max} - 1)$.

4.3.2 Integrated-Mean Weighting

Let the Stokes' Integrated-Mean Averaging Function $\hat{S}(\psi)$ be the staircase-like (piecewise constant) function which assumes the constant value over each ring of the integrated mean value of the Stokes' function on that ring. Thus,

$$\hat{S}(\psi) = \begin{cases} \frac{1}{\cos \psi_0 - \cos \psi_1} \int_{\cos \psi_1}^{\cos \psi_0} S(\cos \psi) d(\cos \psi) & \text{for } \psi_0 \leq \psi < \psi_1 \\ \frac{1}{\cos \psi_1 - \cos \psi_2} \int_{\cos \psi_2}^{\cos \psi_1} S(\cos \psi) d(\cos \psi) & \text{for } \psi_1 \leq \psi < \psi_2 \\ \text{etc.} \end{cases}$$

For notational simplification, the integrated-mean values will be denoted by the symbols $\hat{S}_{(i)}$

$$\hat{S}(\psi) = \begin{cases} \hat{S}_{(1)} & \text{for } \psi_0 \leq \psi < \psi_1 \\ \hat{S}_{(2)} & \text{for } \psi_1 \leq \psi < \psi_2 \\ \text{etc.} \end{cases}$$

The grave accent symbol is used in the notation to evoke an average, since the traditional average symbol (a superscript bar) has another meaning in geodesy when used with a kernel, namely truncation of the kernel at a specified spherical radius.

Values of the $\hat{S}_{(i)}$ may be easily calculated from the analytic expression for the indefinite integral of the Stokes' function:

$$-\int S(\psi) \sin \psi \, d\psi = -4t + 5t^2 + 6t^3 - 7t^4 + 6t^2(1-t^2) \ln t(1+t)$$

where $t = \sin \frac{\psi}{2}$. See Heiskanen-Moritz (1967, pg. 263, equation for Q_0). The value of the function $\hat{S}(\psi)$ at any particular spherical radius ψ will of course depend in general upon the choice of the spherical ring radii ψ_i ; however, these are assumed to be chosen a priori, so the parametric dependence is not explicitly shown in the notation. A typical graph of $\hat{S}(\psi)$ is provided in Figure 4.3.2-1 for a particular choice of spherical ring boundary radii. The shaded region in this figure indicates the area under the Stokes' function curve between two ring radii. The constant value of Stokes' integrated-mean averaging function between these same ring radii is calculated so that the rectangular area under its value (+2 in the figure) is equal to the shaded area.

When the Stokes' integrated-mean averaging function $\hat{S}(\psi)$ is substituted for the classical Stokes' function in the explicit integral form of the Stokes' transformation, the double integral on the (densely-distributed) point gravity anomalies $\Delta g(\psi, \alpha)$ simplifies to a double summation on a finite number of mean gravity anomalies $\overline{\Delta g}_{ij}$:

$$N = \frac{R}{G} \iint \hat{S}(\psi) \Delta g(\psi, \alpha) \frac{d\sigma}{4\pi} = \frac{R}{G} \sum_i \hat{S}_{(i)} \sum_j \frac{A_{ij}}{4\pi} \overline{\Delta g}_{ij}$$

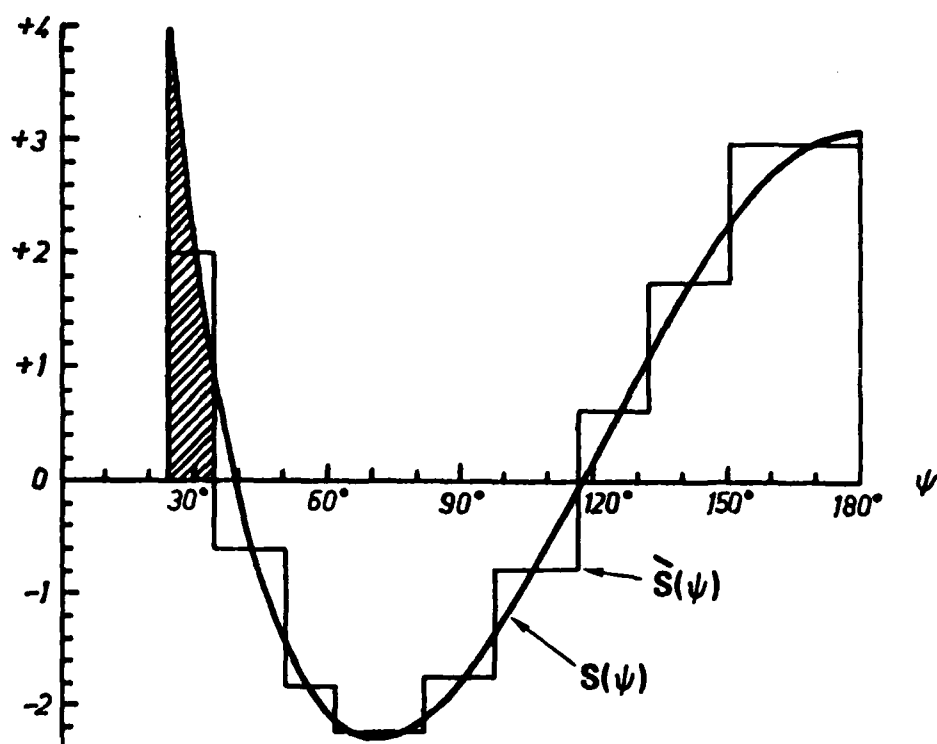
where A_{ij} is the surface area of the (i,j)th compartment on the unit sphere.

Hence, the digital filter representation of this transformation may be written:

$$N = \frac{R}{G} \sum_i \sum_j \hat{w}_{ij} \overline{\Delta g}_{ij}$$

where the weights are

$$\hat{w}_{ij} = \hat{S}_{(i)} \frac{A_{ij}}{4\pi}$$



$\tilde{S}(\psi)$: STOKES' INTEGRATED-MEAN AVERAGING FUNCTION
 $S(\psi)$: CLASSICAL STOKES' FUNCTION

Figure 4.3.2-1. Stokes' Integrated-Mean Averaging Function $\tilde{S}(\psi)$.

The spectrum of this transformation may also be easily derived by again substituting the $\hat{S}(\psi)$ for $S(\psi)$, this time in the spectral equation which again reduces to a summation:

$$\lambda_n\{\hat{S}; \overline{\Delta g} + N\} = \frac{R}{G} \int_{-1}^{+1} \hat{S}(\cos \psi) P_n(\cos \psi) \frac{d(\cos \psi)}{2} = \frac{R}{G} \sum_i \left[\hat{S}_{(i)} \int_{x_i}^{x_{i+1}} P_n(x) \frac{dx}{2} \right]$$

where $x \equiv \cos \psi$ and $x_i = \cos \psi_i$.

The partial derivatives $\partial \lambda_n / \partial x_k$ of the elements of the spectrum with respect to each spherical ring boundary radius of the template (or rather with respect to the consines thereof) may be obtained by differentiating the equation for the spectrum, yielding after some manipulation:

$$\frac{\partial \lambda_n\{\hat{S}; \overline{\Delta g} + N\}}{\partial x_k} = \frac{R}{2G} \left[\hat{S}_{(k)} \hat{P}_{n(k)} - \hat{S}_{(k+1)} \hat{P}_{n(k+1)} + S(x_k) \left[-\hat{P}_{n(k)} + \hat{P}_{n(k+1)} \right] + P_n(x_k) \left[-\hat{S}_{(k)} + \hat{S}_{(k+1)} \right] \right]$$

where

$$\hat{P}_{n(k)} = \frac{1}{x_{k+1} - x_k} \int_{x_k}^{x_{k+1}} P_n(x) dx$$

is the integrated-mean value of the Legendre polynomial over the k^{th} ring. The seemingly unsymmetric indices (k) and $(k+1)$ in the partial derivative expression for $\partial \lambda_n / \partial x_k$ are actually symmetric because they refer to the rings which are separated by the spherical radius ψ_k . The ring and radius indexing convention causes this apparent asymmetry.

The analytic partial derivative expression is extremely simple to implement in a computer algorithm because all of the quantities which enter into it have already been calculated for the evaluation of the spectrum itself with the exception of $S(x_k)$ and $P_n(x_k)$ which are relatively easy to obtain. Hence only a few multiplications and additions are necessary for the computation of the analytic partial. This fortuitous situation is in contrast to most analytic partial derivative evaluations which generally require more computational expense than the evaluation of their primitive. In the present case, the situation results from the use of the integrated-mean, so that higher derivatives do not occur in the partial expression, because of the a priori integral.

4.3.3 Dirac Delta Weighting

Let the Stokes' comb function $\overline{S}(\psi)$ be defined to be the comb-like function which consists of a linear combination of a finite set of Dirac Delta functions weighted according to the value of the Stokes' function at each spike.

$$\overline{S}(\psi) = \sum_i S(\psi_i^{\text{spike}}) \delta(\cos \psi - \cos \psi_i^{\text{spike}})$$

The spherical radii at which the spikes are located will be denoted by ψ_i^{spike} . The Dirac Delta function $\delta(x)$ has the property that it is zero everywhere except when the argument is zero, in which case the function is infinite in such a way that its integral is unity:

$$\int_{-1}^{+1} \delta(x) dx = 1$$

A graph of a typical Stokes' comb function is given in Figure 4.3.3-1.

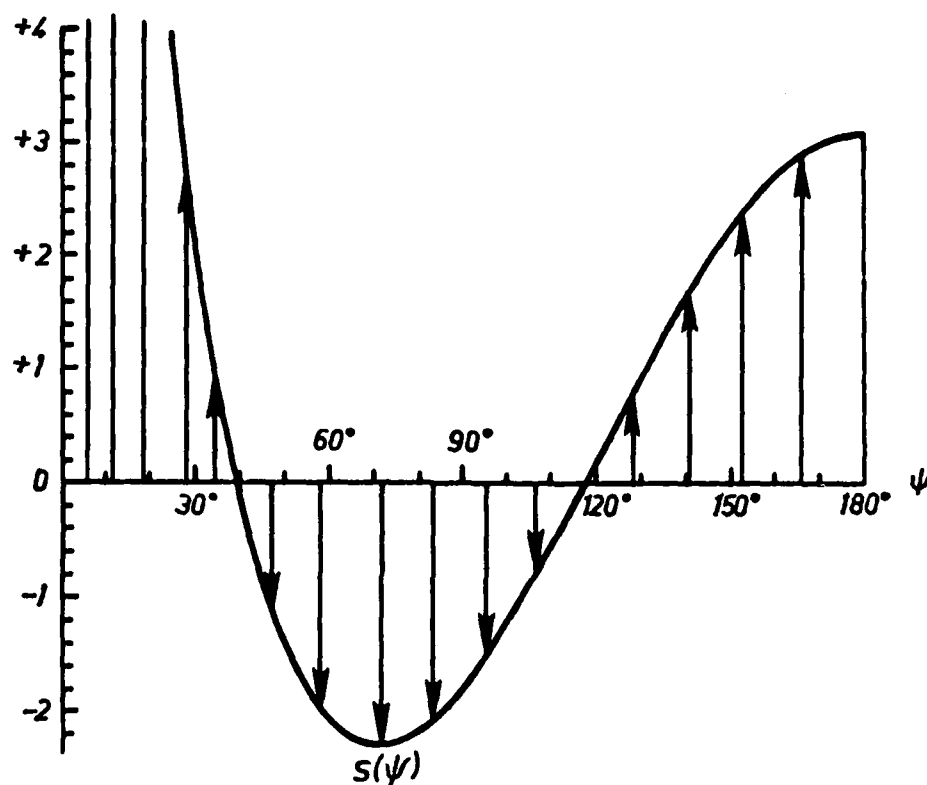
When the Stokes' comb function $\overline{S}(\psi)$ is substituted for the classical Stokes' function $S(\psi)$ in the explicit integral form of the Stokes' transformation the double integral on the densely distributed point gravity anomalies reduces to a summation on the arc-average gravity anomalies $\Delta \widehat{g}_i$ around each spike radius ψ_i^{spike} :

$$N = \frac{R}{G} \iint \overline{S}(\psi) \Delta g(\psi, \alpha) \frac{d\sigma}{4\pi} = \frac{R}{G} \sum_i S(\psi_i^{\text{spike}}) \frac{1}{P} \Delta \widehat{g}_i$$

where P is the total number of spikes. The factor $(1/P)$ plays the same role in this formula as the factor $(A_{ij}/4\pi)$ plays in the previous formulae, namely as the ratio of the weight (area) of current compartment or point to the weight of all compartments or points (before the Stokes' function weighting is applied).

Hence, the digital filter representation of this transformation may be written:

$$N = \frac{R}{G} \sum_i \overline{w}_{ij} \Delta \widehat{g}_i$$



$\overline{S}(\psi)$: STOKES' COMB FUNCTION, INDICATED BY THE VERTICAL ARROWS WHOSE VALUES ARE ACTUALLY INFINITE BUT WHOSE RELATIVE WEIGHTING IS SHOWN BY THEIR RELATIVE HEIGHT.

$S(\psi)$: CLASSICAL STOKES' FUNCTION, INDICATED BY THE SMOOTH CURVE.

Figure 4.3.3-1. Stokes' Comb Function $\overline{S}(\psi)$.

where the weights are

$$\bar{w}_{ij} = S(\psi_i^{\text{spike}}) \frac{1}{P}.$$

The spectrum of this transformation may also be derived:

$$\begin{aligned} \lambda_n \{ \bar{S}; \Delta g + N \} &= \frac{R}{G} \int_{-1}^{+1} \bar{S}(\cos \psi) P_n(\cos \psi) \frac{d(\cos \psi)}{2} \\ &= \frac{R}{G} \frac{1}{2P} \sum_i S(\psi_i^{\text{spike}}) P_n(\cos \psi_i^{\text{spike}}) \end{aligned}$$

making use of the property of the Dirac Delta function. When using this equation to evaluate the spectrum, care should be taken that a sufficient number of spikes are chosen in a well-distributed manner so that a sufficient number of data points enter into the computation. Otherwise aliasing of the spectrum may result from undersampling. This problem is well-known to workers in the field of sampled-data processing. It will not be dealt with here since the input of mean gravity anomalies rather than arc gravity anomalies is more common in geodesy. This example is provided only to show that the spectral theory of discrete summation transformations can include summation over arc anomalies and even point anomalies (by an obvious generalization).

4.3.4 Summary of Discrete Stokes' Transformations

A summary of the mathematical relationships for the various discrete Stokes' summation transformations is given in Figures 4.3.4-1 through 4.3.4-3.

- **TRANSFORMATION: DISCRETE STOKES' SUMMATION
USING MID-POINT STOKES' WEIGHTING**

Input: $\bar{\Delta g}_{ij}$ (mean gravity anomaly for each compartment)
Output: N (geoid height)

- **EXPLICIT FORM**

$$N = \frac{R}{G} \int \int \bar{S}(\psi) \Delta g(\psi, \alpha) \frac{d\sigma}{4\pi} = \frac{R}{G} \sum_i S(\psi_i^{\text{mid}}) \sum_j \frac{\text{AREA}_{ij}}{4\pi} \bar{\Delta g}_{ij}$$

$$N = \frac{R}{G} \sum_i \sum_j \bar{w}_{ij} \bar{\Delta g}_{ij} \quad \text{where} \quad \bar{w}_{ij} = S(\psi_i^{\text{mid}}) \frac{\text{AREA}_{ij}}{4\pi}$$

- **EIGENVALUES**

$$\begin{aligned} \lambda_n &= \frac{R}{G} \int_{-1}^{+1} \bar{S}(\cos \psi) P_n(\cos \psi) \frac{d(\cos \psi)}{2} \\ &= \frac{1}{2} \frac{R}{G} \sum_i \left[S(\psi_i^{\text{mid}}) \int_{\cos \psi_i}^{\cos \psi_{i-1}} P_n(t) dt \right] \end{aligned}$$

Figure 4.3.4-1. Summary of Relationships for the Discrete Stokes' Summation Transformation Using Midpoint Weighting.

- **TRANSFORMATION: DISCRETE STOKES' SUMMATION
USING INTEGRATED-MEAN WEIGHTING**

Input: $\bar{\Delta g}_{ij}$ (mean gravity anomaly for each compartment)
Output: N (geoid height)

- **EXPLICIT FORM**

$$N = \frac{R}{G} \iint \tilde{S}(\psi) \Delta g(\psi, \alpha) \frac{d\sigma}{4\pi} = \frac{R}{G} \sum_i \tilde{S}_{(i)} \sum_j \frac{\text{AREA}_{ij}}{4\pi} \bar{\Delta g}_{ij}$$

$$N = \frac{R}{G} \sum_i \sum_j \tilde{w}_{ij} \bar{\Delta g}_{ij} \quad \text{where } \tilde{w}_{ij} = \tilde{S}_{(i)} \frac{\text{AREA}_{ij}}{4\pi}$$

- **EIGENVALUES**

$$\begin{aligned} \lambda_n &= \frac{R}{G} \int_{-1}^{+1} \tilde{S}(\cos \psi) P_n(\cos \psi) \frac{d(\cos \psi)}{2} \\ &= \frac{1}{2} \frac{R}{G} \sum_i \left[\tilde{S}_{(i)} \int_{\cos \psi_i}^{\cos \psi_{i-1}} P_n(t) dt \right] \end{aligned}$$

Figure 4.3.4-2. Summary of Relationships for the Discrete Stokes' Summation Using Integrated-Mean Weighting.

- **TRANSFORMATION: DISCRETE STOKES' SUMMATION
ON ARC GRAVITY ANOMALIES**

Input: Δg_i (arc gravity anomalies)

Output: N (geoid height)

- **EXPLICIT FORM**

$$N = \frac{R}{G} \iint \bar{S}(\psi) \Delta g(\psi, \alpha) \frac{d\sigma}{4\pi} = \frac{R}{G} \sum_i S(\psi_i^{\text{spike}}) \frac{1}{P} \Delta g_i$$

$$N = \frac{R}{G} \sum_i \bar{w}_{ij} \Delta g_i \quad \text{where } \bar{w}_{ij} = S(\psi_i^{\text{spike}}) \frac{1}{P}$$

- **EIGENVALUES**

$$\lambda_n = \frac{R}{G} \int_{-1}^{+1} \bar{S}(\psi) P_n(\cos\psi) \frac{d(\cos\psi)}{2}$$

$$= \frac{1}{2P} \frac{R}{G} \sum_i S(\psi_i^{\text{spike}}) P_n(\cos\psi_i^{\text{spike}})$$

where P
denotes
total number
of spikes

BEWARE OF ALIASING INTRODUCED BY UNDERSAMPLING

Figure 4.3.4-3. Summary of Relationships for the Discrete Stokes' Summation Transformation on Arc Gravity Anomalies.

4.4 Vening-Meinesz' Discrete Summation Transformations

Discrete summation approximations to the Vening-Meinesz Integral will now be derived which will transform mean gravity anomalies over compartments into the two horizontal gravity disturbance components or equivalently the two deflections of the vertical. Also the spectra corresponding to these summations will be derived. The method used for the derivations will be to select judiciously chosen approximations to the kernel of the Vening-Meinesz' Integral which will reduce the integral to a summation on mean gravity anomalies. The Vening-Meinesz' kernel consists of a spherical radial portion and an azimuthal portion:

$$\underline{K}(\psi, \alpha) = \text{VM}(\psi) \begin{Bmatrix} \cos \alpha \\ \sin \alpha \end{Bmatrix}$$

Approximations to each of these portions will be required. Two such judiciously chosen approximations are presented.

4.4.1 Midpoint Weighting

Let the Vening-Meinesz' midpoint averaging function $\overline{\text{VM}}(\psi)$ be the staircase-like (piecewise constant) function which assumes the constant value VM_i over the i^{th} ring of the classical Vening-Meinesz' function evaluated at the midpoint of that ring ψ_i^{MID} measured in spherical distance ψ between the inner and outer spherical ring boundaries. Thus

$$\overline{\text{VM}}(\psi) = \begin{cases} \text{VM}(\psi_1^{\text{MID}}) & \text{for } \psi_0 < \psi < \psi_1 \\ \text{VM}(\psi_2^{\text{MID}}) & \text{for } \psi_1 < \psi < \psi_2 \\ \text{etc.} \end{cases}$$

where $\psi_i^{\text{MID}} = (\psi_{i-1} + \psi_i)/2$ following the convention that the index of a ring or the midpoint ψ_i^{MID} of the same ring are the same as the index of the outer ring boundary. Thus

$$\overline{\text{VM}}(\psi) = \begin{cases} \overline{\text{VM}}_1 & \text{for } \psi_0 < \psi < \psi_1 \\ \overline{\text{VM}}_2 & \text{for } \psi_1 < \psi < \psi_2 \\ \text{etc.} \end{cases}$$

As described in the discrete Stokes' summation sections, the midpoint averaging functions depend not only upon ψ but also upon the underlying spherical ring radii boundaries of the template, although the dependence is not explicitly indicated in the notation.

A graph of a typical Vening-Meinesz' midpoint averaging function is given in Figure 4.4.1-1 for an arbitrary selection of ring boundary radii.

Similarly, let the cosine and sine midpoint averaging functions $\overline{\cos \alpha}$ and $\overline{\sin \alpha}$ be the staircase-like (piecewise constant) functions which assume the constant value over each compartment of the actual cosine and sine functions evaluated at the mid-azimuth of that compartment.

$$\begin{Bmatrix} \overline{\cos \alpha} \\ \overline{\sin \alpha} \end{Bmatrix} = \begin{Bmatrix} \cos \alpha_{i,j}^{\text{MID}} \\ \sin \alpha_{i,j}^{\text{MID}} \end{Bmatrix} = \begin{Bmatrix} \overline{C}_{ij} \\ \overline{S}_{ij} \end{Bmatrix} \quad \text{for } \alpha_{i,j-1} \leq \alpha < \alpha_{i,j}$$

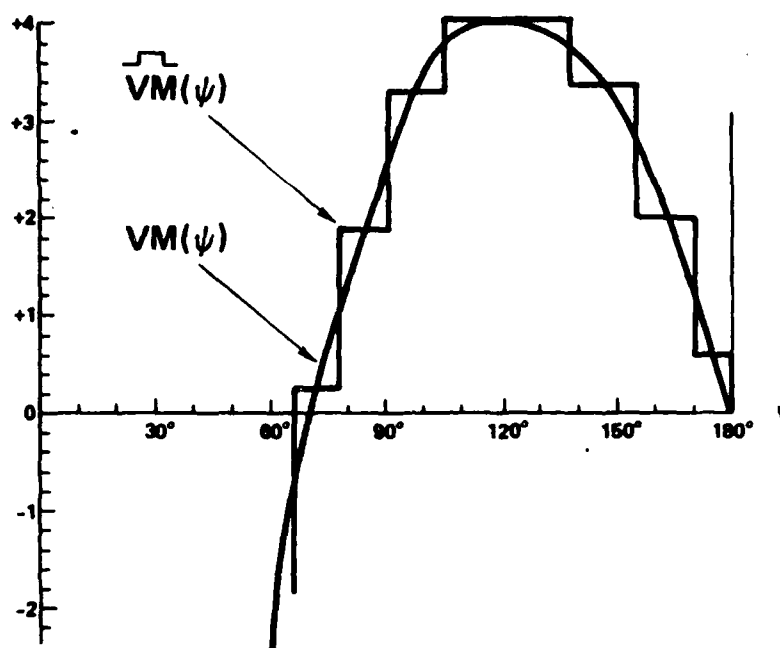
where $\alpha_{ij}^{\text{MID}} = (\alpha_{i,j-1} + \alpha_{i,j})/2$

When the Vening-Meinesz' and the cosine and sine midpoint averaging functions are substituted for the corresponding classical functions in the Vening-Meinesz' Integral, the double integral on the densely distributed point gravity anomalies reduces to a double summation on the mean gravity anomalies over each compartment:

$$\begin{Bmatrix} \delta g_{N-S} \\ \delta g_{E-W} \end{Bmatrix} = \begin{Bmatrix} G_{\xi} \\ G_{\eta} \end{Bmatrix} = \iint \overline{VM}(\psi) \begin{Bmatrix} \overline{\cos \alpha} \\ \overline{\sin \alpha} \end{Bmatrix} \Delta g(\psi, \alpha) \frac{d\sigma}{4\pi} = \sum_i \overline{VM}_i \sum_i \begin{Bmatrix} \overline{C}_{ij} \\ \overline{S}_{ij} \end{Bmatrix} \frac{A_{ij}}{4\pi} \overline{\Delta g}_{ij}$$

Hence, the digital filter representation of this transformation may be written:

$$\begin{Bmatrix} G_{\xi} \\ G_{\eta} \end{Bmatrix} = \sum_i \sum_j \overline{w}_{ij} \overline{\Delta g}_{ij}$$



$\widehat{VM}(\psi)$: VENING-MEINESZ' MIDPOINT AVERAGING FUNCTION
 $VM(\psi)$: CLASSICAL VENING-MEINESZ' FUNCTION

Figure 4.4.1-1. Vening-Meinesz' Midpoint Averaging Function $\widehat{VM}(\psi)$.

where the weights are

$$\bar{w}_{ij} = \bar{VM}_i \begin{Bmatrix} \bar{C}_{ij} \\ \bar{S}_{ij} \end{Bmatrix} \frac{A_{ij}}{4\pi}.$$

The spectrum of the transformation is

$$\begin{aligned} \lambda_{-n}^1 &= 2 \sqrt{\frac{(n-1)!}{(n+1)!}} \iint \bar{VM}(\psi) \begin{Bmatrix} \bar{C}_{ij} \cos \alpha \\ \bar{S}_{ij} \sin \alpha \end{Bmatrix} \begin{Bmatrix} \cos \alpha \\ \sin \alpha \end{Bmatrix} P_n^1(\cos \psi) \frac{d\sigma}{4\pi} \\ &= \frac{2}{\sqrt{n(n+1)}} \sum_i \bar{VM}_i \int_{x_i}^{x_{i-1}} P_n^1(x) \frac{dx}{2} \sum_j \begin{Bmatrix} \bar{C}_{ij} \\ \bar{S}_{ij} \end{Bmatrix} \int_{\alpha_{i,j-1}}^{\alpha_{i,j}} \begin{Bmatrix} \cos \alpha \\ \sin \alpha \end{Bmatrix} \frac{d\alpha}{2\pi} \end{aligned}$$

where $x_i \equiv \cos \psi_i$

4.4.2 Integrated Mean Weighting

Let the Vening-Meinesz Integrated Mean Averaging Function $\bar{VM}(\psi)$ be the staircase-like (piecewise constant) function which assumes the constant value \bar{VM}_i over the i^{th} ring of the integrated-mean value of the classical Vening-Meinesz' function over that ring.

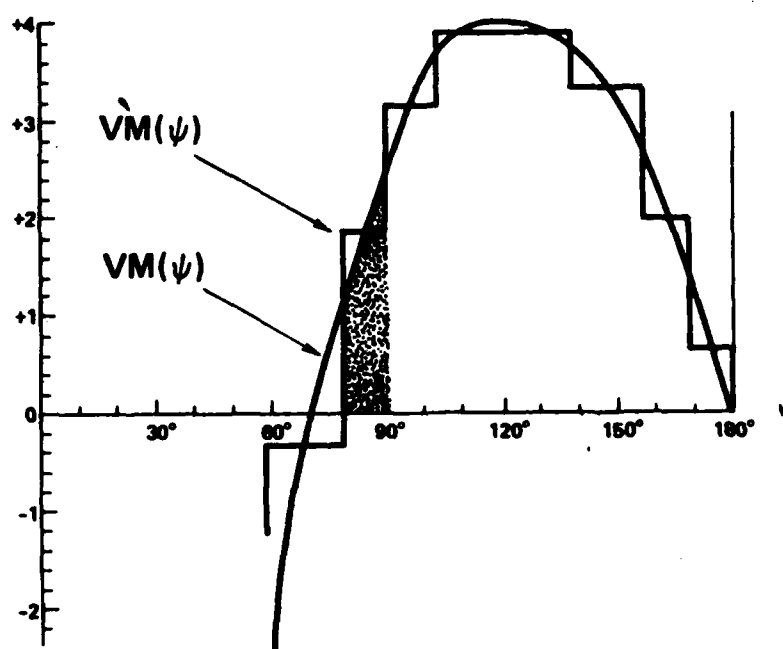
$$\bar{VM}(\psi) = \begin{cases} \bar{VM}_1 & \text{for } \psi_0 < \psi \leq \psi_1 \\ \bar{VM}_2 & \text{for } \psi_1 < \psi \leq \psi_2 \\ \bar{VM}_3 & \text{for } \psi_2 < \psi \leq \psi_3 \\ \text{etc.} \end{cases}$$

where

$$\bar{VM}_i = \frac{1}{x_{i-1} - x_i} \int_{x_i}^{x_{i-1}} VM(x) dx$$

and $x = \cos \psi_i$.

A typical graph of $\bar{VM}(\psi)$ is given in Figure 4.4.2-1 for a particular choice of spherical ring boundary radii. From the definition of this function, the area of the shaded region under the classical Vening-Meinesz' function between each pair of successive ring boundary radii must equal the area of the rectangular block between these radii whose ordinate is the constant value \bar{VM}_i .



$\hat{V}M(\psi)$: VENING-MEINESZ INTEGRATED-MEAN AVERAGING FUNCTION
 $VM(\psi)$: CLASSICAL VENING-MEINESZ FUNCTION.

Figure 4.4.2-1. Vening-Meinesz' Integrated-Mean Averaging Function $\hat{V}M(\psi)$.

Similarly let the cosine and sine integrated-mean averaging functions $\hat{\cos} \alpha$ and $\hat{\sin} \alpha$ be the staircase-like (piecewise constant) functions which assume the constant value over each compartment of the integrated-mean value of the actual cosine and sine functions over that compartment.

$$\begin{aligned} \begin{Bmatrix} \hat{\cos} \alpha \\ \hat{\sin} \alpha \end{Bmatrix} &= \frac{1}{\alpha_{i,j} - \alpha_{i,j-1}} \int_{\alpha_{i,j-1}}^{\alpha_{i,j}} \begin{Bmatrix} \cos \alpha \\ \sin \alpha \end{Bmatrix} d\alpha \\ &= \frac{1}{\alpha_{i,j} - \alpha_{i,j-1}} \begin{Bmatrix} \sin \alpha_{i,j} - \sin \alpha_{i,j-1} \\ -\cos \alpha_{i,j} + \cos \alpha_{i,j-1} \end{Bmatrix} \\ &= \begin{Bmatrix} \hat{c}_{ij} \\ \hat{s}_{ij} \end{Bmatrix} \quad \text{for } \alpha_{i,j-1} \leq \alpha < \alpha_{i,j} \end{aligned}$$

When the Vening-Meinesz', and the cosine and sine integrated-mean averaging functions are substituted for the corresponding classical functions in the Vening-Meinesz' Integral, the double integral on the densely-distributed point gravity reduces to a double summation on the mean gravity anomalies over each compartment:

$$\begin{Bmatrix} G\xi \\ G\eta \end{Bmatrix} = \iint \hat{V}\hat{M}(\psi) \begin{Bmatrix} \cos \alpha \\ \sin \alpha \end{Bmatrix} \Delta g(\psi, \alpha) \frac{d\sigma}{4\pi} = \sum_i \hat{V}\hat{M}_i \sum_j \begin{Bmatrix} \hat{c}_{ij} \\ \hat{s}_{ij} \end{Bmatrix} \frac{A_{ij}}{4\pi} \Delta \bar{g}_{ij}$$

Hence the digital filter representation of this transformation may be written:

$$\begin{Bmatrix} G\xi \\ G\eta \end{Bmatrix} = \sum_i \sum_j \hat{w}_{ij} \Delta \bar{g}_{ij}$$

where the weights are

$$\hat{w}_{ij} = \hat{v}_i \left\{ \begin{matrix} \hat{c}_{ij} \\ \hat{s}_{ij} \end{matrix} \right\} \frac{A_{ij}}{4\pi}$$

The spectrum of the transformation is:

$$\begin{aligned} \lambda_n^1 &= 2 \sqrt{\frac{(n-1)!}{(n+1)!}} \iint \hat{v}_i(\psi) \left\{ \begin{matrix} \cos \alpha \\ \sin \alpha \end{matrix} \right\} \left\{ \begin{matrix} \cos \alpha \\ \sin \alpha \end{matrix} \right\} P_n^1(\cos \psi) \frac{d\sigma}{4\pi} \\ &= \frac{2}{\sqrt{n(n+1)}} \sum_i \hat{v}_i \int_{x_i}^{x_{i-1}} P_n^1(x) \frac{dx}{2} \sum_j \left\{ \begin{matrix} \hat{c}_{i,j} \\ \hat{s}_{i,j} \end{matrix} \right\} \int_{\alpha_{i,j-1}}^{\alpha_{i,j}} \left\{ \begin{matrix} \cos \alpha \\ \sin \alpha \end{matrix} \right\} \frac{d\sigma}{2\pi} \\ &= \frac{2}{\sqrt{n(n+1)}} \sum_i \hat{v}_i \int_{x_i}^{x_{i-1}} P_n^1(x) \frac{dx}{2} \sum_j \frac{1}{2\pi(\alpha_{i,j} - \alpha_{i,j-1})} \left\{ \begin{matrix} (\sin \alpha_{i,j} - \sin \alpha_{i,j-1})^2 \\ (\cos \alpha_{i,j} - \cos \alpha_{i,j-1})^2 \end{matrix} \right\} \\ &= \frac{2}{\sqrt{n(n+1)}} \sum_i \hat{v}_i \int_{x_i}^{x_{i-1}} P_n^1(x) \frac{dx}{2} \sum_j \ell_{ij} \left\{ \begin{matrix} \cos^2[(\alpha_{i,j-1} + \alpha_{i,j})/2] \\ \sin^2[(\alpha_{i,j-1} + \alpha_{i,j})/2] \end{matrix} \right\} \end{aligned}$$

where

$$\ell_{ij} = \frac{\sin^2[(\alpha_{i,j} - \alpha_{i,j-1})/2]}{\pi[(\alpha_{i,j} - \alpha_{i,j-1})/2]}$$

and

$$x_i = \cos \psi_i.$$

The lengthy but straight-forward steps in the derivation of these expressions have been omitted.

The partial derivatives $\partial \lambda_n^1 / \partial x_k$ of the elements of the spectrum with respect to each of the template spherical ring radii (or rather with respect to their cosines) may also be derived. As mentioned in the Stokes' section, these quantities will be necessary in the implementation of a least squares optimization algorithm for the determination of "improved" values of the template ring radii.

By direct differentiation of the equation for the spectrum above,

$$\frac{\partial \lambda_n^1}{\partial x_i} = \frac{2}{\sqrt{n(n+1)}} \left[\begin{aligned} & -\frac{1}{2} \ell_{i+1} (\hat{V}M_{i+1}) \hat{P}_{n,i+1}^1 + \frac{1}{2} \ell_i (\hat{V}M_i) \hat{P}_{n,i}^1 \\ & + VM(x_i) \left[+\frac{1}{2} \ell_{i+1} \hat{P}_{n,i+1}^1 - \frac{1}{2} \ell_i \hat{P}_{n,i}^1 \right] \\ & + P_n^1(x_i) \left[+\frac{1}{2} \ell_{i+1} \hat{V}M_{i+1} - \frac{1}{2} \ell_i \hat{V}M_i \right] \end{aligned} \right]$$

where

$$\ell_i = \sum_j \ell_{ij} \begin{cases} \cos^2[(\alpha_{i,j} + \alpha_{i,j-1})/2] \\ \sin^2[(\alpha_{i,j} + \alpha_{i,j-1})/2] \end{cases}$$

$$x_i = \cos \psi_i$$

and

$$\hat{P}_{n,i}^1 = \frac{1}{x_{i-1} - x_i} \int_{x_i}^{x_{i-1}} P_n^1(x) dx$$

While this equation looks forbidding, it is extremely simple to implement in a computer program since almost all of the quantities appearing in it will already have been computed during the computation of the spectrum λ_n^1 itself. Hence only the few additional multiplications and additions of these quantities as indicated by this equation are necessary to obtain the analytic partial. Again this is an exceptionally fortuitous situation. It avoids the approximate incremental method of calculating the partial, and it avoids the generally prohibitively expensive calculation of the partial.

Similarly, the partial derivatives $\partial \lambda_n^1 / \partial \alpha_{ij}$ of the elements of the spectrum with respect to each of the template compartment boundary azimuths may also be derived. These quantities will be necessary if the azimuths will be adjusted in an optimization program to derive templates with "improved" values of the azimuths.

Again by direct differentiation of the first component of the equation for the spectrum of the discrete Vening-Meinesz' transformation,

$$\frac{\partial \lambda_n^1}{\partial \alpha_{i,j}} = \frac{2}{\sqrt{n(n+1)}} \sum_i \tilde{v}M_i \int_{x_i}^{x_{i-1}} p_n^1(x) \frac{dx}{2} \frac{\partial \ell_i}{\partial \alpha_{i,j}}$$

where

$$\begin{aligned} \frac{\partial \ell_i}{\partial \alpha_{i,j}} = \frac{1}{2\pi} & \left[\left(\frac{\sin \alpha_{i,j+1} - \sin \alpha_{i,j}}{\alpha_{i,j+1} - \alpha_{i,j}} \right) - \left(\frac{\sin \alpha_{i,j} - \sin \alpha_{i,j-1}}{\alpha_{i,j} - \alpha_{i,j-1}} \right) \right] \\ & \left[\left(\frac{\sin \alpha_{i,j+1} - \sin \alpha_{i,j}}{\alpha_{i,j+1} - \alpha_{i,j}} \right) + \left(\frac{\sin \alpha_{i,j} - \sin \alpha_{i,j-1}}{\alpha_{i,j} - \alpha_{i,j-1}} \right) - 2 \cos \alpha_{i,j} \right] \end{aligned}$$

A similar expression could be derived for the partial of the second component of λ_n^1 .

4.4.3 Summary of Discrete Vening-Meinesz' Transformations

A summary of the mathematical relationships for the discrete Vening-Meinesz' summation transformations is given in Figures 4.4.3-1 and 4.4.3-2.

• TRANSFORMATION

DISCRETE VENING-MEINESZ' SUMMATION

USING MIDPOINT WEIGHTING

Input: $\bar{\Delta g}_{ij}$ (mean gravity anomaly in each compartment)

Output: G_{ϵ} (horizontal gravity disturbance vector)

• EXPLICIT FORM

$$G_{\epsilon} = \begin{Bmatrix} G_{\xi} \\ G_{\eta} \end{Bmatrix} = \iint \bar{VM}(\psi) \begin{Bmatrix} \cos \alpha \\ \sin \alpha \end{Bmatrix} \Delta g(\psi, \alpha) \frac{d\sigma}{4\pi} = \sum_i \sum_j \bar{w}_{ij} \bar{\Delta g}_{ij}$$

$$\text{where } \bar{w}_{ij} = \bar{VM}(\psi_i^{\text{mid}}) \begin{Bmatrix} \cos \alpha_{ij}^{\text{mid}} \\ \sin \alpha_{ij}^{\text{mid}} \end{Bmatrix} \frac{\text{AREA}_{ij}}{4\pi}$$

• SPECTRUM (TRANSFER FUNCTION)

$$\lambda_{-n}^1 = 2 \sqrt{\frac{(n-1)!}{(n+1)!}} \iint \bar{VM}(\psi) \begin{Bmatrix} \cos \alpha \\ \sin \alpha \end{Bmatrix} \begin{Bmatrix} \cos \alpha \\ \sin \alpha \end{Bmatrix} P_n^1(\cos \alpha) \frac{d\sigma}{4\pi}$$

$$= \frac{2}{\sqrt{n(n+1)}} \sum_i \bar{VM}(\psi_i^{\text{mid}}) \int_{x_i}^{x_{i-1}} P_n^1(x) \frac{dx}{2}$$

$$\cdot \sum_j \begin{Bmatrix} \cos \alpha_{ij}^{\text{mid}} \\ \sin \alpha_{ij}^{\text{mid}} \end{Bmatrix} \int_{\alpha_{i,j-1}}^{\alpha_{i,j}} \begin{Bmatrix} \cos \alpha \\ \sin \alpha \end{Bmatrix} \frac{d\alpha}{2\pi}$$

where $x_i = \cos \psi_i$

Figure 4.4.3-1. Summary of Relationships for the Discrete Vening-Meinesz' Summation Using Midpoint Weighting.

• TRANSFORMATION

DISCRETE VENING-MEINESZ' SUMMATION
USING INTEGRATED-MEAN WEIGHTING

Input: $\bar{\Delta g}_{ij}$ (mean gravity anomaly in each compartment)
Output: G_{ξ} (horizontal gravity disturbance vector)

• EXPLICIT FORM

$$G_{\xi} = \begin{Bmatrix} G_{\xi} \\ G_{\eta} \end{Bmatrix} = \iint \dot{V}M(\psi) \begin{Bmatrix} \cos \alpha \\ \sin \alpha \end{Bmatrix} \Delta g(\psi, \alpha) \frac{d\sigma}{4\pi}$$

$$= \sum_i \sum_j \dot{w}_{ij} \bar{\Delta g}_{ij} \quad \text{where } \dot{w}_{ij} = \dot{V}M_i \begin{Bmatrix} \dot{C}_{i,j} \\ \dot{S}_{i,j} \end{Bmatrix} \frac{\text{AREA}_{i,j}}{4\pi}$$

• SPECTRUM

$$\lambda_n^1 = 2 \sqrt{\frac{(n-1)!}{(n+1)!}} \iint \dot{V}M(\psi) \begin{Bmatrix} \cos \alpha \\ \sin \alpha \end{Bmatrix} \begin{Bmatrix} \cos \alpha \\ \sin \alpha \end{Bmatrix} P_n^1(\cos \psi) \frac{d\sigma}{4\pi}$$

$$= \frac{2}{\sqrt{n(n+1)}} \sum_i \dot{V}M_i \int_{x_i}^{x_{i-1}} P_n^1(x) \frac{dx}{2} \sum_j \ell_{ij} \begin{Bmatrix} \cos^2 [(\alpha_{i,j-1} + \alpha_{ij})/2] \\ \sin^2 [(\alpha_{i,j-1} + \alpha_{ij})/2] \end{Bmatrix}$$

where $\ell_{ij} = \frac{\sin^2 [(\alpha_{i,j} - \alpha_{i,j-1})/2]}{\pi [(\alpha_{i,j} - \alpha_{i,j-1})/2]}$ and where $x_i = \cos \psi_i$

Figure 4.4.3-2. Summary of Relationships for the Discrete Vening-Meinesz' Summation Using Integrated-Mean Weighting.

4.5 Inner Zone Operators and Their Spectra for First Order Geodetic Transformations

In the numerical evaluation of the discrete Vening-Meinesz' summation at the surface, a small circular region or "cap" centered at the point of evaluation is always excluded due to the singularity of the Vening-Meinesz' kernel at the origin. This spherical cap is called the "inner zone". The contribution of the inner zone in the computation of the deflections or horizontal gravity disturbances is then accounted for by other methods, usually* through the use of the first finite differences of the input quantity to the transformation. The spectra of such operators will now be derived and compared to the theoretical spectrum of a truncated integral transformation.

4.5.1 Dipole Operators and Their Spectra

The simplest case is a "single dipole" finite difference operator which transform an arbitrary input $f(\psi, \alpha)$ into the finite difference

$$f(\psi_0, \alpha) - f(\psi_0, \alpha + \pi)$$

of the two values of the input which lie radially opposite each other at a spherical radius ψ_0 along a diameter having azimuth α . Such an operator may be put into the form of an integral transformation through the use of two Dirac Delta functions.

In the case when the dipole lies in the north-south direction, the spectral results shown in Figure 4.5-1 are deducible. By combining these results with analogous ones for an east-west dipole, the "double dipole" spectrum given in Figure 4.5-2 are obtained. And with another slight generalization, the spectrum of the Rice quadruple dipole operator is derived as specified in Figure 4.5-3.

These finite difference operators and their spectra will be used in the next section to determine the spectra of geodetic inner-zone deflection operators.

4.5.2 Inner Zone Deflection Operators and Their Spectra

Heiskanen-Moritz (1967) have shown that to a low-order approximation the contribution of the inner zone to the two components of the horizontal gravity disturbance is given by:*

* Heiskanen-Moritz, 1967, pp. 120-122; Pick-Picha-Vyskocil, 1973, pp. 262-264.

** page 121, equation 2-232.

• TRANSFORMATION: NORTH-SOUTH DIPOLE

$$\begin{array}{l} \text{Input: } f(\psi, \alpha) \\ \text{Output: } \begin{Bmatrix} f_N - f_S \\ 0 \end{Bmatrix} = \begin{Bmatrix} f(\psi_0, 0) - f(\psi_0, \pi) \\ 0 \end{Bmatrix} \end{array}$$

• EXPLICIT FORM

$$\begin{Bmatrix} f_N - f_S \\ 0 \end{Bmatrix} = \iint [\delta_N - \delta_S] \begin{Bmatrix} \cos \alpha \\ \sin \alpha \end{Bmatrix} f(\psi, \alpha) \frac{d\alpha}{4\pi}$$

• SPECTRUM

$$\begin{aligned} \lambda_n^1 &= \frac{2}{\sqrt{n(n+1)}} \iint [\delta_N - \delta_S] \begin{Bmatrix} \cos \alpha \\ \sin \alpha \end{Bmatrix} P_n^1(\cos \psi) \begin{Bmatrix} \cos \alpha \\ \sin \alpha \end{Bmatrix} \frac{d\alpha}{4\pi} \\ &= \frac{2}{\sqrt{n(n+1)}} P_n^1(\cos \psi_0) \begin{Bmatrix} 2 \\ 0 \end{Bmatrix} \\ &\approx -\sqrt{n(n+1)} \sin \psi_0 \left[1 - \frac{(n-1)(n+2)}{2} \sin^2 \frac{\psi_0}{2} + \dots \right] \begin{Bmatrix} 1 \\ 0 \end{Bmatrix} 2 \\ &\approx -\sqrt{n(n+1)} \psi_0 \begin{Bmatrix} 1 \\ 0 \end{Bmatrix} 2 \end{aligned}$$

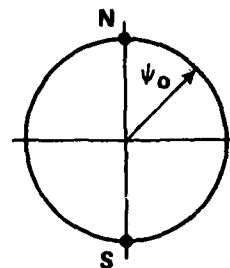
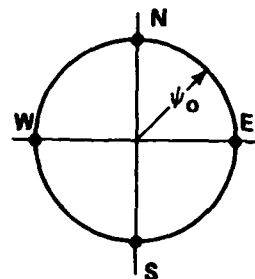


Figure 4.5-1. Summary of Mathematical Relationships for the Single Dipole Finite Difference Operator.

• TRANSFORMATION: NORTH-SOUTH, EAST-WEST DOUBLE DIPOLE

Input: $f(\psi, \alpha)$

$$\text{Output: } \begin{Bmatrix} f_N - f_S \\ f_E - f_W \end{Bmatrix} = \begin{Bmatrix} f(\psi_0, 0) - f(\psi_0, \pi) \\ f(\psi_0, \frac{\pi}{2}) - f(\psi_0, \frac{3\pi}{2}) \end{Bmatrix}$$



• EXPLICIT FORM

$$\begin{Bmatrix} f_N - f_S \\ f_E - f_W \end{Bmatrix} = \iint [(\delta_N - \delta_S) + (\delta_E - \delta_W)] \begin{Bmatrix} \cos \alpha \\ \sin \alpha \end{Bmatrix} f(\psi, \alpha) \frac{d\sigma}{4\pi}$$

• SPECTRUM

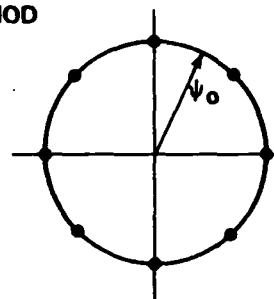
$$\begin{aligned} \lambda_n^1 &= \frac{2}{\sqrt{n(n+1)}} P_n^1(\cos \psi_0) \begin{Bmatrix} 2 \\ 2 \end{Bmatrix} \\ &\approx -\sqrt{n(n+1)} \sin \psi_0 \left[1 - \frac{(n-1)(n+2)}{2} \sin^2 \frac{\psi_0}{2} + \dots \right] \begin{Bmatrix} 1 \\ 1 \end{Bmatrix} 2 \\ &\approx -\sqrt{n(n+1)} \psi_0 \begin{Bmatrix} 1 \\ 1 \end{Bmatrix} 2 \end{aligned}$$

Figure 4.5-2. Summary of Mathematical Relationships for the Double Dipole Finite Difference Operator.

• TRANSFORMATION: RICE'S "THREE-GRADIENT" OR "EIGHT-POINT" METHOD

Input: $f(\psi, \alpha)$

$$\text{Output: } \begin{Bmatrix} \frac{1}{2} (f_N - f_S) + \frac{\sqrt{2}}{4} (f_{NE} - f_{SW}) + \frac{\sqrt{2}}{4} (f_{NW} - f_{SE}) \\ \frac{1}{2} (f_E - f_W) + \frac{\sqrt{2}}{4} (f_{NE} - f_{SW}) - \frac{\sqrt{2}}{4} (f_{NW} - f_{SE}) \end{Bmatrix}$$



• SPECTRUM

$$\begin{aligned} \lambda_n^1 &= \frac{2}{\sqrt{n(n+1)}} \frac{P_n^1(\cos \psi_0)}{2} \begin{Bmatrix} 4 \\ 4 \end{Bmatrix} \\ &\approx -\sqrt{n(n+1)} \sin \psi_0 \left[1 - \frac{(n-1)(n+2)}{2} \sin^2 \frac{\psi_0}{2} + \dots \right] \begin{Bmatrix} 1 \\ 1 \end{Bmatrix}^2 \\ &\approx -\sqrt{n(n+1)} \psi_0 \begin{Bmatrix} 1 \\ 1 \end{Bmatrix}^2 \end{aligned}$$

Figure 4.5-3. Summary of Mathematical Relationships for the Rice Weighted Quadruple Dipole Operator.

$$\begin{Bmatrix} G\xi \\ G\eta \end{Bmatrix}_{\text{INNER ZONE}} = \int_0^{2\pi} \int_0^{s_0} \left(-\frac{2}{s^2} \right) \begin{Bmatrix} \cos \alpha \\ \sin \alpha \end{Bmatrix} \Delta g \frac{s ds d\alpha}{4\pi}$$

where s represents the linear distance $R\psi$ on the surface of a sphere of radius R . By expanding $\Delta g(s, \alpha)$ in a two-dimensional Taylor series, and performing the integration shown above on the result, Heiskanen-Moritz derive that the leading term in the inner zone contribution is*

$$\begin{Bmatrix} G\xi \\ G\eta \end{Bmatrix}_{\text{INNER ZONE}} = -\frac{s_0}{2} \begin{Bmatrix} \frac{\partial}{\partial x} \Delta g \\ \frac{\partial}{\partial y} \Delta g \end{Bmatrix} + \dots$$

where x and y are linear distances along the local north and east directions respectively.

The partial derivatives above may be approximated using the double dipole finite difference operator or the Rice weighted quadruple dipole operator of the previous subsection:

$$\begin{aligned} \begin{Bmatrix} \frac{\partial}{\partial x} \Delta g \\ \frac{\partial}{\partial y} \Delta g \end{Bmatrix} &\approx \begin{Bmatrix} \frac{\Delta g_N - \Delta g_S}{2s_0} \\ \frac{\Delta g_E - \Delta g_W}{2s_0} \end{Bmatrix} = \frac{1}{2s_0} \begin{Bmatrix} \Delta g_N - \Delta g_S \\ \Delta g_E - \Delta g_W \end{Bmatrix} \\ \\ \begin{Bmatrix} \frac{\partial}{\partial x} \Delta g \\ \frac{\partial}{\partial y} \Delta g \end{Bmatrix} &\approx \begin{Bmatrix} \frac{1}{2} \left(\frac{\Delta g_N - \Delta g_S}{2s_0} \right) + \frac{1}{4} \left(\frac{\Delta g_{NE} - \Delta g_{SE}}{\sqrt{2}s_0} \right) + \frac{1}{4} \left(\frac{\Delta g_{NW} - \Delta g_{SW}}{\sqrt{2}s_0} \right) \\ \frac{1}{2} \left(\frac{\Delta g_E - \Delta g_W}{2s_0} \right) + \frac{1}{4} \left(\frac{\Delta g_{NE} - \Delta g_{NW}}{\sqrt{2}s_0} \right) + \frac{1}{4} \left(\frac{\Delta g_{SE} - \Delta g_{SW}}{\sqrt{2}s_0} \right) \end{Bmatrix} \\ &\approx \frac{1}{2s_0} \begin{Bmatrix} \frac{1}{2} (\Delta g_N - \Delta g_S) + \frac{\sqrt{2}}{4} (\Delta g_{NE} - \Delta g_{SW}) + \frac{\sqrt{2}}{4} (\Delta g_{NW} - \Delta g_{SE}) \\ \frac{1}{2} (\Delta g_E - \Delta g_W) + \frac{\sqrt{2}}{4} (\Delta g_{NE} - \Delta g_{SW}) - \frac{\sqrt{2}}{4} (\Delta g_{NW} - \Delta g_{SE}) \end{Bmatrix} \end{aligned}$$

* page 122, equation 2-235.

Consequently, from the spectral results for these dipole operators, it is quickly deduced that the spectrum of the transformation yielding the contribution of the inner zone to the horizontal gravity disturbances via the two approximations is:

$$\lambda_{-n}^1 = \frac{2}{\sqrt{n(n+1)}} \frac{P_n^1(\cos \psi_0)}{(-4)} \begin{Bmatrix} 2 \\ 2 \end{Bmatrix} \approx \sqrt{n(n+1)} \frac{\psi_0}{2} \begin{Bmatrix} 1 \\ 1 \end{Bmatrix}$$

Thus the inner zone can have a rather large effect on the spectrum of a Vening-Meinesz' transformation, especially for high spherical harmonic degree n and large truncation radii ψ_0 .

Just as the transformations involving the double dipole or Rice quadruple dipole operators are approximations to the continuous integral Vening-Meinesz' transformation truncated to a spherical cap, so must the spectrum of these transformations approximate the spectrum of the theoretical truncated Vening-Meinesz transformations. This will be shown to be true (to first order in ψ_0) in the next subsection.

It should be noted, however, that quite a few approximations have been made in the above discussion. Specifically, at the beginning the Vening-Meinesz' Integral was "localized" to a neighborhood of the origin, then the gravity anomalies were expanded in a Taylor series which was truncated, and finally partial derivatives were approximated by finite differences. In a series of papers, Prado (1977a, 1977b) and Adams and Prado (1978) have examined the analogous "flat-earth" transformation converting vertical gravity disturbances δg into horizontal gravity disturbances ($G\xi$, $G\eta$) and placed the spectral theory of this planar transformation on a much more rigorous basis, showing in fact that the outputs and inputs are related by a two-dimensional Hilbert transformation. Their papers also give further references to the mathematical and engineering literature.

4.5.3 The Truncated Vening-Meinesz' Transformation and Its Spectrum

Cook (1951) and deWitte (1967) have investigated the mathematical properties of the truncated Vening-Meinesz' transformation and have calculated some estimates of the contributions of the excluded regions. DeWitte has provided graphs* of the low degree Cook coefficients $q_n(\psi_0)$

* in his Figures 10 and 11

which are closely related to the spectrum of the residual* Vening-Meinesz' transformation, and are analogous to the Molodenskii coefficients $Q_n(\psi_0)$ for the Stokes' kernel. While the Cook coefficients provide theoretically correct expressions describing the spectrum for all truncation radii ψ_0 , the properties of the truncated Vening-Meinesz transformation for small ψ_0 may be more easily seen in a power series expansion about the origin in powers of ψ_0 . The mathematical results are exhibited in Figure 4.5-4.

From the power series in the figure it is seen that indeed the spectrum of the theoretical truncated Vening-Meinesz' transformation matches through first order the spectrum of the inner zone deflection transformations involving the double dipole or Rice quadruple dipole operators.

• TRANSFORMATION: Vening-Meinesz over a circular cap of spherical radius ψ_0 around the origin

• EXPLICIT FORM:

$$\begin{Bmatrix} G\xi \\ G\eta \end{Bmatrix} = \int_0^{2\pi} \int_0^{\psi_0} VM(\psi) \begin{Bmatrix} \cos \alpha \\ \sin \alpha \end{Bmatrix} \Delta g(\psi, \alpha) \frac{\sin \psi d\psi d\alpha}{4\pi}$$

• SPECTRUM

$$\begin{aligned} \lambda_n^1 &= \frac{2}{\sqrt{n(n+1)}} \int_0^{\psi_0} VM(\psi) P_n^1(\cos \psi) \frac{\sin \psi d\psi}{2} \\ &\approx \frac{2}{\sqrt{n(n+1)}} \int_0^{\psi_0} \frac{-1}{2 \sin^2 \frac{\psi}{2}} P_n^1(\cos \psi) \frac{\sin \psi d\psi}{2} \text{ for small } \psi_0 \\ &\approx \sqrt{n(n+1)} \frac{\psi_0}{2} \left[1 - \frac{(n-1)(n+2)}{6} \left(\frac{\psi_0}{2}\right)^2 + \frac{(n-2)(n-1)(n+2)(n+3)}{180} \left(\frac{\psi_0}{2}\right)^4 - \dots \right] \end{aligned}$$

Figure 4.5-4. Summary of Mathematical Relationships for the Truncated Vening-Meinesz' Transformation.

* The term "residual" refers to the "outer zone" where $\psi_0 < \psi \leq \pi$, while "truncated" refers to the "inner zone".

In the comprehensive filter design program (Appendix C), the negative of the series expansion through third order has been incorporated as a correction to the theoretical Vening-Meinesz' spectrum for the entire sphere, since the small spherical cap around the origin is being omitted in the calculation of the spectrum of the discrete Vening-Meinesz' summation transformation. It is thereby tacitly assumed for the purpose of optimal template design that in the actual Vening-Meinesz' summation an almost error-free inner-zone deflection operator has been implemented. More realistic cases could be considered by deriving more accurate approximations to the spectra of the Rice quadruple dipole operator, for instance, and incorporating these expressions instead into the spectral computations.

SECTION 5

SPECIFIC TEMPLATES AND EXAMPLES OF SPECTRA

This chapter describes a number of specific bull's-eye templates for the Stokes' and Vening-Meinesz' discrete summation transformations, and gives tables of values of their compartment boundary parameters. Graphs and listings of the numerical values of the spectra for some of these summation transformations, as well as for the corresponding integral transformations, are also presented to provide an intuitive feeling for these quantities.

5.1 Specific Templates

The values of the compartment boundary parameters for almost all of the bull's-eye templates which have been published in the literature have been derived using the concept of the "equal contribution" of each template subdivision. Since many of the specific templates to be described in this chapter fall into this category and since the relatively good quality of the equal contribution template can be partially explained by spectral theory, the equal contribution concept will be examined in some detail. Templates with parameters determined by other methods will be described in a later subsection entitled "Other Templates".

Under the equal contribution concept, the spherical ring boundary radii and compartment boundary azimuths are selected so that the individual contributions from the template subdivisions to the total output will all be equal in magnitude in the hypothetical case when the subdivision inputs to the summation are all equal. For example, in the Stokes' or Vening-Meinesz' transformations, the boundaries of the subdivisions would be selected so that each subdivision would contribute equally (in magnitude) to the geoid height or deflection of the vertical when the input mean gravity anomaly over each subdivision in one milligal.

Traditionally, the word "subdivision" has meant "compartment". However, "subdivision" is purposely being used here to allow the equal contribution concept to be extended to complete rings or complete sectors rather than being restricted to compartments. In fact, it will be shown that the equal contribution of complete rings and sectors are more natural concepts than that for compartments. Historically, however, before the advent of electronic computers, an equal compartment contribution template (in the form of a physical template to be laid on a gravity anomaly map) would have been a very useful computational aid.

5.1.1 Templates with Compartmental Equal Contribution

In the standard method of implementing the compartmental equal contribution concept, the number of compartments in each ring is chosen a priori according to some ad hoc scheme or "educated guess". Then the spherical ring boundary radii are determined so that each compartment will contribute equal outputs for equal inputs. This involves calculating the total contribution of each ring and dividing by the number of compartments in the ring to find the compartmental contribution. Hence, the contribution of a complete ring will be proportional to the number of compartments in the ring. Finally, for non-zeroth-order transformations only, the spherical sector boundary azimuths are determined so that again each compartment will contribute equal outputs for equal inputs. Examples of the computations are given in Pick-Picha-Vyskocil (1973, pp. 255 and 265-267).

The number of compartments in each ring is often chosen so that it is approximately proportional to the trigonometric sine of the spherical radius ψ of the midpoint of the ring. This is motivated by the fact that the element of area on the surface of the (unit) sphere is

$$d\sigma = \sin\psi \, d\psi \, d\alpha$$

so that with such a choice the compartments have approximately equal area (if the sector boundary azimuths are uniformly partitioned), and approximately equal dimensions (namely $\sin\psi \, d\alpha$ and $d\psi$ when the proportionality constant relating the maximum number of compartments in the $\psi = 90^\circ$ ring to the total number of rings is correctly chosen), and hence have approximately equi-distant midpoints.

Other considerations are also often involved in the a priori choice of the number of compartments in each ring, such as the condition that

the number be divisible by four so that the template can be made bilaterally symmetric.

It should be noted however that the selection of the number of compartments in each ring by the method outlined above requires a pre-existing knowledge of the ring boundary radii, which are precisely the quantities to be determined. In other words, the number of compartments in each ring and the ring boundary radii are mutually dependent quantities under the compartmental equal contribution concept. Thus an exact determination of these quantities would necessitate an iterative solution. This is why published methods are rather ad hoc or based upon "educated guesses".

5.1.1.1 Pick-Picha-Vyskocil Templates

Pick-Picha-Vyskocil (1973) have given values of the template parameters for a 34-ring Stokes' template and a 23-ring Vening-Meinesz template. These are reproduced in Tables 5.1.1-1 and 5.1.1-2. The Vening-Meinesz' template has been derived under the compartmental equal contribution concept, while the Stokes' template has been derived under a modified form of this concept in which the close rings (those with $\psi < 2.9610^\circ$) are more finely subdivided* into compartments and these smaller compartments contribute one tenth that of the compartments in the far rings for equal inputs.

5.1.1.2 Rice and Kazansky Inner Zone Templates

Rice (1952) and Kazansky (1935) have developed templates for the inner zone of the Vening-Meinesz' transformation based on the equal contribution concept. Since the templates are for use only in the inner zone, the Vening-Meinesz' function was approximated by its leading term which permitted the analytical solution for the spherical ring radii

$$\psi_i = a^i \psi_0$$

where "a" is a constant.

In the original Rice paper, ψ_0 corresponds to the distance of 100 meters on the surface of the earth and $a=1.1864$. With 36 compartments in each ring, each compartment contributes one milli-arc-second to the total deflection of the vertical when the compartmental mean gravity anomaly input is one milliga. The values of the original Rice Inner Zone Template parameters are given in Table 5.1.1-3.

* apparently by a factor of ten

RING BOUNDARY RADII

No. of rings	ψ°	r (km)	No. of sectors in ring
1	0.0684	7.606	4
2	0.1753	19.493	6
3	0.3078	34.23	8
4	0.4474	49.75	8
5	0.7116	79.13	16
6	0.9758	108.5	16
7	1.2348	137.3	16
8	1.4883	165.5	16
9	1.9860	220.8	32
10	2.4780	275.5	32
11	2.9610	329.3	32
12	4.148	461	8
13	5.884	654	12
14	8.180	905	16

15	10.488	1166	16
16	12.85	1430	16
17	15.99	1778	20
18	20.17	2243	24
19	25.30		24
20	33.90		24
21	52.0		28
22	61.0		40
23	72.0		64
24	82.3		64
25	94.2		64
26	106.3		42
27	126.3		20
28	135.9		20
29	142.7		20
30	149.0		20
31	155.4		20
32	162.9		20
33	176.4		20
34	180.0		1

Table 5.1.1-1. Pick-Picha-Vyskocil Template Parameters for the Stokes' Transformation.

RING RADII

No. of rings	ψ^2	r (km)	k
1	0.044	4.893	16
2	0.063	7.005	
3	0.089	9.897	
4	0.128	14.23	
5	0.183	20.35	
6	0.261	29.02	
7	0.372	41.4	
8	0.530	58.9	
9	0.753	83.7	
10	1.069	118.9	
10	1.069	118.9	24
11	1.794	199.5	
12	2.966	329.8	
13	4.821	536.1	
14	7.591	844	
15	11.47	1275	33
15	11.47		
16	18.55		
17	28.3		
18	40.8		
19	65.3		23
19	65.3		
20	98.9		
21	114.4		
22	130.5		
23	180.0		

SECTOR AZIMUTHS

Rings 1-10		Rings 10-15	
k	α	k	α
0	0°00'00"	0	0°00'00"
1	14 28 40	1	9 35 40
2	30 00 00	2	19 28 20
3	48 35 30	3	30 00 00
4	90 00 00	4	41 48 40
		5	56 26 30
		6	90 00 00
Rings 15-19		Rings 19-23	
1	3°28'30" *	1	4°59'20" *
2	10 28 30	2	15 07 20
3	17 38 30	3	25 46 20
4	25 06 10	4	37 29 40
5	33 03 20	5	51 30 00
6	41 48 40	6	73 02 40
7	51 59 20	7	119 35 30
8	65 22 50	8	135 55 20
9	104 08 20	9	148 33 00
10	121 57 10	10	159 38 40
11	133 20 30	11	169 59 00
12	142 41 40	12	180 00 00
13	150 59 50		
14	158 40 30		
15	165 58 10		
16	173 02 20		
17	180 00 00		

* As the rings contain an odd number of sectors, the division into sectors does not begin in the zero azimuth.

Table 5.1.1-2. Pick-Picha-Vyskocil Template Parameters for the Vening-Meinesz' Transformation.

In Kazansky's paper, ψ_0 corresponds to 5 km, and $a \approx 1.25$. The values of Kazansky's Inner Zone Template parameters* are given in Table 5.1.1-4.

(n = circle number; r = inner radius)

n	r,km	n	r,km	n	r,km	n	r,km	n	r,km	n	r,km
0	0.100	10	0.554	20	3.068	30	16.94	40	92.22	50	465.5
1	0.119	11	0.657	21	3.641	31	20.09	41	109.0	51	541.5
2	0.141	12	0.780	22	4.320	32	23.83	42	128.7	52	628.1
3	0.167	13	0.926	23	5.125	33	28.25	43	151.9	53	725.9
4	0.198	14	1.099	24	6.081	34	33.48	44	179.1	54	835.9
5	0.235	15	1.304	25	7.216	35	39.67	45	210.9	55	958.5
6	0.279	16	1.547	26	8.560	36	47.00	46	248.0	56	1094.3
7	0.331	17	1.836	27	10.15	37	55.66	47	291.2		
8	0.393	18	2.179	28	12.05	38	65.90	48	341.2		
9	0.467	19	2.586	29	14.29	39	77.97	49	399.0		

Table 5.1.1-3. The Original Rice Inner Zone Template Parameters.

(n = ring number; r = inner radius)

n	r,km	n	r,km	n	r,km	n	r,km
1	5.0	7	20.9	13	86.4	19	341
2	6.4	8	26.5	14	109.1	20	424
3	8.1	9	33.6	15	138	21	524
4	10.2	10	42.6	16	173	22	645
5	13.0	11	54.0	17	218	23	788
6	16.5	12	68.3	18	273	24	955

Table 5.1.1-4. Kazansky Inner Zone Template Parameters

5.1.2 Template with Ring or Sector Equal Contribution

In the method of implementing the ring or sector equal contribution concept, the template subdivisions from which equal contributions are desired are chosen to be complete rings when the compartment boundary radii are being determined, or complete sectors when the compartment boundary azimuths are being determined. Thus the two dimensions are decoupled from each other in the determination of equal contribution

*The author is indebted to Mr. Patrick J. Fell for providing these values.

values of the template parameters. This is consistent with the fact that the Laplace equation, which all harmonic functions satisfy, is separable* in three-dimensional spherical coordinates with the three-dimensional solution being a linear combination of the product of the individual solutions in each separate dimension.

Expressed in mathematical notation, the ring and sector equal contribution concepts impose the conditions:

$$\left| \int_{\psi_{i-1}}^{\psi_i} K(\psi) \sin \psi \, d\psi \right| = \begin{matrix} \text{the same constant} \\ \text{value for all } i \end{matrix}$$

and

$$\left| \int_{\alpha_{i,j-1}}^{\alpha_{i,j}} \underline{A}(\alpha) \, d\alpha \right| = \begin{matrix} \text{the same constant} \\ \text{vector value for all } j \end{matrix}$$

where $K(\psi)$ and $\underline{A}(\alpha)$ are the radial and azimuthal parts of the kernel of the transformation

$$\underline{K}(\psi, \alpha) = K(\psi) \underline{A}(\alpha)$$

For first-order transformations, the sector equal contribution condition becomes

$$\left| \int_{\alpha_{i,j-1}}^{\alpha_{i,j}} \begin{Bmatrix} \cos \alpha \\ \sin \alpha \end{Bmatrix} d\alpha \right| = \left\{ \begin{matrix} |\sin \alpha_{i,j} - \sin \alpha_{i,j-1}| \\ |\cos \alpha_{i,j} - \cos \alpha_{i,j-1}| \end{matrix} \right\} = \begin{matrix} \text{the same constant} \\ \text{value for all } j \end{matrix}$$

It is interesting to compare this condition with the condition that

$$\left| \frac{\sin \alpha_{i,j} - \sin \alpha_{i,j-1}}{\alpha_{i,j} - \alpha_{i,j-1}} \right| = \begin{matrix} \text{the same constant} \\ \text{value for all } j \end{matrix}$$

which may be shown to be a sufficient condition for a partition of the azimuths to yield the lowest possible rms discretization error. The validity of this statement may be established by setting the partial derivative $\partial \lambda_n^1 / \partial \alpha_{i,j}$ of the spectrum with respect to the azimuths equal to zero, but the details will be omitted.

* i.e. multiplicatively decoupleable

It has been found experimentally that the equal contribution templates for complete rings or sectors yield discrete summation transformations with relatively low rms discretization errors. The discretization error, which will be described in Chapter 6, is a measure of the error introduced solely through the approximation of continuous integral transformation by a discrete summation. The equal contribution templates are certainly not optimal templates in the sense of minimizing the rms discretization error. Nevertheless they appear to be good initial guesses in a filter design program.

5.1.2.1 Equal Contribution Calculations for the Stokes' Integral

The problem is to find the values ψ_i of the spherical ring boundary radii such that

$$\left| \int_{\psi_i}^{\psi_{i+1}} S(\psi) \sin \psi \, d\psi \right| = \begin{array}{l} \text{the same constant} \\ \text{value for all } i \end{array}$$

where $S(\psi)$ is the classical Stokes' function. It may be shown* that the integral

$$-\int_0^{\psi} S(\psi) \sin \psi \, d\psi = -4t + 5t^2 + 6t^2 - 7t^4 + 6t^2(1-t^2) \ln t(1+t)$$

where $t = \sin \frac{\psi}{2}$.

Since the Stokes' function has two distinct zeros while $\sin \psi$ is always positive between 0 and π , the integrand will have two distinct zeros, meaning that there will be regions in which cancellations will occur and the integral could have a zero value for the appropriate choices of the ψ_i . For an exact solution these must be removed. An algorithm for performing the computation has been developed by Stanley W. Shepperd,** and is included in PL/I code under the procedure name `EQUI_INTEGRAL_PSI_CALC_STOKES`. The algorithm will calculate the values of the boundary radii ψ_i which yield an equal contribution for each complete ring for any even number of rings. An even number is necessary

* see Heiskanen-Moritz (1967, pp. 262-263)

**Staff Member, Charles Stark Draper Laboratory, Inc.

because of the two zeros of the integrand. The derivation of the algorithm is given in Appendix F.

5.1.2.2 Equal Contribution Calculations for the Analog of Stokes' Integral on Surface Layer Density

The problem of calculating the values of the ring boundary radii for a ring equal contribution template in the transformation converting surface layer densities into geoid height is considerably easier* than in the classical Stokes' transformation due to the facts that the kernel has no zeros and is easily integrable.

The explicit form of the transformation is

$$N = \frac{R}{G} \iint \frac{2}{(2 \sin \frac{\psi}{2})} \mu(\psi, \alpha) \frac{d\sigma}{4\pi}$$

Hence, it is desired to find the ψ_i such that

$$\left| \int_{\psi_i}^{\psi_{i+1}} \frac{2}{(2 \sin \frac{\psi}{2})} \sin \psi \, d\psi \right| = \left| 4 \sin \frac{\psi_{i+1}}{2} - 4 \sin \frac{\psi_i}{2} \right|$$

= the same constant for all i

Now the total integral from 0 to π has the value 4 which must be equally divided among R rings, so each ring contributes $4/R$. Hence the condition to be satisfied is

$$\left| 4 \sin \frac{\psi_{i+1}}{2} - 4 \sin \frac{\psi_i}{2} \right| = \frac{4}{R}$$

with $\psi_0 = 0$ and $\psi_R = \pi$. The solution is

$$\psi_i = 2 \arcsin \frac{i}{R}.$$

5.1.2.3 Equal Contribution Calculations for the Vening-Meinesz' Integral

The problem is to find the values ψ_i of the spherical ring boundary radii such that

$$\left| \int_{\psi_i}^{\psi_{i+1}} \text{VM}(\psi) \sin \psi \, d\psi \right| = \begin{matrix} \text{the same constant} \\ \text{value for all } i \end{matrix}$$

*The author wishes to draw attention to his finding that almost all expressions involving surface layer densities are much simpler and more tractable than those operating on the other geodetic quantities.

where $VM(\psi) = \partial S(\psi)/\partial \psi$ is the classical Vening-Meinesz' function. The author is not aware of any closed-form expression for this integral. Pick-Picha-Vyskocil (1973, page 261) give an expression which involves an infinite series having coefficients which are functions of the Bernoulli and Euler numbers, but this does not appear to be usable practically.

If the classical Vening-Meinesz' function is approximated by discarding all but the "leading" term

$$\frac{-\cos(\psi/2)}{2 \sin^2(\psi/2)}$$

then a solution is possible. This is described in the next section since the resulting kernel is the mathematically exact one for surface layer densities.

5.1.2.4 Equal Contribution Calculations for the Analog of Vening-Meinesz' Integral on Surface Layer Density

The problem of calculating the values of the ring boundary parameters ψ_i for a ring equal contribution template in the transformation converting surface layer densities to deflections of the vertical (or equivalently horizontal gravity disturbances) is not difficult due to the facts that the kernel has no zeros and is easily integrable.

The explicit form of the transformation is

$$\begin{Bmatrix} G\xi \\ G\eta \end{Bmatrix} = \iint \frac{-2 \cos \frac{\psi}{2}}{(2 \sin \frac{\psi}{2})^2} \mu(\psi, \alpha) \begin{Bmatrix} \cos \alpha \\ \sin \alpha \end{Bmatrix} \frac{d\sigma}{4\pi}$$

Hence it is desired to find the ψ_i such that

$$\left| \int_{\psi_i}^{\psi_{i+1}} \frac{-2 \cos \frac{\psi}{2}}{(2 \sin \frac{\psi}{2})^2} \sin \psi \, d\psi \right| = \begin{matrix} \text{constant} \\ \text{for all } i \end{matrix}$$

The indefinite integral may be expressed in closed form as

$$\int \frac{-2 \cos \frac{\psi}{2}}{(2 \sin \frac{\psi}{2})^2} \sin \psi \, d\psi = -2 \left[\log \left| \tan \frac{\psi}{4} \right| + \cos \frac{\psi}{2} \right]$$

The total definite integral from 0 to π is infinite due to the second-order pole at $\psi = 0$. However the total definite integral from a non-zero initial spherical radius ψ_0 to π has the value

$$\int_{\psi_0}^{\pi} \frac{-2 \cos \frac{\psi}{2}}{(2 \sin \frac{\psi}{2})^2} \sin \psi \, d\psi = 2 \log \left| \tan \frac{\psi_0}{4} \right| + 2 \cos \frac{\psi_0}{2}$$

This value must be equally divided among R rings, so the contribution of each ring is

$$I = \left[2 \log \left| \tan \frac{\psi_0}{4} \right| + 2 \cos \frac{\psi_0}{2} \right] / R$$

Thus, the ring radii ψ_i are related by the conditions

$$-2 \log \left| \tan \frac{\psi_{i+1}}{4} \right| - \cos \frac{\psi_{i+1}}{2} = I - 2 \log \left| \tan \frac{\psi_i}{4} \right| - 2 \cos \frac{\psi_i}{2}$$

$$i = 0, 1, 2, \dots (R-1)$$

Once the truncation radius ψ_0 is chosen, the solution of this transcendental equation for each i may be accomplished by a Newton iteration scheme. The author has found that a good initial guess for the iteration is

$$\psi_{i+1} \approx 1.2 \psi_i$$

An algorithm for accomplishing this has been coded in PL/I and incorporated into the comprehensive filter design program listed in an appendix under the procedure name EQUI_INTEGRAL_PSI_CALC_VM_DEN.

Thus the sequence of computations is:

- 1) Select ψ_0 and R
- 2) Compute I
- 3) For $i = 0, 1, \dots (R-1)$ successively,
 - a) Make initial guess of ψ_{i+1} using $\psi_{i+1} = 1.2 \psi_i$.
 - b) Solve the ring boundary radii conditions equation iteratively by a Newton iteration scheme for ψ_{i+1} .

The results of the computation of the ring radii in the 23 and 125-ring cases is given in Tables 5.1.2-1 and 5.1.2-2. The last ring

SPHERICAL RADIUS PSI (DEGREES)

0.0440000	0.0611177	0.0848950	0.1179225	0.1637990	0.2275235	0.3160396	0.4389928	0.6097818	0.8470203
1.1765895	1.6343682	2.2703809	3.1541283	4.3824956	6.0909150	8.4698169	11.7900031	16.4449830	23.0306519
32.5259409	46.7795815	70.6387839	179.9323089						

Table 5.1.2-1. Template Parameters for the 23-Ring Equal Contribution Template with ψ_0 = the initial radius of Pick-Picka-Vyskocil.

SPHERICAL RING RADIUS PSI (DEGREES)

0.0021134	0.0023003	0.0025038	0.0027252	0.0029663	0.0032286	0.0035142	0.0038250	0.0041633	0.0045316
0.0049324	0.0053686	0.0058434	0.0063603	0.0069220	0.0075351	0.0082016	0.0089270	0.0097166	0.0105760
0.0115114	0.0125295	0.0136377	0.0148439	0.0161568	0.0175858	0.0191412	0.0208342	0.0226770	0.0246827
0.0268558	0.0292420	0.0318283	0.0346434	0.0377075	0.0410427	0.0446728	0.0486239	0.0529246	0.0576056
0.0627006	0.0682463	0.0742825	0.0808525	0.0880037	0.0957873	0.1042594	0.1134809	0.1235179	0.1344427
0.1463338	0.1592766	0.1733641	0.1886977	0.2053874	0.2235534	0.2433260	0.2648476	0.2882726	0.3137696
0.3415218	0.3717286	0.4046071	0.4403938	0.4793458	0.5217432	0.5678907	0.6181200	0.6727923	0.7323007
0.7970729	0.8675748	0.9443132	1.0278402	1.1187564	1.2177159	1.3254307	1.4426758	1.5702951	1.7092076
1.8604136	2.0250025	2.2041607	2.3991803	2.6114685	2.8425585	3.0941206	3.3679751	3.6661060	3.9908764
4.3440452	4.7287861	5.1477082	5.6038787	6.1006493	6.6416846	7.2309951	7.8729739	8.5724389	9.3346813
10.1655212	11.0713734	12.0593235	13.1372195	14.3137808	15.5987310	17.0029605	18.5387287	20.2199191	22.0623639
24.0842669	26.3067595	28.7546468	31.4574435	34.4507929	37.7785623	41.49559188	45.6740945	50.4080772	55.8297467
62.1319835	69.6173685	78.8107748	90.7798193	108.4698082	179.9974296				

Table 5.1.2-2. Template Parameters for the 125-Ring Equal Contribution Template with $\psi_0 R = 235$ meters.

radius in these tables should be exactly 180°, rather than the values shown which resulted from the termination criteria used in the Newton iteration scheme. The termination criteria worked very well for all spherical ring radii except the last.

5.1.3 Other Templates

Two templates have been developed by, and are in use at, the Defense Mapping Agency Aerospace Center, St. Louis, Missouri. While the templates are not of the bull's-eye type but are rather of the rectangular grid type, they may be "converted" to bull's-eye type by determining what their form would be if the point of evaluation were the north pole (of the earth) and the spherical radius ψ and spherical azimuth α were identified with colatitude and longitude (on the earth) respectively. In the following sections, this technique will be called "circularization".

5.1.3.1 The Circularized AGEMIT Template

When the circularization process is applied to the surface rectangular grid template employed in the DMAAC AGEMIT computer program, a template with 101 rings is obtained, excluding any inner zone. The rings in this template fall naturally into four groups according to the spherical radius increment between rings. The values of the increments and the starting and terminating index and radius for each group are given in Table 5.1.3-1.

RING GROUP	RING BOUNDARY RADII GROUPS				
	i_{START}	i_{END}	$\psi_{i_{START}}$	$\psi_{i_{END}}$	INCREMENT
I	0	35	5'	3°0'	5'
II	35	51	3°0'	7°0'	15'
III	51	69	7°	25°	1°
IV	69	101	25°	180°	5°

Table 5.1.3-1. Template Parameters for the Circularized AGEMIT Template.

5.1.3.2 The "Rice-DMAAC" Template

This 125-ring template is a combination of modified forms of the Rice Inner Zone template and the circularized AGEMIT template. In the modified Rice template, the first five and the last sixteen rings have been omitted, so that the initial radius corresponds to 235 meters and the final radius to 92,220 meters. An earth radius of 6,371,032 meters is assumed implying that the last spherical ring boundary radius is about 0.829° . In the modified form of the circularized AGEMIT template, the ring boundary radii less than 1° are omitted.

A listing of the actual numerical values of the spherical ring boundary radii of this template is given in Table 5.1.3-2.

5.2 Examples of Spectra

In this section, examples are presented of calculations of actual spectra both for theoretical integral transformations and for discrete summation transformations based on some of the templates described in the previous section. It will be seen that just as the summation transformation is an approximation to the integral transformation in the spatial domain so is the spectrum of the summation transformation an approximation to the spectrum of the integral transformation in the frequency domain. It will also be seen that the values of the template parameters greatly affect the closeness of the approximation in the frequency domain just as it is obvious that they do in the spatial domain.

5.2.1 Stokes' Transformation

Plots have been generated of the spectra of the discrete Stokes' summation transformation for two templates, namely the 34-ring Pick-Picha-Vyskocil template and the 101-ring circularized DMAAC template, as well as of the spectra of the continuous (theoretical) Stokes' integral transformation. The plots show the fundamental characteristics of the spectra, specifically that the spectrum of the summation transformation is "close" to that of the integral transformation but not exactly equal to it. The plots are presented in Figures 5.2.1-1 and 5.2.1-2.

SPHERICAL RING RADII PSI (DEGREES)													
0.0021134	0.0025091	0.0029767	0.0035343	0.0041998	0.0049822	0.0059085	0.0070147	0.0083277	0.0098835				
0.0117271	0.0139124	0.0165115	0.0195961	0.0232563	0.0275910	0.0327441	0.0386505	0.0460900	0.0546875				
0.0648947	0.0769815	0.0912807	0.1083677	0.1285124	0.1523443	0.1806728	0.2143073	0.2540571	0.3010914				
0.3567591	0.4226790	0.5005599	0.5926500	0.7011975	0.8293502	1.0000000	1.0833330	1.1666660	1.2500000				
1.3333330	1.4166660	1.5000000	1.5833330	1.6666660	1.7500000	1.8333330	1.9166660	2.0000000	2.0833330				
2.1666660	2.2500000	2.3333330	2.4166660	2.5000000	2.5833330	2.6666660	2.7500000	2.8333330	2.9166660				
3.0000000	3.2500000	3.5000000	3.7500000	4.0000000	4.2500000	4.5000000	4.7500000	5.0000000	5.2500000				
5.5000000	5.7500000	6.0000000	6.2500000	6.5000000	6.7500000	7.0000000	7.2500000	7.5000000	7.7500000				
11.0000000	12.0000000	13.0000000	14.0000000	15.0000000	16.0000000	17.0000000	18.0000000	19.0000000	20.0000000				
21.0000000	22.0000000	23.0000000	24.0000000	25.0000000	30.0000000	35.0000000	40.0000000	45.0000000	50.0000000				
55.0000000	60.0000000	65.0000000	70.0000000	75.0000000	80.0000000	85.0000000	90.0000000	95.0000000	100.0000000				
105.0000000	110.0000000	115.0000000	120.0000000	125.0000000	130.0000000	135.0000000	140.0000000	145.0000000	150.0000000				
155.0000000	160.0000000	165.0000000	170.0000000	175.0000000	180.0000000								

Table 5.1.3-2. Template Parameters for the 125-Ring "Rice-DMAAC" Template.

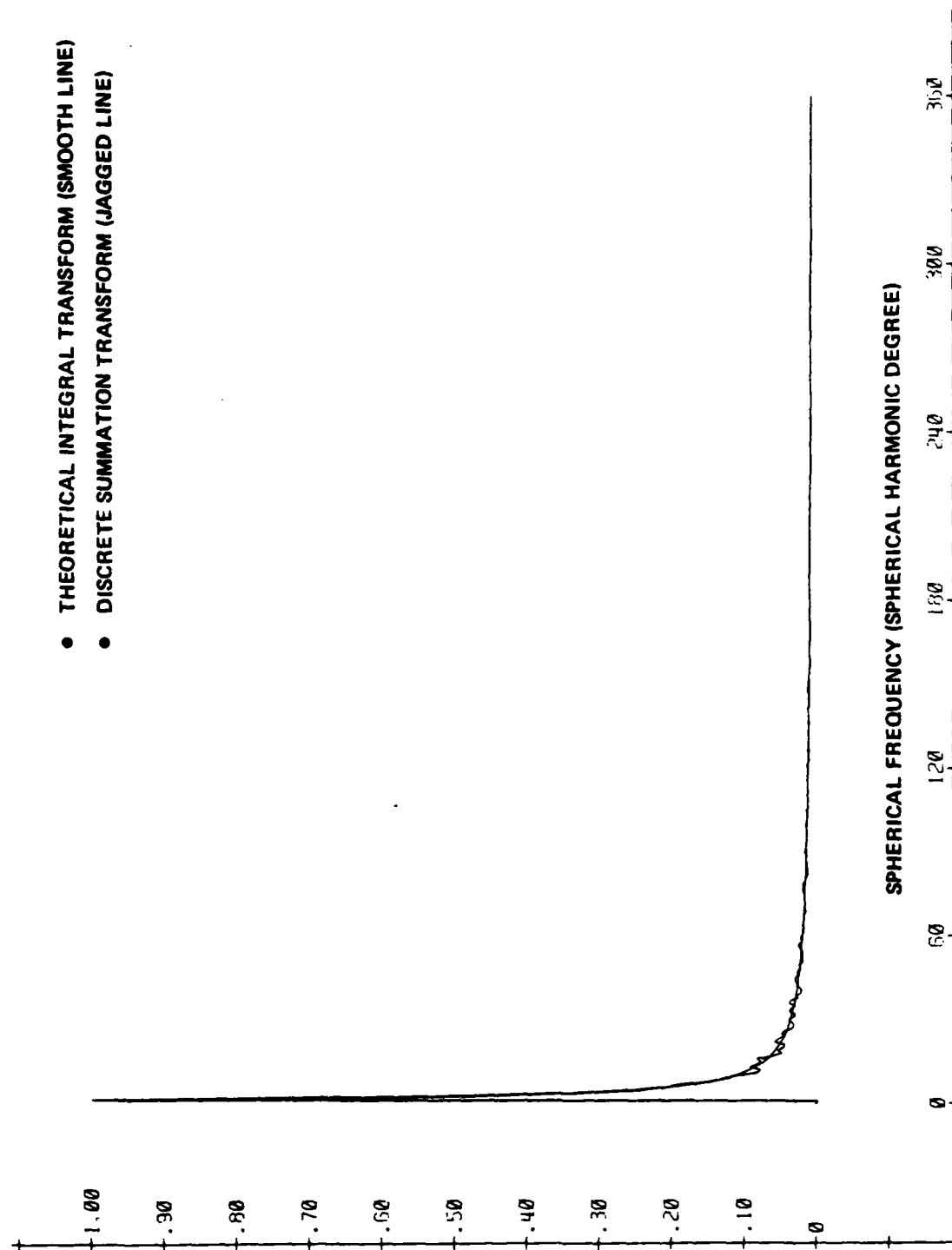


Figure 5.2.1-1a. Spectra of Stokes' Transformation (34-Ring Pick-Picha-Vyskocil Template).

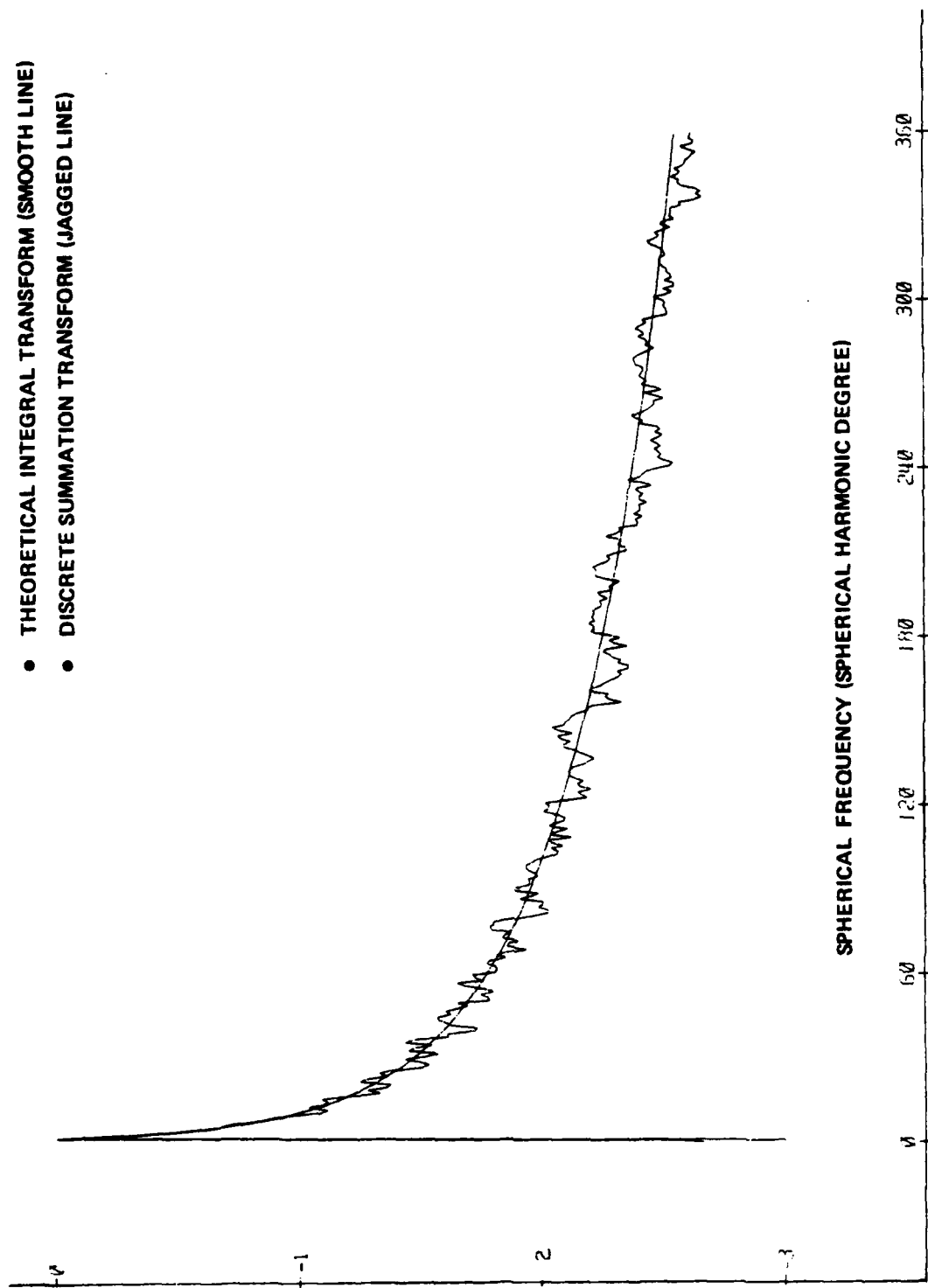


Figure 5.2.1-lb. Log Spectra of Stokes Transformation (34-Ring Pick-Picha-Vyskocil Template).

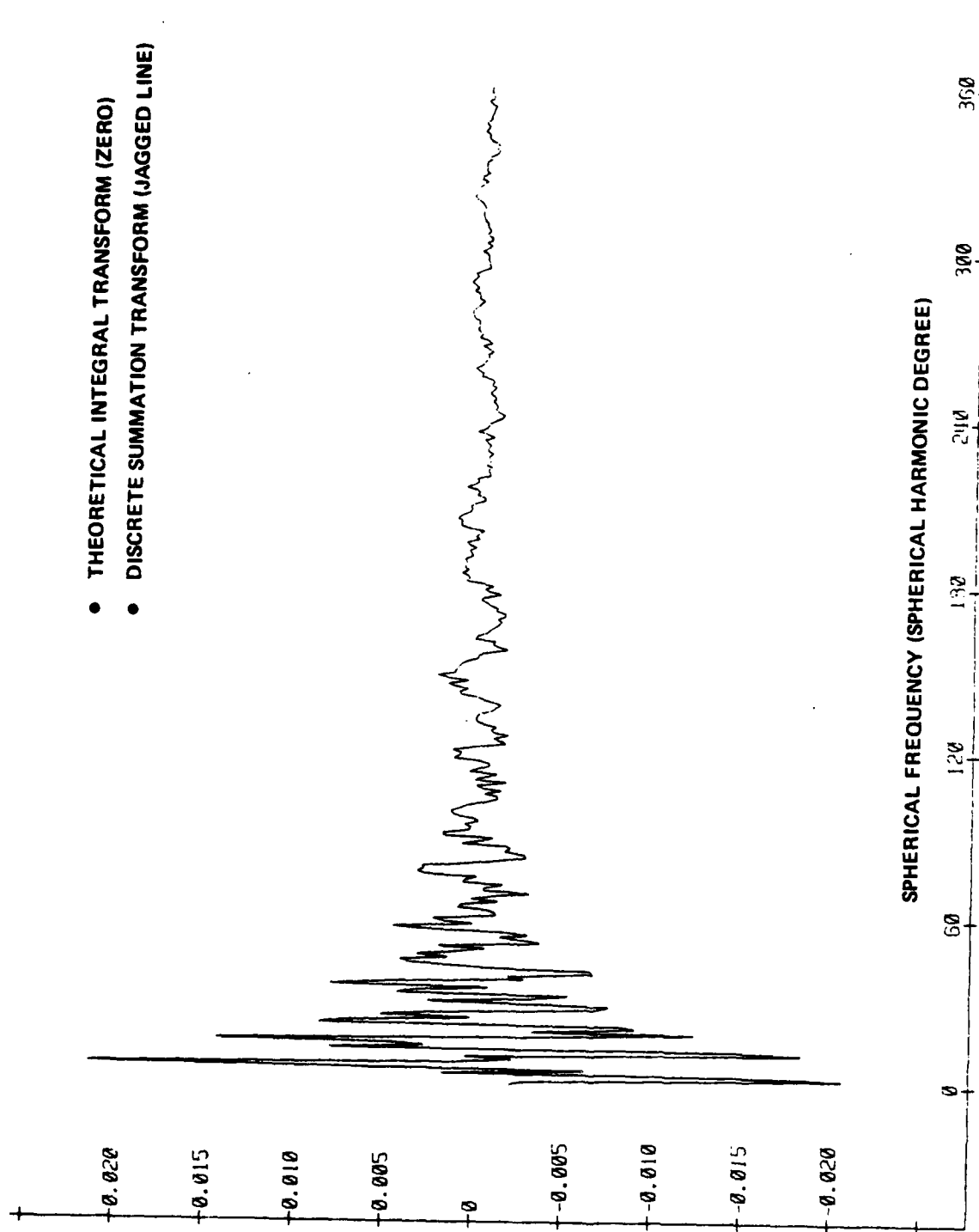


Figure 5.2.1-1c. Difference in Spectra of Stokes' Transformation (34-Ring Pick-Picha-Vyskocil Template).

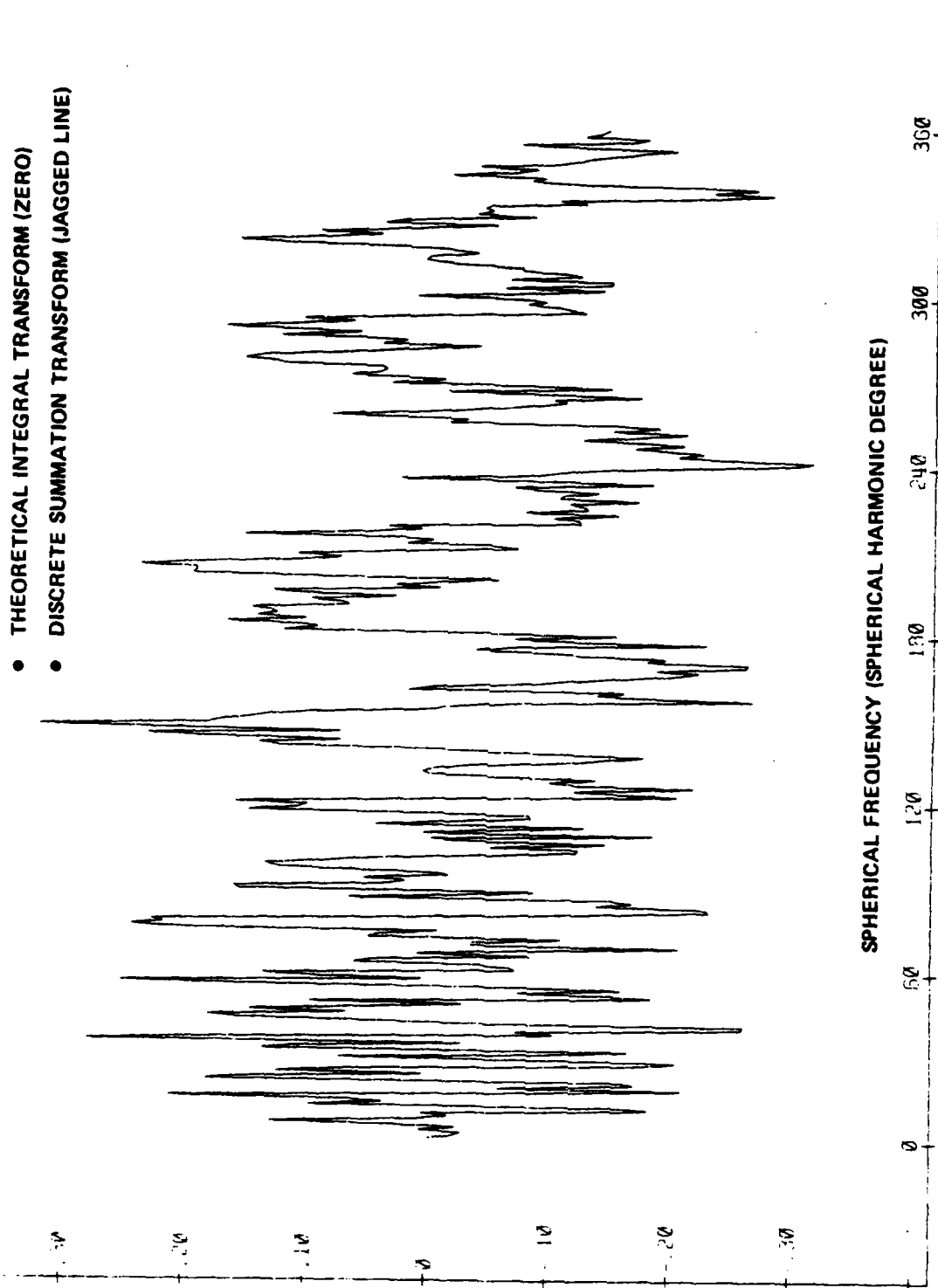


Figure 5.2.1-1d. Relative Difference in Spectra of Stokes' Transformation (34-Ring Pick-Pichavyskocil Template).

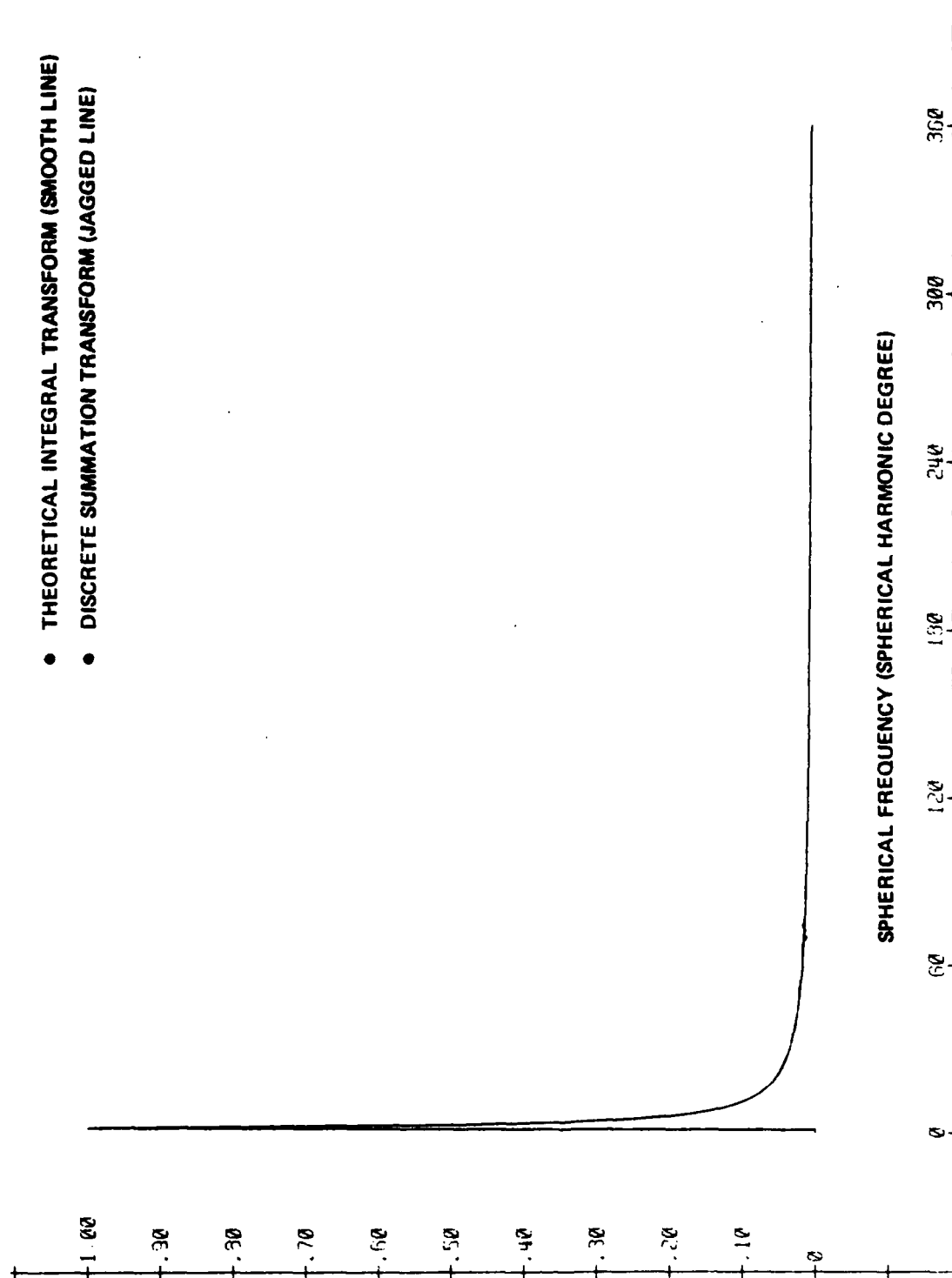


Figure 5.2.1-2a. Spectra of Stokes' Transformation (101-Ring Circularized AGEMIT Template).

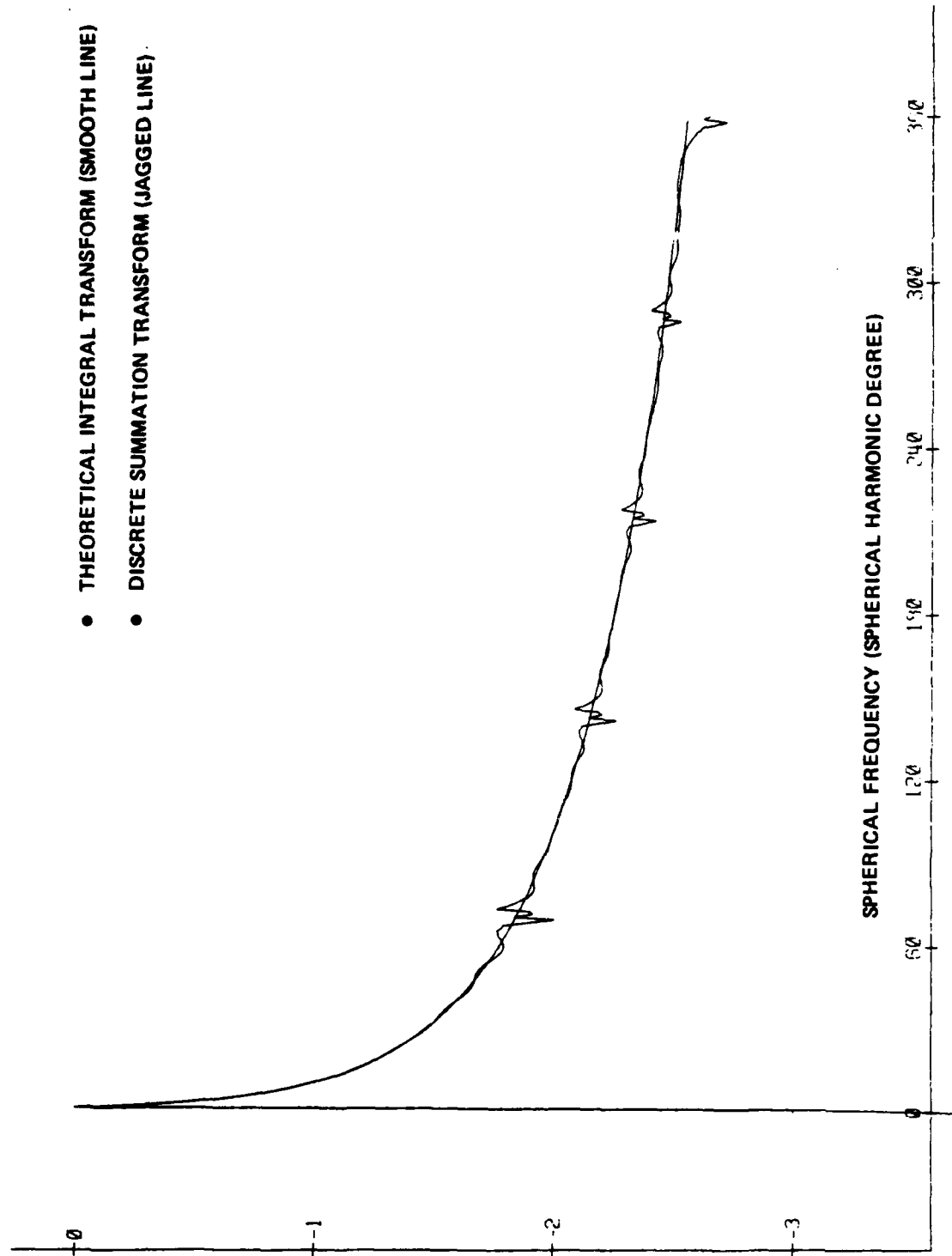


Figure 5.2.1-2b. Log Spectrum of Stokes' Transformation (101-Ring Circularized AGEMIT Template).

- THEORETICAL INTEGRAL TRANSFORM (ZERO)
- DISCRETE SUMMATION TRANSFORM (JAGGED LINE)

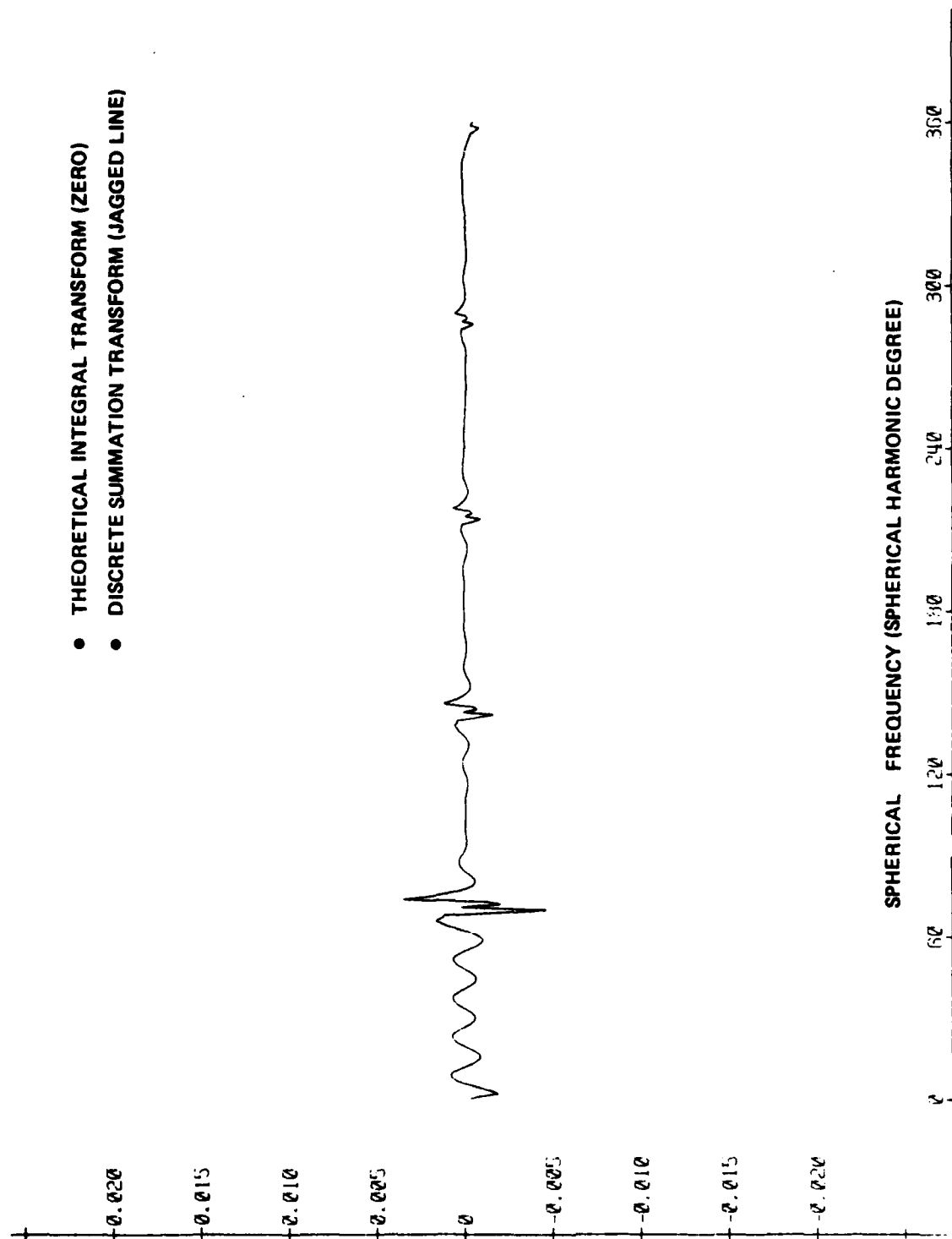


Figure 5.2.1-2c. Difference in Spectra of Stokes' Transformation (101-Ring Circularized AGEMIT Template).

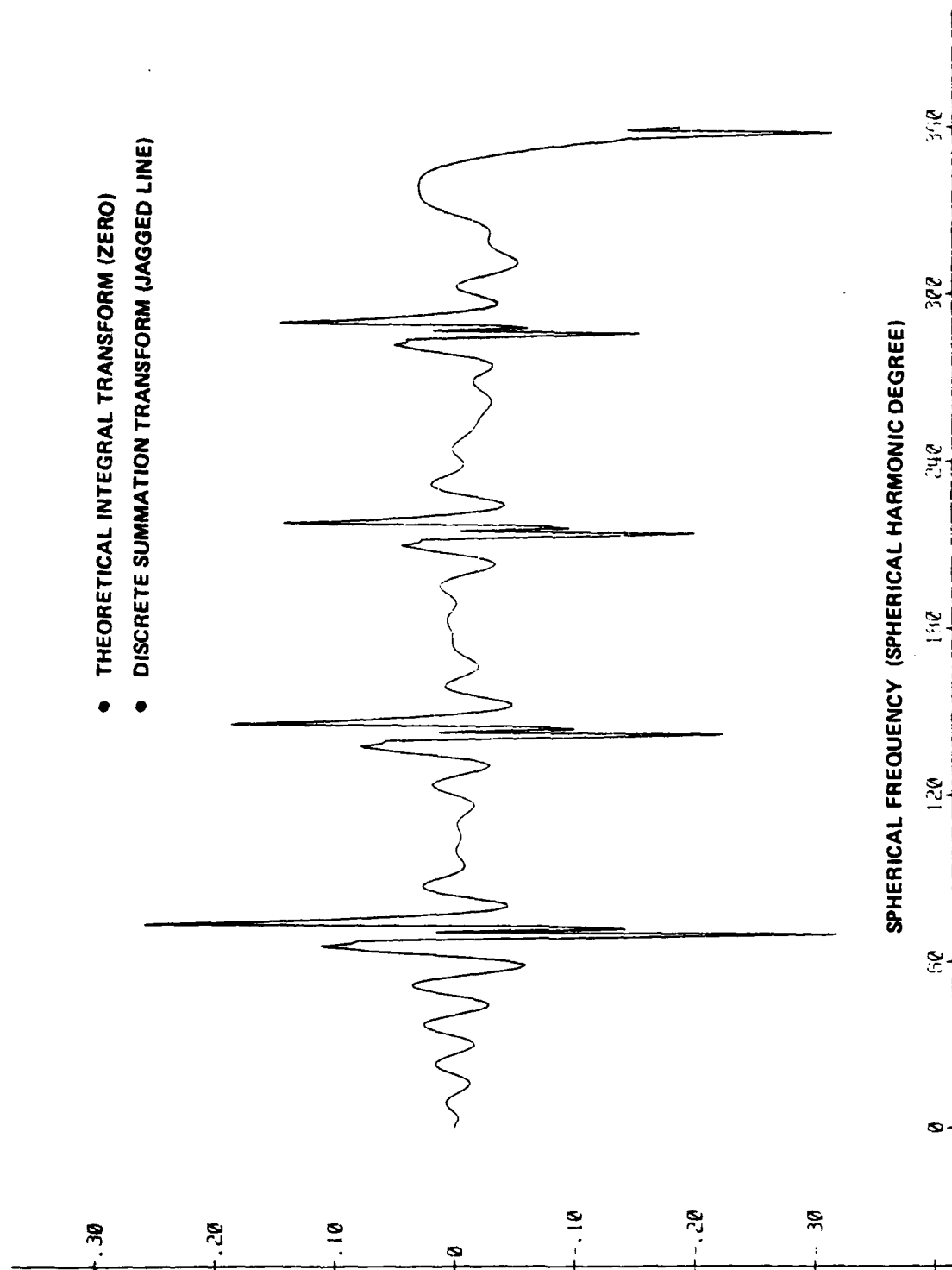


Figure 5.2.1-2d. Relative Difference in Spectra of Stokes' Transformation (101-Ring Circularized AGEMIT Template).

The plots of the spectra are presented in four ways for each template:

- a) The actual values of the spectra of the theoretical and the discrete are plotted on a linear scale.
- b) The actual values of the spectra of the theoretical and the discrete are plotted on a logarithmic scale.
- c) The difference of the spectrum of the discrete summation from the spectrum of the continuous integral is plotted on an enlarged linear scale.
- d) The relative difference of the spectrum of the discrete summation from the spectrum of continuous integral is plotted on an enlarged linear scale. The relative difference is the actual difference divided by the "true" value, which is the value of the continuous integral transformation spectrum in this case. These plots are useful for quickly determining percentage errors.

5.2.2 Vening-Meinesz' Transformation

Plots have not yet been generated of the spectra of the discrete Vening-Meinesz' summation transformation for various templates. However, many computer-generated tabular listings of the spectral values and other associated quantities have been made during the course of this work. Excerpts of two representative listings for the analog of the Vening-Meinesz' transformation on surface layer densities are presented in Figures 5.2.2-1 and 5.2.2-2. Plots of these data would have many of the same features as the plots of the Stokes' spectra in the previous section.

In the figures, the following information is provided by columns:

N: Spherical Frequency (Spherical Harmonic Degree)

ACTUAL SPECTRUM: The numerical value of the spectrum of the discrete summation transformation for the specified spherical frequency.

IDEAL SPECTRUM: The numerical value of the spectrum of the theoretical integral transformation for the specified spherical frequency.

RESIDUAL SPECTRUM: The difference between the actual and ideal spectra.

WEIGHT: The power spectrum of the input to the transformation; specifically, the Tscherning-Rapp degree variances for surface layer densities.

SIGMA(N): The square root of the residual power spectrum of the output of the transformation. This quantity is the product of the square of the residual spectrum and the weight. It is the global rms value of the error in the output of the transformation which is introduced by using the summation rather than the integral for the specified frequency.

SIGMA(N) CUM: The cumulative value of SIGMA(N) up to and including the specified frequency, where cumulative is interpreted in a root-sum-square sense.

N	ACTUAL SPECTRUM	IDEAL SPECTRUM	RESIDUAL SPECTRUM	(mgal ²) WEIGHT	(mgal) SIGMA(N)	(mgal) SIGMA(N) CUM
1	0.931133669627	0.9422660225592	-0.0091320537031	0.02250	0.00137	0.00137
2	0.9268272021619	0.9788953606687	-0.0520681581700	0.75000	0.36065	0.36065
3	1.0418275581510	0.9884131994111	0.0534143559635	96.59352	0.52497	0.63691
4	0.9021409346350	0.9920908130345	-0.0099498778582	51.32411	0.07128	0.64089
5	0.983793988351	0.9937560932788	-0.0099620930851	37.01279	0.06061	0.64375
6	0.9826748933681	0.9945486071942	-0.0118737109005	29.98342	0.06502	0.64702
7	1.0114273394706	0.9949019203693	0.0165254175663	25.75403	0.08366	0.65244
8	1.001094980475	0.9950102884364	0.000846917331	22.78462	0.02911	0.65309
9	0.9905245431492	0.9949713234804	-0.004467784464	20.79462	0.02020	0.65340
10	0.97846008409	0.9948384435176	-0.0160924345255	19.17665	0.07047	0.65719
11	0.747919136530	0.9946428500072	0.0001490636350	17.86884	0.00063	0.65719
12	1.006022958347	0.9944038337364	0.0116190724075	16.80082	0.04763	0.65991
13	1.007620242583	0.9941338451545	-0.0134941786528	15.88904	0.05379	0.66110
14	0.988977466898	0.9938410320882	-0.0048932862910	15.10197	0.01902	0.66138
15	0.9781391241718	0.9935311326433	-0.0149920061231	14.42229	0.05691	0.66382
16	0.9807597310594	0.9932081641395	-0.0124843006133	13.88048	0.04624	0.66543
17	0.9975544489283	0.9928750292130	0.0047194175422	13.25216	0.01710	0.66565
18	1.0060010994512	0.9925338673747	0.0134672299027	12.75648	0.04810	0.66739
19	1.0039171955851	0.9921862836918	0.0117308087647	12.30510	0.04115	0.66866
20	0.991653613768	0.9918335013377	0.0000201110379	11.89144	0.00007	0.66866
21	0.9851157649296	0.9914764656573	-0.0063606934913	11.51030	0.02158	0.66900
22	0.9824043870180	0.9911159165903	-0.0087115280330	11.15741	0.02910	0.66964
23	0.9340550768625	0.9907524399901	-0.0066973504262	10.85933	0.02204	0.67000
24	0.9838276892353	0.9903865045836	-0.006568131547	10.52316	0.02120	0.67034
25	0.987620923227	0.9900184809379	-0.0023975626100	10.23649	0.00767	0.67038
26	0.9943584448740	0.9896487017262	0.0047197416425	9.98727	0.01490	0.67055
27	1.0030122309957	0.9892773955430	0.0137308324060	9.71376	0.04281	0.67191
28	1.0033316532666	0.9890047822964	0.0144760692553	9.47447	0.04456	0.67339
29	0.9953912808249	0.9885310346932	0.0068602450192	9.24809	0.02086	0.67371
30	0.9824691048999	0.9881563000528	-0.0056871920824	9.03349	0.01709	0.67393
1820	0.4806042189468	0.4816112027101	-0.0010069036862	0.29571	0.00055	0.75413
1821	0.480443699853	0.4812843558556	-0.0008406857975	0.29550	0.00046	0.75413
1822	0.4802766747651	0.4809576494733	-0.0006809746867	0.29530	0.00037	0.75413
1823	0.4801180951649	0.4806309336200	-0.0005128984340	0.29509	0.00028	0.75413
1824	0.4799658185327	0.4803044183520	-0.0003305997843	0.29499	0.00018	0.75413
1825	0.4798102709071	0.4799779237262	-0.0001676528191	0.29460	0.00009	0.75413
1826	0.4796499123361	0.4796515097991	-0.0000015974629	0.29448	0.00000	0.75413
1827	0.4794947490238	0.4793251766273	0.0001695723913	0.29428	0.00009	0.75413
1828	0.4793494182149	0.4789989242675	0.0003504939377	0.29407	0.00019	0.75413
1829	0.4792040687562	0.4786727527762	0.0005313158035	0.29197	0.00029	0.75413
1830	0.4790435926787	0.4783466622100	0.0006970304530	0.29367	0.00036	0.75413

Figure 5.2.2-1. Spectra of the Vening-Meinesz' Transformation (23-Ring Equal Contribution Template with $\psi_0 = 0.044^\circ$).

N	ACTUAL SPECTRUM	IDEAL SPECTRUM	RESIDUAL SPECTRUM	(mgal ²) WEIGHT	(mgal) SIGMA(N)	(mgal) SIGMA(N) CUM
1	0.9380893352946	0.9427829594510	-0.0046936233322	0.02250	0.00070	0.00070
2	0.9787351931740	0.9797507215370	-0.0010155283380	47.50000	0.00700	0.00700
3	0.9975915808385	0.9896794306982	0.0079121477902	96.59352	0.07776	0.07808
4	0.9322894474659	0.9937255110595	-0.0614360600710	51.32411	0.08193	0.11318
5	1.0050699130261	0.9957581798047	0.0093117319047	37.01279	0.05665	0.12656
6	0.9928960395101	0.9969175071845	-0.0040214657784	29.98362	0.02202	0.12846
7	0.9973264099035	0.9976372894750	-0.0003108754335	25.75403	0.00150	0.12847
8	0.9990252652526	0.9981119041832	0.0009133808760	22.88992	0.00437	0.12855
9	0.9997336044657	0.9984390336943	0.0012945707422	20.79462	0.00590	0.12868
10	0.9954361763071	0.9986721394258	-0.0032359629404	19.17665	0.01417	0.12946
11	1.0014201539672	0.9989424810777	0.002576727125	17.87684	0.01090	0.12992
12	0.998563176790	0.998693286009	-0.000130109158	16.80082	0.00046	0.12992
13	0.9977083407738	0.9990650859021	-0.0013567449059	15.80904	0.00541	0.13003
14	0.9992986076086	0.9991380305305	0.001605770667	15.10197	0.00062	0.13003
15	1.0012229076212	0.9991938577876	0.0020290496759	14.41229	0.00770	0.13026
16	0.9970427052219	0.9992365904265	-0.0021938851569	13.80048	0.00815	0.13052
17	0.9991801725020	0.9992691352631	-0.000089627554	13.25216	0.00032	0.13052
18	1.0309899768200	0.9992936350695	0.0016963416710	12.75648	0.00606	0.13056
19	0.9990400359127	0.9993116974932	-0.0002716614399	12.30510	0.00095	0.13066
20	0.9972275890422	0.9993245477729	-0.0020969586913	11.59144	0.00723	0.13086
21	1.0010135900966	0.9993331329238	0.0016804570332	11.51030	0.00570	0.13099
22	1.0002755188305	0.9993381942489	0.000371244829	11.15741	0.00313	0.13102
23	0.9977786508319	0.9993403187227	-0.0015616677701	10.82933	0.00514	0.13112
24	0.9986157196099	0.9993399760011	-0.0007242562715	10.52316	0.00235	0.13114
25	1.0012364629690	0.999375454751	0.0018989173695	10.23649	0.00608	0.13129
26	0.9992123444715	0.9993333363170	-0.0001209918410	9.96727	0.00033	0.13129
27	0.9981728580989	0.9993276825172	-0.0011547442991	9.71376	0.00360	0.13134
28	0.9992068124611	0.9993205542954	-0.0001137418294	9.47447	0.00035	0.13134
29	1.0002488783297	0.9993123668495	0.000365116712	9.24809	0.00285	0.13137
30	0.9993937854830	0.9993031871313	0.0000955983414	9.03349	0.00029	0.13137
1420	0.9734125585112	0.9736048655185	-0.0003923068239	0.29571	0.00021	0.13329
1421	0.9734200588344	0.9737864290562	-0.0003663701937	0.29550	0.00020	0.13329
1422	0.9734413873986	0.9737679926626	-0.0003266050480	0.29530	0.00018	0.13329
1423	0.9734612370162	0.9737495562478	-0.0002803190755	0.29509	0.00016	0.13329
1424	0.9734844377943	0.9737311198417	-0.0002466819715	0.29489	0.00013	0.13329
1425	0.9735160153435	0.9737126834444	-0.0001966680866	0.29468	0.00011	0.13329
1426	0.9735440326780	0.9736942470558	-0.0001502143714	0.29448	0.00008	0.13329
1427	0.9735701357897	0.9736758106760	-0.0001056738838	0.29428	0.00006	0.13329
1428	0.9736029778074	0.9736573743050	-0.0000543964852	0.29407	0.00003	0.13329
1429	0.9736336035603	0.9736389379427	-0.0000053343820	0.29387	0.00000	0.13329
1430	0.9736546402500	0.9736205015893	0.0000341386476	0.29367	0.00002	0.13329

Figure 5.2.2-2. Spectra of the Vening-Meinesz' Transformation (125-Ring Equal Contribution Template with $\psi_0 = 0.0021134^\circ = 235$ meters.

SECTION 6

TEMPLATE OPTIMIZATION METHODS FOR DISCRETE SUMMATION TRANSFORMATIONS

6.1 Introduction

In the previous chapters on the spectral theory of discrete summation transformations, it was shown both by analytical expressions and by numerical examples that the spectrum of such a transformation depends parametrically upon the values of the spherical ring boundary radii and the spherical compartment boundary azimuths of the underlying bull's-eye template. Several reasonable ways of selecting the values of these parameters were described under the general concept of the equal contribution of subdivisions of a spherical surface.

In this chapter a method is presented for iteratively deriving the "best" or "optimal" values of these parameters for any transformation. The method is based upon incrementally adjusting the values of the parameters until a particular scalar function of them, the global rms discretization error, has been minimized. The number of rings and the number of compartments in each ring are chosen a priori and held constant during the iterative process.

The minimization of the global rms discretization error is equivalent to the process of making the spectrum of the discrete summation transformation approximate as well as possible the spectrum of the theoretical integral transformation in a weighted least-squares sense. This process of adjusting the parameters in a linear shift-invariant transformation so that its approximate spectrum agrees as well as possible with an ideal spectrum is known in engineering terminology as digital filter design. Hence the derivation of optimal discrete summation approximations to geodetic integral transformations may be called spherical geodetic digital filter design.

To illustrate ideas, an example of the intermediate results of such a filter design computation is presented in Figure 6.1-1. Here the figure-of-merit, namely the global rms discretization error in the

total horizontal gravity disturbance, is decreased at each iteration from an initial value of 0.754 mgal to a final value of 0.519 mgal by means of the incremental adjustment of the spherical ring boundary radii numbered 9 through 22. (The reason that the radii numbered 1 through 8 were not adjusted will be explained in Section 6.3.3 and Appendix E). It is seen in the figure that the radii parameters change gradually during the course of the computation with larger changes occurring in the larger radii. These radii are more directly related to the low frequencies for which the input power spectral density is greater, and thereby have a greater effect upon the total rms discretization error.

SUMMARY OF COMPLETE RUN

	ITER# 1	ITER# 2	ITER# 3	ITER# 4	ITER# 5	ITER# 6	ITER# 7	ITER# 8	ITER# 9	ITER#10
FIGURE OF MERIT	7.54E-01	6.63E-01	6.09E-01	5.78E-01	5.59E-01	5.46E-01	5.36E-01	5.29E-01	5.24E-01	5.19E-01

VALUES OF PARAMETERS

RING#	SPHERICAL RING RADII (DEGREES)									
0	0.044	0.044	0.044	0.044	0.044	0.044	0.044	0.044	0.044	0.044
1	0.061	0.061	0.061	0.061	0.061	0.061	0.061	0.061	0.061	0.061
2	0.085	0.085	0.085	0.085	0.085	0.085	0.085	0.085	0.085	0.085
3	0.118	0.118	0.118	0.118	0.118	0.118	0.118	0.118	0.118	0.118
4	0.164	0.164	0.164	0.164	0.164	0.164	0.164	0.164	0.164	0.164
5	0.228	0.228	0.228	0.228	0.228	0.228	0.228	0.228	0.228	0.228
6	0.316	0.316	0.316	0.316	0.316	0.316	0.316	0.316	0.316	0.316
7	0.439	0.439	0.439	0.439	0.439	0.439	0.439	0.439	0.439	0.439
8	0.610	0.610	0.610	0.610	0.610	0.610	0.610	0.610	0.610	0.610
9	0.847	0.843	0.849	0.850	0.850	0.851	0.851	0.852	0.852	0.853
10	1.177	1.177	1.177	1.178	1.178	1.178	1.178	1.179	1.179	1.179
11	1.634	1.635	1.635	1.635	1.635	1.635	1.635	1.636	1.636	1.636
12	2.270	2.271	2.271	2.271	2.271	2.271	2.271	2.271	2.271	2.271
13	3.154	3.154	3.155	3.155	3.155	3.155	3.155	3.155	3.155	3.155
14	4.382	4.383	4.383	4.383	4.384	4.384	4.384	4.384	4.384	4.384
15	6.091	6.092	6.092	6.092	6.093	6.093	6.093	6.093	6.093	6.093
16	8.470	8.471	8.472	8.472	8.472	8.472	8.472	8.472	8.472	8.471
17	11.790	11.792	11.792	11.793	11.793	11.792	11.792	11.791	11.791	11.790
18	16.445	16.445	16.445	16.444	16.443	16.442	16.441	16.440	16.439	16.439
19	23.031	23.018	23.010	23.005	23.003	23.004	23.007	23.012	23.020	23.030
20	32.523	32.450	32.427	32.434	32.463	32.510	32.571	32.645	32.729	32.822
21	46.780	46.527	46.744	47.207	47.785	48.408	49.033	49.636	50.204	50.728
22	70.639	74.568	77.654	80.082	82.030	83.622	84.943	86.054	86.997	87.804
23	179.932	179.932	179.932	179.932	179.932	179.932	179.932	179.932	179.932	179.932

Figure 6.1-1. Example of Iterative Decrease of the Discretization Error.

The global rms discretization error is only one of a number of scalar quantities which could be chosen as a figure-of-merit of the accuracy of the summation approximation to the theoretical integral transformation. The global maximum discretization error, namely the maximum error in the output of summation transformation over the whole sphere, is another such quantity. Both of these discretization error types have the distinct advantage of possessing a useful physical interpretation. However, the rms error has the additional advantage of being closely related to spectral quantities of the transformation through the Parseval Theorem, and hence of being easy to compute when the residual spectrum and input power spectral density are known. The global rms discretization error and its properties will now be described.

6.2 Global RMS Discretization Error

The global rms discretization error of a discrete summation transformation is the global rms value of the error in the output of the transformation due solely to the use of the summation approximation rather than the rigorously correct integral expression. The rms discretization error depends upon the strengths of the various spherical harmonic frequencies which occur in the input to the transformation; a nominal model such as the Tscherning-Rapp degree variance model is assumed. The term "global" means that the root-mean-square is taken over the whole surface of the (unit) sphere.

The global rms discretization error is given by

$$\left\{ f_{\text{OUT}}^{\text{APPROX}} - f_{\text{OUT}} \right\}_{\text{rms}} = \left[\iint \left[f_{\text{OUT}}^{\text{APPROX}} - f_{\text{OUT}} \right]^2 \frac{d\sigma}{4\pi} \right]^{\frac{1}{2}}$$

By the Parseval Theorem, it is known that

$$\left\{ f_{\text{OUT}} \right\}_{\text{rms}}^2 = \sum_{n=0}^{\infty} |\lambda_n|^2 \left\{ f_{\text{IN}(n)} \right\}_{\text{rms}}^2$$

and

$$\left\{ f_{\text{OUT}}^{\text{APPROX}} \right\}_{\text{rms}}^2 = \sum_{n=0}^{\infty} |\lambda_n^{\text{APPROX}}|^2 \left\{ f_{\text{IN}(n)} \right\}_{\text{rms}}^2$$

Similarly, for the difference transformation

$$\left\{f_{\text{OUT}}^{\text{APPROX}} - f_{\text{OUT}}\right\}_{\text{rms}}^2 = \sum_{n=0}^{\infty} \left| \lambda_n \left\{K^{\text{APPROX}} - K\right\} \right|^2 \left\{f_{\text{IN}(n)}\right\}_{\text{rms}}^2$$

where $\lambda_n \left\{K^{\text{APPROX}} - K\right\}$ is the spectrum of the difference transformation. But by the linear property of the spectrum,

$$\begin{aligned} \lambda_n \left\{K^{\text{APPROX}} - K\right\} &= \lambda_n \left\{K^{\text{APPROX}}\right\} - \lambda_n \left\{K\right\} \\ &= \lambda_n^{\text{APPROX}} - \lambda_n \end{aligned}$$

So the global rms discretization error is

$$\left\{f_{\text{OUT}}^{\text{APPROX}} - f_{\text{OUT}}\right\}_{\text{rms}} = \left[\sum_{n=0}^{\infty} \left| \lambda_n^{\text{APPROX}} - \lambda_n \right|^2 \sigma_n^2 \left\{f_{\text{IN}}\right\} \right]^{1/2}$$

6.2.1 Examples

The global rms discretization errors for a number of specific templates are presented in Table 6.2-1 for the Stokes' transformation and in Table 6.2-2 for the Vening-Meinesz' transformation.

The following points may be observed from these tables:

For the discrete Stokes' transformation:

- a) The global rms geoid height discretization error is substantially lower in the analog transformation from mean surface layer densities to geoid height than in the classical transformation from mean gravity anomalies to geoid height for the 34-ring template, even though the input power spectral density for surface layer density is larger for each frequency than that for gravity anomalies.
- b) The 66-ring Equal Ring Contribution Template seems to have a relatively large discretization error for a template with this many rings. The 34-ring Pick-Picha-Vyskocil template has a slightly lower absolute error for a more gross partition of the spherical surface.

- c) As the number of rings increases, the contribution of the higher frequencies (above spherical harmonic degree 30) becomes relatively greater.

For the discrete Vening-Meinesz' transformation analog which converts mean surface layer densities to deflections:

- a) The 125-ring Rice/AGEMIT template has a discretization error almost half that of the 125-ring equal ring contribution template.
- b) The reduction of the value of the truncation radius ψ_0 towards zero does not necessarily decrease the discretization error. This would imply that there may perhaps exist an optimum (non-zero) value of ψ_0 .

Table 6.2-1. Discretization Error of Various Templates for Stokes' Transformation.

Type	# Rings	Max Degree	rms Error
CLASSICAL STOKES			
Pick-Picha-Vyskocil	34	30	1.29 m
Pick-Picha-Vyskocil	34	1440	1.34 m
Equal Ring Contribution	66	30	1.30 m
Equal Ring Contribution	66	1440	1.64 m
Circularized AGEMIT	101	30	0.108 m
Circularized AGEMIT	101	1440	0.165 m
ANALOG STOKES			
Pick-Picha-Vyskocil	34	30	0.668 m
Pick-Picha-Vyskocil	34	1500	0.689 m

The "RMS ERROR" column gives the global rms discretization error in the geoid height.

Table 6.2-2. Discretization Error of Various Templates for Vening-Meinesz' Transformation.

Type	# Rings	ψ_0 (deg)	Max Degree	rms Error
Pick-Picha-Vyskocil	23	10^{-5}	30	0.445 mgal
Pick-Picha-Vyskocil	23	0.030	1440	0.714 mgal
Equal Ring Contribution	23	0.044	1440	0.754 mgal
Circularized AGEMIT	101	0.030	1440	1.115 mgal
RICE/AGEMIT	125	0.002	1440	0.075 mgal
Equal Ring Contribution	125	0.002	1440	0.133 mgal
Equal Ring Contribution	125	0.001	1440	0.145 mgal

The "RMS ERROR" column gives the global rms discretization error in the total horizontal gravity disturbance.

6.3 Optimization Algorithm

There are a number of algorithms which could be used to determine the values of the template parameters which minimize the global rms discretization error under the inequality constraints that the ring boundary radii and the compartment boundary azimuths must not overlap. Descriptions of such algorithms may be found, for example, in the constrained minimization sections of Luenberger (1973, Part III), Lawson and Hanson (1974, Chapter 23), Dornby (1975, Chapters 7 and 8), and Avriel (1977, Part II). A survey of recent developments in optimization theory is given in Jacobs (1977, Part III).

Under the present effort, however, a simple and quickly implementable algorithm has been employed, namely a Gauss-Newton* scheme to perform an unconstrained minimization step, followed by a "projection" technique to force the satisfaction of inequality constraints. Due to certain convergence difficulties with this algorithm, three simple and also easily implementable variations of it were experimented with additionally. This section describes the main algorithm and the variations.

While neither the algorithm nor the variations provided reductions of several orders of magnitude in the rms discretization error as had

*The Gauss-Newton algorithm is well-known in satellite orbit determination work as "differential correction".

been hoped, the algorithm and the variations did possess sufficient computational power to demonstrate that the spectral theory of spherical geodetic operators as described in the earlier chapters of this document is valid and that it is feasible to derive improved values of the template parameters by means of this theory.

6.3.1 Gauss-Newton Minimization

A brief mathematical description of this process will be given in the notation and terminology of this document for the present application.

Let the P-dimensional vector \underline{x} denote the template parameters, such as the ring boundary radii and compartment boundary azimuths, whose values are to be varied during the optimization. Let the components of the N-dimensional vectors $\underline{\lambda}_{IDEAL}$ and $\underline{\lambda}(\underline{x})$ represent the values of the spectrum for each spherical harmonic frequency n of the continuous integral transformation and a discrete summation approximation thereof, respectively. In principle N would be infinite, but in practice N is a sufficiently large number, such as 1440 which would include the contributions of all wavelengths longer than 15 arc-minutes. Further let the residual spectrum vector $\underline{\Delta\lambda}(\underline{x})$ be the difference $\underline{\lambda}(\underline{x}) - \underline{\lambda}_{IDEAL}$. It is desired to make the residual spectrum as small as possible in a weighted least squares sense, that is to find the solution \underline{x}^* of the weighted least squares problem

$$W \underline{\Delta\lambda}(\underline{x}) = \underline{0}$$

where W is the weighting matrix, or equivalently to minimize the scalar function

$$\phi(\underline{x}) = [W \underline{\Delta\lambda}(\underline{x})]^T [W \underline{\Delta\lambda}(\underline{x})]$$

Since the residual spectrum $\underline{\Delta\lambda}(\underline{x})$ depends non-linearly on the parameter vector \underline{x} , an iterative solution is necessary. Suppose an estimate or initial guess $\hat{\underline{x}}$ of the solution \underline{x}^* is available. By linearizing the residual spectrum about the estimate,

$$\underline{\Delta\lambda}(\underline{x}) = \underline{\Delta\lambda}(\hat{\underline{x}}) + \frac{\partial}{\partial \underline{x}} [\underline{\lambda}(\underline{x})](\underline{x} - \hat{\underline{x}}) + \dots$$

and solving the resulting linearized problem

$$W \frac{\partial [\underline{\lambda}(\underline{x})]}{\partial \underline{x}} (\underline{x} - \hat{\underline{x}}) = -W \underline{\Delta\lambda}(\hat{\underline{x}})$$

in a least-squares sense, an improved estimate

$$\hat{\underline{x}} = \underline{\hat{x}} + (\underline{x} - \underline{\hat{x}})$$

of the solution \underline{x}^* of the non-linear problem is obtained. A new residual spectrum $\underline{\Delta\lambda}(\underline{\hat{x}})$ is now computed based on the improved estimate and the process is repeated.

The solution of the linearized weighted least-squares problem may be written explicitly* as:

$$\underline{\Delta x} = (\underline{x} - \underline{\hat{x}}) = - \left[\left(\frac{\partial \underline{\Delta\lambda}}{\partial \underline{x}} \right)^T W^T W \left(\frac{\partial \underline{\Delta\lambda}}{\partial \underline{x}} \right) \right]^{-1} \left(\frac{\partial \underline{\Delta\lambda}}{\partial \underline{x}} \right)^T W^T W \underline{\Delta\lambda}(\underline{x})$$

However to preserve accuracy in actual computation, the least-squares solution for $\underline{\Delta x}$ should be obtained by a robust numerical method** applied directly to the overconstrained system, rather than through the theoretical expression above which would involve the inversion of a $P \times P$ matrix. In the present study, the subroutine MLSQ from the IBM Scientific Subroutine Package (IBM, 1968) was used to perform this function.

6.3.1.1 Standard (Input) Weighting

By taking the weighting matrix W used in the solution of the weighted least-squares problem of the previous section to be the diagonal matrix whose elements are the degree standard deviations of the input geodetic quantity $f_{IN}(\psi, \alpha)$,

$$W_{nn} = \sigma_n \{f_{IN}\}$$

it will result that the scalar objective function to be minimized

$$\phi(\underline{x}) = [W \underline{\Delta\lambda}(\underline{x})]^T [W \underline{\Delta\lambda}(\underline{x})]$$

is the global mean-square discretization error in the output. Under this scheme of weighting, heavier emphasis is assigned to those spherical harmonic degrees which contribute more to the input power.

This is the most natural choice for the weighting matrix W . However, other choices are of course possible. Some of these will be examined in Sections 6.3.4.2 and 6.3.4.3.

* See Dahlquist and Björk (1977, pg. 443).

** such as one involving Householder transformations. See Lawson and Hanson (1974, Chapter 11).

A degree variance model widely cited in the literature is that of Tscherning and Rapp (1974, pg. 30, eqn. 68). It is given by any of the following equivalent forms:

$$\sigma_n^2\{N\} = \frac{R^2}{G^2} \begin{cases} 0 & n = 0,1 \\ A' & n = 2 \\ A/(n-1)(n-2)(n+24) & n \geq 3 \end{cases}$$

$$\sigma_n^2\{\Delta g\} = \frac{R^2}{G^2} \begin{cases} 0 & n = 0,1 \\ A' & n = 2 \\ A(n-1)/(n-2)(n+24) & n \geq 3 \end{cases}$$

$$\sigma_n^2\{d_{kg}\} = \frac{R^2}{G^2} \begin{cases} 0 & n = 0,1 \\ A'(2+k)^2 & n = 2 \\ A(n+k)^2/(n-1)(n-2)(n+24) & n \geq 3 \end{cases}$$

where $A' = 7.6 \text{ mgal}^2$ and $A = 425.28 \text{ mgal}^2$. This model was used in the comprehensive filter design computer program.

6.3.2 Satisfaction of the Inequality Constraints

After a tentative differential correction $\Delta \underline{x}$ to the current estimate $\hat{\underline{x}}$ of the parameter vector has been determined from the Gauss-Newton scheme, it remains to check whether the new estimate $\hat{\underline{x}} = \hat{\underline{x}} + \Delta \underline{x}$ satisfies the inequality constraints that parameters of the same type do not overlap.

For example, if the parameters in the parameter vector \underline{x} are all cosines of the spherical ring boundary radii ψ_i with

$$x_i = \cos \psi_i$$

then the inequality constraints on \underline{x} will be of the form

$$x_0 > x_1 > x_2 > \dots > x_I$$

corresponding to the "natural" inequalities

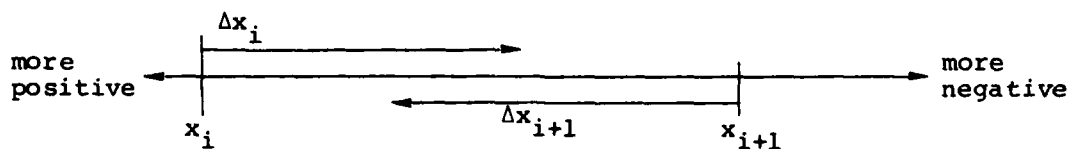
$$\psi_0 < \psi_1 < \psi_2 < \dots < \psi_I$$

If the components of the new estimate do not initially satisfy such inequalities, then the algorithm described in the following paragraphs is used to force satisfaction.

The inequality constraint satisfaction scheme is composed of two main subcases, namely the cases when the tentative adjacent increments which cause overlapping are in opposite directions or in the same direction.

Case 1a: When the adjacent increments are in opposite directions (i.e. have opposite sign) and are directed towards each other, then the two increments will each be reduced by the same constant fraction or percentage so that the overlap is not only eliminated but also so that a gap is introduced between the new estimates of adjacent independent parameters. The size of the gap is taken to be a fixed fraction of the total interval between the adjacent parameters.

Mathematically, let Δx_i and Δx_{i+1} be the overlapping increments directed towards each other. For definiteness, assume $\Delta x_i < 0$ and $\Delta x_{i+1} > 0$. Then the overlapping is expressed by the condition: $x_i + \Delta x_i < x_{i+1} + \Delta x_{i+1}$, as shown by the sketch:



Let $\Delta x'_i$ and $\Delta x'_{i+1}$ indicate the increments which will be used in place of Δx_i and Δx_{i+1} so that there will not be overlap and so that:

- i) the relative strength of the original increments will be preserved:

$$\frac{\Delta x_i}{\Delta x_{i+1}} = \frac{\Delta x'_i}{\Delta x'_{i+1}}$$

- ii) a "gap" will be left between the new estimates $(x_i + \Delta x'_i)$ and $(x_{i+1} + \Delta x'_{i+1})$ which is a fixed fraction of the difference between the previous estimates x_i and x_{i+1} :

$$(x_i - x_{i+1})a = (-\Delta x'_i + \Delta x'_{i+1})$$

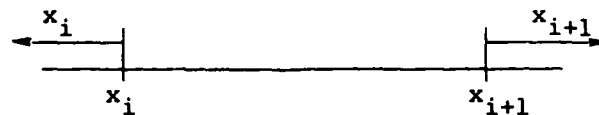
By solving these equations for $\Delta x'_i$ and $\Delta x'_{i+1}$ it is found that

$$\Delta x'_i = \Delta x_i \left[\frac{(x_i - x_{i+1})a}{(-\Delta x_i + \Delta x_{i+1})} \right]$$

and

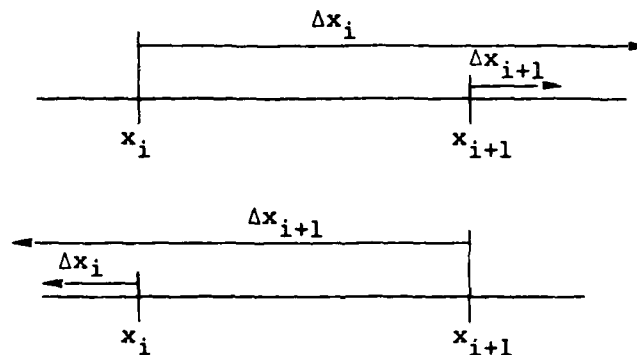
$$\Delta x'_{i+1} = \Delta x_{i+1} \left[\frac{(x_i - x_{i+1})a}{(-\Delta x_i + \Delta x_{i+1})} \right]$$

Case 1b: When the adjacent increments are in opposite directions (i.e. have opposite sign) but are directed away from each other, there cannot be overlapping as seen in the sketch:



so this case is non-existent.

Cases 2a and 2b: When the adjacent increments are in the same direction (i.e., have the same sign) and one of the increments is so large in magnitude that overlapping occurs as shown in the sketches:



then the larger increment (in magnitude) is set to a specified fraction of the current difference between adjacent estimates.

Mathematically,

$$x_i + \Delta x_i < x_{i+1} + \Delta x_{i+1}$$

is the overlapping condition in both subcases, although in subcase 2a both Δx_i and Δx_{i+1} are negative, while in subcase 2b both Δx_i and Δx_{i+1} are positive. Then

$$\text{if } \Delta x_i < 0, \Delta x_i' = -b(x_i - x_{i+1})$$

$$\text{if } \Delta x_i > 0, \Delta x_i' = +b(x_i - x_{i+1})$$

This assumes that pairs of increments are being checked in order of increasing i .

The foregoing algorithm to force the satisfaction of the inequality constraints is certainly not the best method of handling constrained minimization, but it is quickly and easily implementable in a computer program.

6.3.3 Exclusion of Small Ring Radii Parameters from Differential Adjustment

As has been mentioned, only the contributions of the spherical harmonic degrees up through a finite number N are included in the actual numerical computations. Consequently, the contributions of the higher degrees, or equivalently the higher frequencies or shorter wavelengths, are neglected. Therefore any parameters which are principally related to these neglected degrees should be held fixed during the iterative optimization process, because no information is being obtained to permit the rational adjustment of these parameters and because small random errors in the computations could induce large erroneous increments in them.

The spherical boundary radii close to the origin are indeed principally related to the higher harmonic degrees. In fact, it may be shown that if the Stokes' or Vening-Meinesz' Integrals are carried out only over a spherical cap having a spherical radius $\psi_0^{(n)}$ which is the smallest zero of the Molodenskii function $Q_n(\psi)$ or the Cook function $q_n(\psi)$ respectively, then the contribution of the n^{th} spherical harmonic frequency is completely accounted for in the mean; the contribution of the neglected part of the sphere is identically zero for this frequency (in the mean). The first zeros of the Molodenskii function $Q_n(\psi)$ and

the Cook function $q_n(\psi)$ are approximately $1/(n-1)$ and $2/(n-1)$ radians respectively for n larger than 10 or so.

Computational examples will be exhibited in Appendix E which show numerically that large erroneous increments do indeed occur for the close ring boundary radii, and that the higher the degree N of spherical harmonics considered, the smaller the spherical radius separating the unreasonable increments from the reasonable increments, as would be expected.

An approximate rule-of-thumb for the limiting spherical radius ψ_{LIMIT} inside of which all spherical ring boundary parameters ψ_i should be excluded from differential adjustment is:

$$\psi_{\text{LIMIT}} = \frac{900^\circ}{N}$$

In some cases, especially those with a small total number of rings (e.g., 23), ψ_{LIMIT} may be too large, perhaps by as much as a factor of two. In other cases, especially those with a large number of rings (e.g., 125), ψ_{LIMIT} may be too small, perhaps by as much as a factor of one third. However, the rule-of-thumb provides roughly the right order of magnitude.

The exclusion of the close spherical ring boundary radii from differential adjustment during the iterative optimization procedure has the byproduct of reducing the overall computational burden. Not only is the (fairly short) calculation of the partials of the spectrum with respect to the radii avoided, but also the dimensions of the least-squares normal equations are decreased and hence so is the execution time required for their solution. For the Stokes' transformation, the reduction is not great since typically only about 5% to 10% of the ring radii will lie inside the limiting radius ψ_{LIMIT} . However, for the Vening-Meinesz' transformation, the reduction is often substantial since 30% to 60% of the ring radii typically lie within ψ_{LIMIT} .

6.3.4 Variations in the Optimization Algorithm

Due to various difficulties in the convergence of the optimization process, three easy-to-implement variations in the optimization algorithm were experimented with. These variations generally worked in the expected manner, alleviating some of the problems encountered, but usually for only a few iterations. They are no substitute for more powerful optimization algorithms.

The three variations are original with the author, and are described in the following subsections.

6.3.4.1 Damping of the Increments

The differential correction Δx in the independent parameters which is produced by each iteration of the Gauss-Newton optimization process does not always lead to a decrease in the rms discretization error. Sometimes it causes an increase. This is because the Gauss-Newton method is not rigorously a "descent" method such as Steepest Descent or Conjugate Gradients. In descent methods, the figure of merit is always decreased at each iteration; however the calculations are generally more involved.

In some Vening-Meinesz' cases, especially those with a large number of parameters, it was observed that several descent steps occurred followed by one or more ascent steps followed by more descent steps, etc. Sometimes a parameter oscillation developed with several parameters assuming alternate values in alternate iterations. It was conjectured that better progress to the true minimum could be made if a slower but non-oscillatory descent could be achieved.

To implement such an idea, the partial derivatives in the Vening-Meinesz case were adjusted (specifically, made larger) by changing the multiplicative factor

$$\frac{2}{\sqrt{n(n+1)}}$$

appearing at the front of the exact expression to the factor

$$\frac{2}{[n(n+1)]^p}$$

where $p < 0.5$. With larger than normal partial derivatives, the algorithm calculates that a smaller than normal increment Δx is required to counteract the same observed residuals. Thus the increments are damped and the descent to the minimum is slowed.

The increment damping variation of the optimization algorithm generally works computationally as expected, as will be shown by examples in Section 7.4.1.

6.3.4.2 Output Weighting

Rather than using the degree standard deviations of the input geodetic quantity $f_{IN}(\psi, \alpha)$ to the transformation as the weights in the (diagonal) weighting matrix of the least squares problem

$$W_{nn} = \sigma_n \{f_{IN}\}$$

the Output Weighting Variation of the optimization algorithm uses the degree standard deviations of the output geodetic quantity f_{OUT} :

$$\begin{aligned} W_{nn} &= \sigma_n \{f_{OUT}\} \\ &= |\lambda_n^{\text{APPROX}} - \lambda_n| \sigma_n \{f_{IN}\} \end{aligned}$$

The idea of using this weighting scheme came from a study of the details of the algorithm of Kahng (1972) for general least p^{th} power approximation with $2 < p < \infty$. Kahng's method for the general problem is based upon iteratively solving a weighted least-squares sub-problem where the weights are the $(p-2)$ power of the absolute values of the residuals resulting from the previous iteration. In other words, the weights used in the next iteration are a power of the output errors of the present iteration.

Output weighting is more directly suggested by the fact that rms discretization error is the root-sum-square of the output degree standard deviations. Hence it will be more quickly minimized if the weights for each degree are chosen proportional to the output contribution for the degree in question.

A numerical example is provided by Figure 6.3.4-1. The degree variances $\sigma_n^2\{\mu\}$ of the input surface layer density μ based on the Tscherning-Rapp model are listed in mgal^2 in the column "DEG VAR IN". The rms discretization error contributed by the current spherical harmonic degree and by all degrees up through the current degree are listed in mgal in the columns "SIGMA" and "CUM SIGMA" respectively.* From the SIGMA column it is seen that degrees three through six each introduce very large values into the cumulative rms discretization error. In fact, the total discretization error through degree 1440 is 0.13321 of

* SIGMA is the product of the absolute value of RESID SPECTRUM and the square root of DEG VAR IN.

N	ACTUAL SPECTRUM	IDEAL SPECTRUM	RESID SPECTRUM	REL RESID	DEG VAR IN	WEIGHT	SIGMA	CUM SIGMA
1	0.9380893307	0.9427829594	-0.0046936274	-0.004978	0.02250	0.49568	0.00070	0.00070
2	0.9787351945	0.9797507214	-0.0010155269	-0.001037	47.50000	48.98647	0.00700	0.00703
3	0.9975915764	0.9896794306	0.0079121441	0.007995	96.47556	6039.56250	0.07771	0.07803
4	0.9622894533	0.9937255109	-0.0114360601	-0.011508	51.26143	6704.14453	0.08188	0.11311
5	1.0050699120	0.9957581796	0.0093117319	0.009351	36.96759	3205.39795	0.05662	0.12649
6	0.9928960378	0.9969175069	-0.0040214658	-0.004034	29.94680	484.30493	0.02201	0.12839
7	0.9973264111	0.9976372692	-0.0003108780	-0.000312	25.72258	2.48596	0.00158	0.12840
8	0.9990252653	0.9981119038	0.0009133813	0.000915	22.86196	19.07294	0.00437	0.12847
9	0.9977336013	0.9984390333	0.0012945679	0.001297	20.76922	34.80725	0.00590	0.12861
10	0.9954361773	0.9986721390	-0.0032359615	-0.003240	19.15324	200.56207	0.01416	0.12938
11	1.0014201530	0.9988424806	0.0025776722	0.002581	17.85501	118.63570	0.01089	0.12984
12	0.9988563151	0.9989693281	-0.0001130130	-0.000113	16.78030	0.21432	0.00046	0.12984
13	0.9977083390	0.9970650854	-0.0013567463	-0.001358	15.86963	29.21217	0.00540	0.12995
14	0.9992986091	0.9991380299	0.0001605791	0.000161	15.08352	0.38894	0.00062	0.12995
15	1.0012229027	0.9991938572	0.0020290455	0.002031	14.39469	59.26331	0.00770	0.13018
16	0.9979427037	0.9992365898	-0.0021938859	-0.002196	13.78363	66.34245	0.00315	0.13044
17	0.9991801732	0.9992691346	-0.0000889613	-0.000089	13.23598	0.10475	0.00032	0.13044
18	1.0009899754	0.9992936343	0.0016963410	0.001698	12.74090	36.66286	0.00605	0.13058
19	0.9990400305	0.9993116967	-0.0002716661	-0.000272	12.29007	0.90704	0.00095	0.13058
20	0.9972275907	0.9993245469	-0.0020969561	-0.002098	11.87692	52.22549	0.00723	0.13078
21	1.0010135907	0.9993331321	0.0016804584	0.001682	11.49624	32.46468	0.00570	0.13091
22	1.0002755142	0.9993381933	0.0009373203	0.000938	11.14379	9.79060	0.00313	0.13094
23	0.9977786476	0.9993403178	-0.0015616701	-0.001563	10.81610	26.37845	0.00514	0.13104
24	0.9986157229	0.9993399750	-0.0007242518	-0.000725	10.51031	5.51308	0.00235	0.13106
25	1.0012364612	0.9993375444	0.0018989167	0.001900	10.22398	36.86649	0.00607	0.13121
26	0.9972123394	0.9993333352	-0.0001209958	-0.000121	9.95510	0.14574	0.00038	0.13121
27	0.9931728566	0.9993276014	-0.0011547448	-0.001156	9.70190	12.93685	0.00360	0.13126
28	0.9992060146	0.9993205531	-0.0001137386	-0.000114	9.46290	0.12242	0.00035	0.13126
29	1.0002468970	0.9993123657	0.0009365112	0.000937	9.23680	8.10116	0.00285	0.13129
30	0.9993987821	0.9993031859	0.0000955962	0.000096	9.02246	0.08245	0.00029	0.13129
31	0.9991105932	0.9992931379	-0.0001825447	-0.000183	8.81889	0.29387	0.00054	0.13129
32	0.9984196878	0.9992823268	-0.0008626387	-0.000863	8.62523	6.41843	0.00253	0.13131
33	0.9993189923	0.9992708424	0.0000481500	0.000048	8.44069	0.01957	0.00014	0.13131
34	1.0004383990	0.9992587616	0.0011796372	0.001181	8.26459	11.50053	0.00339	0.13136
35	0.9996457189	0.9992461507	0.0003995681	0.000400	8.09630	1.29261	0.00114	0.13136
36	0.9975240179	0.9992330670	-0.0017090491	-0.001710	7.93528	23.17775	0.00481	0.13145
37	0.9988512639	0.9992195602	-0.0003682962	-0.000369	7.78103	1.05543	0.00103	0.13145
38	1.0006642920	0.9992056738	0.0014586181	0.001460	7.63309	16.23990	0.00403	0.13151
39	0.9993057840	0.9991914456	0.0006143383	0.000615	7.49106	2.82721	0.00168	0.13153
40	0.9780668087	0.9991769091	-0.0010901003	-0.001091	7.35456	8.73956	0.00296	0.13156
41	0.9987382173	0.9991620935	-0.0004238761	-0.000424	7.22326	1.29781	0.00114	0.13156
42	0.9992352097	0.9991470249	0.0000881848	0.000088	7.09684	0.05519	0.00023	0.13156
43	0.9994373176	0.9991317262	0.0003055914	0.000306	6.97502	0.65137	0.00081	0.13157
44	0.9997404214	0.9991162179	0.0006242034	0.000625	6.85754	2.67190	0.00163	0.13158
45	0.9994038652	0.9991005182	0.0003033669	0.000304	6.74415	0.62067	0.00079	0.13158
46	0.9979211409	0.9990046434	-0.0011635025	-0.001165	6.63464	8.98157	0.00300	0.13161
47	0.9983296447	0.9990666081	-0.0007389633	-0.000740	6.52830	3.56516	0.00189	0.13163
48	0.9998228519	0.9990524253	0.0007704264	0.000771	6.42644	3.81446	0.00195	0.13164
49	1.0001335680	0.9990361070	0.0010974610	0.001099	6.32737	7.62081	0.00276	0.13167
50	0.9969787249	0.9990196637	-0.0000409388	-0.000041	6.23144	0.01044	0.00010	0.13167

Figure 6.3.4-1. Example of Output Weighting.

which 0.12839 is already contributed by degrees one through six. Thus in a minimization it is imperative to quickly reduce the contributions of these degrees.

In the standard implementation, the input degree variances $\sigma_n^2\{\mu\}$ would be used as weights, while in the variant implementation the output-related quantities

$$w_{nn}^2 = \left(|\lambda_n^{\text{APPROX}} - \lambda_n|^2 \sigma_n^2\{\mu\} 10^6 \right)$$

listed in the "WEIGHT" column are used.*

It is seen immediately that in the standard implementation the weights for degrees three through six are not sufficiently large to counteract the effect of the 1436 other degrees whose weights are smaller but still non-negligible. On the other hand, in the variant implementation, the weights for degrees three through six are much larger and do counteract the other 1436 degrees.

In actual optimization computer runs, this heuristic explanation is vindicated numerically. Specific examples will be given in Section 7.4.2.

6.3.4.3 Power Emphasis of the Input or Output Weighting

As an additional means of emphasizing or de-emphasizing certain of the weights of the weighted least-squares procedure, an idea is borrowed from the increment damping variation and from Kahng's original p^{th} power algorithm, namely that the preliminary weight as calculated by either the input or output weighting methods be raised to a specific power and the result used as the actual weight. This provides a simple and convenient way of smoothly increasing and decreasing the weights to adjust them relatively for specific purposes while still maintaining the underlying input or output weight orderings. The actual power to which the preliminary weights are raised provides the user with a one-parameter family of possible "distortions" of the underlying weighting.

As with the other two variations in the optimization algorithm, the power emphasis variation is a quickly implementable ad hoc scheme. The results of using this variation will be discussed in Section 7.4.3.

*The factor 10^6 serves no purpose other than to scale the WEIGHT values for printing and possibly to prevent exponent underflow in the least squares subroutine.

SECTION 7

TEMPLATE OPTIMIZATION RESULTS

7.1 Summary

The basic template optimization results which have been achieved during the course of the present work are summarized in Figure 7.1-1. All of these results have been attained using the optimization algorithm and variations described in the previous chapter.

From the figure, it is seen that moderate reductions in the global rms discretization error have been obtained for both the Stokes' and Vening-Meinesz' discrete summation transformations for several choices of the number of rings in the template. Specifically, the reductions have been from the values listed "current" column, which correspond to a published or a currently-used template, to the values listed in the "reduced" column, which correspond to the improved template.

In some cases, further reduction of the discretization error seems likely since this figure-of-merit was still being consistently reduced in each iteration at the time the optimization process was halted (due to computer time limitations or other extraneous reasons). In other cases, further reduction appears stymied. This may be due to a contorted shape of the multi-dimensional surface on which the minimization is being performed or to the lack of powerfulness of the optimization algorithms used. Alternatively, the minimum rms discretization error corresponding to the optimal template may actually have been reached.* This possibility is suggested by the fact that variations in the optimization algorithm yielded very similar results. However, it is not yet known whether any of the values in the "reduced" column are the true minima.

* Since some error must be introduced by the discrete summation approximation, the minimum rms discretization error has a non-zero value.

It had been hoped that reductions of several orders of magnitude in the global rms discretization error would be achieved. It is still possible that this will be true.

Details of the optimization results presented in the figure, as well as several related results and the results of the experimentation with the optimization algorithm variations, are presented in the following sections.

		<u>RMS DISCRETIZATION ERROR</u>	
		CURRENT	REDUCED
• STOKES' TRANSFORMATION			
(MEAN GRAVITY ANOMALIES TO GEOID HEIGHT)			
- 34-RING CASE:	1.336 M	→	0.434 M
- 101-RING CASE:	0.165 M	→	0.097 M
• STOKES' TRANSFORMATION ANALOG			
(MEAN SURFACE LAYER DENSITIES TO GEOID HEIGHT)			
- 34-RING CASE:	0.687 M	→	0.219 M
• VENING-MEINESZ' TRANSFORMATION ANALOG			
(MEAN SURFACE LAYER DENSITIES TO HORIZONTAL GRAVITY DISTURBANCES)			
- 23-RING CASE:	0.754 MGAL	→	0.519 MGAL
- 125-RING CASE (EQUAL-INTEGRAL)	0.133 MGAL	→	0.082 MGAL
- 125-RING CASE (DMAAC-RICE)	0.075 MGAL	→	0.063 MGAL

Figure 7.1-1. Summary of Basic Optimization Results.

7.2 Template Optimization Results for the Stokes' Transformation

Four main results have been obtained for the discrete Stokes' summation transformation, in particular three for the classic transformation converting gravity anomalies to geoid height and one for the analog transformation converting surface layer densities to geoid height. The three results for the classic transformation are for templates with 34, 66, and 101 rings, while that for the analog transformation is for a template with 34 rings.

7.2.1 Classic Stokes' Transformation

Summaries of the intermediate results during the optimization process on a discrete classic Stokes' summation transformation are given in Figures 7.2.1-1, 7.2.1-2, and 7.2.1-3 for templates of 34, 66 and 101 rings, respectively.

The following points may be noted from these figures:

- a) In the 34-ring case, the rms discretization error is being reduced steadily but has not achieved a minimum after 10 iterations.
- b) Both of the two "gaps" of about 20° in the initial template parameters around the zeros of the classic Stokes' function have been eliminated during the course of the optimization. Even though the Pick-Picha-Vyskocil template is not an equal ring contribution template, it has been derived on equal contribution considerations and hence has these gaps (around 39° and 118°).
- c) In the 66-ring case, the rms discretization error appears to have reached a plateau after two or three iterations at a level of about 1.00 meter. This is much larger than expected, as is the initial discretization error of 1.64 meters, for a template with so many rings. Intuitively, the more rings in the template the lower the discretization error is expected to be, at least for "reasonable" spherical boundary radii partitions.
- d) In the 66-ring case, the exact equal integral template has a "gap" between the ring boundary radii #19 and #20 of about 20° corresponding to the first zero of the classic Stokes'

function at 39° , and a ring boundary radius (#52) equaling the second zero of the function near 118° with the adjacent ring radii being about 10° away on each side. During the course of the optimization, the first gap is eliminated, the ring radius at the second zero remains fairly constant and the distances to the adjacent ring radii are both reduced slightly to about 8.5° as if the "virtual" gap at this radius were being eliminated.

- e) In the 101-ring case, the rms discretization error seems to have been reduced to a minimum of about 0.100 meters, which scarcely changed during the last five iterations. However, in reality, almost all of the ring radii increments between ring #18 and #52 are being severely restricted so as not to overlap by the inequality constraint algorithm. When this severe restriction occurs, the optimization is greatly hindered, so the value attained is probably not the minimum possible.

In the figures, a horizontal line indicates the division between the parameters which were and were not allowed to vary, while a vertical line indicates the division between convergence and divergence of the iteration process.

SUMMARY OF COMPLETE RUN

	ITER# 0	ITER# 1	ITER# 2	ITER# 3	ITER# 4	ITER# 5	ITER# 6	ITER# 7	ITER# 8	ITER# 9	ITER#10
FIGURE OF MERIT	1.336	0.729	0.559	0.506	0.485	0.471	0.462	0.454	0.446	0.442	0.434
VALUES OF PARAMETERS											
RING# SPHERICAL RING RADII (DEGREES)											
0	0.000	0.000	0.000	0.000	0.000	0.000	0.000	0.000	0.000	0.000	0.000
1	0.068	0.068	0.068	0.068	0.068	0.068	0.068	0.068	0.068	0.068	0.068
2	0.175	0.175	0.175	0.175	0.175	0.175	0.175	0.175	0.175	0.175	0.175
3	0.308	0.308	0.308	0.308	0.308	0.308	0.308	0.308	0.308	0.308	0.308
4	0.447	0.447	0.447	0.447	0.447	0.447	0.447	0.447	0.447	0.447	0.447
5	0.712	0.712	0.712	0.712	0.712	0.712	0.712	0.712	0.712	0.712	0.712
6	0.976	0.912	1.009	1.053	1.180	1.226	1.142	1.307	1.242	1.360	1.277
7	1.235	1.177	1.310	1.402	1.680	1.582	1.801	1.742	1.986	1.826	2.063
8	1.488	1.771	1.646	1.971	2.116	2.460	2.346	2.601	2.553	2.853	2.712
9	1.986	2.117	2.435	2.527	2.923	3.054	3.438	3.305	3.624	3.595	3.927
10	2.478	2.585	3.116	3.453	3.684	4.058	4.247	4.587	4.534	4.876	4.683
11	2.961	3.641	3.937	4.461	4.720	5.095	5.403	5.680	5.928	6.039	6.335
12	4.148	4.745	5.241	5.628	6.052	6.370	6.763	7.070	7.369	7.595	7.825
13	5.864	6.260	6.722	7.188	7.602	8.018	8.394	8.776	9.102	9.401	9.665
14	8.100	8.143	8.637	9.116	9.573	10.021	10.440	10.844	11.218	11.557	11.867
15	10.488	10.517	11.050	11.548	12.041	12.522	12.968	13.396	13.794	14.166	14.510
16	12.850	13.606	14.027	14.626	15.136	15.642	16.101	16.540	16.948	17.336	17.693
17	15.990	17.075	17.856	18.473	19.018	19.524	19.975	20.404	20.803	21.186	21.549
18	20.170	21.502	22.613	23.329	23.856	24.327	24.736	25.126	25.492	25.848	26.191
19	25.300	27.563	28.746	29.428	29.853	30.216	30.536	30.852	31.159	31.467	31.773
20	33.500	35.905	36.808	37.062	37.200	37.363	37.545	37.758	37.986	38.229	38.479
21	52.000	48.782	47.076	46.330	46.061	45.980	46.019	46.119	46.263	46.430	46.613
22	61.000	59.534	57.965	57.144	56.883	56.629	56.632	56.621	56.705	56.783	56.869
23	72.000	80.662	79.977	84.426	81.896	84.120	82.966	83.787	83.412	83.645	83.549
24	82.000	86.084	89.601	90.333	91.679	91.570	91.939	91.945	92.088	92.123	92.191
25	94.200	95.903	97.865	99.171	99.962	100.391	100.633	100.781	100.893	100.975	101.044
26	106.300	108.313	109.165	109.686	110.038	110.267	110.406	110.501	110.569	110.622	110.664
27	126.300	123.921	122.568	121.911	121.592	121.440	121.353	121.304	121.269	121.244	121.223
28	135.900	135.620	134.898	134.222	133.730	133.406	133.181	133.016	132.883	132.770	132.667
29	142.700	144.309	145.592	145.939	145.875	145.726	145.556	145.375	145.194	145.013	144.834
30	149.000	151.420	154.589	157.105	158.116	158.387	158.365	158.215	158.015	157.780	157.528
31	155.400	157.846	161.058	164.191	166.793	169.674	171.154	171.401	171.274	170.939	170.650
32	162.900	165.654	170.283	175.611	178.017	178.281	178.430	178.509	178.647	178.792	178.871
33	176.400	178.390	179.280	179.678	179.856	179.901	178.780	178.684	179.411	179.153	179.050
34	180.000	180.000	180.000	180.000	180.000	180.000	180.000	180.000	180.000	180.000	180.000

Figure 7.2.1-1. Summary of 34-Ring Template Optimization for the Classic Stokes' Transformation.

SUMMARY OF COMPLETE RUN

ITER# 0 ITER# 1 ITER# 2 ITER# 3

FIGURE OF MERIT

1.64E+00 1.12E+00 1.02E+00 1.01E+00

VALUES OF PARAMETERS

RING#	SPHERICAL RING RADII (DEGREES)			
0	0.000	0.000	0.000	0.000
1	1.510	1.510	1.510	1.510
2	2.918	2.467	2.955	2.726
3	4.274	3.066	3.328	3.402
4	5.602	4.570	3.420	3.670
5	6.916	5.888	4.663	4.755
6	8.228	7.198	6.172	6.646
7	9.545	8.507	7.415	8.626
8	10.877	9.826	10.570	9.364
9	12.231	11.161	12.261	12.141
10	13.618	12.521	14.237	13.271
11	15.046	16.242	15.262	16.267
12	16.528	17.780	16.692	17.895
13	18.080	19.403	19.973	18.249
14	19.721	20.113	20.822	21.531
15	21.482	20.995	21.705	22.474
16	23.406	21.879	22.662	23.446
17	25.569	23.853	23.638	26.440
18	28.118	26.097	28.832	29.324
19	31.449	34.997	35.517	35.235
20	50.091	46.266	43.652	43.599
21	52.792	54.650	50.751	49.807
22	55.108	56.777	57.105	54.197
23	57.189	58.727	59.395	60.105
24	59.107	59.561	60.282	60.377
25	60.909	60.462	60.660	60.566
26	62.623	61.254	61.057	61.867
27	64.269	62.954	64.264	63.471
28	65.862	64.539	65.858	64.584
29	67.413	66.173	66.561	65.999
30	68.933	67.719	67.334	66.716
31	70.429	69.234	68.023	69.004
32	71.908	70.726	71.908	70.946
33	73.375	72.202	73.376	73.903
34	74.837	73.669	74.035	74.218
35	76.298	75.130	74.766	74.583
36	77.764	76.592	75.423	74.897
37	79.240	78.060	76.886	77.686
38	80.732	81.110	78.673	80.746
39	82.244	81.867	81.262	81.856
40	83.785	82.553	82.004	82.691
41	85.361	84.101	82.863	83.912
42	86.982	85.964	87.047	86.003
43	88.658	87.317	87.778	87.193
44	90.402	89.007	88.623	87.947
45	92.233	90.768	89.359	89.770
46	94.174	92.621	91.138	92.815
47	96.259	96.628	93.235	93.620
48	98.541	97.969	98.036	99.115
49	101.108	99.053	101.177	101.717
50	104.133	101.710	105.091	105.441
51	108.063	112.387	108.992	109.069
52	117.662	118.496	117.458	117.554
53	127.798	124.958	125.714	125.729
54	132.306	135.209	134.309	134.302
55	133.958	136.752	135.515	138.098
56	139.209	138.377	139.512	139.429
57	142.241	139.600	143.542	144.236
58	145.155	147.432	149.713	148.288
59	143.024	150.308	150.622	150.704
60	150.904	153.243	150.725	150.715
61	153.858	156.308	157.089	156.340
62	156.958	159.603	158.733	157.409
63	160.316	161.200	159.912	158.964
64	164.133	163.101	165.388	161.652
65	168.915	175.049	166.882	166.753
66	180.000	180.000	180.000	180.000

Figure 7.2.1-2. Summary of 66-Ring Template Optimization for the Classic Stokes' Transformation Beginning with an Equal Ring Contribution Template.

SUMMARY OF COMPLETE RUN

	ITER# 0	ITER# 1	ITER# 2	ITER# 3	ITER# 4	ITER# 5	ITER# 6	ITER# 7	ITER# 8	ITER# 9	ITER#10
FIGURE OF MERIT	0.165	0.132	0.118	0.115	0.108	0.103	0.101	0.101	0.099	0.100	0.097
VALUES OF PARAMETERS											
RING# SPHERICAL RING RADII (DEGREES)											
0	0.000	0.000	0.000	0.000	0.000	0.000	0.000	0.000	0.000	0.000	0.000
1	0.083	0.083	0.083	0.083	0.083	0.083	0.083	0.083	0.083	0.083	0.083
2	0.167	0.167	0.167	0.167	0.167	0.167	0.167	0.167	0.167	0.167	0.167
3	0.250	0.250	0.250	0.250	0.250	0.250	0.250	0.250	0.250	0.250	0.250
4	0.333	0.333	0.333	0.333	0.333	0.333	0.333	0.333	0.333	0.333	0.333
5	0.417	0.417	0.417	0.417	0.417	0.417	0.417	0.417	0.417	0.417	0.417
6	0.500	0.500	0.500	0.500	0.500	0.500	0.500	0.500	0.500	0.500	0.500
7	0.583	0.583	0.583	0.583	0.583	0.583	0.583	0.583	0.583	0.583	0.583
8	0.667	0.667	0.667	0.667	0.667	0.667	0.667	0.667	0.667	0.667	0.667
9	0.750	0.750	0.750	0.750	0.750	0.750	0.750	0.750	0.750	0.750	0.750
10	0.833	0.833	0.833	0.833	0.833	0.833	0.833	0.833	0.833	0.833	0.833
11	0.917	0.917	0.917	0.917	0.917	0.917	0.917	0.917	0.917	0.917	0.917
12	1.000	1.000	1.000	1.000	1.000	1.000	1.000	1.000	1.000	1.000	1.000
13	1.083	1.017	1.017	1.017	1.017	1.017	1.017	1.017	1.017	1.017	1.017
14	1.167	1.101	1.034	1.034	1.034	1.034	1.034	1.034	1.034	1.034	1.034
15	1.250	1.271	1.137	1.056	1.056	1.056	1.056	1.056	1.056	1.056	1.056
16	1.333	1.313	1.280	1.167	1.079	1.079	1.079	1.079	1.079	1.079	1.079
17	1.417	1.350	1.321	1.288	1.192	1.102	1.084	1.080	1.080	1.080	1.080
18	1.500	1.567	1.396	1.628	1.363	1.228	1.397	1.153	1.095	1.083	1.080
19	1.583	1.650	1.680	1.691	1.696	1.436	1.649	1.450	1.218	1.593	1.202
20	1.667	1.688	1.721	1.711	1.706	1.698	1.701	1.659	1.673	1.681	1.692
21	1.750	1.730	1.739	1.744	1.718	1.708	1.706	1.715	1.702	1.695	1.699
22	1.833	1.767	1.753	1.753	1.746	1.755	1.718	1.751	1.758	1.713	1.708
23	1.917	1.938	1.902	1.767	1.783	1.774	1.759	1.781	1.774	1.776	1.781
24	2.000	1.979	1.946	1.832	1.816	1.836	1.787	1.801	1.785	1.782	2.069
25	2.083	2.150	2.015	2.130	1.895	1.876	1.844	1.830	1.915	2.159	2.181
26	2.167	2.188	2.158	2.189	2.233	1.967	2.263	1.935	2.216	2.245	2.224
27	2.250	2.229	2.196	2.243	2.322	2.332	2.346	2.280	2.330	2.302	2.256
28	2.333	2.354	2.255	2.342	2.359	2.350	2.465	2.474	2.427	2.446	2.331
29	2.417	2.396	2.363	2.410	2.393	2.493	2.500	2.491	2.501	2.483	2.453
30	2.500	2.521	2.422	2.508	2.517	2.522	2.515	2.503	2.539	2.635	2.514
31	2.583	2.563	2.529	2.544	2.535	2.531	2.675	2.548	2.658	2.674	2.700
32	2.667	2.688	2.588	2.574	2.550	2.710	2.725	2.685	2.722	2.706	2.765
33	2.750	2.729	2.696	2.610	2.749	2.768	2.754	2.731	2.761	2.780	2.790
34	2.833	2.854	2.755	2.782	2.825	2.806	2.828	2.769	2.784	2.792	2.805
35	2.917	2.896	2.863	2.836	2.863	2.833	2.843	2.831	2.815	2.803	2.832
36	3.000	2.934	3.242	2.942	2.916	2.874	2.864	2.950	3.240	2.905	2.881
37	3.250	3.314	3.346	3.396	3.039	3.334	2.972	3.308	3.472	3.288	2.986
38	3.500	3.439	3.408	3.436	3.404	3.592	3.387	3.512	3.619	3.502	3.332
39	3.750	3.814	3.517	3.490	3.638	3.652	3.604	3.646	3.667	3.677	3.533
40	4.000	3.939	4.242	3.674	3.656	4.199	3.768	3.728	3.707	3.697	3.681
41	4.250	4.314	4.414	4.678	4.438	4.499	4.260	3.842	4.184	3.807	4.175
42	4.500	4.439	4.741	4.767	4.696	4.628	4.525	4.564	4.564	4.262	4.503
43	4.750	4.814	4.845	4.819	4.850	4.878	4.679	4.641	4.580	4.567	4.639
44	5.000	4.939	4.908	4.858	5.186	5.224	4.949	4.734	4.957	4.657	4.938
45	5.250	5.051	5.465	5.265	5.443	5.353	5.250	5.011	5.031	5.341	5.370
46	5.500	5.565	5.575	5.487	5.517	5.584	5.396	5.532	5.480	5.893	5.374
47	5.750	5.690	5.723	5.606	5.576	5.794	6.141	6.132	5.992	6.461	6.335
48	6.000	6.201	6.038	5.792	6.501	6.330	6.463	6.442	6.555	6.879	7.057
49	6.250	6.402	6.242	6.577	6.580	6.926	6.890	7.167	7.103	7.166	7.489
50	6.500	6.550	6.650	6.964	7.161	7.493	7.326	7.168	7.336	7.567	7.937

Figure 7.2.1-3. Summary of 101-Ring Template Optimization for the Classic Stokes' Transformation.

51	6.750	6.683	7.127	7.210	7.684	8.085	7.974	7.793	7.624	8.027	8.268
52	7.000	7.463	7.817	7.674	8.182	8.298	8.128	8.316	8.354	8.651	8.777
53	8.000	8.235	8.457	8.846	8.326	8.628	8.956	8.938	8.708	8.809	8.914
54	9.000	9.066	9.285	9.216	9.314	9.136	9.589	9.594	9.621	9.475	9.553
55	10.000	9.915	10.170	9.675	9.829	10.035	10.368	10.317	10.277	10.357	10.103
56	11.000	10.670	10.909	10.765	11.063	11.043	11.050	11.035	10.940	10.984	11.020
57	12.000	11.783	11.962	11.979	11.805	12.049	11.910	11.725	11.773	11.657	11.623
58	13.000	12.701	12.848	12.793	12.569	12.839	12.698	12.719	12.660	12.275	12.488
59	14.000	13.690	13.721	13.612	13.635	13.788	13.783	13.646	13.395	13.549	13.461
60	15.000	14.701	14.831	14.596	14.776	14.624	14.646	14.475	14.328	14.423	14.466
61	16.000	15.923	15.730	15.680	15.672	15.524	15.607	15.523	15.556	15.488	15.552
62	17.000	16.597	16.643	16.878	16.817	16.672	16.738	16.629	16.708	16.671	16.758
63	18.000	17.797	17.724	17.758	17.955	17.891	17.836	17.823	17.823	17.849	17.966
64	19.000	18.730	18.772	18.827	19.104	19.103	19.037	19.155	19.247	19.257	19.153
65	20.000	19.895	20.050	20.202	20.304	20.433	20.575	20.700	20.719	20.681	20.432
66	21.000	20.655	20.527	20.440	20.810	20.579	20.912	21.180	21.217	21.493	21.841
67	22.000	21.586	21.727	21.754	22.027	22.222	22.620	22.834	23.089	23.298	23.564
68	23.000	22.568	23.050	23.560	23.977	24.178	24.499	24.814	25.054	25.285	25.456
69	24.000	23.770	24.846	25.490	26.063	26.469	26.726	27.044	27.307	27.550	27.721
70	25.000	26.297	27.354	27.973	28.586	29.005	29.317	29.598	29.842	30.069	30.265
71	30.000	30.194	30.707	31.192	31.606	31.967	32.253	32.490	32.717	32.916	33.004
72	35.000	34.687	34.736	34.893	35.079	35.331	35.558	35.740	35.915	36.077	36.216
73	40.000	39.475	39.180	39.097	39.050	39.153	39.239	39.350	39.459	39.551	39.640
74	45.000	44.371	43.901	43.652	43.480	43.378	43.324	43.328	43.346	43.399	43.410
75	50.000	49.306	48.788	48.420	48.155	47.954	47.792	47.658	47.613	47.587	47.561
76	55.000	54.325	53.825	53.431	53.141	52.813	52.545	52.343	52.258	52.180	52.226
77	60.000	59.534	59.055	58.647	58.419	58.070	57.672	57.523	57.414	57.357	57.344
78	65.000	65.319	64.734	64.573	64.278	64.070	63.637	63.630	63.341	63.461	63.372
79	70.000	74.808	78.385	75.438	77.560	75.972	78.541	76.522	78.382	77.246	78.073
80	75.000	79.252	79.660	82.017	80.696	81.539	80.879	82.747	81.695	82.242	81.761
81	80.000	81.973	83.799	84.171	85.611	84.780	85.252	85.388	85.957	85.568	85.844
82	85.000	85.624	87.031	87.861	88.348	88.879	88.735	88.910	89.200	89.363	89.282
83	90.000	90.274	90.926	91.459	91.960	92.295	92.497	92.641	92.801	92.952	93.147
84	95.000	95.170	95.311	95.534	95.982	96.198	96.328	96.463	96.576	96.778	96.925
85	100.000	99.887	99.989	100.054	100.250	100.415	100.475	100.602	100.655	100.790	100.871
86	105.000	104.805	104.729	104.808	104.847	104.853	104.860	104.939	105.012	105.020	105.086
87	110.000	109.786	109.621	109.625	109.623	109.543	109.516	109.504	109.598	109.555	109.669
88	115.000	114.772	114.633	114.541	114.445	114.364	114.367	114.309	114.320	114.289	114.307
89	120.000	119.789	119.654	119.531	119.409	119.320	119.294	119.252	119.163	119.157	119.063
90	125.000	124.776	124.667	124.508	124.413	124.342	124.304	124.232	124.144	124.103	124.071
91	130.000	129.828	129.725	129.632	129.550	129.468	129.365	129.317	129.280	129.197	129.140
92	135.000	134.979	134.856	134.743	134.667	134.635	134.536	134.492	134.454	134.423	134.397
93	140.000	140.066	139.999	139.881	139.849	139.859	139.791	139.762	139.741	139.768	139.764
94	145.000	145.110	145.164	145.128	145.147	145.232	145.187	145.194	145.197	145.198	145.191
95	150.000	150.299	150.401	150.580	150.658	150.734	150.776	150.817	150.788	150.745	150.678
96	155.000	155.518	155.692	155.947	156.267	156.257	156.386	156.445	156.400	156.308	156.239
97	160.000	160.738	161.254	161.576	162.152	161.947	162.200	162.238	162.168	161.997	161.921
98	165.000	165.924	166.936	167.113	168.064	167.752	168.077	168.007	167.748	167.574	167.233
99	170.000	170.904	172.262	172.937	174.502	173.028	173.349	173.172	172.532	173.499	172.190
100	175.000	177.765	178.693	177.457	178.278	174.875	174.250	173.837	176.404	178.392	174.863
101	180.000	180.000	180.000	180.000	180.000	180.000	180.000	180.000	180.000	180.000	180.000

Figure 7.2.1-3. (continued)

7.2.2 Analog Stokes' Transformation

A summary of the intermediate results during the optimization process on a 34-ring discrete Stokes' summation for the analog transformation converting surface layer densities to geoid height is given in Figure 7.2.2-1. The initial estimate of the template parameters is that of the Pick-Picha-Vyskocil template (for the classic Stokes' summation).

The following points may be noted from the figure:

- a) The spherical ring boundary radii numbered 28 through 33 have merged together by the tenth iteration to the approximate value 153.2° . Hence five of the parameters have become "locked". If the program had the astuteness to recognize this situation, remove the "locked" variables, and insert them as five new independent variables throughout the range of variation, an entirely different set of results might have been obtained.
- b) As in the classic Stokes' case, the "gap" between the ring boundary radii around the first zero in the classic Stokes' function was eliminated during the optimization.

7.2.3 Discussion of Stokes' Transformation Results

The optimization process for the discrete Stokes' summation transformation generally appears to be working well. Moderate decreases in the global rms discretization error have been achieved in all cases. Certainly, larger decreases are desired, but it is not yet clear how close the results are to the true minima.

SUMMARY OF COMPLETE RUN

	ITER# 0	ITER# 1	ITER# 2	ITER# 3	ITER# 4	ITER# 5	ITER# 6	ITER# 7	ITER# 8	ITER# 9	ITER#10
FIGURE OF MERIT	0.689	0.318	0.243	0.226	0.219	0.230	0.222	0.220	0.220	0.231	0.223

VALUES OF PARAMETERS

RING# SPHERICAL RING RADII (DEGREES)

0	0.000	0.000	0.000	0.000	0.000	0.000	0.000	0.000	0.000	0.000	0.000
1	0.058	0.068	0.068	0.068	0.068	0.068	0.063	0.068	0.068	0.068	0.068
2	0.175	0.175	0.175	0.175	0.175	0.175	0.175	0.175	0.175	0.175	0.175
3	0.303	0.308	0.308	0.308	0.308	0.308	0.308	0.308	0.308	0.308	0.308
4	0.447	0.447	0.447	0.447	0.447	0.447	0.447	0.447	0.447	0.447	0.447
5	0.712	0.712	0.712	0.712	0.712	0.712	0.712	0.712	0.712	0.712	0.712
6	0.976	0.924	1.001	1.123	1.131	1.269	1.179	1.420	1.336	1.443	1.331
7	1.235	1.192	1.326	1.456	1.825	1.654	1.903	1.939	2.234	1.954	2.236
8	1.498	1.837	1.690	2.056	2.272	2.814	2.586	2.858	2.844	3.293	3.030
9	1.986	2.211	2.630	2.650	3.185	3.494	4.041	3.673	4.125	4.124	4.640
10	2.478	2.664	3.350	3.931	4.082	4.607	4.909	5.415	5.200	5.606	5.672
11	2.961	3.941	4.301	5.150	5.267	5.833	6.021	6.808	6.593	7.062	7.033
12	4.148	5.091	5.960	6.396	7.297	7.098	7.871	8.133	9.035	8.520	9.200
13	5.884	6.630	7.546	8.574	8.826	9.893	9.591	10.469	10.645	11.553	11.015
14	8.180	8.400	9.840	10.547	11.634	11.865	12.815	12.551	13.528	13.514	14.439
15	10.438	10.865	12.390	13.180	14.352	14.572	15.478	15.464	16.130	16.299	16.973
16	12.850	14.777	15.129	17.127	17.130	18.564	18.207	19.423	18.866	19.950	19.692
17	15.990	18.411	19.734	20.704	21.633	21.905	22.720	22.657	23.468	23.168	23.973
18	20.170	22.698	25.140	25.067	26.354	26.147	27.037	26.986	27.499	27.637	27.828
19	25.300	28.686	30.558	31.435	31.111	31.963	31.655	32.294	32.140	32.566	32.576
20	33.900	36.549	37.752	37.610	37.757	37.634	37.886	37.849	38.038	38.095	38.257
21	52.000	48.222	45.928	45.363	45.028	44.884	44.835	44.832	44.842	44.915	44.987
22	61.000	58.951	55.974	54.561	53.968	53.630	53.465	53.362	53.307	53.327	53.356
23	72.000	70.026	67.499	65.903	65.083	64.611	64.343	64.162	64.046	64.008	63.987
24	82.000	81.281	80.275	79.525	78.930	78.482	78.162	77.927	77.757	77.641	77.557
25	94.200	94.980	95.854	96.091	95.849	95.550	95.263	95.038	94.852	94.668	94.522
26	106.300	108.178	110.817	113.039	114.292	114.892	115.100	115.149	115.103	114.971	114.819
27	126.300	124.899	127.307	130.773	133.664	135.575	136.738	137.393	137.727	137.659	137.656
28	135.900	135.502	138.366	143.667	147.603	150.548	151.041	152.614	152.925	153.101	153.116
29	142.700	143.056	145.098	148.655	151.326	152.173	152.810	153.003	153.145	153.159	153.144
30	149.000	149.150	149.602	152.030	152.339	152.971	153.052	153.181	153.199	153.185	153.164
31	155.400	155.180	152.667	153.491	153.119	153.295	153.213	153.251	153.234	153.242	153.197
32	162.900	161.317	156.120	155.215	153.828	153.649	153.365	153.327	153.266	153.258	153.245
33	176.400	168.580	162.532	163.602	162.291	159.882	155.777	153.831	153.427	153.298	153.266
34	180.000	180.000	180.000	180.000	180.000	180.000	180.000	180.000	180.000	180.000	180.000

Figure 7.2.2-1. Summary of 34-Ring Template Optimization for the Stokes' Transformation Analog.

7.3 Template Optimization Results for the Vening-Meinesz' Transformation

Five main results have been obtained for the discrete Vening-Meinesz' summation transformation, all of the five being for the analog transformation converting surface layer densities to deflections (strictly, to horizontal gravity disturbance components). Two of the five main cases are for transformations with 23-ring templates, while the other three are for 125-ring templates.

7.3.1 Vening-Meinesz' 23-Ring Template

The two results for the 23-ring case begin with different initial values of the estimated spherical ring boundary radii, one using the equal ring contribution template and the other using the Pick-Picha-Vyskocil template. A summary of the intermediate results of the iterative optimization process for these cases is given in Figures 7.3.1-1 and 7.3.1-2.

The following observations may be made from these figures:

- a) For a small number of spherical ring boundary radii, the equal ring contribution template is a better starting point for the optimization process than the Pick-Picha-Vyskocil template in the sense that the optimization progresses faster to a lower rms discretization error in spite of starting at a slightly higher value of this figure-of-merit.
- b) The optimum values of the spherical ring boundary radii do not seem to have been reached when the runs were terminated, as the rms discretization error was still decreasing consistently at this point.

SUMMARY OF COMPLETE RUN

	ITER# 1	ITER# 2	ITER# 3	ITER# 4	ITER# 5	ITER# 6	ITER# 7	ITER# 8	ITER# 9	ITER#10
FIGURE OF MERIT	7.54E-01	6.63E-01	6.09E-01	5.78E-01	5.59E-01	5.46E-01	5.36E-01	5.29E-01	5.24E-01	5.19E-01

VALUES OF PARAMETERS

RING#	SPHERICAL RING RADII (DEGREES)									
0	0.044	0.044	0.044	0.044	0.044	0.044	0.044	0.044	0.044	0.044
1	0.061	0.061	0.061	0.061	0.061	0.061	0.061	0.061	0.061	0.061
2	0.085	0.085	0.085	0.085	0.085	0.085	0.085	0.085	0.085	0.085
3	0.118	0.118	0.118	0.118	0.118	0.118	0.118	0.118	0.118	0.118
4	0.164	0.164	0.164	0.164	0.164	0.164	0.164	0.164	0.164	0.164
5	0.228	0.228	0.228	0.228	0.228	0.228	0.228	0.228	0.228	0.228
6	0.316	0.316	0.316	0.316	0.316	0.316	0.316	0.316	0.316	0.316
7	0.439	0.439	0.439	0.439	0.439	0.439	0.439	0.439	0.439	0.439
8	0.610	0.610	0.610	0.610	0.610	0.610	0.610	0.610	0.610	0.610
9	0.847	0.848	0.849	0.850	0.850	0.851	0.851	0.852	0.852	0.853
10	1.177	1.177	1.177	1.178	1.178	1.178	1.178	1.179	1.179	1.179
11	1.634	1.635	1.635	1.635	1.635	1.635	1.635	1.636	1.636	1.636
12	2.270	2.271	2.271	2.271	2.271	2.271	2.271	2.271	2.271	2.271
13	3.154	3.154	3.155	3.155	3.155	3.155	3.155	3.155	3.155	3.155
14	4.332	4.333	4.333	4.333	4.334	4.334	4.334	4.334	4.334	4.334
15	6.091	6.092	6.092	6.092	6.093	6.093	6.093	6.093	6.093	6.093
16	8.470	8.471	8.472	8.472	8.472	8.472	8.472	8.472	8.472	8.471
17	11.790	11.792	11.792	11.793	11.793	11.792	11.792	11.791	11.791	11.790
18	16.445	16.445	16.445	16.444	16.443	16.442	16.441	16.440	16.439	16.439
19	23.031	23.018	23.019	23.005	23.003	23.004	23.007	23.012	23.020	23.030
20	32.523	32.450	32.427	32.434	32.463	32.510	32.571	32.645	32.729	32.822
21	46.780	46.527	46.744	47.207	47.705	48.408	49.033	49.636	50.204	50.728
22	70.639	74.560	77.654	80.092	82.030	83.622	84.943	86.054	86.997	87.804
23	179.932	179.932	179.932	179.932	179.932	179.932	179.932	179.932	179.932	179.932

Figure 7.3.1-1. Summary of 23-Ring Template Optimization for the Vening-Meinesz' Analog Transformation, Beginning from an Equal Ring Contribution Template.

SUMMARY OF COMPLETE RUN

	ITER# 0	ITER# 1	ITER# 2	ITER# 3	ITER# 4	ITER# 5
FIGURE OF MERIT	7.14E-01	6.72E-01	6.48E-01	6.34E-01	6.27E-01	6.24E-01

VALUES OF PARAMETERS

RING#	SPHERICAL RING RADII (DEGREES)					
0	0.030	0.030	0.030	0.030	0.030	0.030
1	0.044	0.044	0.044	0.044	0.044	0.044
2	0.063	0.063	0.063	0.063	0.063	0.063
3	0.089	0.089	0.089	0.089	0.089	0.089
4	0.128	0.128	0.128	0.128	0.128	0.128
5	0.183	0.183	0.183	0.183	0.183	0.183
6	0.261	0.261	0.261	0.261	0.261	0.261
7	0.372	0.372	0.372	0.372	0.372	0.372
8	0.530	0.530	0.530	0.530	0.530	0.530
9	0.753	0.753	0.753	0.753	0.753	0.753
10	1.069	1.103	1.130	1.152	1.170	1.185
11	1.754	1.799	1.809	1.819	1.831	1.842
12	2.966	2.955	2.947	2.943	2.942	2.942
13	4.821	4.787	4.758	4.735	4.716	4.701
14	7.591	7.540	7.502	7.471	7.444	7.420
15	11.470	11.553	11.597	11.607	11.598	11.575
16	18.550	18.399	18.252	18.126	18.028	17.946
17	28.300	28.059	27.844	27.649	27.489	27.359
18	40.800	41.129	41.369	41.570	41.664	41.691
19	65.300	64.998	64.744	64.494	64.191	63.852
20	98.600	97.762	96.499	95.025	93.656	92.407
21	114.400	115.725	116.621	117.133	117.460	117.637
22	130.500	129.337	128.799	128.807	129.002	129.535
23	180.000	180.000	180.000	180.000	180.000	180.000

Figure 7.3.1-2. Summary of 23-Ring Template Optimization for the Vening-Meinesz' Analog Transformation, Beginning from the Pick-Picha-Vyskocil Template.

7.3.2 Vening Meinesz' 125-Ring Template

The three results for the 125-ring case consist of two results which begin with an equal ring contribution template and one which begins with the circularized AGEMIT template. A summary of the intermediate results of the optimization process is given in Figures 7.3.2-1, 7.3.2-2, and 7.3.2-3.

The following points may be noted from these figures:

- a) While the circularized AGEMIT template has a lower initial rms discretization error than the equal ring contribution template for this relatively large number of spherical ring boundary radii, and while this lower figure-of-merit is consistently maintained throughout the optimization process, neither template seems to lead to an optimization run with a large reduction of discretization error. This may be due to the nature of the response surface in the vicinity of the template parameter values (which may be relatively "far" from their optimum values), or to the lack of powerfulness of the optimization algorithm for large dimensions.
- b) The optimization beginning with the equal ring contribution template may have reached a local minimum on the sixth iteration with an rms discretization error of about 0.082 mgal. The likelihood of this being the case is strengthened by the rough agreement of the independent optimization run (Figure 7.3.2-2) which converges to approximately the same minimum (0.084 mgal) although the steps are different due to the use of a variant algorithm. Both optimization runs begin to diverge or oscillate after this point.

SUMMARY OF COMPLETE RUN

	ITER# 0	ITER# 1	ITER# 2	ITER# 3	ITER# 4	ITER# 5	ITER# 6	ITER# 7	ITER# 8	ITER# 9	ITER#10
FIGURE OF MERIT	1.33E-01	1.21E-01	1.13E-01	1.02E-01	9.13E-02	8.49E-02	8.21E-02	8.22E-02	8.64E-02	8.99E-02	9.04E-02
VALUES OF PARAMETERS											
RING# SPHERICAL RING RADII (DEGREES)											
0	0.002	0.002	0.002	0.002	0.002	0.002	0.002	0.002	0.002	0.002	0.002
1	0.002	0.002	0.002	0.002	0.002	0.002	0.002	0.002	0.002	0.002	0.002
2	0.003	0.003	0.003	0.003	0.003	0.003	0.003	0.003	0.003	0.003	0.003
3	0.003	0.003	0.003	0.003	0.003	0.003	0.003	0.003	0.003	0.003	0.003
4	0.003	0.003	0.003	0.003	0.003	0.003	0.003	0.003	0.003	0.003	0.003
5	0.003	0.003	0.003	0.003	0.003	0.003	0.003	0.003	0.003	0.003	0.003
6	0.004	0.004	0.004	0.004	0.004	0.004	0.004	0.004	0.004	0.004	0.004
7	0.004	0.004	0.004	0.004	0.004	0.004	0.004	0.004	0.004	0.004	0.004
8	0.004	0.004	0.004	0.004	0.004	0.004	0.004	0.004	0.004	0.004	0.004
9	0.005	0.005	0.005	0.005	0.005	0.005	0.005	0.005	0.005	0.005	0.005
10	0.005	0.005	0.005	0.005	0.005	0.005	0.005	0.005	0.005	0.005	0.005
11	0.005	0.005	0.005	0.005	0.005	0.005	0.005	0.005	0.005	0.005	0.005
12	0.006	0.006	0.006	0.006	0.006	0.006	0.006	0.006	0.006	0.006	0.006
13	0.006	0.006	0.006	0.006	0.006	0.006	0.006	0.006	0.006	0.006	0.006
14	0.007	0.007	0.007	0.007	0.007	0.007	0.007	0.007	0.007	0.007	0.007
15	0.008	0.008	0.008	0.008	0.008	0.008	0.008	0.008	0.008	0.008	0.008
16	0.008	0.008	0.008	0.008	0.008	0.008	0.008	0.008	0.008	0.008	0.008
17	0.009	0.009	0.009	0.009	0.009	0.009	0.009	0.009	0.009	0.009	0.009
18	0.010	0.010	0.010	0.010	0.010	0.010	0.010	0.010	0.010	0.010	0.010
19	0.011	0.011	0.011	0.011	0.011	0.011	0.011	0.011	0.011	0.011	0.011
20	0.012	0.012	0.012	0.012	0.012	0.012	0.012	0.012	0.012	0.012	0.012
21	0.013	0.013	0.013	0.013	0.013	0.013	0.013	0.013	0.013	0.013	0.013
22	0.014	0.014	0.014	0.014	0.014	0.014	0.014	0.014	0.014	0.014	0.014
23	0.015	0.015	0.015	0.015	0.015	0.015	0.015	0.015	0.015	0.015	0.015
24	0.016	0.016	0.016	0.016	0.016	0.016	0.016	0.016	0.016	0.016	0.016
25	0.018	0.018	0.018	0.018	0.018	0.018	0.018	0.018	0.018	0.018	0.018
26	0.019	0.019	0.019	0.019	0.019	0.019	0.019	0.019	0.019	0.019	0.019
27	0.021	0.021	0.021	0.021	0.021	0.021	0.021	0.021	0.021	0.021	0.021
28	0.023	0.023	0.023	0.023	0.023	0.023	0.023	0.023	0.023	0.023	0.023
29	0.025	0.025	0.025	0.025	0.025	0.025	0.025	0.025	0.025	0.025	0.025
30	0.027	0.027	0.027	0.027	0.027	0.027	0.027	0.027	0.027	0.027	0.027
31	0.029	0.029	0.029	0.029	0.029	0.029	0.029	0.029	0.029	0.029	0.029
32	0.032	0.032	0.032	0.032	0.032	0.032	0.032	0.032	0.032	0.032	0.032
33	0.035	0.035	0.035	0.035	0.035	0.035	0.035	0.035	0.035	0.035	0.035
34	0.038	0.038	0.038	0.038	0.038	0.038	0.038	0.038	0.038	0.038	0.038
35	0.041	0.041	0.041	0.041	0.041	0.041	0.041	0.041	0.041	0.041	0.041
36	0.045	0.045	0.045	0.045	0.045	0.045	0.045	0.045	0.045	0.045	0.045
37	0.049	0.049	0.049	0.049	0.049	0.049	0.049	0.049	0.049	0.049	0.049
38	0.053	0.053	0.053	0.053	0.053	0.053	0.053	0.053	0.053	0.053	0.053
39	0.058	0.058	0.058	0.058	0.058	0.058	0.058	0.058	0.058	0.058	0.058
40	0.063	0.063	0.063	0.063	0.063	0.063	0.063	0.063	0.063	0.063	0.063
41	0.068	0.068	0.068	0.068	0.068	0.068	0.068	0.068	0.068	0.068	0.068
42	0.074	0.074	0.074	0.074	0.074	0.074	0.074	0.074	0.074	0.074	0.074
43	0.081	0.081	0.081	0.081	0.081	0.081	0.081	0.081	0.081	0.081	0.081
44	0.088	0.088	0.088	0.088	0.088	0.088	0.088	0.088	0.088	0.088	0.088
45	0.096	0.096	0.096	0.096	0.096	0.096	0.096	0.096	0.096	0.096	0.096
46	0.104	0.104	0.104	0.104	0.104	0.104	0.104	0.104	0.104	0.104	0.104
47	0.113	0.113	0.113	0.113	0.113	0.113	0.113	0.113	0.113	0.113	0.113
48	0.124	0.124	0.124	0.124	0.124	0.124	0.124	0.124	0.124	0.124	0.124
49	0.134	0.134	0.134	0.134	0.134	0.134	0.134	0.134	0.134	0.134	0.134
50	0.146	0.146	0.146	0.146	0.146	0.146	0.146	0.146	0.146	0.146	0.146
51	0.159	0.159	0.159	0.159	0.159	0.159	0.159	0.159	0.159	0.159	0.159
52	0.173	0.173	0.173	0.173	0.173	0.173	0.173	0.173	0.173	0.173	0.173
53	0.189	0.189	0.189	0.189	0.189	0.189	0.189	0.189	0.189	0.189	0.189
54	0.205	0.205	0.205	0.205	0.205	0.205	0.205	0.205	0.205	0.205	0.205
55	0.224	0.224	0.224	0.224	0.224	0.224	0.224	0.224	0.224	0.224	0.224
56	0.243	0.243	0.243	0.243	0.243	0.243	0.243	0.243	0.243	0.243	0.243
57	0.265	0.265	0.265	0.265	0.265	0.265	0.265	0.265	0.265	0.265	0.265
58	0.283	0.288	0.289	0.288	0.288	0.288	0.288	0.288	0.288	0.288	0.288
59	0.314	0.314	0.314	0.314	0.314	0.314	0.314	0.314	0.314	0.314	0.314

Figure 7.3.2-1. Summary of 125-Ring Template Optimization for the Vening-Meinesz' Analog Transformation, Beginning from an Equal Ring Contribution Template. (Damping = 0.5)

60	0.342	0.342	0.342	0.342	0.342	0.342	0.342	0.342	0.342	0.342	0.342
61	0.372	0.372	0.372	0.372	0.372	0.372	0.372	0.372	0.372	0.372	0.372
62	0.405	0.405	0.405	0.405	0.405	0.405	0.405	0.405	0.405	0.405	0.405
63	0.440	0.440	0.440	0.440	0.440	0.440	0.440	0.440	0.440	0.440	0.440
64	0.479	0.479	0.479	0.479	0.479	0.479	0.479	0.479	0.479	0.479	0.479
65	0.522	0.522	0.522	0.522	0.522	0.522	0.522	0.522	0.522	0.522	0.522
66	0.568	0.568	0.568	0.568	0.568	0.568	0.568	0.568	0.568	0.568	0.568
67	0.618	0.618	0.618	0.618	0.618	0.618	0.618	0.618	0.618	0.618	0.618
68	0.673	0.673	0.673	0.673	0.673	0.673	0.673	0.673	0.673	0.673	0.673
69	0.732	0.733	0.733	0.733	0.733	0.733	0.734	0.734	0.743	0.756	0.690
70	0.797	0.797	0.796	0.796	0.795	0.794	0.794	0.794	0.794	0.765	0.801
71	0.868	0.868	0.868	0.869	0.870	0.870	0.870	0.871	0.900	0.902	0.870
72	0.944	0.944	0.945	0.944	0.944	0.944	0.943	0.944	0.910	0.900	1.015
73	1.028	1.028	1.027	1.027	1.027	1.027	1.027	1.027	1.052	1.040	1.064
74	1.119	1.119	1.120	1.120	1.120	1.121	1.121	1.122	1.105	1.109	1.090
75	1.218	1.217	1.217	1.216	1.216	1.216	1.216	1.216	1.226	1.224	1.237
76	1.325	1.326	1.326	1.327	1.327	1.327	1.327	1.328	1.323	1.325	1.313
77	1.443	1.442	1.442	1.442	1.442	1.442	1.442	1.442	1.445	1.444	1.453
78	1.570	1.571	1.571	1.571	1.571	1.572	1.572	1.573	1.571	1.573	1.574
79	1.709	1.709	1.709	1.709	1.709	1.710	1.710	1.710	1.712	1.711	1.708
80	1.860	1.861	1.861	1.861	1.861	1.862	1.863	1.863	1.862	1.861	1.864
81	2.025	2.025	2.025	2.025	2.026	2.026	2.027	2.027	2.020	2.031	2.028
82	2.204	2.204	2.204	2.205	2.205	2.205	2.206	2.206	2.206	2.206	2.207
83	2.399	2.399	2.399	2.400	2.400	2.401	2.401	2.402	2.402	2.402	2.403
84	2.611	2.612	2.612	2.612	2.613	2.613	2.614	2.614	2.614	2.615	2.615
85	2.843	2.843	2.843	2.844	2.845	2.846	2.846	2.846	2.847	2.848	2.840
86	3.094	3.095	3.096	3.097	3.098	3.099	3.100	3.100	3.100	3.101	3.101
87	3.368	3.369	3.369	3.370	3.371	3.372	3.372	3.373	3.373	3.375	3.376
88	3.666	3.667	3.667	3.667	3.668	3.669	3.670	3.671	3.673	3.675	3.676
89	3.991	3.991	3.991	3.991	3.993	3.996	3.997	3.999	4.001	4.003	4.004
90	4.344	4.344	4.344	4.344	4.346	4.349	4.351	4.355	4.357	4.359	4.360
91	4.729	4.729	4.730	4.733	4.736	4.738	4.740	4.741	4.742	4.743	4.743
92	5.148	5.148	5.149	5.153	5.157	5.159	5.160	5.161	5.161	5.163	5.165
93	5.604	5.605	5.609	5.611	5.614	5.616	5.618	5.620	5.624	5.626	5.632
94	6.101	6.104	6.107	6.110	6.113	6.117	6.121	6.124	6.125	6.127	6.133
95	6.642	6.648	6.652	6.655	6.660	6.665	6.669	6.671	6.672	6.677	6.681
96	7.231	7.235	7.238	7.242	7.248	7.254	7.259	7.262	7.262	7.272	7.276
97	7.873	7.876	7.877	7.879	7.883	7.889	7.894	7.897	7.906	7.911	7.915
98	8.572	8.576	8.576	8.577	8.580	8.584	8.588	8.596	8.602	8.606	8.609
99	9.335	9.332	9.334	9.339	9.344	9.347	9.354	9.362	9.365	9.368	9.369
100	10.166	10.169	10.165	10.172	10.180	10.192	10.214	10.227	10.237	10.247	10.256
101	11.071	11.076	11.074	11.076	11.081	11.105	11.119	11.128	11.134	11.140	11.144
102	12.059	12.072	12.075	12.078	12.101	12.115	12.124	12.129	12.132	12.135	12.137
103	13.137	13.144	13.144	13.156	13.185	13.205	13.221	13.234	13.244	13.253	13.260
104	14.314	14.308	14.314	14.335	14.356	14.373	14.390	14.402	14.412	14.422	14.432
105	15.599	15.596	15.600	15.605	15.615	15.624	15.627	15.629	15.629	15.627	15.626
106	17.003	17.022	17.059	17.104	17.144	17.173	17.193	17.204	17.211	17.217	17.219
107	18.539	18.609	18.662	18.714	18.766	18.807	18.842	18.866	18.884	18.902	18.924
108	20.220	20.294	20.296	20.289	20.312	20.356	20.403	20.454	20.510	20.570	20.632
109	22.062	22.069	22.090	22.097	22.100	22.082	22.044	21.989	21.929	21.868	21.807
110	24.004	24.108	24.112	24.153	24.215	24.274	24.328	24.370	24.406	24.439	24.471
111	26.307	26.238	26.195	26.180	26.199	26.242	26.286	26.313	26.329	26.341	26.352
112	28.755	28.859	28.929	28.983	29.017	29.024	29.013	28.999	28.984	28.971	28.959
113	31.457	31.591	31.741	31.907	32.050	32.172	32.202	32.303	32.498	32.615	32.718
114	34.451	34.606	34.717	34.857	35.073	35.318	35.588	35.894	36.014	36.070	36.099
115	37.779	37.775	37.508	37.155	36.910	36.741	36.576	36.345	36.239	36.183	36.155
116	41.496	41.238	41.298	41.446	41.514	41.464	41.341	41.171	40.971	40.760	40.500
117	45.674	45.771	45.793	45.999	46.309	46.671	47.038	47.379	47.691	47.980	48.246
118	50.408	50.562	50.721	50.813	50.926	51.043	51.128	51.146	51.118	51.063	50.987
119	55.830	56.600	57.205	57.790	58.326	58.698	58.950	59.177	59.389	59.526	59.766
120	62.132	62.047	61.867	61.838	62.086	62.572	63.146	63.564	63.886	64.177	64.458
121	69.617	69.249	68.509	68.164	68.433	68.774	68.988	69.068	69.112	69.202	69.385
122	78.811	79.119	80.433	82.324	84.124	85.613	86.814	87.776	88.617	89.409	90.204
123	90.780	93.236	94.147	94.449	94.925	95.325	95.550	95.508	95.339	95.093	94.755
124	108.470	110.141	111.377	113.269	115.635	117.644	119.155	120.112	120.709	121.349	121.854
125	179.997	179.997	179.997	179.997	179.997	179.997	179.997	179.997	179.997	179.997	179.997

Figure 7.3.2-1. (continued)

SUMMARY OF COMPLETE RUN

	ITER# 1	ITER# 2	ITER# 3	ITER# 4	ITER# 5	ITER# 6
FIGURE OF MERIT	1.33E-01	1.02E-01	8.48E-02	1.13E-01	1.31E-01	1.08E-01

VALUES OF PARAMETERS

RING#	SPHERICAL RING RADII (DEGREES)					
0	0.002	0.002	0.002	0.002	0.002	0.002
1	0.002	0.002	0.002	0.002	0.002	0.002
2	0.003	0.003	0.003	0.003	0.003	0.003
3	0.003	0.003	0.003	0.003	0.003	0.003
4	0.003	0.003	0.003	0.003	0.003	0.003
5	0.003	0.003	0.003	0.003	0.003	0.003
6	0.004	0.004	0.004	0.004	0.004	0.004
7	0.004	0.004	0.004	0.004	0.004	0.004
8	0.004	0.004	0.004	0.004	0.004	0.004
9	0.005	0.005	0.005	0.005	0.005	0.005
10	0.005	0.005	0.005	0.005	0.005	0.005
11	0.005	0.005	0.005	0.005	0.005	0.005
12	0.006	0.006	0.006	0.006	0.006	0.006
13	0.006	0.006	0.006	0.006	0.006	0.006
14	0.007	0.007	0.007	0.007	0.007	0.007
15	0.008	0.008	0.008	0.008	0.008	0.008
16	0.008	0.008	0.008	0.008	0.008	0.008
17	0.009	0.009	0.009	0.009	0.009	0.009
18	0.010	0.010	0.010	0.010	0.010	0.010
19	0.011	0.011	0.011	0.011	0.011	0.011
20	0.012	0.012	0.012	0.012	0.012	0.012
21	0.013	0.013	0.013	0.013	0.013	0.013
22	0.014	0.014	0.014	0.014	0.014	0.014
23	0.015	0.015	0.015	0.015	0.015	0.015
24	0.016	0.016	0.016	0.016	0.016	0.016
25	0.018	0.018	0.018	0.018	0.018	0.018
26	0.019	0.019	0.019	0.019	0.019	0.019
27	0.021	0.021	0.021	0.021	0.021	0.021
28	0.023	0.023	0.023	0.023	0.023	0.023
29	0.025	0.025	0.025	0.025	0.025	0.025
30	0.027	0.027	0.027	0.027	0.027	0.027
31	0.029	0.029	0.029	0.029	0.029	0.029
32	0.032	0.032	0.032	0.032	0.032	0.032
33	0.035	0.035	0.035	0.035	0.035	0.035
34	0.038	0.038	0.038	0.038	0.038	0.038
35	0.041	0.041	0.041	0.041	0.041	0.041
36	0.045	0.045	0.045	0.045	0.045	0.045
37	0.049	0.049	0.049	0.049	0.049	0.049
38	0.053	0.053	0.053	0.053	0.053	0.053
39	0.058	0.058	0.058	0.058	0.058	0.058
40	0.063	0.063	0.063	0.063	0.063	0.063
41	0.068	0.068	0.068	0.068	0.068	0.068
42	0.074	0.074	0.074	0.074	0.074	0.074
43	0.081	0.081	0.081	0.081	0.081	0.081
44	0.088	0.088	0.088	0.088	0.088	0.088
45	0.096	0.096	0.096	0.096	0.096	0.096
46	0.104	0.104	0.104	0.104	0.104	0.104
47	0.113	0.113	0.113	0.113	0.113	0.113
48	0.124	0.124	0.124	0.124	0.124	0.124
49	0.134	0.134	0.134	0.134	0.134	0.134
50	0.146	0.146	0.146	0.146	0.146	0.146
51	0.159	0.159	0.159	0.159	0.159	0.159
52	0.173	0.173	0.173	0.173	0.173	0.173
53	0.189	0.189	0.189	0.189	0.189	0.189
54	0.205	0.205	0.205	0.205	0.205	0.205
55	0.224	0.224	0.224	0.224	0.224	0.224
56	0.243	0.243	0.243	0.243	0.243	0.243
57	0.265	0.265	0.265	0.265	0.265	0.265
58	0.288	0.288	0.288	0.288	0.288	0.288
59	0.314	0.314	0.314	0.314	0.314	0.314

Figure 7.3.2-2. Summary of 125-Ring Template Optimization for the Vening-Meinesz' Analog Transformation, Beginning from an Equal Ring Contribution Template. (Damping = 0.25)

60	0.342	0.342	0.342	0.342	0.342	0.342
61	0.372	0.372	0.372	0.372	0.372	0.372
62	0.405	0.405	0.405	0.405	0.405	0.405
63	0.440	0.440	0.440	0.440	0.440	0.440
64	0.479	0.479	0.479	0.479	0.479	0.479
65	0.522	0.522	0.522	0.522	0.522	0.522
66	0.568	0.568	0.568	0.568	0.568	0.568
67	0.618	0.618	0.618	0.618	0.618	0.618
68	0.673	0.673	0.673	0.673	0.673	0.673
69	0.732	0.732	0.732	0.732	0.732	0.732
70	0.797	0.815	0.844	0.925	0.933	0.777
71	0.868	0.850	0.944	0.958	0.950	0.937
72	0.944	0.936	0.999	0.926	0.964	0.953
73	1.028	1.003	1.113	1.024	1.184	1.012
74	1.117	1.144	1.184	1.221	1.239	1.248
75	1.218	1.194	1.325	1.291	1.274	1.265
76	1.325	1.356	1.403	1.341	1.301	1.279
77	1.443	1.414	1.568	1.437	1.609	1.368
78	1.570	1.604	1.622	1.650	1.664	1.671
79	1.709	1.674	1.656	1.668	1.673	1.676
80	1.860	1.724	1.700	1.689	1.604	1.631
81	2.025	1.868	1.871	1.888	1.897	1.934
82	2.204	2.068	2.070	2.073	2.065	2.071
83	2.399	2.264	2.287	2.295	2.290	2.301
84	2.611	2.531	2.534	2.541	2.536	2.546
85	2.843	2.794	2.797	2.803	2.799	2.809
86	3.094	3.067	3.068	3.069	3.066	3.074
87	3.369	3.340	3.353	3.357	3.362	3.371
88	3.666	3.661	3.657	3.657	3.658	3.659
89	3.991	3.994	3.995	3.997	3.999	3.997
90	4.344	4.345	4.346	4.346	4.347	4.346
91	4.729	4.729	4.729	4.728	4.730	4.730
92	5.148	5.146	5.149	5.150	5.149	5.149
93	5.604	5.598	5.599	5.604	5.606	5.610
94	6.101	6.100	6.097	6.099	6.101	6.102
95	6.642	6.645	6.639	6.637	6.633	6.633
96	7.231	7.235	7.225	7.222	7.219	7.217
97	7.873	7.875	7.877	7.880	7.874	7.877
98	8.572	8.575	8.579	8.582	8.580	8.580
99	9.335	9.335	9.342	9.343	9.341	9.341
100	10.166	10.168	10.170	10.171	10.165	10.164
101	11.071	11.069	11.067	11.066	11.065	11.064
102	12.059	12.059	12.057	12.056	12.054	12.050
103	13.137	13.133	13.136	13.139	13.142	13.141
104	14.314	14.317	14.315	14.315	14.320	14.320
105	15.599	15.601	15.602	15.598	15.608	15.609
106	17.093	16.993	17.007	17.015	17.025	17.034
107	18.539	18.535	18.544	18.543	18.549	18.557
108	20.220	20.227	20.230	20.233	20.233	20.242
109	22.062	22.071	22.085	22.089	22.087	22.090
110	24.084	24.096	24.100	24.113	24.121	24.130
111	26.307	26.319	26.326	26.333	26.341	26.348
112	28.755	28.775	28.789	28.792	28.797	28.790
113	31.457	31.483	31.487	31.493	31.485	31.493
114	34.451	34.474	34.469	34.478	34.491	34.501
115	37.779	37.773	37.788	37.818	37.837	37.840
116	41.496	41.495	41.502	41.483	41.447	41.407
117	45.674	45.701	45.633	45.566	45.512	45.448
118	50.408	50.356	50.307	50.237	50.170	50.117
119	55.830	55.608	55.450	55.338	55.281	55.253
120	62.132	61.926	61.817	61.911	62.070	62.213
121	69.617	69.877	70.179	70.185	70.110	70.044
122	78.811	78.860	78.677	78.544	78.458	78.392
123	90.780	91.525	93.204	94.325	94.904	95.253
124	108.470	113.447	117.084	119.626	121.557	122.842
125	180.000	180.000	180.000	180.000	180.000	180.000

Figure 7.3.2-2. (continued)

SUMMARY OF COMPLETE RUN

	ITER# 0	ITER# 1	ITER# 2	ITER# 3	ITER# 4	ITER# 5	ITER# 6
FIGURE OF MERIT	7.49E-02	7.02E-02	6.91E-02	6.71E-02	6.55E-02	6.42E-02	6.33E-02

VALUES OF PARAMETERS

RING#	SPHERICAL RING RADII (DEGREES)						
0	0.002	0.002	0.002	0.002	0.002	0.002	0.002
1	0.003	0.003	0.003	0.003	0.003	0.003	0.003
2	0.003	0.003	0.003	0.003	0.003	0.003	0.003
3	0.004	0.004	0.004	0.004	0.004	0.004	0.004
4	0.004	0.004	0.004	0.004	0.004	0.004	0.004
5	0.005	0.005	0.005	0.005	0.005	0.005	0.005
6	0.006	0.006	0.006	0.006	0.006	0.006	0.006
7	0.007	0.007	0.007	0.007	0.007	0.007	0.007
8	0.008	0.008	0.008	0.008	0.008	0.008	0.008
9	0.010	0.010	0.010	0.010	0.010	0.010	0.010
10	0.012	0.012	0.012	0.012	0.012	0.012	0.012
11	0.014	0.014	0.014	0.014	0.014	0.014	0.014
12	0.017	0.017	0.017	0.017	0.017	0.017	0.017
13	0.020	0.020	0.020	0.020	0.020	0.020	0.020
14	0.023	0.023	0.023	0.023	0.023	0.023	0.023
15	0.028	0.028	0.028	0.028	0.028	0.028	0.028
16	0.033	0.033	0.033	0.033	0.033	0.033	0.033
17	0.039	0.039	0.039	0.039	0.039	0.039	0.039
18	0.046	0.046	0.046	0.046	0.046	0.046	0.046
19	0.055	0.055	0.055	0.055	0.055	0.055	0.055
20	0.065	0.065	0.065	0.065	0.065	0.065	0.065
21	0.077	0.077	0.077	0.077	0.077	0.077	0.077
22	0.091	0.091	0.091	0.091	0.091	0.091	0.091
23	0.103	0.103	0.103	0.103	0.103	0.103	0.103
24	0.129	0.129	0.129	0.129	0.129	0.129	0.129
25	0.152	0.152	0.152	0.152	0.152	0.152	0.152
26	0.181	0.181	0.181	0.181	0.181	0.181	0.181
27	0.214	0.214	0.214	0.214	0.214	0.214	0.214
28	0.254	0.254	0.254	0.254	0.254	0.254	0.254
29	0.301	0.301	0.301	0.301	0.301	0.301	0.301
30	0.357	0.357	0.357	0.357	0.357	0.357	0.357
31	0.423	0.423	0.423	0.423	0.423	0.423	0.423
32	0.501	0.501	0.501	0.501	0.501	0.501	0.501
33	0.593	0.593	0.593	0.593	0.593	0.593	0.593
34	0.701	0.701	0.701	0.701	0.701	0.701	0.701
35	0.829	0.830	0.830	0.830	0.830	0.830	0.830
36	1.000	0.994	0.991	0.988	0.934	0.931	0.977
37	1.003	1.006	1.000	1.076	1.076	1.074	1.074
38	1.167	1.157	1.167	1.173	1.173	1.176	1.175
39	1.250	1.270	1.239	1.231	1.231	1.228	1.230
40	1.333	1.298	1.329	1.335	1.336	1.336	1.334
41	1.417	1.437	1.432	1.425	1.428	1.424	1.426
42	1.500	1.479	1.481	1.486	1.485	1.489	1.489
43	1.583	1.620	1.626	1.629	1.631	1.631	1.632
44	1.667	1.647	1.639	1.636	1.634	1.633	1.633
45	1.750	1.751	1.753	1.752	1.749	1.748	1.746
46	1.833	1.844	1.849	1.853	1.859	1.863	1.867
47	1.917	1.904	1.896	1.891	1.886	1.883	1.879
48	2.000	2.005	2.010	2.010	2.009	2.008	2.007
49	2.083	2.083	2.088	2.089	2.093	2.095	2.099
50	2.167	2.157	2.152	2.149	2.146	2.143	2.141
51	2.250	2.258	2.265	2.267	2.268	2.268	2.268
52	2.333	2.329	2.324	2.326	2.327	2.328	2.329
53	2.417	2.417	2.416	2.410	2.407	2.404	2.402
54	2.500	2.499	2.501	2.508	2.512	2.517	2.521
55	2.583	2.587	2.590	2.585	2.581	2.575	2.571
56	2.667	2.657	2.650	2.652	2.654	2.657	2.659
57	2.750	2.762	2.773	2.779	2.783	2.782	2.780
58	2.833	2.828	2.815	2.807	2.806	2.803	2.805
59	2.917	2.912	2.918	2.920	2.919	2.919	2.918

Figure 7.3.2-3. Summary of 125-Ring Template Optimization for the Vening-Meinesz' Analog Transformation, Beginning from Circularized AGEMIT Template.

60	3.000	3.000	3.009	3.012	3.015	3.018	3.021
61	3.250	3.240	3.247	3.246	3.245	3.245	3.245
62	3.500	3.501	3.501	3.501	3.501	3.501	3.501
63	3.750	3.747	3.746	3.745	3.743	3.742	3.742
64	4.000	4.001	4.002	4.003	4.003	4.004	4.004
65	4.250	4.247	4.245	4.244	4.242	4.241	4.241
66	4.500	4.501	4.502	4.503	4.504	4.505	4.506
67	4.750	4.747	4.746	4.744	4.743	4.741	4.740
68	5.000	4.995	4.995	4.995	4.995	4.995	4.996
69	5.250	5.243	5.239	5.237	5.234	5.232	5.230
70	5.500	5.496	5.497	5.498	5.498	5.498	5.498
71	5.750	5.745	5.743	5.742	5.740	5.738	5.736
72	6.000	6.000	6.000	6.001	6.002	6.003	6.005
73	6.250	6.244	6.240	6.237	6.234	6.231	6.228
74	6.500	6.498	6.498	6.498	6.497	6.497	6.497
75	6.750	6.749	6.749	6.750	6.751	6.752	6.753
76	7.000	7.016	7.033	7.050	7.066	7.080	7.095
77	8.000	7.908	7.981	7.977	7.973	7.971	7.970
78	9.000	8.993	8.984	8.977	8.970	8.965	8.959
79	10.000	9.993	9.985	9.979	9.973	9.968	9.961
80	11.000	10.992	10.985	10.979	10.974	10.969	10.965
81	12.000	11.988	11.980	11.974	11.968	11.963	11.960
82	13.000	13.006	13.013	13.018	13.021	13.024	13.027
83	14.000	13.971	13.946	13.925	13.905	13.890	13.878
84	15.000	15.012	15.028	15.041	15.048	15.056	15.065
85	16.000	15.972	15.946	15.924	15.903	15.882	15.862
86	17.000	17.002	17.004	17.008	17.014	17.020	17.026
87	18.000	18.003	18.007	18.015	18.024	18.029	18.032
88	19.000	18.970	18.942	18.923	18.909	18.894	18.870
89	20.000	20.023	20.044	20.071	20.104	20.132	20.154
90	21.000	20.971	20.948	20.928	20.908	20.890	20.869
91	22.000	21.995	21.992	21.994	21.997	22.000	22.004
92	23.000	22.995	22.997	23.005	23.014	23.022	23.029
93	24.000	23.955	23.925	23.910	23.903	23.902	23.906
94	25.000	25.153	25.294	25.422	25.538	25.642	25.735
95	30.000	30.009	30.004	29.969	29.932	29.900	29.873
96	35.000	34.949	34.905	34.853	34.821	34.780	34.738
97	40.000	39.966	39.948	39.935	39.921	39.905	39.884
98	45.000	44.981	44.963	44.946	44.927	44.906	44.886
99	50.000	49.957	49.930	49.908	49.887	49.866	49.847
100	55.000	54.893	54.807	54.728	54.656	54.593	54.535
101	60.000	59.910	59.845	59.775	59.733	59.716	59.684
102	65.000	64.922	64.873	64.849	64.831	64.813	64.793
103	70.000	69.925	69.877	69.850	69.829	69.810	69.793
104	75.000	74.946	74.916	74.894	74.877	74.861	74.846
105	80.000	79.947	79.913	79.893	79.877	79.861	79.845
106	85.000	84.940	84.900	84.873	84.852	84.849	84.830
107	90.000	89.933	89.893	89.874	89.861	89.850	89.841
108	95.000	94.923	94.875	94.853	94.840	94.829	94.819
109	100.000	99.920	99.871	99.844	99.827	99.814	99.802
110	105.000	104.911	104.853	104.822	104.802	104.785	104.772
111	110.000	109.921	109.874	109.848	109.832	109.822	109.814
112	115.000	114.939	114.907	114.886	114.894	114.894	114.896
113	120.000	119.954	119.935	119.939	119.949	119.958	119.966
114	125.000	124.961	124.950	124.964	124.984	125.002	125.017
115	130.000	129.949	129.922	129.913	129.909	129.906	129.903
116	135.000	134.943	134.943	134.932	134.926	134.921	134.918
117	140.000	139.984	139.978	139.977	139.978	139.980	139.983
118	145.000	145.019	145.037	145.051	145.063	145.073	145.080
119	150.000	150.049	150.079	150.093	150.096	150.099	150.075
120	155.000	155.053	155.130	155.151	155.160	155.150	155.144
121	160.000	159.989	159.940	159.873	159.797	159.724	159.659
122	165.000	164.681	164.483	164.482	164.555	164.634	164.714
123	170.000	169.960	169.970	169.892	169.727	169.624	169.615
124	175.000	174.772	174.822	174.915	174.924	174.912	174.969
125	180.000	180.000	180.000	180.000	180.000	180.000	180.000

Figure 7.3.2-3. (continued)

7.3.3 Discussion of Vening-Meinesz' Transformation Results

The optimization process for the discrete Vening-Meinesz' summation transformation has been demonstrated to work. However, only marginal to mediocre decreases in the global rms discretization error have generally been obtained. Nevertheless, the feasibility of the process has been proven and one or two fairly good runs indicate that the possibility of some significant reductions do exist.

Some possible reasons for the marginal to mediocre results are:

- i) The optimization runs generally require extensive use of the "projection" algorithm to force satisfaction of the inequality constraints (i.e. to prevent overlapping of parameters). This is very detrimental to convergence.
- ii) Typically, a much larger percentage of the ring boundary radii are closer to the origin in the Vening-Meinesz' case, and have therefore been excluded from adjustment during optimization. These parameters may have a larger effect than previously thought.
- iii) The Gauss-Newton algorithm used in the optimization runs implicitly assumes a quadratic surface model in the neighborhood of the current values of the parameters. This is because of the linearization of the least-squares problem. A true Newton method involves a matrix of second partial derivatives in addition, which has been neglected in this implementation. This can be of importance if the response surface is highly non-linear.*

*Dahlquist-Björk (1974, pg. 444); Dennis [1977, pg. 296, where the second partial derivative term is called $\mathcal{S}(\mathbf{x})$].

7.4 Template Optimization Results Using Variations in the Optimization Algorithm

7.4.1 Increment Damping Variation

The variation of the optimization algorithm which involves the damping of the increments to the independent template parameters was described in Section 6.3.4.1. The increment damping variation seems to perform well the function for which it was intended for templates with a relatively small number of ring radii, but gives the opposite behavior for templates with a relatively large number of ring radii.

The behavior of the optimization variation for 23-ring templates is illustrated by two principal cases which have as their initial estimate of template parameters the Pick-Picha-Vyskocil template and the equal ring contribution template.

In the Pick-Picha-Vyskocil case, the summary of the intermediate results of optimization process is given in Figure 7.4.1-1(a,b,c), from which it is seen that:

- a) With no damping (figure a), the figure-of-merit decreases for two iterations and then increases for the following eight iterations. The ring boundary radii numbered 21 and 22, seem to oscillate in alternate iterations between two regions of values, one of which is emphasized by circles in the figure. If the oscillation could be controlled, a minimum might be reached more easily.
- b) With moderate damping (figure b), the figure-of-merit decreases monotonically for at least five iterations although at a much slower rate. The oscillation in ring boundary radii #21 and #22 has been suppressed as desired. The damping parameter value is 0.25, which is slightly too strong; the spherical ring radii parameter #20 is not making sufficiently rapid enough progress to a value of about 92° . [The computer printout of the summary is not available because the run stopped on maximum time before it had been printed; however, the values listed in the summary have been assembled from a more detailed listing of the run.]
- c) With extremely high damping (figure c), the figure-of-merit decreases extremely slowly as the parameters change extremely slowly. The damping parameter has the value 0.0, which occurred accidentally.

SUMMARY OF COMPLETE RUN

	ITER# 0	ITER# 1	ITER# 2	ITER# 3	ITER# 4	ITER# 5	ITER# 6	ITER# 7	ITER# 8	ITER# 9	ITER#10
FIGURE OF MERIT	7.14E-01	6.37E-01	6.36E-01	6.55E-01	6.70E-01	6.96E-01	7.11E-01	7.26E-01	7.33E-01	7.48E-01	7.48E-01

VALUES OF PARAMETERS

RING# SPHERICAL RING RADII (DEGREES)

0	0.030	0.030	0.030	0.030	0.030	0.030	0.030	0.030	0.030	0.030	0.030
1	0.044	0.044	0.044	0.044	0.044	0.044	0.044	0.044	0.044	0.044	0.044
2	0.063	0.063	0.063	0.063	0.063	0.063	0.063	0.063	0.063	0.063	0.063
3	0.089	0.089	0.089	0.089	0.089	0.089	0.089	0.089	0.089	0.089	0.089
4	0.128	0.128	0.128	0.128	0.128	0.128	0.128	0.128	0.128	0.128	0.128
5	0.183	0.183	0.183	0.183	0.183	0.183	0.183	0.183	0.183	0.183	0.183
6	0.261	0.261	0.261	0.261	0.261	0.261	0.261	0.261	0.261	0.261	0.261
7	0.372	0.372	0.372	0.372	0.372	0.372	0.372	0.372	0.372	0.372	0.372
8	0.530	0.530	0.530	0.530	0.530	0.530	0.530	0.530	0.530	0.530	0.530
9	0.753	0.750	0.750	0.750	0.750	0.750	0.750	0.750	0.750	0.750	0.750
10	1.069	1.153	1.213	1.249	1.276	1.293	1.308	1.317	1.326	1.332	1.337
11	1.794	1.855	1.913	1.956	1.992	2.017	2.041	2.057	2.073	2.085	2.093
12	2.966	2.957	3.030	3.072	3.113	3.145	3.175	3.198	3.221	3.238	3.251
13	4.821	4.775	4.790	4.821	4.859	4.892	4.927	4.954	4.962	5.004	5.021
14	7.591	7.516	7.516	7.531	7.558	7.584	7.616	7.642	7.671	7.694	7.710
15	11.470	11.653	11.691	11.691	11.694	11.702	11.720	11.735	11.754	11.765	11.772
16	13.550	13.265	13.114	13.039	12.987	12.970	12.951	12.943	12.927	12.906	12.890
17	28.300	28.032	27.780	27.657	27.528	27.492	27.395	27.351	27.254	27.171	27.119
18	40.890	42.186	42.271	42.235	42.020	41.945	41.696	41.505	41.340	41.172	41.078
19	65.300	64.666	64.277	63.951	63.619	63.177	62.790	62.444	62.128	61.911	61.780
20	93.600	92.944	92.839	91.675	92.107	90.140	90.635	89.170	89.970	89.269	89.619
21	114.400	127.026	116.627	127.559	109.118	127.806	113.438	129.772	113.552	133.550	107.697
22	130.500	153.418	130.478	169.556	133.185	159.533	130.117	158.260	133.339	169.687	138.413
23	180.000	180.000	180.000	180.000	180.000	180.000	180.000	180.000	180.000	180.000	180.000

Figure 7.4.1-la. Comparison of Vening-Meinesz' Optimization Using Increment Damping Variation. No Damping (damping parameter = 0.50).

SUMMARY OF COMPLETE RUN

	ITER# 0	ITER# 1	ITER# 2	ITER# 3	ITER# 4	ITER# 5
--	---------	---------	---------	---------	---------	---------

Figure of Merit

	.71433	.70587	.69903	.69422	.69037	?
--	--------	--------	--------	--------	--------	---

Values of Parameters

Ring # Spherical Ring Radii (Degrees)

...

20	98.600	97.244	96.294	95.676	95.181	94.753
21	114.400	117.809	121.985	123.970	124.641	124.660
22	130.500	135.509	142.189	147.264	149.403	149.924
23	180.000	180.000	180.000	180.000	180.000	180.000

Figure 7.4.1-lb. Comparison of Vening-Meinesz' Optimization Using Increment Damping Variation. Moderate Damping (damping parameter = 0.25).

SUMMARY OF COMPLETE RUN

	ITER# 0	ITER# 1	ITER# 2	ITER# 3	ITER# 4	ITER# 5
FIGURE OF MERIT						
	7.14E-01	7.14E-01	7.13E-01	7.12E-01	7.11E-01	7.11E-01
VALUES OF PARAMETERS						
RING# SPHERICAL RING RADII (DEGREES)						
0	0.030	0.030	0.030	0.030	0.030	0.030
1	0.044	0.044	0.044	0.044	0.044	0.044
2	0.063	0.063	0.063	0.063	0.063	0.063
3	0.089	0.089	0.089	0.089	0.089	0.089
4	0.128	0.128	0.128	0.128	0.128	0.128
5	0.183	0.183	0.183	0.183	0.183	0.183
6	0.261	0.261	0.261	0.261	0.261	0.261
7	0.372	0.372	0.372	0.372	0.372	0.372
8	0.530	0.530	0.530	0.530	0.530	0.530
9	0.753	0.752	0.751	0.751	0.750	0.750
10	1.069	1.069	1.069	1.069	1.069	1.069
11	1.794	1.794	1.794	1.794	1.794	1.794
12	2.966	2.966	2.966	2.966	2.965	2.965
13	4.821	4.821	4.820	4.820	4.820	4.819
14	7.591	7.590	7.590	7.589	7.588	7.588
15	11.470	11.472	11.474	11.475	11.477	11.479
16	18.550	18.546	18.542	18.538	18.534	18.530
17	28.300	28.296	28.291	28.287	28.283	28.278
18	40.800	40.822	40.843	40.864	40.884	40.905
19	65.300	65.272	65.244	65.217	65.190	65.163
20	98.600	98.472	98.344	98.217	98.090	97.965
21	114.400	114.467	114.535	114.606	114.679	114.753
22	130.500	130.653	130.807	130.963	131.120	131.280
23	180.000	180.000	180.000	180.000	180.000	180.000

Figure 7.4.1-lc. Comparison of Vening-Meinesz' Optimization Using Increment Damping Variation. Extremely High Damping (damping parameter = 0.00).

In the Equal Ring Contribution Template case, an analogous situation occurs. A summary of the intermediate results of the optimization process is given in Figure 7.4.1-2(b,c)*, from which it may be observed that:

With moderate damping (figure b), the figure-of-merit decreases slowly and nonmonotonically as do the values of the template parameters. The change is, however, slightly faster than that for the Pick-Picha-Vyskocil template (Figure 7.4.1-lb), although the damping parameter is stronger here than it is there.

With high damping (figure c), the figure-of-merit and the values of the parameters change more slowly than with moderate damping, as expected.

*The 23-ring equal ring contribution case with no damping was not run, so no Figure "a" appears.

SUMMARY OF COMPLETE RUN

ITER# 1 ITER# 2 ITER# 3 ITER# 4 ITER# 5 ITER# 6 ITER# 7 ITER# 8 ITER# 9 ITER#10
 FIGURE OF MERIT
 7.54E-01 6.63E-01 6.09E-01 5.78E-01 5.59E-01 5.46E-01 5.36E-01 5.29E-01 5.24E-01 5.19E-01

VALUES OF PARAMETERS

RING# SPHERICAL RING RADII (DEGREES)

0	0.044	0.044	0.044	0.044	0.044	0.044	0.044	0.044	0.044	0.044
1	0.061	0.061	0.061	0.061	0.061	0.061	0.061	0.061	0.061	0.061
2	0.085	0.085	0.085	0.085	0.085	0.085	0.085	0.085	0.085	0.085
3	0.118	0.118	0.118	0.118	0.118	0.118	0.118	0.118	0.118	0.118
4	0.164	0.164	0.164	0.164	0.164	0.164	0.164	0.164	0.164	0.164
5	0.228	0.228	0.228	0.228	0.228	0.228	0.228	0.228	0.228	0.228
6	0.316	0.316	0.316	0.316	0.316	0.316	0.316	0.316	0.316	0.316
7	0.439	0.439	0.439	0.439	0.439	0.439	0.439	0.439	0.439	0.439
8	0.610	0.610	0.610	0.610	0.610	0.610	0.610	0.610	0.610	0.610
9	0.847	0.848	0.849	0.850	0.850	0.851	0.851	0.852	0.852	0.853
10	1.177	1.177	1.177	1.178	1.178	1.178	1.178	1.179	1.179	1.179
11	1.634	1.635	1.635	1.635	1.635	1.635	1.635	1.636	1.636	1.636
12	2.270	2.271	2.271	2.271	2.271	2.271	2.271	2.271	2.271	2.271
13	3.154	3.154	3.155	3.155	3.155	3.155	3.155	3.155	3.155	3.155
14	4.382	4.383	4.383	4.383	4.384	4.384	4.384	4.384	4.384	4.384
15	6.091	6.092	6.092	6.092	6.093	6.093	6.093	6.093	6.093	6.093
16	8.470	8.471	8.472	8.472	8.472	8.472	8.472	8.472	8.472	8.471
17	11.790	11.792	11.792	11.793	11.793	11.792	11.792	11.791	11.791	11.790
18	16.445	16.445	16.445	16.445	16.443	16.442	16.441	16.440	16.439	16.439
19	23.031	23.018	23.010	23.005	23.003	23.004	23.007	23.012	23.020	23.030
20	32.523	32.450	32.427	32.434	32.463	32.510	32.571	32.645	32.729	32.822
21	46.780	46.527	46.744	47.207	47.785	48.408	49.033	49.636	50.204	50.728
22	70.639	74.568	77.654	80.082	82.030	83.622	84.943	86.054	86.997	87.804
23	179.932	179.932	179.932	179.932	179.932	179.932	179.932	179.932	179.932	179.932

Figure 7.4.1-2b. Comparison of Vening-Meinesz' Optimization Using Increment Damping. Moderate Damping (damping parameter = 0.20).

SUMMARY OF COMPLETE RUN

ITER# 1 ITER# 2 ITER# 3 ITER# 4 ITER# 5 ITER# 6 ITER# 7 ITER# 8 ITER# 9 ITER#10
 FIGURE OF MERIT
 7.54E-01 7.26E-01 7.01E-01 6.78E-01 6.59E-01 6.42E-01 6.29E-01 6.17E-01 6.08E-01 6.00E-01

VALUES OF PARAMETERS

RING# SPHERICAL RING RADII (DEGREES)

0	0.044	0.044	0.044	0.044	0.044	0.044	0.044	0.044	0.044	0.044
1	0.061	0.061	0.061	0.061	0.061	0.061	0.061	0.061	0.061	0.061
2	0.085	0.085	0.085	0.085	0.085	0.085	0.085	0.085	0.085	0.085
3	0.118	0.118	0.118	0.118	0.118	0.118	0.118	0.118	0.118	0.118
4	0.164	0.164	0.164	0.164	0.164	0.164	0.164	0.164	0.164	0.164
5	0.228	0.228	0.228	0.228	0.228	0.228	0.228	0.228	0.228	0.228
6	0.316	0.316	0.316	0.316	0.316	0.316	0.316	0.316	0.316	0.316
7	0.439	0.439	0.439	0.439	0.439	0.439	0.439	0.439	0.439	0.439
8	0.610	0.610	0.610	0.610	0.610	0.610	0.610	0.610	0.610	0.610
9	0.847	0.847	0.848	0.848	0.848	0.849	0.849	0.849	0.849	0.850
10	1.177	1.177	1.177	1.177	1.177	1.177	1.177	1.177	1.177	1.177
11	1.634	1.634	1.634	1.634	1.635	1.635	1.635	1.635	1.635	1.635
12	2.270	2.270	2.270	2.270	2.270	2.270	2.270	2.270	2.270	2.270
13	3.154	3.154	3.154	3.154	3.154	3.154	3.154	3.154	3.154	3.154
14	4.382	4.383	4.383	4.383	4.383	4.383	4.383	4.383	4.383	4.383
15	6.091	6.091	6.091	6.091	6.091	6.091	6.092	6.092	6.092	6.092
16	8.470	8.470	8.470	8.471	8.471	8.471	8.471	8.471	8.471	8.471
17	11.790	11.790	11.791	11.791	11.791	11.791	11.792	11.792	11.792	11.792
18	16.445	16.445	16.445	16.445	16.444	16.444	16.444	16.444	16.443	16.443
19	23.031	23.026	23.022	23.018	23.014	23.010	23.007	23.004	23.001	22.998
20	32.523	32.490	32.461	32.434	32.411	32.390	32.371	32.355	32.342	32.330
21	46.780	46.634	46.502	46.390	46.298	46.228	46.179	46.151	46.142	46.150
22	70.639	71.750	72.309	73.807	74.739	75.603	76.403	77.139	77.817	78.440
23	179.932	179.932	179.932	179.932	179.932	179.932	179.932	179.932	179.932	179.932

Figure 7.4.1-2c. Comparison of Vening-Meinesz' Optimization Using Increment Damping Variation. High Damping (damping parameter = 0.10).

Finally, the results in a 125-ring case are exhibited in Figure 7.4.1-3(a,b). They are opposite to the previous results. In the "moderately damped" case (figure b) the figure-of-merit requires less than half as many iterations to achieve the same reduced values as in the "undamped" case (figure a). In particular, to reduce the figure-of-merit from 0.133 to 0.102, requires only one iteration in the damped case but three in the undamped case. And to reduce it from 0.102 to .0848 again requires only one iteration in the damped case but two iterations in the undamped case. The reasons for these contradictory results are not known.

SUMMARY OF COMPLETE RUN

	ITER# 0	ITER# 1	ITER# 2	ITER# 3	ITER# 4	ITER# 5	ITER# 6	ITER# 7	ITER# 8	ITER# 9	ITER#10
FIGURE OF MERIT	1.33E-01	1.21E-01	1.13E-01	1.02E-01	9.13E-02	8.49E-02	8.21E-02	8.22E-02	8.64E-02	8.99E-02	9.04E-02

VALUES OF PARAMETERS

RING# SPHERICAL RING RADII (DEGREES)

68	0.673	0.673	0.673	0.673	0.673	0.673	0.673	0.673	0.673	0.673	0.673
69	0.732	0.733	0.733	0.733	0.733	0.734	0.734	0.734	0.743	0.756	0.690
70	0.797	0.797	0.796	0.796	0.795	0.794	0.794	0.794	0.794	0.765	0.801
71	0.868	0.868	0.868	0.869	0.870	0.870	0.870	0.871	0.900	0.902	0.870
72	0.944	0.944	0.945	0.944	0.944	0.944	0.943	0.944	0.910	0.908	1.015
73	1.028	1.028	1.027	1.027	1.027	1.027	1.027	1.027	1.052	1.040	1.064
74	1.119	1.119	1.120	1.120	1.120	1.121	1.121	1.122	1.105	1.109	1.090
75	1.218	1.217	1.217	1.216	1.216	1.216	1.216	1.216	1.226	1.224	1.237
76	1.325	1.326	1.326	1.327	1.327	1.327	1.327	1.328	1.323	1.325	1.313
77	1.443	1.442	1.442	1.442	1.442	1.442	1.442	1.442	1.445	1.444	1.453
78	1.570	1.571	1.571	1.571	1.571	1.572	1.572	1.573	1.571	1.573	1.574
79	1.709	1.709	1.709	1.709	1.709	1.710	1.710	1.710	1.712	1.711	1.708
80	1.860	1.861	1.861	1.861	1.861	1.862	1.863	1.863	1.862	1.861	1.864
81	2.025	2.025	2.025	2.025	2.025	2.026	2.027	2.027	2.028	2.031	2.028
82	2.204	2.204	2.204	2.205	2.205	2.205	2.206	2.206	2.206	2.206	2.207
83	2.399	2.399	2.399	2.400	2.400	2.401	2.401	2.402	2.402	2.402	2.403
84	2.611	2.612	2.612	2.612	2.613	2.613	2.614	2.614	2.614	2.615	2.615
85	2.843	2.843	2.843	2.844	2.845	2.846	2.846	2.846	2.847	2.848	2.848
86	3.094	3.095	3.096	3.097	3.098	3.099	3.100	3.100	3.100	3.101	3.101
87	3.368	3.369	3.369	3.370	3.371	3.372	3.372	3.373	3.374	3.375	3.376
88	3.666	3.667	3.667	3.667	3.668	3.669	3.670	3.671	3.673	3.675	3.676
89	3.991	3.991	3.991	3.991	3.993	3.996	3.997	3.999	4.001	4.003	4.004
90	4.344	4.344	4.344	4.344	4.346	4.349	4.351	4.355	4.357	4.359	4.360
91	4.729	4.729	4.730	4.733	4.736	4.738	4.740	4.741	4.742	4.743	4.743
92	5.148	5.148	5.149	5.153	5.157	5.159	5.160	5.161	5.161	5.163	5.165
93	5.604	5.605	5.609	5.611	5.614	5.616	5.618	5.620	5.624	5.626	5.632
94	6.101	6.104	6.107	6.110	6.113	6.117	6.121	6.124	6.125	6.127	6.133
95	6.642	6.640	6.652	6.655	6.660	6.665	6.669	6.671	6.672	6.677	6.681
96	7.231	7.235	7.238	7.242	7.248	7.254	7.259	7.262	7.265	7.272	7.276
97	7.873	7.876	7.877	7.879	7.883	7.889	7.894	7.897	7.906	7.911	7.915
98	8.572	8.576	8.576	8.577	8.580	8.584	8.588	8.596	8.602	8.606	8.609
99	9.335	9.332	9.334	9.339	9.344	9.347	9.354	9.362	9.365	9.368	9.369
100	10.166	10.169	10.165	10.172	10.180	10.192	10.214	10.227	10.237	10.247	10.256
101	11.071	11.076	11.074	11.076	11.081	11.105	11.119	11.128	11.134	11.140	11.144
102	12.059	12.072	12.075	12.078	12.101	12.115	12.124	12.129	12.132	12.135	12.137
103	13.137	13.144	13.144	13.156	13.185	13.205	13.221	13.234	13.244	13.253	13.260
104	14.314	14.308	14.314	14.335	14.356	14.373	14.390	14.402	14.412	14.422	14.432
105	15.599	15.596	15.600	15.605	15.615	15.624	15.627	15.629	15.629	15.627	15.626
106	17.003	17.022	17.059	17.104	17.144	17.173	17.193	17.204	17.211	17.217	17.219
107	18.539	18.609	18.662	18.714	18.766	18.807	18.842	18.866	18.884	18.902	18.924
108	20.220	20.294	20.296	20.289	20.312	20.356	20.403	20.454	20.510	20.570	20.632
109	22.062	22.069	22.090	22.097	22.100	22.082	22.044	21.989	21.929	21.868	21.807
110	24.004	24.108	24.112	24.153	24.215	24.274	24.328	24.370	24.406	24.439	24.471
111	26.307	26.238	26.195	26.180	26.199	26.242	26.286	26.313	26.329	26.341	26.352
112	28.755	28.059	28.929	28.903	29.017	29.024	29.013	28.999	28.984	28.971	28.959
113	31.457	31.591	31.741	31.907	32.050	32.172	32.232	32.383	32.498	32.615	32.718
114	34.451	34.606	34.717	34.857	35.073	35.318	35.530	35.894	36.014	36.070	36.099
115	37.779	37.775	37.500	37.155	36.910	36.741	36.576	36.345	36.239	36.183	36.155
116	41.496	41.233	41.290	41.446	41.514	41.464	41.341	41.171	40.971	40.760	40.580
117	45.674	45.771	45.793	45.999	46.309	46.671	47.038	47.379	47.691	47.980	48.246
118	50.408	50.562	50.721	50.813	50.926	51.043	51.128	51.146	51.118	51.063	50.987
119	55.830	56.600	57.205	57.790	58.326	58.693	58.950	59.177	59.389	59.586	59.766
120	62.132	62.047	61.867	61.838	62.086	62.572	63.146	63.564	63.886	64.177	64.458
121	69.617	69.249	68.509	68.164	68.433	68.774	68.988	69.068	69.112	69.202	69.305
122	78.811	79.119	80.433	82.324	84.124	85.613	86.814	87.776	88.617	89.409	90.204
123	90.780	93.236	94.147	94.449	94.925	95.325	95.550	95.508	95.339	95.093	94.755
124	108.470	110.141	111.377	113.269	115.635	117.644	119.155	120.112	120.739	121.349	121.854
125	179.997	179.997	179.997	179.997	179.997	179.997	179.997	179.997	179.997	179.997	179.997

Figure 7.4.1-3a. Comparison of Vening-Meinesz' Optimization Using Increment Damping. No Damping (damping parameter = 0.50).

SUMMARY OF COMPLETE RUN

	ITER# 1	ITER# 2	ITER# 3	ITER# 4	ITER# 5	ITER# 6
FIGURE OF MERIT	1.33E-01	1.02E-01	8.48E-02	1.13E-01	1.31E-01	1.08E-01

VALUES OF PARAMETERS

RING# SPHERICAL RING RADII (DEGREES)

	0.673	0.673	0.673	0.673	0.673	0.673
68	0.673	0.673	0.673	0.673	0.673	0.673
69	0.732	0.732	0.732	0.732	0.732	0.732
70	0.797	0.815	0.844	0.925	0.933	0.777
71	0.860	0.850	0.944	0.958	0.950	0.937
72	0.944	0.956	0.999	0.986	0.964	0.953
73	1.028	1.008	1.113	1.024	1.184	1.012
74	1.119	1.144	1.184	1.221	1.239	1.248
75	1.218	1.194	1.325	1.291	1.274	1.265
76	1.325	1.356	1.403	1.341	1.301	1.279
77	1.443	1.414	1.568	1.437	1.609	1.368
78	1.570	1.604	1.622	1.650	1.664	1.671
79	1.709	1.674	1.656	1.668	1.673	1.676
80	1.860	1.724	1.700	1.689	1.604	1.681
81	2.025	1.858	1.871	1.888	1.897	1.934
82	2.204	2.068	2.070	2.073	2.065	2.071
83	2.399	2.284	2.287	2.295	2.290	2.301
84	2.611	2.531	2.534	2.541	2.536	2.546
85	2.843	2.794	2.797	2.803	2.799	2.809
86	3.094	3.067	3.068	3.069	3.066	3.074
87	3.368	3.340	3.353	3.357	3.362	3.371
88	3.666	3.661	3.657	3.657	3.658	3.659
89	3.991	3.994	3.995	3.997	3.999	3.997
90	4.344	4.345	4.346	4.346	4.347	4.346
91	4.729	4.729	4.729	4.728	4.730	4.730
92	5.148	5.145	5.149	5.150	5.149	5.149
93	5.604	5.593	5.599	5.604	5.606	5.610
94	6.101	6.100	6.097	6.099	6.101	6.102
95	6.642	6.645	6.639	6.637	6.633	6.633
96	7.231	7.235	7.225	7.222	7.219	7.217
97	7.873	7.875	7.877	7.880	7.874	7.877
98	8.572	8.575	8.579	8.582	8.580	8.580
99	9.335	9.335	9.342	9.343	9.341	9.341
100	10.166	10.168	10.170	10.171	10.165	10.164
101	11.071	11.069	11.067	11.066	11.065	11.064
102	12.059	12.059	12.057	12.056	12.054	12.050
103	13.137	13.139	13.136	13.139	13.142	13.141
104	14.314	14.317	14.315	14.315	14.320	14.320
105	15.599	15.601	15.602	15.598	15.608	15.609
106	17.003	16.998	17.007	17.015	17.025	17.034
107	18.539	18.535	18.544	18.543	18.549	18.557
108	20.220	20.227	20.230	20.233	20.233	20.242
109	22.062	22.071	22.065	22.089	22.087	22.090
110	24.084	24.096	24.100	24.113	24.121	24.130
111	26.307	26.319	26.326	26.333	26.341	26.348
112	28.755	28.775	28.789	28.792	28.797	28.790
113	31.457	31.483	31.487	31.493	31.485	31.493
114	34.451	34.474	34.469	34.478	34.491	34.501
115	37.779	37.773	37.768	37.818	37.837	37.840
116	41.496	41.495	41.502	41.483	41.447	41.407
117	45.674	45.701	45.633	45.566	45.512	45.448
118	50.408	50.356	50.307	50.237	50.170	50.117
119	55.830	55.608	55.450	55.338	55.281	55.253
120	62.132	61.926	61.817	61.911	62.070	62.213
121	69.617	69.877	70.179	70.185	70.110	70.044
122	78.811	78.860	78.677	78.544	78.458	78.392
123	90.780	91.525	93.204	94.325	94.904	95.253
124	100.470	113.447	117.084	119.626	121.557	122.842
125	180.000	180.000	180.000	180.000	180.000	180.000

Figure 7.4.1-3b. Comparison of Vening-Meinesz' Optimization Using Increment Damping. Moderate Damping (damping parameter = 0.25).

7.4.2 Output Weighting Variation

The variation of the optimization algorithm which uses output weighting was described in Section 6.3.4.2. This variation performs well the immediate function for which it was intended, namely to reduce the rms discretization error more rapidly than the standard algorithm (using input weighting) by heavily overweighting large output residuals in the least squares solutions. However, the optimization variation seems to provide mixed final results, at least on the basis of the relatively few cases run.

In particular, in a Vening-Meinesz' case, the rms discretization error is rapidly reduced in one iteration to a level which previously required six iterations to attain, but the convergence then becomes unstable. In a Stokes' case, the convergence is consistent over three iterations but it does not seem to be as rapid as might be expected, although an examination of the detailed printout reveals the optimization variation is performing as designed.

Iterative rms errors are shown in Figure 7.4.2-1(a,b) for a 125-ring Vening-Meinesz' optimization starting from a Circularized AGEMIT template. With standard input weighting (figure a), the figure-of-merit decreases slowly from 0.1332 mgal to 0.0821 mgal in six iterations. However with output weighting (figure b), the figure-of-merit is reduced immediately to 0.0815 mgal in a single iteration, but subsequent iterations cause the figure-of-merit to oscillate at a higher value.

SUMMARY OF COMPLETE RUN

	ITER# 0	ITER# 1	ITER# 2	ITER# 3	ITER# 4	ITER# 5	ITER# 6	ITER# 7	ITER# 8	ITER# 9	ITER#10
FIGURE OF MERIT	1.33E-01	1.21E-01	1.13E-01	1.02E-01	9.13E-02	8.49E-02	8.21E-02	8.22E-02	8.64E-02	8.99E-02	9.04E-02

Figure 7.4.2-1a. Example of Vening-Meinesz' Optimization Run Using Standard Weighting.

SUMMARY OF COMPLETE RUN

	ITER# 0	ITER# 1	ITER# 2	ITER# 3	ITER# 4	ITER# 5	ITER# 6	ITER# 7	ITER# 8	ITER# 9	ITER#10
FIGURE OF MERIT	1.33E-01	8.15E-02	6.71E-02	8.99E-02	9.39E-02	1.45E-01	9.41E-02	8.98E-02	9.12E-02	1.05E-01	1.01E-01

Figure 7.4.2-1b. Example of Vening-Meinesz' Optimization Run Using Output Weighting.

A more detailed set of results is given in Figure 7.4.2-2(a,b,c,d) to illustrate how the output weighting variation works numerically. The sequence of four individual listings provides the low degree residuals on the first four passes of a 66-ring Classic Stokes' optimization, beginning with an equal ring contribution template. The following observations can be made:

- a) On the initial pass (figure a), very large output residuals occur for degrees 3, 6, 7, 8, 11, and 12 as shown in meters in the SIGMA column. These are heavily weighted by the corresponding weights shown in the WEIGHT column. Under the standard a priori weighting the residuals would only have been weighted by the values shown in the DEG VAR IN column.
- b) On the first iteration (figure b), the very large output residuals have been much reduced although some medium large ones remain.
- c) On the second iteration (figure c), the medium large residuals are reduced further.
- d) Finally on the third iteration (figure d), no harmonic degree contributes more than 0.1 meter to the rms discretization error, and the contributions are more evenly spread throughout all degrees.

N	ACTUAL SPECTRUM	IDEAL SPECTRUM	RESID SPECTRUM	REL RESID	DEG VAR IN	WEIGHT	SIGMA	CUM SIGMA
0	-0.0000000000	0.0000000000	-0.0000000000	0.000000	0.00000	0.00000	0.00000	0.00000
1	-0.0037093003	0.0000000000	-0.0037093002	0.000000	0.00000	0.00000	0.00000	0.00000
2	0.9855297639	1.0000000000	-0.0144702345	-0.014470	322.03928	67431.00000	0.25967	0.25967
3	0.4854559047	0.5000000000	-0.0145340934	-0.029068	1334.86223	281976.06250	0.53101	0.59111
4	0.3250120262	0.3333333333	-0.0083213039	-0.024964	965.39143	66847.62500	0.25855	0.64518
5	0.2477549190	0.2500000000	-0.0022451810	-0.008981	828.53518	4176.50781	0.06463	0.64841
6	0.2118126460	0.2000000000	0.0118126459	0.059063	750.66000	104773.93750	0.32369	0.72471
7	0.1873065575	0.1666666667	0.0206398889	0.123839	697.57316	297169.56250	0.54513	0.90685
8	0.1563881854	0.1428571429	0.0135310404	0.094717	657.00250	120289.93750	0.34683	0.97091
9	0.1303717268	0.1250000000	0.0053717233	0.042974	624.09143	18008.40625	0.13420	0.98014
10	0.1052069804	0.1111111111	-0.0059041306	-0.053137	596.27118	20785.26563	0.14417	0.99069
11	0.0814298991	0.1000000000	-0.0185700990	-0.185701	572.08381	197262.18750	0.44416	1.08570
12	0.0724732599	0.0909090909	-0.0184358284	-0.202794	550.63067	187148.12500	0.43261	1.16871
13	0.0737547066	0.0833333333	-0.0095786266	-0.114944	531.32108	48748.75391	0.22079	1.18939
14	0.0763192465	0.0769230769	-0.0006038302	-0.007850	513.74632	187.31750	0.01369	1.18946
15	0.0813236081	0.0714285714	0.0098950361	0.138530	497.61136	48721.96875	0.22073	1.20977
16	0.0802580257	0.0666666667	0.0135913566	0.203870	482.69572	89165.93750	0.29861	1.24608
17	0.0720900855	0.0625000000	0.0095900819	0.153441	468.82966	43118.10156	0.20765	1.26326
18	0.0610276208	0.0583235294	0.0022040913	0.037470	455.07929	2214.66943	0.04706	1.26414
19	0.0496436676	0.0555555556	-0.0059118867	-0.106414	443.73669	15508.77344	0.12453	1.27026
20	0.0434718695	0.0526315789	-0.0091597065	-0.174034	432.31334	36271.17969	0.19045	1.28446
21	0.0422327270	0.0500000000	-0.0077672713	-0.155345	421.53544	25431.44141	0.15947	1.29432
22	0.0412892788	0.0476190476	-0.0063297674	-0.132925	411.34070	16480.75391	0.12838	1.30067
23	0.0450381462	0.0454545455	-0.0003663991	-0.008061	401.67587	53.92427	0.00734	1.30069
24	0.0459704136	0.0434782609	0.0024921526	0.057320	392.49500	2437.71729	0.04937	1.30163
25	0.0409919830	0.0416666667	-0.0006746836	-0.016192	383.75809	174.68588	0.01322	1.30169
26	0.0405553272	0.0400000000	0.0005553272	0.013883	375.43000	115.77818	0.01076	1.30174
27	0.0395683388	0.0334615335	0.0011068003	0.028777	367.47972	450.16504	0.02122	1.30191
28	0.0338889155	0.0370370370	-0.0031481213	-0.084999	359.87965	3566.64746	0.05972	1.30328
29	0.0359343921	0.0357142857	0.0002201084	0.006163	352.60512	17.08258	0.00413	1.30329
30	0.0355412629	0.0344827586	0.0020585041	0.059697	345.63397	1464.60254	0.03827	1.30385
31	0.0297360857	0.0333333333	-0.0035972474	-0.107917	338.94621	4386.02734	0.06623	1.30553
32	0.0290709279	0.0322580645	-0.0031871365	-0.098801	332.52372	3377.72217	0.05812	1.30682
33	0.0285809977	0.0312500000	-0.0026690022	-0.085408	326.35002	3234.77759	0.04822	1.30771
34	0.0225125925	0.0303303030	-0.0077904351	-0.257084	320.41009	19445.96484	0.13945	1.31512
35	0.0250291219	0.0294117647	-0.0043826401	-0.149010	314.69017	6044.41797	0.07775	1.31742
36	0.0292238078	0.0285714286	0.0006523791	0.022833	309.17765	131.58554	0.01147	1.31747
37	0.0266595757	0.0277777778	-0.0011182020	-0.040255	303.88091	379.93994	0.01949	1.31761
38	0.0282520221	0.0270270270	0.0012249949	0.045325	298.72925	448.27637	0.02117	1.31778
39	0.0290753150	0.0263157895	0.0027595253	0.104662	293.77277	2237.07373	0.04730	1.31863
40	0.0229563447	0.0255410256	-0.0026846607	-0.104703	288.98230	2082.84277	0.04564	1.31942
41	0.0209341335	0.0250000000	-0.0040658638	-0.162635	284.34935	4700.64453	0.06856	1.32120
42	0.0213527790	0.0243902439	-0.0030374648	-0.124536	279.86600	2582.09717	0.05081	1.32218
43	0.0184515911	0.0233095238	-0.0053579323	-0.225033	275.52489	7909.61328	0.08894	1.32517
44	0.0192304464	0.0232558140	-0.0040253662	-0.173091	271.31916	4396.33594	0.06630	1.32683
45	0.0211524440	0.0227272727	-0.0015748285	-0.069292	267.24239	662.78369	0.02574	1.32708
46	0.0196853811	0.0222222222	-0.0025368410	-0.114158	263.28857	1694.40967	0.04116	1.32771
47	0.0189859998	0.0217391304	-0.0027531306	-0.126644	259.45210	1966.57617	0.04435	1.32845
48	0.0193155695	0.0212765957	-0.0019610261	-0.092168	255.72768	983.43213	0.03136	1.32882
49	0.0182337808	0.0203333333	-0.0025995523	-0.124779	252.11038	1703.67896	0.04128	1.32946
50	0.0181876777	0.0204081633	-0.0022204854	-0.108804	248.59554	1225.71362	0.03501	1.32993
51	0.0185162384	0.0200000000	-0.0014837615	-0.074168	245.17878	539.77271	0.02323	1.33013
52	0.0180409969	0.0195078431	-0.0015668441	-0.079909	241.85596	593.75635	0.02437	1.33035
53	0.0166001580	0.0192307692	-0.0026306103	-0.136792	238.62319	1651.29858	0.04964	1.33097
54	0.0149664644	0.0183579245	-0.0039014600	-0.206777	235.47631	3504.28418	0.05987	1.33232
55	0.0137764776	0.0183185185	-0.0047420375	-0.256070	232.41332	5226.25701	0.07229	1.33428
56	0.0130022218	0.0181818182	-0.0051795952	-0.284878	229.42945	6155.17578	0.07845	1.33658
57	0.0132653153	0.0173571429	-0.0045918263	-0.257142	226.52208	4776.18750	0.06911	1.33837
58	0.0145773246	0.0175439596	-0.0029665348	-0.169092	223.65026	1968.53003	0.04437	1.33910

Figure 7.4.2-2a. Iteration #0 of a Stokes' Optimization Run Using Output Weighting.

N	ACTUAL SPECTRUM	IDEAL SPECTRUM	RESID SPECTRUM	REL RESID	DEG VAR IN	WEIGHT	SIGMA	CUM SIGMA
0	-0.0000000000	0.0000000000	-0.0000000000	0.000000	0.00000	0.00000	0.00000	0.00000
1	-0.0000434992	0.0000000000	-0.0000434992	0.000000	0.00000	0.00000	0.00000	0.00000
2	0.9918916901	1.0000000000	-0.0081083067	-0.008108	322.03928	21172.35156	0.14551	0.14551
3	0.4939480322	0.5000000000	-0.0060519651	-0.012104	1334.86223	46891.01953	0.22111	0.26469
4	0.3296772785	0.3333333333	-0.0036560546	-0.010968	965.39143	12904.12891	0.11360	0.28804
5	0.2464799639	0.2500000000	-0.0035200361	-0.014080	828.53518	10266.08984	0.10132	0.30534
6	0.2015902158	0.2000000000	0.0015902158	0.007951	750.86000	1898.76367	0.04357	0.30844
7	0.1722599395	0.1666666667	0.0055932701	0.033560	697.57316	21823.34375	0.14773	0.34199
8	0.1477207036	0.1428571429	0.0048635602	0.034045	657.00250	15540.87500	0.12466	0.36400
9	0.1271832174	0.1250000000	0.0021832173	0.017466	624.09143	2974.69238	0.05454	0.36806
10	0.1094111718	0.1111111111	-0.0016999391	-0.015299	596.27118	1723.10010	0.04151	0.37040
11	0.0997503975	0.1000000000	-0.0002496024	-0.002496	572.08381	35.64156	0.00597	0.37045
12	0.0864487499	0.0909090909	-0.0044603385	-0.049064	550.63067	10954.57813	0.10466	0.38495
13	0.0780060517	0.0833333333	-0.0052472800	-0.062967	531.32108	14629.35938	0.12095	0.40350
14	0.0767456135	0.0769230769	-0.0001774634	-0.002307	513.74632	16.17953	0.00402	0.40352
15	0.0712810953	0.0714285714	-0.0001474762	-0.002065	497.61136	10.82266	0.00329	0.40354
16	0.0620251486	0.0666666667	-0.0046415180	-0.069623	482.69572	10399.04297	0.10198	0.41622
17	0.0640267975	0.0625000000	0.0015267974	0.024429	468.82966	1092.89307	0.03306	0.41753
18	0.0594731137	0.0583235294	0.0006495842	0.011043	455.87929	192.36264	0.01387	0.41776
19	0.0513928041	0.0555555556	-0.0041627511	-0.074930	443.73669	7689.20516	0.06769	0.42687
20	0.0537954989	0.0526315789	0.0011639199	0.022114	432.31334	585.65045	0.02420	0.42755
21	0.0510194489	0.0500000000	0.0010194487	0.020389	421.53544	438.09106	0.02093	0.42806
22	0.0476583643	0.0476190476	0.0000393167	0.000326	411.34070	0.63585	0.00080	0.42806
23	0.0476397604	0.0454545455	0.0021852148	0.048075	401.67507	1918.06763	0.04380	0.43030
24	0.0461539381	0.0434782609	0.0026756772	0.061541	392.49500	2809.96875	0.05301	0.43355
25	0.0456537202	0.0416666667	0.0039870515	0.095689	383.75009	6100.43359	0.07811	0.44053
26	0.0391018772	0.0400000000	-0.0008981228	-0.022453	375.43000	302.83081	0.01740	0.44087
27	0.0337591429	0.0334615335	-0.0047023930	-0.122262	367.47972	8125.89063	0.09014	0.45000
28	0.0352940084	0.0370370370	-0.0017430284	-0.047062	359.87965	1093.36743	0.03307	0.45121
29	0.0249639480	0.0357142857	-0.0107504353	-0.301012	352.60512	40751.22266	0.20187	0.49431
30	0.0260402707	0.0344827586	-0.0084424876	-0.244832	345.63397	24635.26172	0.15696	0.51863
31	0.0326164134	0.0333333333	-0.0007169198	-0.021508	338.94621	174.20950	0.01320	0.51880
32	0.0307558923	0.0322580645	-0.0015021721	-0.046567	332.52372	750.34668	0.02739	0.51952
33	0.0340529454	0.0312500000	0.0028029452	0.089694	326.35002	2563.96948	0.05064	0.52198
34	0.0357953663	0.0303030303	0.0054923333	0.181247	320.41009	9665.39844	0.09831	0.53116
35	0.0313703697	0.0294117647	0.0019586049	0.066593	314.69017	1207.19336	0.03474	0.53229
36	0.0268281526	0.0285714286	-0.0017432759	-0.061015	309.17765	939.59399	0.03065	0.53318
37	0.0221301075	0.0277777778	-0.0056476668	-0.203316	303.86091	9691.98828	0.09845	0.54219
38	0.0207187563	0.0270270270	-0.0063082688	-0.233406	298.72925	11837.70313	0.10903	0.55304
39	0.0203564050	0.0263157895	-0.0059593041	-0.226457	293.77277	10433.11719	0.10214	0.56240
40	0.0202260595	0.0256410256	-0.0054149628	-0.211184	288.98230	8473.46438	0.09205	0.56988
41	0.0235941251	0.0250000000	-0.0014158748	-0.056635	284.34935	570.03540	0.02388	0.57038
42	0.0248350630	0.0243902439	0.0004448190	0.018238	279.86600	55.37538	0.00744	0.57043
43	0.0233165203	0.0238095238	-0.0004930033	-0.020706	275.52489	66.96693	0.00818	0.57049
44	0.0233635488	0.0232558140	0.0001077348	0.004633	271.31916	3.14914	0.00177	0.57049
45	0.0237904004	0.0227272727	0.0010631275	0.046778	267.24239	302.04785	0.01738	0.57075
46	0.0213873737	0.0222222222	-0.0008348485	-0.037568	263.28857	183.50476	0.01355	0.57092
47	0.0216544019	0.0217391304	-0.0000847286	-0.003898	259.45210	1.86259	0.00136	0.57092
48	0.0221655972	0.0212765957	0.0008890014	0.041783	255.72768	202.10759	0.01422	0.57109
49	0.0180523013	0.0208333333	-0.0027810319	-0.133490	252.11038	1949.85645	0.04416	0.57280
50	0.0180453096	0.0204081633	-0.0023628536	-0.115780	248.59554	1387.92798	0.03725	0.57401
51	0.0171733427	0.0200000000	-0.0028260571	-0.141303	245.17878	1958.14429	0.04425	0.57571
52	0.0142183493	0.0186078431	-0.0053894930	-0.274864	241.85596	7025.09766	0.08382	0.58173
53	0.0159417545	0.0192307692	-0.0032890146	-0.171029	238.62319	2501.33398	0.05081	0.58400
54	0.0169903149	0.0186679245	-0.0018776094	-0.099513	235.47681	830.15381	0.02831	0.58471
55	0.0160192327	0.0185165185	-0.0024992859	-0.134961	232.41332	1451.75342	0.03010	0.58595
56	0.0165556807	0.0181818182	-0.0016261293	-0.089437	229.42945	606.67920	0.02463	0.58646
57	0.0166142778	0.0178571429	-0.0012428649	-0.069600	226.52208	349.91138	0.01871	0.58676
58	0.0134139840	0.0175438596	-0.0041298755	-0.235403	223.68826	3815.19629	0.06177	0.59000

Figure 7.4.2-2b. Iteration #1 of a Stokes' Optimization Run Using Output Weighting.

N	ACTUAL SPECTRUM	IDEAL SPECTRUM	RESID SPECTRUM	REL RESID	DEG VAR IN	WEIGHT	SIGMA	CUM SIGMA
0	-0.0000000000	0.0000000000	-0.0000000000	0.000000	0.00000	0.00000	0.00000	0.00000
1	0.0003421743	0.0000000000	0.0003421742	0.000000	0.00000	0.00000	0.00000	0.00000
2	0.9946647164	1.0000000000	-0.0053152815	-0.005315	322.03928	9098.32031	0.09539	0.09539
3	0.4969295715	0.5000000000	-0.0030704283	-0.006141	1334.06223	12584.44922	0.11218	0.14725
4	0.3313029576	0.3333333333	-0.0020303756	-0.006091	965.39143	3979.75342	0.06309	0.16020
5	0.2470288964	0.2500000000	-0.0029711034	-0.011884	828.53518	7313.61547	0.08552	0.18159
6	0.2007166341	0.2000000000	0.0007166339	0.003583	750.86000	385.61450	0.01964	0.18265
7	0.1691776363	0.1666666667	0.0025109695	0.015066	697.57316	4398.17578	0.06632	0.19432
8	0.1428901678	0.1428571429	0.0000330242	0.000231	657.00250	0.71652	0.00085	0.19432
9	0.1259166178	0.1250000000	0.0009166177	0.007333	624.09143	524.35400	0.02290	0.19567
10	0.1108623794	0.1111111111	-0.0002487316	-0.002239	596.27118	36.88971	0.00607	0.19576
11	0.0975068791	0.1000000000	-0.0024931207	-0.024731	572.08381	3555.87280	0.05963	0.20464
12	0.0891384994	0.0909090909	-0.0017705914	-0.019477	550.63067	1726.22363	0.04155	0.20882
13	0.0816676648	0.0833333333	-0.0016656683	-0.019988	531.32108	1474.12402	0.03839	0.21232
14	0.0745244672	0.0769230769	-0.0023986096	-0.031182	513.74632	2955.75098	0.05437	0.21917
15	0.0696858707	0.0714285714	-0.0017427006	-0.024398	497.61136	1511.24605	0.03887	0.22259
16	0.0645091312	0.0666666667	-0.0021575354	-0.032363	482.69572	2246.92847	0.04740	0.22758
17	0.0620183503	0.0625000000	-0.0004816495	-0.007706	468.82966	108.76202	0.01043	0.22782
18	0.0563832280	0.0588235294	-0.0024403012	-0.041485	455.87929	2714.79272	0.05210	0.23370
19	0.0542505052	0.0555555556	-0.0013050502	-0.023491	443.73669	755.75244	0.02749	0.23531
20	0.0526453575	0.0526315789	0.0000137786	0.000262	432.31334	0.08207	0.00029	0.23531
21	0.0473513324	0.0500000000	-0.0026486674	-0.052973	421.53544	2957.25586	0.05438	0.24151
22	0.0457109521	0.0476190476	-0.0019080953	-0.040070	411.34070	1497.62036	0.03870	0.24459
23	0.0459112038	0.0454545455	0.0004566582	0.010046	401.67587	83.76414	0.00915	0.24477
24	0.0420074252	0.0434782609	-0.0014708354	-0.033829	392.49500	849.10620	0.02914	0.24649
25	0.0410798424	0.0416666667	-0.0005868240	-0.014034	383.75809	132.15186	0.01150	0.24676
26	0.0400749909	0.0400000000	0.0000749909	0.001875	375.43000	2.11128	0.00145	0.24677
27	0.0376363063	0.0384615385	-0.0008252321	-0.021456	367.47972	250.25664	0.01582	0.24727
28	0.0354807692	0.0370370370	-0.0015562677	-0.042019	359.87965	871.61719	0.02952	0.24903
29	0.0328894892	0.0357142857	-0.0028247964	-0.079094	352.60512	2813.60303	0.05304	0.25462
30	0.0327951007	0.0344827586	-0.0016876578	-0.048942	345.63397	984.43042	0.03138	0.25654
31	0.0318960430	0.0333333333	-0.0014372901	-0.043119	338.94621	700.19580	0.02646	0.25790
32	0.0301340726	0.0321580645	-0.0021239917	-0.065844	332.52372	1500.12744	0.03873	0.26079
33	0.0319423351	0.0312500000	0.0006923350	0.022155	326.35002	156.42857	0.01251	0.26109
34	0.0300143329	0.0303030303	-0.0002886974	-0.009527	320.41009	26.70494	0.00517	0.26115
35	0.0289111303	0.0294117647	-0.0005006343	-0.017022	314.69017	78.87227	0.00888	0.26130
36	0.0305064499	0.0285714286	0.0019350213	0.067726	309.17765	1157.65601	0.03402	0.26350
37	0.0260891950	0.0277777778	-0.0016885826	-0.060789	303.86091	866.40161	0.02943	0.26514
38	0.0244251641	0.0270270270	-0.0026018629	-0.096269	298.72925	2022.30444	0.04497	0.26893
39	0.0265386986	0.0263157895	0.0002229091	0.008471	293.77277	14.59711	0.00332	0.26896
40	0.0224877932	0.0256410256	-0.0031532352	-0.122976	288.98230	2873.31958	0.05360	0.27424
41	0.0204003425	0.0250000000	-0.0045996569	-0.183986	284.34935	6015.93359	0.07756	0.28500
42	0.0267177032	0.0243902439	0.0023274592	0.095426	279.86600	1516.05249	0.03894	0.28765
43	0.0228402122	0.0235095238	-0.0009693115	-0.040711	275.52489	258.87329	0.01609	0.28810
44	0.0215243649	0.0232558140	-0.0017314488	-0.074452	271.31916	813.39160	0.02852	0.28951
45	0.0237230023	0.0227272727	0.0009957294	0.043812	267.24239	264.96436	0.01628	0.28996
46	0.0167980894	0.0222222222	-0.0054241307	-0.244086	263.28057	7746.26172	0.08801	0.30303
47	0.0148733489	0.0217391304	-0.0068657808	-0.315826	259.45210	12230.29297	0.11059	0.32258
48	0.0139816836	0.0212765957	-0.0072949119	-0.342861	255.72768	13608.73438	0.11666	0.34302
49	0.0138665501	0.0208333333	-0.0074668002	-0.357441	252.11038	13980.28516	0.11824	0.36283
50	0.0153498242	0.0204081633	-0.0050593370	-0.247859	248.59554	6360.75391	0.07975	0.37149
51	0.0182422672	0.0200000000	-0.0017577326	-0.087887	245.17878	757.51001	0.02752	0.37251
52	0.0191535821	0.0196078431	-0.0004542610	-0.023167	241.65596	49.90768	0.00706	0.37258
53	0.0168414822	0.0192307692	-0.0003892870	-0.020243	238.62319	36.16199	0.00601	0.37262
54	0.0184541521	0.0180679245	-0.0004137722	-0.021930	235.47681	40.31535	0.00635	0.37263
55	0.0153749840	0.0185185185	-0.0031435345	-0.169751	232.41332	2296.66382	0.04792	0.37575
56	0.0141606633	0.0181818182	-0.0040211529	-0.221163	229.42945	3709.79736	0.06091	0.38065
57	0.0137689207	0.0178571429	-0.0040862193	-0.228940	226.52208	3785.98315	0.06153	0.38559
58	0.0123186627	0.0175438596	-0.0052251965	-0.297836	223.60826	6107.28516	0.07815	0.39343

Figure 7.4.2-2c. Iteration #2 of a Stokes' Optimization Run Using Output Weighting.

N	ACTUAL SPECTRUM	IDEAL SPECTRUM	RESID SPECTRUM	REL RESID	DEG VAR IN	WEIGHT	SIGMA	CUM SIGMA
0	-0.0000000000	0.0000000000	-0.0000000000	0.000000	0.00000	0.00000	0.00000	0.00000
1	0.0004841557	0.0000000000	0.0004841557	0.000000	0.00000	0.00000	0.00000	0.00000
2	0.9952545462	1.0000000000	-0.0047454536	-0.004745	322.03928	7252.10547	0.08516	0.08516
3	0.4974255820	0.5000000000	-0.0025744180	-0.005149	1334.86223	8646.96875	0.09406	0.12688
4	0.3320486735	0.3333333333	-0.0012846598	-0.003854	965.39143	1593.23438	0.03992	0.13301
5	0.2472054422	0.2500000000	-0.0027145576	-0.010858	828.53518	6105.32813	0.07814	0.15426
6	0.1009227511	0.2000000000	0.0009227509	0.004614	750.86000	639.33398	0.02529	0.15632
7	0.1690815426	0.1666666667	0.0024143759	0.014489	697.57316	4067.93535	0.06378	0.16683
8	0.1426045312	0.143571429	-0.0002526115	-0.001768	657.00250	41.92499	0.00647	0.16896
9	0.1258340664	0.1250000000	0.0008340662	0.006673	624.09143	434.15910	0.02084	0.17024
10	0.1101260353	0.1111111111	-0.0009850727	-0.008866	596.27118	578.60229	0.02405	0.17193
11	0.0969333889	0.1000000000	-0.0030661109	-0.030661	572.08381	5378.17969	0.07334	0.18692
12	0.0882036311	0.0909090909	-0.0027054597	-0.029760	550.63067	4030.34741	0.06349	0.19740
13	0.0809784125	0.0833333333	-0.0023549208	-0.028259	531.32108	2946.52173	0.05428	0.20473
14	0.0745201954	0.0769230769	-0.0024028814	-0.031237	513.74632	2966.28933	0.05446	0.21105
15	0.0704429538	0.0714285714	-0.0009856124	-0.013799	497.61136	483.39502	0.02199	0.21299
16	0.0666572395	0.0666666667	-0.0000094272	-0.000141	482.69572	0.04290	0.00021	0.21299
17	0.0642330473	0.0625000000	0.0017332472	0.027732	468.82966	1406.43237	0.03753	0.21627
18	0.0578798178	0.0523235294	-0.0009437115	-0.016043	455.87929	406.00195	0.02015	0.21721
19	0.0550750058	0.0555555556	-0.0004805496	-0.008550	443.73669	102.47119	0.01012	0.21744
20	0.0525021321	0.0526315789	-0.0001294468	-0.002459	432.31334	7.24405	0.00269	0.21746
21	0.0470022226	0.0500000000	-0.0029977772	-0.059556	421.53544	3788.19897	0.06155	0.22600
22	0.0451753587	0.0476190476	-0.0024436889	-0.051317	411.34070	2456.36816	0.04956	0.23137
23	0.0456629707	0.0454545455	0.0002084252	0.004585	401.67587	17.44922	0.00418	0.23141
24	0.0422112099	0.0434782609	-0.0012670509	-0.029142	392.49500	630.11816	0.02510	0.23277
25	0.0409585161	0.0416666667	-0.0007081504	-0.016996	383.75809	192.44585	0.01397	0.23318
26	0.0400991117	0.0400000000	0.0000991117	0.002478	375.43000	3.68790	0.00192	0.23319
27	0.0370635600	0.0394515395	-0.0013979783	-0.036347	367.47972	718.18140	0.02690	0.23472
28	0.0357110617	0.0370370370	-0.0013259752	-0.035801	359.87965	632.74365	0.02515	0.23607
29	0.0337472707	0.0357142857	-0.0019670150	-0.055076	352.60512	1364.28125	0.03694	0.23894
30	0.0330012655	0.0344827586	-0.0014814930	-0.042563	345.63397	758.60449	0.02754	0.24052
31	0.0319311273	0.0333333333	-0.0014022058	-0.042066	338.94621	666.42920	0.02582	0.24190
32	0.0296213093	0.0322580645	-0.0026367551	-0.081739	332.52372	2311.86328	0.04808	0.24664
33	0.0318331020	0.0312500000	0.0006331019	0.020259	326.35002	130.80696	0.01144	0.24690
34	0.0297378408	0.0303030303	-0.0005651894	-0.018651	320.41009	102.35149	0.01012	0.24711
35	0.0283954209	0.0294117647	-0.0010163437	-0.034556	314.69017	325.06030	0.01803	0.24776
36	0.0305239516	0.0285714286	0.0019525229	0.068338	309.17765	1178.69189	0.03433	0.25013
37	0.0251169660	0.0277777778	-0.0026608116	-0.095789	303.86091	2151.31006	0.04639	0.25440
38	0.0230896865	0.0270270270	-0.0039373375	-0.145681	298.72925	4631.08594	0.06805	0.26334
39	0.0244410738	0.0263157895	-0.0018747156	-0.071239	293.77277	1032.48120	0.03213	0.26529
40	0.0205926229	0.0256410256	-0.0050484017	-0.196888	288.98230	7365.10547	0.05532	0.27083
41	0.0207709545	0.0253000000	-0.0042290427	-0.169162	284.34935	5085.52734	0.07131	0.28780
42	0.0263299107	0.0243902439	0.0019396667	0.079526	279.86600	1052.94165	0.03245	0.28963
43	0.0232471531	0.0238095238	-0.0006623705	-0.023620	275.52489	87.13765	0.00933	0.28978
44	0.0223181334	0.0232558140	-0.0009376805	-0.040320	271.31916	238.55552	0.01545	0.29019
45	0.0248106796	0.0227272727	0.0020834068	0.091670	267.24239	1159.98779	0.03406	0.29218
46	0.0194949918	0.0222222222	-0.0027272303	-0.122725	263.28857	1958.20369	0.04425	0.29551
47	0.0172438511	0.0217391304	-0.0044952780	-0.206783	259.45210	5242.87891	0.07241	0.30426
48	0.0181083200	0.0212765957	-0.0031682756	-0.148909	255.72768	2566.98657	0.05067	0.30844
49	0.0164031270	0.0208333333	-0.0044302046	-0.212650	252.11038	4948.09375	0.07034	0.31636
50	0.0166607179	0.0204081633	-0.0037474453	-0.183625	248.59554	3491.11304	0.05909	0.32183
51	0.0166174288	0.0200000000	-0.0013825712	-0.069129	245.17878	468.65967	0.02165	0.32256
52	0.0185968459	0.0196078431	-0.0010109970	-0.051561	241.85596	247.20453	0.01572	0.32294
53	0.0193958158	0.0192307692	0.0001650466	0.008582	238.62319	6.50018	0.00255	0.32295
54	0.0192349938	0.0182679245	0.0004170693	0.022105	235.47681	40.96042	0.00640	0.32302
55	0.0164769425	0.015185185	-0.0020415760	-0.110245	232.41332	968.70605	0.03112	0.32451
56	0.0155409099	0.0181818182	-0.0026409081	-0.145250	229.42945	1600.13159	0.04000	0.32697
57	0.0144733027	0.0170571429	-0.0033838400	-0.189495	226.52208	2593.76196	0.05093	0.33091
58	0.0123587018	0.0175438596	-0.0051851571	-0.295554	221.68826	6014.04688	0.07755	0.33908

Figure 7.4.2-2d. Iteration #3 of a Stokes' Optimization Run Using Output Weighting.

7.4.3 Power Emphasis Variation

The power emphasis variation of the optimization algorithm was described in Section 6.3.4.3. Only two sets of comparison cases have been run, one with and without power emphasis of the input weighting, and the other with and without power emphasis of the output weighting. All cases were for a 125-ring analog Vening-Meinesz' optimization.

While the variation can be shown to be performing its function as expected in these cases, namely to reduce the larger residuals of a few harmonic degrees more rapidly than under standard optimization, the variation did not lead to significant improvements in the overall minimization of rms discretization error, and sometimes it led to worse errors, especially in the higher degree regime. Consequently the detailed results will not be presented here.

7.4.4 Discussion of the Results of the Optimization Algorithm Variations

The three ad hoc variations in the optimization algorithm did not provide any results which could not be obtained by the standard algorithm. However, the output weighting variation did strongly increase the rate of convergence.

SECTION 8

SUMMARY AND CONCLUSIONS

A general theory and method have been developed by which more accurate and efficient summation approximations can be derived for any of the integral transformations of geodesy. The theory and method were applied to the Stokes' and Vening-Meinesz' Integrals, and improved summations were determined which have lower rms discretization errors than those presently in use. While the results to date are not dramatic, they do indicate that the theory is valid and the method is feasible. The approach may be interpreted as spherical digital filter design for geodetic transformations.

In particular, during the course of this study a comprehensive spectral theory was derived for the spherical integral transformations of geodesy and for their spherical summation approximations. Many analytic and numerical examples of the spectra of such transformations were determined. A catalog of the spatial and frequency domain representations of about 100 spherical integral transformations was compiled. Analytic expressions for the first partial derivatives of the spectra with respect to the template compartment boundary parameters were derived for use in the Gauss-Newton optimization (filter design) process. A method of calculating the spherical ring boundary radii of an equal-ring-contribution template was developed for the Stokes' and Vening-Meinesz' transformations. And an explanation of the longevity and relative success of the equal-ring-contribution template was found within the spectral theory of discrete summation transformations.

A comprehensive geodetic filter design computer program was formulated, coded, compiled, checked out, and executed which: a) computes and compares the spectra of various geodetic integral transformations and their associated discrete summation approximations, b) calculates the partial derivatives of the spectra with respect to the template parameters, c) numerically optimizes the template ring boundary radii by an iterative least-squares differential correction procedure. The

comprehensive filter design computer program is highly structured for ease of modification, is written in PL/I, and uses mnemonic names extensively based on geodetic terminology to enable rapid comprehension by others.

The program was executed for the Stokes' and Vening-Meinesz' transformations for a variety of numbers of template rings using the main optimization algorithm and several variations. The rms discretization error of current templates (introduced by the use of the discrete summation rather than the integral transformation) was reduced by amounts between 16% and 68%. Reductions of one or two orders of magnitude (90% or 99%) are desired but were not attained in the results to date, primarily due to limitations in the optimization algorithm and in particular to the handling of the inequality constraints between the parameters. However, in certain cases there is circumstantial evidence that an actual minimum may have been reached. The optimization algorithm was intentionally rudimentary in order that most of the effort could be devoted to the development of the theory. Suggested improvements to it are recommended.*

In summary, the spherical integral transformations of geodesy and their discrete summation approximations have been interpreted from a spectral-theoretic or spherical digital filter viewpoint. Besides unfolding a deeper understanding of the data-processing being performed by the theoretical transformations and their approximations, the approach has the immediate benefit of enabling optimal templates to be determined for the discrete summations used in computer algorithms.

* in the following chapter

SECTION 9

RECOMMENDATIONS FOR FURTHER INVESTIGATION

Based on the theory, results, and understanding which have been achieved to date, the following subjects are recommended for future research and study.

General Theory

1) An investigation of the possibility of extending the spectral theory of discrete summation transformations to the case of rectangular grid patterns (based on latitude and longitude). Until now, only bull's-eye templates have been considered since it would seem that only these are shift-invariant with a change of the point-of-evaluation. However, it is possible to define convolution in either "geographic" or "local spherical polar" coordinates, and the spectrum is a double integral which may be evaluated in any surface coordinates. Thus it might be possible to develop a theory of discrete summations over rectangular grids.

2) An investigation of techniques for incorporating known statistical uncertainties in the input data into the design of optimal templates for discrete summation transformations. In the present design of optimal filters the input data is assumed to be perfect or error-free.

3) An extension of the digital filter design optimization process to include adjustment of the filter weight parameters as well as the template parameters. Currently the filter weight parameters are held fixed at a pre-selected value (e.g. the integrated-mean value of a kernel over a compartment). In traditional filter design, it is the filter weight parameters which are adjusted rather than grid parameters.

Specific Transformations

1) A derivation of the details of the spectral theory of discrete summation approximations to Molodenskii's Integral, and an application of the optimization (filter design) process to determine optimal templates for this summation. Molodenskii's transformation has greatly increased in importance in recent years due to the expanding availability of satellite altimetry data.

2) A development of a method of easily calculating the integral of the classical Vening-Meinesz' function, so that the integrated-mean weighting scheme can be applied to the discrete summation approximation of the classical Vening-Meinesz' transformation. Currently the analysis and optimization has been limited to the analog of the Vening-Meinesz' transformation having surface layer densities as input rather than gravity anomalies, due to the much more tractable nature of this transformation.

3) A derivation of the spectral theory of discrete summation approximations to the Poisson-deWitte transformation, and an application of the optimization process to determine optimal templates for this summation. DeWitte (1969) has described his recommended method of calculating the three anomalous gravity vector components at altitude, which is partially based on the Poisson kernel. However his investigations, documented in a series of papers, seem to have been generally overlooked by subsequent investigators.

4) A derivation of the partial derivatives of the spectrum of discrete summation transformations with respect to template parameters when the filter weights are chosen by methods other than the integrated-mean value scheme. While the integrated-mean value method corresponds nicely to physical intuition and has the advantage that the partial derivative of the spectrum does not involve the partial derivative of the kernel, it has the disadvantage that the integral of the kernel must be known. Such an integral may be more difficult to compute than the partial derivative of the kernel.

5) An extension of the filter design process to non-traditional geodetic transformations such as those involving gravity gradient tensor components.

Optimization Methods

1) A derivation of the second partial derivatives of the spectrum of the Stokes' and Vening-Meinesz' discrete summations and incorporation of the resulting expressions into the optimization algorithm. The present Gauss-Newton method neglects the second derivative terms and hence is not a pure Newton method with second-order convergence. The difference can be significant when the relationship of the spectra to the parameters is highly non-linear.* Like the first partial derivative expressions, the second partials will seem complicated but should be relatively easy to compute from other quantities which have already had to be calculated in the determination of the spectrum. Moreover, the matrix of second partials will be tridiagonal, thus facilitating manipulations with it. Due to the relative simplicity of this approach, it appears to offer the possibility of a large gain (second-order convergence) for a small price.

2) The incorporation of alternative methods of handling the inequality constraints among the template parameters in the optimization algorithm. The present method, while quick and easy to implement, does not seem to work well especially when there are a large number of parameters.

3) The investigation of other non-linear optimization techniques which might improve computational efficiency in the filter design program. A detailed survey of such techniques is given in Avriel (1976), and recent developments in the non-linear least-squares case are described by Dennis (1977) and Gill and Murray (1978).

4) The replacement of the current least-squares optimization algorithm by a Chebyshev algorithm to minimize the maximum error between the ideal spectrum and the spectrum of the summation approximation rather than the sum-of-squares error.

5) The inclusion of stopping criteria in the optimization algorithm. Currently, the user specifies the number of iterations to be executed. Stopping criteria might provide a rational means of determining whether the true minimum rms discretization error has been reached. It might also prevent the somewhat random divergence observed on some optimization runs after several convergent iterations. Dennis (1977, section 3, pg. 272ff) gives a specific criterion which he has found very reliable and which has a geometric interpretation.

* Dahlquist-Björk (1974, pg. 444); Dennis (1977, pg. 296).

As is apparent from the above, while much development of the theory and its applications have been achieved, many possible areas of further research and development remain to be explored.

APPENDIX A

DEFINITIONS AND NOTATIONS FOR THE ASSOCIATED LEGENDRE FUNCTIONS

The associated Legendre functions $P_n^m(x)$ of n^{th} degree and m^{th} order are defined by

$$P_n^m(x) = (-1)^m (1-x^2)^{m/2} \frac{d^m}{dx^m} P_n(x)$$

or equivalently by

$$P_n^m(\cos \psi) = \sin^m \psi \frac{d}{\sin \psi d\psi} \left(\frac{d}{\sin \psi d\psi} \left[\dots \frac{d P_n(\cos \psi)}{\sin \psi d\psi} \right] \right)$$

where $P_n(x)$ is the Legendre polynomial of n^{th} degree.

This definition follows that of Hobson, and this family of functions is therefore called Hobson's associated Legendre functions.*

The explicit expressions for the first few associated Legendre functions are:

$$P_0^0(\cos \psi) = P_0(\cos \psi) = 1$$

$$P_1^0(\cos \psi) = P_1(\cos \psi) = \cos \psi$$

$$P_1^1(\cos \psi) = -\sin \psi$$

$$P_2^0(\cos \psi) = P_2(\cos \psi) = \frac{3}{2} \cos^2 \psi - \frac{1}{2}$$

$$P_2^1(\cos \psi) = -3 \sin^2 \psi \cos \psi$$

$$P_2^2(\cos \psi) = +3 \sin^2 \psi$$

* See Whittaker and Watson (1927, pg. 325); Robin (1957, Vol. I, pg. 70, 107).

Numerical values of the coefficients in the expressions up to degree and order 25 have been given by Peasley (1976).

The associated Legendre functions satisfy a variety of three-term recurrence relations:

$$\cdot P_n^{m+2}(x) + 2(m+1) \frac{x}{\sqrt{1-x^2}} P_n^{m+1}(x) + (n-m)(n+m+1) P_n^m(x) = 0$$

$$(0 \leq m \leq n-2)$$

$$\cdot (2n+1)x P_n^m(x) = (n-m+1) P_{n+1}^m(x) + (n+m) P_{n-1}^m(x) = 0$$

$$(0 \leq m \leq n-1)$$

$$\cdot (2n+1)\sqrt{1-x^2} P_n^{m-1}(x) = P_{n-1}^m(x) - P_{n+1}^m(x)$$

A very complete list is given in Erdélyi (1953, Section 3.8, pp. 160-161).

The closely related functions $P_{nm}(x)$ used by many authors* differ only in sign for odd order m :

$$P_{nm}(x) = (1-x^2)^{m/2} \frac{d^m}{dx^m} P_n(x) = (-1)^m P_n^m(x)$$

or equivalently

$$P_{nm}(\cos \psi) = (-1)^m P_n^m(\cos \psi)$$

This family of functions is called Ferrers' associated Legendre functions.**

It should be noted that the notational convention for these two families of functions is not completely standardized in the literature. Some authors reverse the notations given above and use $P_n^m(x)$ to denote the Ferrers' family or $P_{n,m}(x)$ to denote the Hobson family. This document follows the convention of Magnus and Oberhettinger (1949), Erdélyi (1953), Courant and Hilbert (1953), Robin (1957), and Gradshteyn and Ryzhik (1965). However, the reverse convention is used by Frank and von Mises (1930), Jahnke and Emde (1945), Vogel (1953), Morse and

* e.g. Heiskanen-Moritz (1967, pg. 22ff).

** See Whittaker and Watson (1927, pg. 323); Robin (1957, Vol. I, pg. 70, 107).

Feshbach (1953), Pick-Picha-Vyskocil (1973), and DiDonato (1977). Therefore, when comparing equations or transformations in this document with other sources, the reader should always first ascertain from fundamental definitions which notational convention is being followed in the other source.

An example of the problems which can be encountered from the existence of two "nearly" identical families is found in Abramowitz and Stegun (1965). On page 334, equation 8.6.6 defines the associated Legendre functions following the Hobson convention; but on page 338, Figure 8.2 depicts a graph of three of these functions following the Ferrers convention.

The reader should also be warned that Erdélyi (1953) and Gradshteyn and Ryzhik (1965) use italics [$P_n^m(x)$] to denote another form of associated Legendre functions defined in the complex plane. This document is concerned only with Legendre functions on the real interval between -1 and +1, which these authors denote by roman characters [$P_n^m(x)$].

The reader may wonder why the Hobson (P_n^m) family has been chosen in the fundamental definition of the spherical spectral transform rather than the Ferrers (P_{nm}) family. The reason is based upon the spectral expansions of the Stokes' and Vening-Meinesz' kernels:

$$S(\psi) = + \sum_{n=2}^{\infty} \frac{2n+1}{n-1} P_n(\cos \psi)$$

$$\frac{dS(\psi)}{d\psi} = + \sum_{n=2}^{\infty} \frac{2n+1}{n-1} P_n^1(\cos \psi) = - \sum_{n=2}^{\infty} \frac{2n+1}{n-1} P_{n1}(\cos \psi)$$

If the Ferrers' family were used in the spherical spectral transform definition,* the resulting spectrum of the Vening-Meinesz' integral transformation would be negative. To eliminate this inconvenience the Hobson family has been selected as fundamental.

If the vertical deflections ξ and η had been defined with the opposite sign convention, the corresponding Vening-Meinesz' integral

* as in the original exposition of the author's study, Robertson (1977a).

formulae would then carry an inelegant negative sign, but the deflections would then be the positive surface gradient of the geoid height, and the spectrum could be made positive by choosing Ferrers' family to be fundamental. Under the standard convention, the Vening-Meinesz' formula carry no negative sign, but the deflections must be the negative surface gradient of the geoid height [Heiskanen-Moritz (1967, pg. 114)].

APPENDIX B

RECURSION RELATIONS FOR THE INDEFINITE INTEGRALS OF THE ASSOCIATED LEGENDRE FUNCTIONS

In order to efficiently compute the spectrum of a discrete summation geodetic transformation for an arbitrary template, it is imperative to utilize recursion relations for the indefinite integrals of the associated Legendre functions. Such relations do not seem to have appeared in the classical or modern literature. However, very recently DiDonato (1977) has published elegant expressions for these recursion relations for arbitrary degree and order, and the derivations thereof. Also, Paul (1978) will soon publish his recursion relations.

At the time when the author was originally implementing his spectral theory of the discrete Vening-Meinesz' transformation in a computer program (late fall 1977), he was not yet aware of DiDonato's or Paul's work, nor was he able to derive similar recursions within a limited time.* Therefore because of the desirability of validating his theory quickly, the author instead derived a recursive computational procedure for the analytic expressions of the indefinite integral of the associated Legendre function $P_n^1(x)$ of arbitrary degree and first order. The derivation was based upon several fundamental ideas of his colleague Stanley W. Shepperd, whose contributions the author wishes to acknowledge. This procedure was programmed, verified and used in the early versions of the discrete Vening-Meinesz' spectral calculation subroutine.

Due to certain numerical difficulties with this procedure which occurred for higher degrees, an attempt was made to derive another recursive set of analytic expressions for the indefinite integrals of $P_n^1(x)$ based on slightly different principles and using Calvez and Genin's (1977) algorithm. Before this was completed, the author became aware of DiDonato's obviously superior recursion relations, and implemented them instead.

* He overly restricted his investigation to recursions involving only integrals of functions of lower degree.

All of these recursion relations are described briefly in the following sections.

B.1 Shepperd-Robertson Recursion

The Shepperd-Robertson recursion relations for the analytic expressions of the indefinite integral of the associated Legendre functions $P_n^1(x)$ is based upon the validity of the following expansions:

$$P_n^1(x) = - \sum_{k=0}^{n-1} b_{n,k} x^k \sqrt{1-x^2}$$

and

$$\int x^k \sqrt{1-x^2} dx = -(1-x^2)^{3/2} \sum_{j=0}^{k-1} c_{k,j} x^j + d_k (x\sqrt{1-x^2} + \arcsin x)$$

where $b_{n,k}$, $c_{n,k}$, and d_k are constants. Thus, upon inserting the second equation into the indefinite integral of the first and regrouping terms it is seen that the integral of $P_n^1(x)$ may be expressed as

$$\int P_n^1(x) dx = +(1-x^2)^{3/2} \sum_{j=0}^{n-2} e_{n,j} x^j + f_n (x\sqrt{1-x^2} + \arcsin x)$$

where

$$e_{n,j} = \sum_{k=j+1}^{n-1} b_{n,k} c_{k,j}$$

$$f_n = \sum_{j=0}^{n-2} b_{n,k} d_k$$

Recursion relations will be developed for the $b_{n,k}$, $c_{k,j}$ and d_k constants in the next subsection, and the $e_{n,j}$ and f_n constants can be easily calculated therefrom. The definite integral over an arbitrary ring is then determined as the difference of two indefinite integral evaluations.

The Shepperd-Robertson recursion relations were coded into the earliest versions of the discrete Vening-Meinesz' spectrum calculation subroutine. They worked well up to about degree 50. Above this degree a numerical instability gradually began to set in with erroneous

digits first appearing in the least significant places and finally in all places. Nevertheless the algorithm enabled an early numerical verification of the author's theory of the discrete Vening-Meinesz' spectrum. A short analysis of the cause of the instability will be given in subsection B.1.2.

B.1.1 Coefficients in the Shepperd-Robertson Recursion

The $b_{n,k}$ coefficients can be shown* to have the values:

$$b_{n,k} = \begin{cases} 0 & \left[\begin{array}{l} n+k \text{ even} \\ 0 \leq k \leq n \end{array} \right] \text{ or } [k \geq n] \\ \frac{(-1)^{\frac{n-k-1}{2}} (n+k+1)!}{2^n \left(\frac{n+k+1}{2}\right)! \left(\frac{n-k-1}{2}\right)! k!} & \left[\begin{array}{l} n \geq 1 \\ n+k \text{ odd} \\ 0 \leq k \leq n-1 \end{array} \right] \end{cases}$$

Several of the lower-indexed values of $b_{n,k}$ are listed in matrix form in Table B-1.

The $b_{n,k}$ coefficients can be shown to satisfy the following recursion relations:

n odd

$$b_{1,0} = 1$$

$$b_{n+2,0} = -\frac{n+2}{n+1} b_{n,0} \quad (\text{down left column})$$

$$b_{n,k+2} = -\frac{(n+k+2)(n-k-1)}{(k+2)(k+1)} b_{n,k}$$

$$\text{where } k = 0, 2, 4, \dots \quad (\text{across row})$$

n even

$$b_{2,1} = 3$$

$$b_{n+2,1} = -\frac{n+3}{n} b_{n,1} \quad (\text{down left column})$$

$$b_{n,k+2} = -\frac{(n+k+2)(n-k-1)}{(k+2)(k+1)} b_{n,k}$$

$$\text{where } k = 1, 3, 5, \dots \quad (\text{across row})$$

* Heiskanen-Moritz (1967, pg. 24, equation 1-62). Their expression has to be reformulated to obtain the expansion used here.

$$P_n^1(x) = - \sum_{k=0}^{n-1} b_{n,k} x^k \sqrt{1-x^2} \quad [n \geq 1]$$

$n \backslash k$	0	1	2	3	4
0	0	0	0	0	0
1	1	0	0	0	0
2	0	3	0	0	0
3	$-\frac{3}{2}$	0	$\frac{5 \cdot 3}{2}$	0	0
4	0	$-\frac{5 \cdot 3}{2}$	0	$\frac{7 \cdot 5 \cdot 3}{3 \cdot 2 \cdot 1}$	0
5	$\frac{5 \cdot 3}{4 \cdot 2}$	0	$-\frac{5 \cdot 3 \cdot 7 \cdot 2}{4 \cdot 2}$	0	$\frac{9 \cdot 7 \cdot 5 \cdot 3}{3 \cdot 4 \cdot 2}$
6	0	$\frac{7 \cdot 5 \cdot 3}{4 \cdot 2}$	0	$\frac{9 \cdot 7 \cdot 5 \cdot 3 \cdot 4}{4 \cdot 3 \cdot 2 \cdot 2}$	0

Table B-1. The $b_{n,k}$ coefficients.

The $c_{k,j}$ and d_k coefficients can be shown to have the following values:*

$$c_{k,j} = \begin{cases} \frac{1}{k+2} \frac{(k-1)!!}{k!!} \frac{(j+1)!!}{j!!} & \begin{cases} k \geq 1 \\ k+j \text{ even} \\ 0 \leq j \leq k-1 \end{cases} \\ 0 & [k+j \text{ odd}] \end{cases}$$

$$d_k = \begin{cases} \frac{1}{k+2} \frac{(k-1)!!}{k!!} & [k \text{ even}] \\ 0 & [k \text{ odd}] \end{cases}$$

Several of the lower-indexed values of the $c_{n,k}$ and d_k are listed in Tables B-2 and B-3.

The $c_{n,k}$ and d_k coefficients are easily seen to satisfy the following recursion relations:

$$\begin{cases} c_{k,k-1} = \frac{1}{k+2} & (\text{diagonal}) \\ c_{k+2,j} = \frac{k+1}{k+3} c_{k,j} & \begin{cases} \text{down columns} \\ \text{from diagonal} \end{cases} \end{cases}$$

$$\begin{cases} d_0 = \frac{1}{2} \\ d_{k+2} = \frac{k+1}{k+3} d_k \end{cases}$$

* The double factorial notation (!!) indicates that only alternate integers appear: $6!! = 6 \cdot 4 \cdot 2$; $5!! = 5 \cdot 3 \cdot 1$.

$$\int x^k \sqrt{1-x^2} dx = -(1-x^2)^{3/2} \sum_{j=0}^{k-1} c_{k,j} x^j + d_k (x\sqrt{1-x^2} + \arcsin x)$$

$k \backslash j$	0	1	2	3	4	5
0	0	0	0	0	0	0
1	$\frac{1}{3}$	0	0	0	0	0
2	0	$\frac{1}{4}$	0	0	0	0
3	$\frac{2}{5 \cdot 3}$	0	$\frac{1}{5}$	0	0	0
4	0	$\frac{3}{6 \cdot 4}$	0	$\frac{1}{6}$	0	0
5	$\frac{4 \cdot 2}{7 \cdot 5 \cdot 3}$	0	$\frac{4}{7 \cdot 5}$	0	$\frac{1}{7}$	0
6	0	$\frac{5 \cdot 3}{8 \cdot 6 \cdot 4}$	0	$\frac{5}{8 \cdot 6}$	0	$\frac{1}{8}$

Table B-2. The $c_{k,j}$ coefficients.

k	d_k
0	$\frac{1}{2}$
1	0
2	$\frac{1}{4 \cdot 2}$
3	0
4	$\frac{3}{6 \cdot 4 \cdot 2}$
5	0
6	$\frac{5 \cdot 3}{8 \cdot 6 \cdot 4 \cdot 2}$

Table B-3. The d_k coefficients.

B.1.2 Instability Analysis of the Shepperd-Robertson Recursion

The predominant cause of the numerical instability of the Shepperd-Robertson recursion relations is the large magnitudes and relative magnitudes of the "polynomial" coefficients $b_{n,k}$ of the associated Legendre function $P_n^1(x)$ which occur for large degree n .

It can be shown that the "diagonal" coefficient $b_{n,n-1}$ has the value

$$b_{n,n-1} = \frac{1 \cdot 3 \cdot 5 \cdot 7 \cdots (2n-1)}{1 \cdot 2 \cdot 3 \cdot 4 \cdots (n-1)} = \frac{2^n (n-\frac{1}{2})!}{\sqrt{\pi} (n-1)!}$$

while the "left column" coefficients $b_{n,0}$ and $b_{n,1}$ have the magnitudes

$$|b_{n,0}| = \frac{(n+1)!}{2^n \left(\frac{n+1}{2}\right)! \left(\frac{n-1}{2}\right)!} \quad [n \text{ odd}]$$

$$|b_{n,1}| = \frac{(n+2)!}{2^n \left(\frac{n+2}{2}\right)! \left(\frac{n-2}{2}\right)!} \quad [n \text{ even}]$$

Using Stirling's formula, the Legendre Duplication formula, and the asymptotic expression for the exponential,

$$n! \sim n^{n+\frac{1}{2}} e^{-n} \sqrt{2\pi}$$

$$(2n)! = \frac{1}{\sqrt{\pi}} 2^{2n} n! (n-\frac{1}{2})!$$

$$e^x \sim (1 + \frac{x}{n})^n$$

the following approximate expressions may be inferred:

$$b_{n,n-1} \sim \frac{2^n \sqrt{n-1}}{\sqrt{\pi}}$$

$$|b_{n,0}| \sim \sqrt{\frac{2}{\pi}} \frac{n}{\sqrt{n-1}} \quad [n \text{ odd}]$$

$$|b_{n,1}| \sim \sqrt{\frac{2}{\pi}} (n+1) \sqrt{n-2} \quad [n \text{ even}]$$

Degree n	"Left columns"		"Diagonal" $b_{n,n-1}$
	$b_{n,0}$	$b_{n,1}$	
25	4.1	93.6	9.3 10^7
50	5.7	273.5	4.4 10^{15}
75	7.0	507.8	1.8 10^{23}
100	8.0	785.8	7.1 10^{30}
125	9.0	1101.6	2.7 10^{38}
150	9.8	1451.1	9.8 10^{45}

Table B-4. Estimates of certain $b_{n,k}$ coefficients.

Some numerical values of these approximations are presented in Table B-4. It is immediately seen that around degree 50 numerical significance will begin to be lost in summations when the computations are carried out on a computer having about sixteen decimal digits of precision.

B.2 Robertson-Clenshaw* Recursion

In order to attempt to overcome the numerical difficulties encountered in the Shepperd-Robertson recursion relations, the possibility of expanding the indefinite integral of the associated Legendre function $P_n^1(x)$ in a linear combination of these functions themselves was investigated. In other words, an expansion of the form

$$\int P_n^1(x) dx = +(1-x^2) \sum_{k=1}^{n-1} h_{n,k} P_k^1(x) + f_n(x\sqrt{1-x^2} + \arcsin x)$$

was sought, where the $h_{n,k}$ are constant coefficients to be determined. If recursions could be derived for these coefficients, then Calvez and Genin's (1977) algorithm could be used to perform the summation directly without separately recursing on the $P_n^1(x)$.

This approach offers the possibility that the $h_{n,k}$ might be "well-behaved", since the problems of large numbers might be entirely embedded in the $P_n^1(x)$ functions, which appear explicitly. This possibility is further suggested by the following heuristic argument: The associated Legendre functions $P_n^1(x)$ have the expansion

$$P_n^1(x) = -\sqrt{1-x^2} \sum_{k=0}^{n-1} b_{n,k} x^k$$

Thus from the integral expansion, the $h_{n,k}$ coefficients are determined by the equations

$$\sum_{k=1}^{n-1} b_{n,k} \sum_{j=1}^{k-1} c_{k,j} x^j = \sum_{k=1}^{n-1} h_{n,k} \sum_{j=1}^{k-1} b_{k,j} x^j$$

which is to hold for all values of x . By reordering the summation, and using matrix notation, this may be written as

$$B C \underline{x} = H B \underline{x}$$

*Clenshaw's name is used because Clenshaw (1955) first suggested the summation technique which Calvez and Genin's (1977) paper generalizes. The Tscherning-Rapp (1974) covariance models use Clenshaw summation. For a detailed description, see Luke (1975, pp. 475-482).

Hence $H = BCB^{-1}$, so that with the reasonable $c_{k,j}$ coefficients, it appears that the $h_{n,k}$ coefficients will also be reasonable, since intuitively large coefficients in the B matrix will be counteracted by correspondingly small elements in the B^{-1} matrix.

Let the elements of the B^{-1} matrix be denoted by $\beta_{j,\ell}$. Some values of the lower-indexed $\beta_{j,\ell}$ and $h_{n,k}$ coefficients are listed in Tables B-5 and B-6.

$j \backslash \ell$	0	1	2	3	4	5
0	0	1	0	0	0	0
1	0	0	$\frac{1}{3}$	0	0	0
2	0	$\frac{1}{5}$	0	$\frac{2}{5 \cdot 3}$	0	0
3	0	0	$\frac{1}{7}$	0	$\frac{3 \cdot 2 \cdot 1}{7 \cdot 5 \cdot 3}$	0
4	0	$\frac{3}{7 \cdot 5}$	0	$\frac{2 \cdot 2}{9 \cdot 5}$	0	$\frac{3 \cdot 2 \cdot 2 \cdot 2}{9 \cdot 7 \cdot 5 \cdot 3}$

$$\sqrt{1-x^2} x^j = - \sum_{\ell=1}^{j+1} \beta_{j,\ell} P_{\ell}^1(x)$$

Table B-5. The $\beta_{j,\ell}$ coefficients.

$n \backslash k$	0	1	2	3	4
0	0	0	0	0	0
1	0	0	0	0	0
2	0	-1	0	0	0
3	0	0	$-\frac{5}{8}$	0	0
4	0	$-\frac{19}{30}$	0	$-\frac{7}{15}$	0

$$\int P_n^1(x) dx = +(1-x^2) \sum_{k=1}^{n-1} h_{n,k} P_n^1(x) + \dots$$

Table B-6. The $h_{n,k}$ coefficients.

The $\beta_{j,l}$ coefficients may actually be determined analytically. Beginning with the identity that

$$\sqrt{1-x^2} x^j = - \sum_{l=1}^{n+1} \beta_{j,l} P_l^1(x) \quad [j \geq 1]$$

and multiplying by $P_n^1(x)$ and integrating,

$$\begin{aligned} \int_{-1}^{+1} \sqrt{1-x^2} P_n^1(x) dx &= - \sum_{l=1}^{j+1} \beta_{j,l} \int_{-1}^{+1} P_n^1(x) P_l^1(x) dx \\ &= -\beta_{j,n} \frac{2}{2n+1} \frac{(n+1)!}{(n-1)!} \end{aligned}$$

Thus

$$\beta_{j,n} = \begin{cases} 0 & [j+n \text{ even}] \\ -2 \int_0^1 \sqrt{1-x^2} x^j P_n^1(x) dx \cdot \frac{2n+1}{2} \frac{(n-1)!}{(n+1)!} & [j+n \text{ odd}] \end{cases}$$

To evaluate the integral, use is made of Erdélyi (1954, Vol. II, pg. 313, eqn. 18.1.4). This yields, after some manipulation:

$$\beta_{j,n} = \begin{cases} 0 & [j+n \text{ even}] \\ + \frac{\left(\frac{1}{2}\right)!}{2^j} \frac{2n+1}{2} \frac{j!}{\left(\frac{j+2+n}{2}\right)! \left(\frac{j+1-n}{2}\right)!} & [j+n \text{ odd}] \end{cases}$$

From this expression, recursion relations could be derived for the $\beta_{j,n}$ coefficients, and a computational procedure could undoubtedly be established for the $h_{n,k}$ coefficients.

At about this point in the development of a stable recursion for the indefinite integrals of the associated Legendre functions, the author became aware of DiDonato's algorithm.

B.3 DiDonato Recursion

DiDonato (1977) has stated and derived elegant recursion relations for the indefinite integrals of the Ferrers' associated Legendre function $P_{nm}^1(x)$ of arbitrary degree n and order m^* .

Using the notation convention of this document they may be stated as follows for the first order:

$$P_1^1(\cos \psi) = -\sin \psi$$

$$P_2^1(\cos \psi) = -3 \sin \psi \cos \psi$$

$$P_{n+1}^1(\cos \psi) = \left[(2n+1)(\cos \psi) P_n^1(\cos \psi) - (n+1) P_{n-1}^1(\cos \psi) \right] / n$$

*The reader is warned that DiDonato uses the reverse notation convention.

Letting $I_n^m = \int P_n^m(x) dx$,

$$I_1^1 = - \left[\cos \psi \sin \psi + \arcsin(\cos \psi) + \frac{\pi}{2} \right] / 2$$

$$I_2^1 = -\sin^2 \psi P_1^1(\cos \psi)$$

$$I_{n+1}^1 = \frac{(n-1)(n+1)}{(n+2)(n)} I_{n-1}^1 - \frac{2n+1}{(n+2)(n)} \sin^2 \psi P_n^1(\cos \psi)$$

In a computer program it is necessary to run two recursions simultaneously, one for the odd indices, beginning with I_1^1 , and one for the even indices beginning with I_2^1 .

The notation I_n^m is used here for the indefinite integral of Hobson's associated Legendre Function in order to distinguish this quantity from DiDonato's S_n^m which denotes the indefinite integral of Ferrers' associated Legendre Function.

This algorithm has been implemented in the comprehensive filter design computer program (Appendix C), and the author has had no difficulties with its use. Although DiDonato also gives a normalized form of the recursive relations and states that it "may be needed in order to keep the results ... from becoming excessively large", the author has not found this to be necessary up through degree 1500.

B.4 Paul Recursion

The author has not yet seen Paul's (1978) recursion relations for the indefinite integrals of the associated Legendre functions.

APPENDIX C

LISTING OF THE COMPREHENSIVE FILTER DESIGN COMPUTER PROGRAM

PL/I OPTIMIZING COMPILER

VERSION 1 RELEASE 3.0 PTF 64

PAGE 1

OPTIONS SPECIFIED

OBJ,GN,NEST,S,OPT(TIME)

OPTIONS USED

AGGREGATE	NOCOUNT	ATTRIBUTES(SHORT)
GONUMBER	NODECK	CHARSET(60,EBCDIC)
INCLUDE	NOESD	NCCOMPILE(S)
INSOURCE	NOFLOW	FLAG(I)
LMESSAGE	NOGOSTMT	LINECOUNT(55)
MAP	NOIMPRECISE	MARGINS(2,72,1)
NEST	NOINTERRUPT	OPTIMIZE(TIME)
NUMBER	NOLIST	SEQUENCE(73,80)
OBJECT	NOMACRO	SIZE(499408)
OPTIONS	NOMARGINI	NOSYNTAX(S)
SOURCE	NOMDECK	XREF(SHORT)
STORAGE	NOOFFSET	TERMINAL(NOAGGREGATE,
	NOSTMT	NOATTRIBUTES,
		NOESD,
		NOINSOURCE,
		NOLIST,
		NOMAP,
		NOOFFSET,
		NOOPTIONS,
		NOSOURCE,
		NOSTORAGE,
		NOXREF)

SOURCE LISTING

NUMBER LEV NT

```

10 0 FITFILT: PROCEDURE(PARAMETERS) OPTIONS(MAIN) REORDER;
20 1 0 DCL PARAMETERS CHAR(100) VARYING;
30 1 0 DCL PI FLOAT BINARY(53) INITIAL(3.14159265358979);
40 1 0 DCL DEGTO RAD FLOAT BINARY(53) INITIAL((PI/180));
50 1 0 DCL RADTO DEG FLOAT BINARY(53) INITIAL((1/DEGTORAD));

70 1 0 DCL (IMIN, IMAX) FIXED BINARY;
80 1 0 DCL (NMIN INITIAL(0), NMAX INITIAL(1440)) FIXED BINARY;
90 1 0 DCL (ITERMIN INITIAL(0), ITERMAX INITIAL(1)) FIXED BINARY;

110 1 0 DCL KERNEL_NAME CHAR(31) VARYING INITIAL('STOKES');
120 1 0 DCL PSI_TEMPLATE_NAME CHAR(31) VARYING INITIAL('PICK_PICHA_VYSKOCIL');
130 1 0 DCL ALPHA_TEMPLATE_NAME CHAR(31) VARYING
    INITIAL('PICK_PICHA_VYSKOCIL');
150 1 0 DCL ALPHA_TEMPLATE_TYPE_NAME CHAR(31) VARYING INITIAL('CONTINUOUS');

170 1 0 DCL VARIABLES CHAR(10) VARYING INITIAL('PSI_ONLY');
180 1 0 DCL ALTITUDE FLOAT BINARY(53) INITIAL(0);
190 1 0 DCL RADIUS_RATIO FLOAT BINARY(53) INITIAL(1);
200 1 0 DCL PSIZERO FLOAT BINARY INITIAL(3E-2);
210 1 0 DCL NRINGS FIXED BINARY INITIAL(66);
220 1 0 DCL NSECTORS FIXED BINARY INITIAL(24);

240 1 0 DCL PRINT_LEVEL FIXED BINARY INITIAL(30);
250 1 0 DCL PLOT_SWITCH FIXED BINARY INITIAL(0);
260 1 0 DCL SAVE_RESULTS_SWITCH FIXED BINARY INITIAL(0);
270 1 0 DCL VARBLERES FILE OUTPUT;

300 1 0 PUT EDIT('EXPLICIT INPUT TO PROGRAM')(A); PUT SKIP(2);
310 1 0 GET DATA(KERNEL_NAME,
    PSI_TEMPLATE_NAME,
    ALPHA_TEMPLATE_NAME,
    ALPHA_TEMPLATE_TYPE_NAME,
    VARIABLES, ALTITUDE,
    ITERMIN, ITERMAX,
    NMAX,
    PSIZERO,
    NRINGS,
    NSECTORS,
    PRINT_LEVEL, PLOT_SWITCH, SAVE_RESULTS_SWITCH,
    DAMPING_POWER, WEIGHT_POWER, WEIGHT_TYPE) COPY;

```


NUMBER LEV NT

```

470 1 0 DCL DAMPING_POWER FLOAT BINARY INITIAL(0.5);
480 1 0 DCL WEIGHT_POWER FLOAT BINARY INITIAL(1.0);
490 1 0 DCL WEIGHT_TYPE CHAR(6) VARYING INITIAL('INPUT');
500 1 0 IF LENGTH(PARAMEters)>0 THEN DO;
510 1 1 GET STRING(PARAMEters(1:'))
      DATA(DAMPING_POWER,WEIGHT_POWER,WEIGHT_TYPE);
530 1 1 PUT SKIP DATA(DAMPING_POWER,WEIGHT_POWER,WEIGHT_TYPE);
540 1 1 END;

570 1 0 PUT SKIP(5) EDIT('EXPLICIT AND IMPLICIT(DEFAULT) INPUT TO PROGRAM')(A);
580 1 0 PUT SKIP(2) DATA(KERNEL_NAME,
      PSI_TEMPLATE_NAME,
      ALPHA_TEMPLATE_NAME,
      VARIABLES, ALTITUDE,
      ITERMIN, ITERMAX,
      NMAX,
      PSIZERO,
      NRINGS,
      NSECTORS,
      PRINT_LEVEL, PLOT_SWITCH, SAVE_RESULTS_SWITCH,
      DAMPING_POWER, WEIGHT_POWER, WEIGHT_TYPE);

730 1 0 DCL (KERNEL_FUNCTION_NOT_KNOWN,
      KERNEL_INTEGRAL_NOT_KNOWN,
      KERNEL_SPECTRUM_NOT_KNOWN) CONDITION INTERNAL;
760 1 0 DCL NOMINAL_COS_PSI_NOT_KNOWN CONDITION INTERNAL;

780 1 0 ON CONDITION(KERNEL_FUNCTION_NOT_KNOWN) STOP;
790 1 0 ON CONDITION(KERNEL_INTEGRAL_NOT_KNOWN) STOP;
800 1 0 ON CONDITION(KERNEL_SPECTRUM_NOT_KNOWN) STOP;
810 1 0 ON CONDITION(NOMINAL_COS_PSI_NOT_KNOWN) STOP;

830 1 0 DCL KERNEL_ORDER FIXED BINARY;
840 1 0 KERNEL_ORDER=KERNEL_ORDER_SET(KERNEL_NAME);
850 1 0 IMAX=IMAX_SET(KERNEL_NAME,PSI_TEMPLATE_NAME);
860 1 0 DCL JMAX(IMAX) FIXED BINARY CONTROLLED;
870 1 0 IF KERNEL_ORDER=1 THEN DO;
880 1 1 ALLOCATE JMAX;
890 1 1 CALL JMAX_SET(KERNEL_NAME,ALPHA_TEMPLATE_NAME,
      ALPHA_TEMPLATE_TYPE_NAME,IMAX,JMAX);
910 1 1 DCL JMAXMAX FIXED BINARY;
920 1 1 JMAXMAX=MAXIMUM(JMAX);
930 1 1 END;

```

PL/I OPTIMIZING COMPILER FITFLT: PROCEDURE(PARAMEters) OPTIONS(MAIN) REORDER;

NUMBER LEV NT

```

970 1 0 ALLOCATE CORE-BEGIN;

1010 2 0 DCL (I,J,N,ITER,VAR) FIXED BINARY;
1020 2 0 DCL NN FLOAT BINARY(53);

1040 2 0 DCL PSI(ITERMIN:ITERMAX,0:IMAX) FLOAT BINARY(53);
1050 2 0 DCL COS_PSI(0:IMAX) FLOAT BINARY(53);
1060 2 0 DCL SIN_PSI(0:IMAX) FLOAT BINARY(53);

1080 2 0 DCL KERNEL(0:IMAX) FLOAT BINARY(53);
1090 2 0 DCL (INTEGRAL_KERNEL, MEAN_KERNEL)(1:IMAX) FLOAT BINARY(53);

1110 2 0 DCL (PN,PN_PREV,PN_NEXT)(0:IMAX) FLOAT BINARY(53);
1120 2 0 DCL (INTEGRAL_PN, MEAN_PN)(1:IMAX) FLOAT BINARY(53);

/* VARIABLES FOR KERNEL_ORDER=1 */
1160 2 0 DCL ALPHA(ITERMIN:ITERMAX, IMAX, 0:JHAXMAX)
      FLOAT BINARY(53) CONTROLLED;
1180 2 0 DCL D_ALPHA(IMAX,0:JHAXMAX) FLOAT BINARY(53) CONTROLLED;

1200 2 0 DCL (PN1,PN1_PREV,PN1_NEXT)(0:IMAX) FLOAT BINARY(53) CONTROLLED;
1210 2 0 DCL (INTEGRAL_PN1, MEAN_PN1)(1:IMAX) FLOAT BINARY(53) CONTROLLED;
1220 2 0 DCL 1 INTEGRAL_PN1_INDEF(0:IMAX) CONTROLLED,
      2 PREV, (3 ODD, 3 EVEN) FLOAT BINARY(53),
      2 HERE
      2 NEXT, (3 ODD, 3 EVEN) FLOAT BINARY(53);

1270 2 0 DCL RING_FACTOR(IMAX) FLOAT BINARY(53) CONTROLLED;
1280 2 0 DCL (ALPHA_SUM2,ALPHA_DIFF2) FLOAT BINARY(53);

1320 2 0 DCL SPECTRUM FLOAT BINARY(53);
1330 2 0 DCL VARMAX FIXED BINARY;
1340 2 0 DCL WEIGHT(0:NMAX) FLOAT BINARY;
1350 2 0 DCL PARTIAL(NMAX,VARMAX) FLOAT BINARY CONTROLLED;
1360 2 0 DCL RESID_SPECTRUM(NMIN:NMAX) FLOAT BINARY CONTROLLED;
1370 2 0 DCL RELATIVE_RESIDUAL(NMAX,1) FLOAT BINARY;
1380 2 0 DCL WEIGHTED_RESIDUAL(NMAX,1) FLOAT BINARY;
1390 2 0 DCL X(0:VARMAX+1) FLOAT BINARY(53) CONTROLLED;
1400 2 0 DCL DX(VARMAX) FLOAT BINARY(53) CONTROLLED;
1410 2 0 DCL (DEG_SIG_OUTPUT_RESID,DEG_SIG_OUTPUT_RESID_CUM) FLOAT BINARY(53);
1420 2 0 DCL (DEG_VAR_OUTPUT_RESID,DEG_VAR_OUTPUT_RESID_CUM) FLOAT BINARY(53);
1430 2 0 DCL FIGURE_OF_MERIT(ITERMIN:ITERMAX) FLOAT BINARY;

```

PL/I OPTIMIZING COMPILER FITFLT: PROCEDURE(PARAMEters) OPTIONS(MAIN) REORDER;

NUMBER LEV NT

```

1480  2  0  DCL KERNEL_FUNCTION_GENERIC (KERNEL_FUNCTION_AT_SURFACE WHEN(*,*),
/* SUBROUTINES */
1500  2  0  DCL KERNEL_SPECTRUM_GENERIC (KERNEL_SPECTRUM_AT_SURFACE WHEN(*,*)) );
1520  2  0  DCL KERNEL_NOMINAL_COS_PSI_GENERIC
(KERNEL_NOMINAL_COS_PSI_SURFACE WHEN(*,*,*)),
1550  2  0  DCL MLSQ_ENTRY( (*,*) BINARY FLOAT, (*,*) BINARY FLOAT,
BINARY FIXED, BINARY FIXED, BINARY FIXED);
00001450
00001460
00001470
00001480
00001490
00001500
00001510
00001520
00001530
00001540
00001550
00001560
00001570
00001580

```

PL/I OPTIMIZING COMPILER FITFILT: PROCEDURE(PARAMEters) OPTIONS(MAIN) REORDER;

NUMBER LEV NT

```

1600 2 0 FIXED_FORMAT: FORMAT(SKIP, 10 F(12,7));
1610 2 0 FLOAT_FORMAT: FORMAT(SKIP, 10 E(12,3));

1630 2 0 NMIN=KERNEL_ORDER;
1640 2 0 ALLOCATE RESID_SPECTRUM;
1650 2 0 IF KERNEL_ORDER=1 THEN
    ALLOCATE ALPHA, D_ALPHA, INTEGRAL_PNI, MEAN_PNI,
    PNI, PNI_PREV, PNI_NEXT, INTEGRAL_PNI_INDEF,
    RING_FACTOR;
1690 2 0 RADIUS_RATIO=RADIUS_RATIO_CALC(ALTITUDE);

1720 2 0 ITER_LOOP_INIT: IF ITERMIN=0 THEN DO;
1730 2 1 IF RADIUS_RATIO=1 THEN
    CALL KERNEL_NOMINAL_COS_PSI
    (KERNEL_NAME,PSI_TEMPLATE_NAME,IMAX,COS_PSI);
1760 2 1 ELSE CALL KERNEL_NOMINAL_COS_PSI
    (KERNEL_NAME,PSI_TEMPLATE_NAME,RADIUS_RATIO,IMAX,COS_PSI);
1780 2 1 IF KERNEL_ORDER=1 THEN
    CALL KERNEL_NOMINAL_ALPHA
    (ALPHA_TEMPLATE_TYPE_NAME,IMAX,IMAX,ALPHA);

1810 2 1 END;
1820 2 0 ELSE DO;
1830 2 1 GET DATA(COS_PSI);
1840 2 1 PSIZE=ACOS(COS_PSI(0))*RADTODEG;
1850 2 1 IF KERNEL_ORDER=1 THEN GET DATA(ALPHA);
1860 2 1 END;

1880 2 0 DO I=0 TO IMAX UNTIL(COS_PSI(I)<COS(5*PI/NMAX));
1890 2 1 IMIN=I;
1900 2 1 END;
1910 2 0 IF VARIABLES='PSI ONLY' THEN VARMAX=IMAX-IMIN-1;
1920 2 0 ALLOCATE PARTIAL_X, DX;

1950 2 0 ITER_LOOP: DO ITER=ITERMIN TO ITERMAX;
1970 2 1 IF SAVE_RESULTS_SWITCH>0 THEN
    PUT FILE(VARIABLES) DATA(ITER,COS_PSI,ALPHA) SKIP(3);

2030 2 1 N_LOOP_INIT: DO;
2040 2 2 RADIUS_RATIO: DO I=0 TO IMAX;
2050 2 3 SIN_PSI(I)=SQRT(1-COS_PSI(I))*SQRT(1+COS_PSI(I));
2060 2 3 IF RADIUS_RATIO=1 THEN
    KERNEL(I)=KERNEL_FUNCTION(KERNEL_NAME,COS_PSI(I));

```

PL/I OPTIMIZING COMPILER FITFLT: PROCEDURE(PARAMEters) OPTIONS(MAIN) REORDER;

NUMBER LEV NT

```

2080 2 3 ELSE
2100 2 3 END RADII_INIT;
2120 2 2 RING_INIT: DO I=1 TO IMAX;
2130 2 3 INTEGRAL_KERNEL(I)=KERNEL_INTEGRAL_INDEF(KERNEL_NAME,COS_PSI(I),RADIUS_RATIO);
2150 2 3 MEAN_KERNEL(I)=INTEGRAL_KERNEL(I)/(COS_PSI(I-1)-COS_PSI(I));
2160 2 3 END RING_INIT;
2180 2 2 PSI(ITER,*)=ACOS(COS_PSI)*RADTODEG;
2190 2 2 IF PRINT_LEVEL>0 THEN DO;
2200 2 3 PUT PAGE EDIT('START OF ITERATION NUMBER',ITER)(A,F(8));
2210 2 3 PUT SKIP(2) EDIT('SPHERICAL RING RADII PSI (DEGREES)')(A)
      (PSI(ITER,*))(R(FIXED_FORMAT));
2230 2 3 PUT SKIP(2) EDIT('COSINES OF PSI VALUES')(A)
      (COS_PSI(ITER,*))(R(FIXED_FORMAT));
2250 2 3 PUT SKIP(2) EDIT('KERNEL VALUES AT SPHERICAL RING RADII PSI')(A)
      (KERNEL(I,R(FLOAT_FORMAT)));
2270 2 3 PUT SKIP(2) EDIT('KERNEL MEAN-INTEGRATED VALUES BETWEEN RING RADII')(A)
      (MEAN_KERNEL(I,R(FLOAT_FORMAT)));
2290 2 3 PUT SKIP(2) EDIT('INTEGRAL OF KERNEL BETWEEN RING RADII')(A)
      (INTEGRAL_KERNEL(I,R(FLOAT_FORMAT)));
2320 2 3 END;
2350 2 2 IF KERNEL_ORDER=1 THEN DO;
2360 2 3 IF ALPHA_TEMPLATE_TYPE_NAME = 'CONTINUOUS' THEN
      IF PRINT_LEVEL>5 THEN DO;
2380 2 4 PUT SKIP(3) EDIT('COMPARTMENT BOUNDARY AZIMUTHS')(A);
2390 2 4 DO I=1 TO IMAX;
2400 2 5 PUT SKIP EDIT('RING NUMBER',I)(A,F(8))
      ((ALPHA(ITER,I,J)*RADTODEG DO J=1 TO JMAX(I))(R(FIXED_FORMAT)));
2420 2 5 END;
2430 2 4 END;
2450 2 3 IF ALPHA_TEMPLATE_TYPE_NAME='CONTINUOUS' THEN
      DO I=1 TO IMAX;
2470 2 4 RING_FACTOR(I)=0.5;
2480 2 4 END;
2490 2 3 ELSE
      DO I=1 TO IMAX;
2510 2 4 RING_FACTOR(I)=0;
2520 2 4 DO J=0 TO JMAX(I)-1;
2530 2 5 ALPHA_SUM2=(ALPHA(ITER,I,J+1)+ALPHA(ITER,I,J))/2;
2540 2 5 ALPHA_DIFF2=(ALPHA(ITER,I,J+1)-ALPHA(ITER,I,J))/2;
2550 2 5 RING_FACTOR(I)=RING_FACTOR(I)+
      SIN(ALPHA_DIFF2)*2*COS(ALPHA_SUM2)**2/ALPHA_DIFF2;

```

PL/I OPTIMIZING COMPILER FITFLT: PROCEDURE(PARAMEters) OPTIONS(MAIN) REORDER;

NUMBER LEV NT

```

2570 2 5 END;
2590 2 4 RING_FACTOR(I)=RING_FACTOR(I)/PI;
2590 2 4 END;
2590 2 4 END;
2600 2 3 IF PRINT_LEVEL>0 THEN
      PUT SKIP(2) EDIT('RING FACTOR',I(A)
        (RING_FACTOR)/(FIXED_FORMAT));
2630 2 3 END;
2650 2 2 IF PRINT_LEVEL>=10 THEN
      PUT PAGE EDIT('N','ACTUAL SPECTRUM','IDEAL SPECTRUM',
        'RESID SPECTRUM','REL RESID','DEG VAR IN','WEIGHT','SIGMA',
        'CUM SIGMA')
        (X(4),A,X(4),A,X(2),A,X(2),A,X(4),A,X(5),A,X(9),A,X(3),A);
2700 2 2 DEG_VAR_OUTPUT_RESID_CUM=0;
2710 2 2 END N_LOOP_INIT;

2750 2 1 N_LOOP: DO N=NNIN TO NMAX;
2760 2 2 NN=FLOAT(N,53);
2770 2 2 SPECTRUM=0;

2810 2 2 I_LOOP: DO I=1 TO IMAX;
2820 2 3 IF KERNEL_ORDER=0 THEN DO;
2830 2 4 CALL INTEGRAL_PN_CALC;
2840 2 4 SPECTRUM=SPECTRUM+MEAN_KERNEL(I)*INTEGRAL_PN(I)/2;
2850 2 4 IF N=0 THEN
      IF I>IMIN+1 & I<=IMAX THEN
        PARTIAL(N,I-IMIN-1)=MEAN_KERNEL(I-1)*MEAN_PN(I-1)/2
        -MEAN_KERNEL(I)*MEAN_PN(I)/2
        -KERNEL(I-1)*(MEAN_PN(I-1)-MEAN_PN(I))/2
        -PN(I-1)*(MEAN_KERNEL(I-1)-MEAN_KERNEL(I))/2;
2910 2 4 END;

2940 2 3 IF KERNEL_ORDER=1 THEN DO;
2950 2 4 CALL INTEGRAL_PN_CALC;
2960 2 4 SPECTRUM=SPECTRUM+MEAN_KERNEL(I)*INTEGRAL_PN(I)*RING_FACTOR(I)
        /SQRT(N)*(NR+1));
2990 2 4 IF VARIABLES='PSI_ONLY' THEN DO;
2990 2 5 IF I>IMIN+1 & I<=IMAX THEN DO;
3000 2 6 PARTIAL(N,I-IMIN-1)=MEAN_KERNEL(I-1)*MEAN_PN(I-1)*RING_FACTOR(I-1)/2
        -MEAN_KERNEL(I)*MEAN_PN(I)*RING_FACTOR(I)/2
        -KERNEL(I-1)*(MEAN_PN(I-1)-MEAN_PN(I))*RING_FACTOR(I-1)
        -MEAN_PN(I)*(MEAN_KERNEL(I-1)-MEAN_KERNEL(I))*RING_FACTOR(I-1)/2
        -PN(I-1)*(MEAN_KERNEL(I-1)-MEAN_KERNEL(I))/2;

```

PL/I OPTIMIZING COMPILER FITFILT: PROCEDURE(PARAMEters) OPTIONS(MAIN) REORDER;

```

NUMBER  LEV  NT
3060    2    6  IF DAMPING_POWER=0.5 THEN
3080    2    6  PARTIAL(N,I-IMIN-1)=2*PARTIAL(N,I-IMIN-1)/SQRT(NN*(NN+1));
3100    2    6  ELSE
3110    2    5  PARTIAL(N,I-IMIN-1)=2*PARTIAL(N,I-IMIN-1)/(NN*(NN+1))*DAMPING_POWER;
3120    2    4  END;
3130    2    3  END I_LOOP;

3170    2    2  RESID_SPECTRUM(N)=SPECTRUM-KERNEL_SPECTRUM(KERNEL_NAME,N);
3180    2    2  IF KERNEL_SPECTRUM(KERNEL_NAME,N)=0 THEN
3200    2    2  ELSE RELATIVE_RESIDUAL=0;
3210    2    2  DEG_VAR_OUTPUT_RESID
3230    2    2  =RESID_SPECTRUM(N)**2*DEG_VAR_INPUT(KERNEL_NAME,N);
3240    2    3  WHEN('INPUT')
3260    2    3  WHEN('OUTPUT')
3280    2    3  WHEN('HEIGHT')
3290    2    2  WHEN('HEIGHT')=(DEG_VAR_OUTPUT_RESID**1E+6)**WEIGHT_POWER;
3310    2    2  END;
3320    2    2  DEG_VAR_OUTPUT_RESID_CUM=DEG_VAR_OUTPUT_RESID_CUM
3330    2    2  +DEG_VAR_OUTPUT_RESID;
3310    2    2  DEG_SIG_OUTPUT_RESID=SQRT(DEG_VAR_OUTPUT_RESID);
3320    2    2  DEG_SIG_OUTPUT_RESID_CUM=SQRT(DEG_VAR_OUTPUT_RESID_CUM);
3330    2    2  IF (PRINT_LEVEL>=10 & N<=60) |
3340    2    2  (PRINT_LEVEL>=15 & N<=360) |
3350    2    2  (PRINT_LEVEL>=20 & N<=720) |
3360    2    2  (PRINT_LEVEL>=25 & N<=1440) |
3370    2    2  (PRINT_LEVEL>=30) THEN
3380    2    2  PUT SKIP EDIT(IN,SPECTRUM,KERNEL_SPECTRUM(KERNEL_NAME,N),
3390    2    2  RESID_SPECTRUM(N),
3400    2    2  RELATIVE_RESIDUAL,
3410    2    2  DEG_VAR_INPUT(KERNEL_NAME,N),
3420    2    2  WEIGHT(N),
3430    2    2  DEG_SIG_OUTPUT_RESID,DEG_SIG_OUTPUT_RESID_CUM)
3440    2    2  (X(2),F(5),3 F(16,10),X(4),F(9,6),X(3),F(11,5),X(2),F(13,5),
3450    2    2  2 F(10,5) );
3460    2    2  END N_LOOP;

3500    2    1  FIGURE_OF_MERIT(ITER)=DEG_SIG_OUTPUT_RESID_CUM;
3510    2    1  IF PRINT_LEVEL>0
3520    2    1  THEN PUT SKIP(4)
3530    2    1  EDIT('CUMULATIVE DEGREE SIGMA OF RESIDUAL THRU DEGREE ',
3540    2    1  NMAX,' IS ',DEG_SIG_OUTPUT_RESID_CUM/(A,F(5),A,F(15,5)));

```

PL/I OPTIMIZING COMPILER FITFIL: PROCEDURE(PARAMEters) OPTIONS(MAIN) REORDER;

NUMBER LEV NT

```

3550  2  1  IF ITER=ITERMAX THEN LEAVE ITER_LOOP;

3600  2  1  IF VARIABLES='PSI_ONLY' THEN
      DO I=IMIN TO IMAX;
3620  2  2  X(I-IMIN)=COS_PSI(I);
3630  2  2  END;
3640  2  1  CALL INCREMENT_CALC;
3650  2  1  IF VARIABLES='PSI_ONLY' THEN DO;
3660  2  2  DO I=IMIN+1 TO IMAX-1;
3670  2  3  COS_PSI(I)=COS_PSI(I)+DX(I-IMIN);
3680  2  3  END;
3690  2  2  IF KERNEL_ORDER/=0 THEN
      DO I=1 TO IMAX;
3710  2  3  DO J=0 TO JMAX(I);
3720  2  4  ALPHA(ITER+1,I,J)=ALPHA(ITER,I,J);
3730  2  4  END;
3740  2  3  END;
3750  2  2  END;
3760  2  1  END ITER_LOOP;

3800  2  0  CALL SUMMARY;

      /* END OF MAIN PROGRAM */
00003550
00003560
00003570
00003580
00003590
00003600
00003610
00003620
00003630
00003640
00003650
00003660
00003670
00003680
00003690
00003700
00003710
00003720
00003730
00003740
00003750
00003760
00003770
00003780
00003790
00003800
00003810
00003820

```


PL/I OPTIMIZING COMPILER FITFIT: PROCEDURE(PARAMETERS) OPTIONS(MAIN) REORDER;

NUMBER LEV NT

```

3840 2 0 RADIUS_RATIO_CALC: PROC(ALTITUDE) RETURNS(FLOAT BINARY(53));
3850 3 0 DCL ALTITUDE FLOAT BINARY(53);
3860 3 0 RETURN(6371032/(6371032*ALTITUDE));
3870 3 0 END RADIUS_RATIO_CALC;

```

```

00003840
00003850
00003860
00003870

```

```

3890 2 0 INTEGRAL_PN_CALC: PROCEDURE;
3900 3 0 IF I=1 THEN DO I=0,1;
3910 3 1 CALL PN_CALC;
3920 3 1 END;
3930 3 0 ELSE CALL PN_CALC;
3940 3 0 INTEGRAL_PN(I)=
      ((PN_NEXT(I-1))-PN_NEXT(I))-(PN_PREV(I-1)-PN_PREV(I))/(2*NN+1);
3960 3 0 MEAN_PN(I)=INTEGRAL_PN(I)/(COS_PSI(I-1)-COS_PSI(I));

3980 3 0 PN_CALC: PROCEDURE;
3990 4 0 IF N=0 THEN DO;
4000 4 1 PN_PREV(I)=1; PN(I)=1; PN_NEXT(I)=COS_PSI(I); END;
4010 4 0 ELSE DO;
4020 4 1 PN_PREV(I)=PN(I); PN(I)=PN_NEXT(I);
4030 4 1 PN_NEXT(I)=((2*NN+1)*COS_PSI(I)*PN(I)-NN*PN_PREV(I))/(NN+1); END;
4040 4 0 END PN_CALC;
4050 3 0 END INTEGRAL_PN_CALC;

```

```

00003890
00003900
00003910
00003920
00003930
00003940
00003950
00003960
00003970
00003980
00003990
00004000
00004010
00004020
00004030
00004040
00004050

```

PL/I OPTIMIZING COMPILER FITFLT: PROCEDURE(PARAHETERS) OPTIONS(MAIN) REORDER;

NUMBER LEV NT

```

4070 2 0 INTEGRAL_PNL_CALC: PROCEDURE;
4080 3 0 IF I=1 THEN DO I=0,1;
4090 3 1 CALL INTEGRAL_PNL_INDEF_CALC;
4100 3 1 END;
4110 3 0 ELSE CALL INTEGRAL_PNL_INDEF_CALC;
4120 3 0 INTEGRAL_PNL(I)=
      INTEGRAL_PNL_INDEF(I-1).HERE-INTEGRAL_PNL_INDEF(I).HERE;
4140 3 0 MEAN_PNL(I)=INTEGRAL_PNL(I)/(COS_PSI(I-1)-COS_PSI(I));

4160 3 0 INTEGRAL_PNL_INDEF_CALC: PROCEDURE;
4170 4 0 IF N=1 THEN DO: PNL_PREV(I)=0; PNL(I)=-SIN_PSI(I);
4180 4 1 PNL_NEXT(I)=3*COS_PSI(I)*PNL(I); END;
4190 4 0 ELSE DO: PNL_PREV(I)=PNL(I); PNL(I)=PNL_NEXT(I);
4200 4 1 PNL_NEXT(I)=(12*N+1)*COS_PSI(I)*PNL(I)-(N+1)*PNL_PREV(I)/NN;END;
4210 4 0 IF MOD(N,2)=1 THEN
      IF N=1 THEN DO;
4230 4 1 INTEGRAL_PNL_INDEF(I).PREV.EVEN=0;
4240 4 1 INTEGRAL_PNL_INDEF(I).HERE=
      -(COS_PSI(I)*SIN_PSI(I)+ASIN(COS_PSI(I))*PI/2)/2;
4260 4 1 INTEGRAL_PNL_INDEF(I).NEXT.EVEN=-(SIN_PSI(I)*2)*PNL(I);
4270 4 1 END;
4280 4 0 ELSE DO;
4290 4 1 INTEGRAL_PNL_INDEF(I).PREV.EVEN=INTEGRAL_PNL_INDEF(I).NEXT.EVEN;
4300 4 1 INTEGRAL_PNL_INDEF(I).HERE=INTEGRAL_PNL_INDEF(I).NEXT.ODD;
4310 4 1 INTEGRAL_PNL_INDEF(I).NEXT.EVEN=
      (NN-1)*(NN+1)/(NN*(NN+2))*INTEGRAL_PNL_INDEF(I).PREV.EVEN
      -(2*NN+1)/(NN*(NN+2))*SIN_PSI(I)*2*PNL(I);
4340 4 1 END;
4350 4 0 ELSE
      IF N=2 THEN DO;
4370 4 1 INTEGRAL_PNL_INDEF(I).PREV.ODD=INTEGRAL_PNL_INDEF(I).HERE;
4380 4 1 INTEGRAL_PNL_INDEF(I).HERE=INTEGRAL_PNL_INDEF(I).NEXT.EVEN;
4390 4 1 INTEGRAL_PNL_INDEF(I).NEXT.ODD=(3*INTEGRAL_PNL_INDEF(I).PREV.ODD
      -5*SIN_PSI(I))*2*PNL(I)/8;
4410 4 1 END;
4420 4 0 ELSE DO;
4430 4 1 INTEGRAL_PNL_INDEF(I).PREV.ODD=INTEGRAL_PNL_INDEF(I).NEXT.ODD;
4440 4 1 INTEGRAL_PNL_INDEF(I).HERE=INTEGRAL_PNL_INDEF(I).NEXT.EVEN;
4450 4 1 INTEGRAL_PNL_INDEF(I).NEXT.ODD=
      (NN-1)*(NN+1)/(NN*(NN+2))*INTEGRAL_PNL_INDEF(I).PREV.ODD
      -(2*NN+1)/(NN*(NN+2))*SIN_PSI(I)*2*PNL(I);
4480 4 1 END;
4490 4 0 END INTEGRAL_PNL_INDEF_CALC;
4500 3 0 END INTEGRAL_PNL_CALC;

```

PL/I OPTIMIZING COMPILER FITFLT: PROCEDURE(PARAMETERS) OPTIONS(MAIN) REORDER;

```

NUMBER LEV NT
4520 2 0 INCREMENT_CALC: PROCEDURE;
4530 3 0 DCL (OVERRATIO,OVERRATIO_FIGHT)(VARMAX) FLOAT BINARY;
4540 3 0 FIXED_FORMAT: FORMAT(SKIP, 10 F(12.7));

4560 3 0 DO N=1 TO NMAX;
4570 3 1 DO VAR=1 TO VARMAX;
4580 3 2 PARTIAL(N,VAR)=HEIGHT(N)*PARTIAL(N,VAR); END;
4590 3 1 WEIGHTED_RESIDUAL(N,1)=HEIGHT(N)*RESID_SPECTRUM(N); END;
4600 3 0 CALL %LSQ( PARTIAL, WEIGHTED_RESIDUAL, NMAX, VARMAX, 1);
4610 3 0 DO VAR=1 TO VARMAX: DX(VAR)=-WEIGHTED_RESIDUAL(VAR,1); END;

4630 3 0 IF PRINT_LEVEL>=8 THEN DO;
4640 3 1 PUT PAGE EDIT('SUMMARY OF DIFFERENTIAL CORRECTION')(A);
4650 3 1 PUT SKIP(4) EDIT('RAW INCREMENTS IN INDEPENDENT VARIABLES')(A)
      (DX) (R(FIXED_FORMAT));
4670 3 1 PUT SKIP(4);
4680 3 1 END;

4700 3 0 DO VAR=1 TO VARMAX;
4710 3 1 IF X(VAR)+DX(VAR)<X(VAR+1)+X(VAR)+DX(VAR) THEN DO;
4720 3 2 IF DX(VAR)<0 THEN OVERRATIO(VAR)=-DX(VAR)/(X(VAR)-X(VAR+1));
4730 3 2 ELSE OVERRATIO(VAR)=+DX(VAR)/(X(VAR+1)-X(VAR));
4740 3 2 IF PRINT_LEVEL>=8 THEN
      PUT SKIP EDIT('INCREMENT # 'VAR,' OVERSHOT BY A FACTOR OF ',
        OVERRATIO(VAR) ) (A,F(4),X(12),A,E(15.4) );
4770 3 2 DX(VAR) = DX(VAR)*0.8/OVERRATIO(VAR);
4780 3 2 END;
4790 3 1 END;

4800 3 0 DO VAR=1 TO VARMAX-1;
4810 3 1 IF X(VAR)+DX(VAR)<X(VAR+1)+DX(VAR+1) THEN DO;
4820 3 2 OVERRATIO_FIGHT(VAR)= (-DX(VAR)+DX(VAR+1))/(X(VAR)-X(VAR+1));
4830 3 2 IF PRINT_LEVEL>=8 THEN
      PUT SKIP EDIT('INCREMENTS # 'VAR,' AND 'VAR+1',
        FOUGHT BY A FACTOR OF ',OVERRATIO_FIGHT(VAR) )
        (A,F(4),A,F(4),X(2),A,E(16.4) );
4870 3 2 IF SIGN(DX(VAR))=-SIGN(DX(VAR+1)) THEN DO;
4880 3 3 DX(VAR)=DX(VAR)*0.5/OVERRATIO_FIGHT(VAR);
4890 3 3 DX(VAR+1)=DX(VAR+1)*0.5/OVERRATIO_FIGHT(VAR);
4900 3 3 END;
4910 3 2 ELSE DX(VAR)=0.8*SIGN(DX(VAR))*(X(VAR)-X(VAR+1));
4920 3 2 END;
4930 3 1 END;
4940 3 0 IF PRINT_LEVEL>=8 THEN
      PUT SKIP(4) EDIT('FINAL INCREMENTS IN INDEPENDENT VARIABLES')(A)
      (DX)(R(FIXED_FORMAT));

4970 3 0 END INCREMENT_CALC;

```

PL/1 OPTIMIZING COMPILER FITFILT: PROCEDURE(PARAMETERS) OPTIONS(MAIN) REORDER;

NUMBER LEV NT

```

4990 2 0 SUMMARY: PROCEDURE;
5000 3 0 IF PRINT_LEVEL>0 THEN DO;
5010 3 1 PUT PAGE EDIT('SUMMARY OF COMPLETE RUN') (A);
5020 3 1 PUT SKIP(2) EDIT('      ')(A)
      ((' ITER#',ITER DO ITER=ITERMIN TO ITERMAX))(A,F(2),X(2) );
5040 3 1 PUT SKIP(2) EDIT('FIGURE OF MERIT')(A);
5050 3 1 PUT SKIP EDIT('      ')(A)
      (('FIGURE OF MERIT(ITER) DO ITER=ITERMIN TO ITERMAX))(E(10,2));
5070 3 1 PUT SKIP(2) EDIT('VALUES OF PARAMETERS')(A);
5080 3 1 PUT SKIP(1) EDIT('RINGS', 'SPHERICAL RING RADII (DEGREES)')(A,X(2),A);
5090 3 1 DO I=0 TO IMAX;
5100 3 2 PUT SKIP EDIT(I)(F(5))
      (('PSI(ITER,I) DO ITER=ITERMIN TO ITERMAX))(F(10,3));
5120 3 2 END;
5130 3 1 END;
5140 3 0 END SUMMARY;

```

PL/I OPTIMIZING COMPILER FITFIL: PROCEDURE(PARAMEters) OPTIONS(MAIN) REORDER;

NUMBER LEV NT

```

5160 2 0 DEG_VAR_INPUT: PROC(KERNEL_NAME,N) RETURNS(FLOAT BINARY(53))
      REDUCIBLE;
5180 3 0 DCL KERNEL_NAME CHAR(31) VARYING;
5190 3 0 DCL N FIXED BINARY;
5200 3 0 DCL NN FLOAT BINARY(53) INITIAL(N);
5210 3 0 DCL K FLOAT BINARY(53);
5220 3 0 DCL ROVERGSQ FLOAT BINARY(53)
      INITIAL(((6378160**3/3.986012E14)**2));

5250 3 0 SELECT(KERNEL_NAME);
5260 3 1 WHEN('STOKES','HEIGHT_FROM_ANOMALY')
      GO TO STOKES;
5280 3 1 WHEN('HEIGHT_FROM_VARIATION')
      GO TO HEIGHT_FROM_VARIATION;
5300 3 1 WHEN('HEIGHT_FROM_DENSITY')
      GO TO HEIGHT_FROM_DENSITY;
5320 3 1 WHEN('HEIGHT_FROM_DISTURBANCE')
      GO TO HEIGHT_FROM_DISTURBANCE;
5340 3 1 WHEN('VENING MEINESZ','DEFLECTION_FROM_ANOMALY')
      GO TO VENING_MEINESZ;
5360 3 1 WHEN('DEFLECTION_FROM_VARIATION')
      GO TO DEFLECTION_FROM_VARIATION;
5380 3 1 WHEN('DEFLECTION_FROM_DENSITY')
      GO TO DEFLECTION_FROM_DENSITY;
5400 3 1 WHEN('HILBERT','DEFLECTION_FROM_DISTURBANCE')
      GO TO DEFLECTION_FROM_DISTURBANCE;
5420 3 1 WHEN('DISTURBANCE_FROM_ANOMALY')
      GO TO DISTURBANCE_FROM_ANOMALY;
5440 3 1 WHEN('DISTURBANCE_FROM_VARIATION')
      GO TO DISTURBANCE_FROM_VARIATION;
5460 3 1 WHEN('DISTURBANCE_FROM_DENSITY')
      GO TO DISTURBANCE_FROM_DENSITY;
5480 3 1 END;

5500 3 0 STOKES:HEIGHT_FROM_ANOMALY: K=-1; GO TO HEIGHT_COMMON;
5510 3 0 HEIGHT_FROM_VARIATION: K=0; GO TO HEIGHT_COMMON;
5520 3 0 HEIGHT_FROM_DENSITY: K=0.5; GO TO HEIGHT_COMMON;
5530 3 0 HEIGHT_FROM_DISTURBANCE: K=1; GO TO HEIGHT_COMMON;
5540 3 0 HEIGHT_COMMON:SELECT(N);
5550 3 1 WHEN(0,1) RETURN(0);
5560 3 1 WHEN(2) RETURN(ROVERGSQ*7.6E-10*(NN+K)**2);
5570 3 1 OTHERWISE RETURN
      (ROVERGSQ*425.28E-10*(NN+K)**2/((NN-1)*(NN-2)*(NN-24)));
5590 3 1 END;

5610 3 0 VENING_MEINESZ:DEFLECTION_FROM_ANOMALY;
5620 3 0 DISTURBANCE_FROM_ANOMALY: K=-1; GO TO DEFLECTION_COMMON;
5630 3 0 DEFLECTION_FROM_VARIATION:

```

NUMBER LEV MT

```

5640 3 0      DISTURBANCE_FROM_VARIATION: K=0; GO TO DEFLECTION_COMMON;
5650 3 0      DEFLECTION_FROM_DENSITY:
5660 3 0      DISTURBANCE_FROM_DENSITY: K=0.5; GO TO DEFLECTION_COMMON;
5670 3 0      HILBERT:DEFLECTION_FROM_DISTURBANCE: K=1; GO TO DEFLECTION_COMMON;
5680 3 0      DEFLECTION_COMMON: SELECT(1);
5690 3 1      WHEN(1) RETURN(1E-2*(NN+K)**2);
5700 3 1      WHEN(2) RETURN(7.6*(NN+K)**2);
5710 3 1      OTHERWISE RETURN(425.28*(NN+K)**2/( (NN-1)*(NN-2)*(NN+24) ));
5720 3 1      END;
5740 3 0      END DEG_VAR_INPUT;

```

```

00005640
00005650
00005660
00005670
00005680
00005690
00005700
00005710
00005720
00005730
00005740

```

PL/I OPTIMIZING COMPILER FITFLT: PROCEDURE(PARAMEters) OPTIONS(MAIN) REORDER;

NUMBER LEV NT

```

5760 2 0 KERNEL_FUNCTION_AT_SURFACE:
5780 3 0 PROC(KERNEL_NAME,COS_PSI) RETURNS(FLOAT BINARY(53)) REDUCIBLE;
5790 3 0 DCL KERNEL_NAME CHAR(31) VARYING;
5800 3 0 DCL COS_PSI FLOAT BINARY(53);
5810 3 0 DCL SIN_HALF_PSI FLOAT BINARY(53) INITIAL((SQRT((1-COS_PSI)/2)));
5820 3 0 DCL COS_HALF_PSI FLOAT BINARY(53) INITIAL((SQRT((1+COS_PSI)/2)));
5830 3 0 IF COS_PSI=1 | SIN_HALF_PSI=0 THEN RETURN(0); ELSE
5840 3 0 SELECT(KERNEL_NAME):
5850 3 1 WHEN('STOKES','HEIGHT_FROM_ANOMALY')
5860 3 1 GO TO STOKES;
5870 3 1 WHEN('HEIGHT_FROM_VARIATION')
5880 3 1 GO TO HEIGHT_FROM_VARIATION;
5890 3 1 WHEN('HEIGHT_FROM_DENSITY')
5900 3 1 GO TO HEIGHT_FROM_DENSITY;
5910 3 1 WHEN('HEIGHT_FROM_DISTURBANCE')
5920 3 1 GO TO HEIGHT_FROM_DISTURBANCE;
5930 3 1 WHEN('MALKIN','HEIGHT_FROM_OUT_PARTIAL')
5940 3 1 GO TO HEIGHT_FROM_OUT_PARTIAL;
5950 3 1 WHEN('VENING_MEINSEZ','DEFLECTION_FROM_ANOMALY')
5960 3 1 GO TO VENING_MEINSEZ;
5970 3 1 WHEN('DEFLECTION_FROM_VARIATION')
5980 3 1 GO TO DEFLECTION_FROM_VARIATION;
5990 3 1 WHEN('DEFLECTION_FROM_DENSITY')
6000 3 1 GO TO DEFLECTION_FROM_DENSITY;
6010 3 1 WHEN('HILBERT','DEFLECTION_FROM_DISTURBANCE')
6020 3 1 GO TO DEFLECTION_FROM_DISTURBANCE;
6030 3 1 WHEN('DISTURBANCE_FROM_ANOMALY')
6040 3 1 GO TO DISTURBANCE_FROM_ANOMALY;
6050 3 1 WHEN('DISTURBANCE_FROM_VARIATION')
6060 3 1 GO TO DISTURBANCE_FROM_VARIATION;
6070 3 1 WHEN('DISTURBANCE_FROM_DENSITY')
6080 3 1 GO TO DISTURBANCE_FROM_DENSITY;
6090 3 1 END;
6110 3 0 STOKES: HEIGHT_FROM_ANOMALY:
6120 3 0 RETURN(1/SIN_HALF_PSI-6*SIN_HALF_PSI+1-5*COS_PSI
6130 3 0 -3*COS_PSI*LOG(SIN_HALF_PSI+SIN_HALF_PSI**2));
6140 3 0 HEIGHT_FROM_VARIATION:
6150 3 0 RETURN(1/SIN_HALF_PSI-2-3*COS_PSI-LOG(SIN_HALF_PSI+SIN_HALF_PSI**2));
6160 3 0 HEIGHT_FROM_DENSITY:
6170 3 0 RETURN(1/SIN_HALF_PSI);
6180 3 0 HEIGHT_FROM_DISTURBANCE:
6190 3 0 RETURN(1/SIN_HALF_PSI-LOG(1+1/SIN_HALF_PSI));
6200 3 0 MALKIN:HEIGHT_FROM_OUT_PARTIAL:
6210 3 0 RETURN(-COS_HALF_PSI/SIN_HALF_PSI);
6230 3 0 DISTURBANCE_FROM_ANOMALY:

```

PL/1 OPTIMIZING COMPILER FITFLT: PROCEDURE(PARAMETERS) OPTIONS(MAIN) REORDER;

NUMBER LEV NT

```

DISTURBANCE_FROM_VARIATION:
DISTURBANCE_FROM_DENSITY:
SIGNAL_CONDITION(KERNEL_FUNCTION_NOT_KNOWN):

6260    3    0    VENDING MEYER: DEFLECTION FROM ANOMALY:
                  RETURN(-COS_HALF_PSI/(2*SIN_HALF_PSI**2)
                  +16*SIN_HALF_PSI*COS_HALF_PSI-6*COS_HALF_PSI
                  -3/(2*SIN_HALF_PSI*COS_HALF_PSI)+1/(2*COS_HALF_PSI)
                  +6*SIN_HALF_PSI*COS_HALF_PSI
                  *LOG(SIN_HALF_PSI*(1+SIN_HALF_PSI)) );
6340    3    0    DEFLECTION FROM VARIATION:
                  RETURN(COS_HALF_PSI*(-1-2*SIN_HALF_PSI-2*SIN_HALF_PSI**2
                  +12*SIN_HALF_PSI**3+12*SIN_HALF_PSI**4)
                  /(2*SIN_HALF_PSI**2*(1+SIN_HALF_PSI)) );
6380    3    0    DEFLECTION FROM DENSITY:
                  RETURN(-COS_HALF_PSI/(2*SIN_HALF_PSI**2)) );
6400    3    0    HILBERT: DEFLECTION FROM DISTURBANCE:
                  RETURN(-COS_HALF_PSI/(2*SIN_HALF_PSI**2*(1+SIN_HALF_PSI)));
6430    3    0    END KERNEL_FUNCTION_AT_SURFACE;

```


PL/I OPTIMIZING COMPILER FITFLT: PROCEDURE(PARAMETERS) OPTIONS(MAIN) REORDER;

```

NUMBER  LEV  NT
6450   2   0   KERNEL_FUNCTION_AT_ALTITUDE: PROC(KERNEL_NAME,COS_PSI,RADIUS_RATIO)
        RETURNS(FLOAT_BINARY(53)) REDUCIBLE;
6470   3   0   DCL KERNEL_NAME CHAR(31) VARYING;
6480   3   0   DCL COS_PSI FLOAT_BINARY(53);
6490   3   0   DCL SIN_PSI FLOAT_BINARY(53);
6500   3   0   DCL RADIUS_RATIO FLOAT_BINARY(53);
6510   3   0   DCL D FLOAT_BINARY(53)
        INITIAL((SQRT(1-2*RADIUS_RATIO*COS_PSI*RADIUS_RATIO**2)));

6540   3   0   SELECT(KERNEL_NAME);
6550   3   1   WHEN('STOKES','HEIGHT_FROM_ANOMALY')
        GO TO STOKES;
6570   3   1   WHEN('HEIGHT_FROM_VARIATION')
        GO TO HEIGHT_FROM_VARIATION;
6590   3   1   WHEN('HEIGHT_FROM_DENSITY')
        GO TO HEIGHT_FROM_DENSITY;
6610   3   1   WHEN('HEIGHT_FROM_DISTURBANCE')
        GO TO HEIGHT_FROM_DISTURBANCE;
6630   3   1   WHEN('VENING_MEINESZ','DEFLECTION_FROM_ANOMALY')
        GO TO VENING_MEINESZ;
6650   3   1   WHEN('DEFLECTION_FROM_VARIATION')
        GO TO DEFLECTION_FROM_VARIATION;
6670   3   1   WHEN('DEFLECTION_FROM_DENSITY')
        GO TO DEFLECTION_FROM_DENSITY;
6690   3   1   WHEN('HILBERT','DEFLECTION_FROM_DISTURBANCE')
        GO TO DEFLECTION_FROM_DISTURBANCE;
6710   3   1   WHEN('DISTURBANCE_FROM_ANOMALY')
        GO TO DISTURBANCE_FROM_ANOMALY;
6730   3   1   WHEN('DISTURBANCE_FROM_VARIATION')
        GO TO DISTURBANCE_FROM_VARIATION;
6750   3   1   WHEN('DISTURBANCE_FROM_DENSITY')
        GO TO DISTURBANCE_FROM_DENSITY;
6770   3   1   END;

6790   3   0   STOKES:HEIGHT_FROM_ANOMALY:
        RETURN(RADIUS_RATIO*(2/D*(1-3*D-RADIUS_RATIO*COS_PSI*
        (5+3*LOG((1-RADIUS_RATIO*COS_PSI*D)/2)))));
6820   3   0   HEIGHT_FROM_VARIATION: SIGNAL_CONDITION(KERNEL_FUNCTION_NOT_KNOWN);
6830   3   0   HEIGHT_FROM_DENSITY: RETURN(2*RADIUS_RATIO/D);
6840   3   0   HEIGHT_FROM_DISTURBANCE: SIGNAL_CONDITION(KERNEL_FUNCTION_NOT_KNOWN);
6850   3   0   DISTURBANCE_FROM_ANOMALY:
        RETURN(-RADIUS_RATIO**2*((1-RADIUS_RATIO**2/D**3+4/D+1-6*D
        -RADIUS_RATIO*COS_PSI*(13+6*LOG((1-RADIUS_RATIO*COS_PSI*D)/2)))));

6890   3   0   DISTURBANCE_FROM_VARIATION:
        SIGNAL_CONDITION(KERNEL_FUNCTION_NOT_KNOWN);
6910   3   0   DISTURBANCE_FROM_DENSITY:
        RETURN(-2*RADIUS_RATIO**2*(1-RADIUS_RATIO*COS_PSI/D**3));

```

PL/I OPTIMIZING COMPILER FITFILT: PROCEDURE(PARAMETERS) OPTIONS(MAIN) REORDER;

NUMBER LEV NT

```

6950 3 0 VENING_MEINESZ: DEFLECTION_FROM_ANOMALY:
      SIN_PSI=SQRT(1-COS_PSI)*SQRT(1+COS_PSI);
6970 3 0 RETURN(RADIUS_RATIO**3*SIN_PSI*(2/D**3*6/D-8
      -3*(1-RADIUS_RATIO)*COS_PSI-D)/(D*SIN_PSI**2)
      -3*LOG((1-RADIUS_RATIO)*COS_PSI+D/2));
7000 3 0 DEFLECTION_FROM_VARIATION: SIGNAL_CONDITION(KERNEL_FUNCTION_NOT_KNOWN);
7010 3 0 DEFLECTION_FROM_DENSITY:
      SIN_PSI=SQRT(1-COS_PSI)*SQRT(1+COS_PSI);
7030 3 0 RETURN(2*SIN_PSI*(RADIUS_RATIO/D)**3);
7040 3 0 HILBERT:DEFLECTION_FROM_DISTURBANCE:
      SIGNAL_CONDITION(KERNEL_FUNCTION_NOT_KNOWN);

7070 3 0 END KERNEL_FUNCTION_AY_ALTITUDE;

```

```

00006930
00006940
00006950
00006960
00006970
00006980
00006990
00007000
00007010
00007020
00007030
00007040
00007050
00007060
00007070

```

PL/I OPTIMIZING COMPILER FITFLT: PROCEDURE(PARAMEters) OPTIONS(MAIN) REORDER;

NUMBER LEV MT

```

7090 2 0 KERNEL_INTEGRAL_INDEF:PROC(KERNEL_NAME,COS_PSI)
      RETURNS(FLOAT BINARY(53)) REDUCIBLE;
7110 3 0 DCL KERNEL_NAME CHAR(31) VARYING;
7120 3 0 DCL COS_PSI FLOAT BINARY(53);
7130 3 0 DCL SIN_HALF_PSI FLOAT BINARY(53) INITIAL((SQRT((1-COS_PSI)/2)));
7140 3 0 DCL COS_HALF_PSI FLOAT BINARY(53) INITIAL((SQRT((1+COS_PSI)/2)));

7160 3 0 SELECT(KERNEL_NAME);
7170 3 1 WHEN('STOKES','HEIGHT_FROM_ANOMALY')
      GO TO STOKES;
7190 3 1 WHEN('HEIGHT_FROM_VARIATION')
      GO TO HEIGHT_FROM_VARIATION;
7210 3 1 WHEN('HEIGHT_FROM_DENSITY')
      GO TO HEIGHT_FROM_DENSITY;
7230 3 1 WHEN('HEIGHT_FROM_DISTURBANCE')
      GO TO HEIGHT_FROM_DISTURBANCE;
7250 3 1 WHEN('MALKIN','HEIGHT_FROM_OUT_PARTIAL')
      GO TO HEIGHT_FROM_OUT_PARTIAL;
7270 3 1 WHEN('VENING MEINESZ','DEFLECTION_FROM_ANOMALY')
      GO TO VENING_MEINESZ;
7290 3 1 WHEN('DEFLECTION_FROM_VARIATION')
      GO TO DEFLECTION_FROM_VARIATION;
7310 3 1 WHEN('DEFLECTION_FROM_DENSITY')
      GO TO DEFLECTION_FROM_DENSITY;
7330 3 1 WHEN('HILBERT','DEFLECTION_FROM_DISTURBANCE')
      GO TO DEFLECTION_FROM_DISTURBANCE;
7350 3 1 WHEN('DISTURBANCE_FROM_ANOMALY')
      GO TO DISTURBANCE_FROM_ANOMALY;
7370 3 1 WHEN('DISTURBANCE_FROM_VARIATION')
      GO TO DISTURBANCE_FROM_VARIATION;
7390 3 1 WHEN('DISTURBANCE_FROM_DENSITY')
      GO TO DISTURBANCE_FROM_DENSITY;
7410 3 1 END;

7430 3 0 STOKES:HEIGHT_FROM_ANOMALY:
      IF SIN_HALF_PSI=0 THEN
        RETURN((SIN_HALF_PSI*(-4*SIN_HALF_PSI*(1+5*SIN_HALF_PSI*
          (+6-7*SIN_HALF_PSI)))+1.5*(1-COS_PSI)*(1+COS_PSI)*
          LOG(SIN_HALF_PSI*(1+SIN_HALF_PSI))));
      ELSE RETURN(0);
7480 3 0 HEIGHT_FROM_VARIATION: SIGNAL CONDITION(KERNEL_INTEGRAL_NOT_KNOWN);
7490 3 0 HEIGHT_FROM_DENSITY: RETURN(-4*SIN_HALF_PSI);
7500 3 0 HEIGHT_FROM_DISTURBANCE: RETURN(-4*SIN_HALF_PSI);
7510 3 0 HEIGHT_FROM_DISTURBANCE: SIGNAL CONDITION(KERNEL_INTEGRAL_NOT_KNOWN);
7520 3 0 MALKIN:HEIGHT_FROM_OUT_PARTIAL:
      SIGNAL CONDITION(KERNEL_INTEGRAL_NOT_KNOWN);

7550 3 0 DISTURBANCE_FROM_ANOMALY:
      DISTURBANCE_FROM_VARIATION:

```

PL/I OPTIMIZING COMPILER FITFLT: PROCEDURE(PARAMETERS) OPTIONS(MAIN) REORDER;

NUMBER LEV NT

7600	3	0	DISTURBANCE FROM DENSITY:	00007570
			SIGNAL CONDITION(KERNEL_INTEGRAL_NOT_KNOWN);	00007580
				00007590
				00007600
7620	3	0	VENING MEINERZ: DEFLECTION FROM ANOMALY:	00007610
			SIGNAL CONDITION(KERNEL_INTEGRAL_NOT_KNOWN);	00007620
				00007630
				00007640
7640	3	0	DEFLECTION FROM VARIATION:	00007650
			SIGNAL CONDITION(KERNEL_INTEGRAL_NOT_KNOWN);	00007660
				00007670
				00007680
7660	3	0	DEFLECTION FROM DENSITY:	00007690
			RETURN(LOG((1-COS_HALF_PSI)/(1+COS_HALF_PSI))+2*COS_HALF_PSI);	
			HYLBERT: DEFLECTION FROM DISTURBANCE:	
			SIGNAL CONDITION(KERNEL_INTEGRAL_NOT_KNOWN);	
7690	3	0	END KERNEL_INTEGRAL_INDEF;	

PL/I OPTIMIZING COMPILER FITFLT: PROCEDURE(PARAMETERS) OPTIONS(MAIN) REORDER;

NUMBER LEV NT

```

7710 2 0 KERNEL_SPECTRUM_AT_SURFACE:
      PROCT(KERNEL_NAME,N) RETURNS(FLOAT BINARY(53)) REDUCIBLE;
7730 3 0 DCL KERNEL_NAME CHAR(31) VARYING;
7740 3 0 DCL N FIXED BINARY;
7750 3 0 DCL NN FLOAT BINARY(53) INITIAL(N);

7770 3 0 SELECT(KERNEL_NAME);
7780 3 1 WHEN('STOKES','HEIGHT_FROM_ANOMALY')
      GO TO STOKES;
7800 3 1 WHEN('HEIGHT_FROM_VARIATION')
      GO TO HEIGHT_FROM_VARIATION;
7820 3 1 WHEN('HEIGHT_FROM_DENSITY')
      GO TO HEIGHT_FROM_DENSITY;
7840 3 1 WHEN('HEIGHT_FROM_DISTURBANCE')
      GO TO HEIGHT_FROM_DISTURBANCE;
7860 3 1 WHEN('MALKIN','HEIGHT_FROM_OUT_PARTIAL')
      GO TO HEIGHT_FROM_OUT_PARTIAL;
7880 3 1 WHEN('VENING_MEINESZ','DEFLECTION_FROM_ANOMALY')
      GO TO VENING_MEINESZ;
7900 3 1 WHEN('DEFLECTION_FROM_VARIATION')
      GO TO DEFLECTION_FROM_VARIATION;
7920 3 1 WHEN('DEFLECTION_FROM_DENSITY')
      GO TO DEFLECTION_FROM_DENSITY;
7940 3 1 WHEN('HILBERT','DEFLECTION_FROM_DISTURBANCE')
      GO TO DEFLECTION_FROM_DISTURBANCE;
7960 3 1 WHEN('DISTURBANCE_FROM_ANOMALY')
      GO TO DISTURBANCE_FROM_ANOMALY;
7980 3 1 WHEN('DISTURBANCE_FROM_VARIATION')
      GO TO DISTURBANCE_FROM_VARIATION;
8000 3 1 WHEN('DISTURBANCE_FROM_DENSITY')
      GO TO DISTURBANCE_FROM_DENSITY;
8020 3 1 END;

8040 3 0 STOKES: HEIGHT_FROM_ANOMALY:
      IF N=0 | N=1 THEN RETURN(0); ELSE RETURN(1/(NN-1));
8050 3 0 IF N=0 | N=1 THEN RETURN(0); ELSE RETURN(1/NN);
8060 3 0 HEIGHT_FROM_VARIATION: IF N=0 THEN RETURN(0); ELSE RETURN(1/NN);
8070 3 0 HEIGHT_FROM_DENSITY: RETURN(1/(NN+0.5));
8080 3 0 HEIGHT_FROM_DISTURBANCE: RETURN(1/(NN+1));
8090 3 0 MALKIN:HEIGHT_FROM_OUT_PARTIAL: RETURN(-MALKIS(N));

8110 3 0 DISTURBANCE_FROM_ANOMALY:
8120 3 0 IF N=0 | N=1 THEN RETURN(0); ELSE RETURN((NN+1)/(NN-1));
8130 3 0 DISTURBANCE_FROM_VARIATION:
8140 3 0 IF N=0 THEN RETURN(0); ELSE RETURN((NN+1)/NN);
8150 3 0 DISTURBANCE_FROM_DENSITY:
      RETURN((NN+1)/(NN+0.5));

8180 3 0 VENING_MEINESZ:DEFLECTION_FROM_ANOMALY:

```

PL/I OPTIMIZING COMPILER FITFLT: PROCEDURE(PARAMEters) OPTIONS(MAIN) REORDER;

NUMBER LEV NT

```

      IF N=0 | N=1 THEN RETURN(0);
      ELSE RETURN(SQRT(NN*(NN+1)))/(NN-1)-SMALL_CAP_SPECTRUM(N);
8200 3 0 DEFLECTION_FROM_VARIATION:
8210 3 0 IF N=0 THEN RETURN(0);
      ELSE RETURN(SQRT(NN*(NN+1)))/NN-SMALL_CAP_SPECTRUM(N);
8230 3 0 DEFLECTION_FROM_DENSITY:
8240 3 0 RETURN(SQRT(NN*(NN+1)))/(NN+0.5)-SMALL_CAP_SPECTRUM(N);
      RETURN(DEFLECTION_FROM_DISTURBANCE:
8260 3 0 HILBERT: DEFLECTION_FROM_DISTURBANCE:
      RETURN(SQRT(NN*(NN+1)))/(NN+1)-SMALL_CAP_SPECTRUM(N);
      -00008280
8290 3 0 SMALL_CAP_SPECTRUM: PROC(N) RETURNS(FLOAT BINARY(53));
8300 4 0 DCL N FIXED BINARY;
8310 4 0 DCL NN FLOAT BINARY(53) INITIAL(N);
8320 4 0 RETURN( SQRT(NN*(NN+1))*
      (+PSIZERO*DEGTORAD/2
      -(NN-1)*(NN+2)*(PSIZERO*DEGTORAD)**3/48) );
8350 4 0 END SMALL_CAP_SPECTRUM;
      -00008360
8370 3 0 WALLIS: PROC(N) RETURNS(FLOAT BINARY(53));
8380 4 0 DCL N FIXED BINARY;
8390 4 0 DCL NN FLOAT BINARY(53) INITIAL(N);
8400 4 0 END WALLIS;
      -00008420
8420 3 0 END KERNEL_SPECTRUM_AT_SURFACE;

```

PL/I OPTIMIZING COMPILER FITFLT: PROCEDURE(PARAMEters) OPTIONS(MAIN) REORDER:

```

NUMBER  LEV  NT
8440   2   0  KERNEL_SPECTRUM_AT_ALTITUDE:
          PROC(KERNEL_NAME,N,RADIUS_RATIO) RETURNS(FLOAT BINARY(53))
          REDUCIBLE:
8470   3   0  DCL KERNEL_NAME CHAR(31) VARYING;
8480   3   0  DCL N FIXED BINARY;
8490   3   0  DCL RADIUS_RATIO FLOAT BINARY(53);
8500   3   0  DCL NN FLOAT BINARY(53) INITIAL(N);

8520   3   0  SELECT(KERNEL_NAME);
8530   3   1  WHEN('STOKES','HEIGHT_FROM_ANOMALY')
              GO TO STOKES;
8550   3   1  WHEN('HEIGHT_FROM_VARIATION')
              GO TO HEIGHT_FROM_VARIATION;
8570   3   1  WHEN('HEIGHT_FROM_DENSITY')
              GO TO HEIGHT_FROM_DENSITY;
8590   3   1  WHEN('HEIGHT_FROM_DISTURBANCE')
              GO TO HEIGHT_FROM_DISTURBANCE;
8610   3   1  WHEN('VENING_MEINERZ','DEFLECTION_FROM_ANOMALY')
              GO TO VENING_MEINERZ;
8630   3   1  WHEN('DEFLECTION_FROM_VARIATION')
              GO TO DEFLECTION_FROM_VARIATION;
8650   3   1  WHEN('DEFLECTION_FROM_DENSITY')
              GO TO DEFLECTION_FROM_DENSITY;
8670   3   1  WHEN('HILBERT','DEFLECTION_FROM_DISTURBANCE')
              GO TO DEFLECTION_FROM_DISTURBANCE;
8690   3   1  WHEN('DISTURBANCE_FROM_ANOMALY')
              GO TO DISTURBANCE_FROM_ANOMALY;
8710   3   1  WHEN('DISTURBANCE_FROM_VARIATION')
              GO TO DISTURBANCE_FROM_VARIATION;
8730   3   1  WHEN('DISTURBANCE_FROM_DENSITY')
              GO TO DISTURBANCE_FROM_DENSITY;
8750   3   1  END;

8770   3   0  STOKES:HEIGHT_FROM_ANOMALY:
              HEIGHT_FROM_VARIATION:
              HEIGHT_FROM_DENSITY:
              VENING_MEINERZ:DEFLECTION_FROM_ANOMALY:
              DEFLECTION_FROM_VARIATION:
              DEFLECTION_FROM_DENSITY:
              HILBERT:
              RETURN(RADIUS_RATIO**N);
              KERNEL_SPECTRUM_AT_SURFACE(KERNEL_NAME,N));

8670   3   0  DISTURBANCE_FROM_ANOMALY:
              DISTURBANCE_FROM_VARIATION:
              DISTURBANCE_FROM_DENSITY:
              RETURN(-(RADIUS_RATIO**(N+2)))#
              KERNEL_SPECTRUM_AT_SURFACE(KERNEL_NAME,N));

```

PL/I OPTIMIZING COMPILER FITFILT: PROCEDURE(PARAMETERS) OPTIONS(MAIN) REORDER;

NUMBER LEV NT

8920 3 0 END KERNEL_SPECTRUM_AT_ALTITUDE; 00008920

PL/I OPTIMIZING COMPILER FITFLT: PROCEDURE(PARAMETERS) OPTIONS(MAIN) REORDER;

NUMBER LEV NT

```

8940 2 0 KERNEL_NOMINAL_COS_PSI_SURFACE:
      PROC(KERNEL_NAME,PSI_TEMPLATE_NAME,IMAX,COS_PSI);
8960 3 0 DCL KERNEL_NAME CHAR(31) VARYING;
8970 3 0 DCL PSI_TEMPLATE_NAME CHAR(31) VARYING;
8980 3 0 DCL IMAX FIXED BINARY;
8990 3 0 DCL COS_PSI(*) FLOAT BINARY(53);

9010 3 0 DCL PSI23(0:23) FLOAT BINARY
      INITIAL(PSIZEZERO, 0.044,0.063,0.089,0.128,0.183,
      0.261,0.372,0.530,0.753,1.069,1.794,2.966,4.821,7.591,11.47,18.55,
      28.3,40.8,65.3,98.6,114.4,130.5,180.0);
9050 3 0 DCL PSI34(0:34) FLOAT BINARY INITIAL(PSIZEZERO,
      0.0664,0.1753,0.3078,0.4474,0.7116,0.9758,1.2348,
      1.4883,1.9860,2.4780,2.9610,4.148,5.884,8.180,10.488,
      12.85,15.99,20.17,25.30,33.90,52.0,61.0,72.0,82.3,94.2,
      106.3,126.3,135.9,142.7,149.0,155.4,162.9,176.4,180.0);
9100 3 0 DCL PSI101(0:101) FLOAT BINARY INITIAL(PSIZEZERO,
      (+5/60),(+10/60),(+15/60),(+20/60),(+25/60),(+30/60),
      (+35/60),(+40/60),(+45/60),(+50/60),(+55/60),
      1,(1+5/60),(1+10/60),(1+15/60),(1+20/60),(1+25/60),(1+30/60),
      (1+35/60),(1+40/60),(1+45/60),(1+50/60),(1+55/60),
      2,(2+5/60),(2+10/60),(2+15/60),(2+20/60),(2+25/60),(2+30/60),
      (2+35/60),(2+40/60),(2+45/60),(2+50/60),(2+55/60),
      3,(3+15/60),(3+30/60),(3+45/60),4,(4+15/60),(4+30/60),(4+45/60),
      5,(5+15/60),(5+30/60),(5+45/60),6,(6+15/60),(6+30/60),(6+45/60),
      7,8,9,10,11,12,13,14,15,16,17,18,19,20,21,22,23,24,
      25,30,35,40,45,50,55,60,65,70,75,80,85,90,95,100,105,110,115,
      120,125,130,135,140,145,150,155,160,165,170,175,180 );
9220 3 0 DCL PSIRICE(0:35) FLOAT BINARY STATIC
      INITIAL( 235.279,331.393,467.554,657.760,926.1099,1304.1547,
      1836.2179,2586.3068,3641.4320,5125.6081,7216.8560,10150,
      12050,14290,16940,20090,23830,28250,33480,39670,47000,
      55640,65900,77970,92220);

9280 3 0 SELECT(KERNEL_NAME);
9290 3 1 WHEN('STOKES','HEIGHT_FROM_ANOMALY')
      GO TO STOKES;
9310 3 1 WHEN('HEIGHT_FROM_VARIATION')
      GO TO HEIGHT_FROM_VARIATION;
9330 3 1 WHEN('HEIGHT_FROM_DENSITY')
      GO TO HEIGHT_FROM_DENSITY;
9350 3 1 WHEN('HEIGHT_FROM_DISTURBANCE')
      GO TO HEIGHT_FROM_DISTURBANCE;
9370 3 1 WHEN('MALKIN','HEIGHT_FROM_OUT_PARTIAL')
      GO TO HEIGHT_FROM_OUT_PARTIAL;
9390 3 1 WHEN('VENING_MEINESZ','DEFLECTION_FROM_ANOMALY')
      GO TO VENING_MEINESZ;
9410 3 1 WHEN('DEFLECTION_FROM_VARIATION')

```


PL/I OPTIMIZING COMPILER FITFILT: PROCEDURE(PARAMETERS) OPTIONS(MAIN) REORDER:

NUMBER LEV NT

9920	3	1	END: RETURN;	(PSIZERO,NRINGS,CDS_PSI);	00009910
					00009920
					00009930

PL/I OPTIMIZING COMPILER FITFILT: PROCEDURE(PARAMEters) OPTIONS(MAIN) REORDER;

NUMBER LEV NT

```

9950 3 0 EQUI INTEGRAL_PSI_CALC_STOKES:
      PROCEDURE(NRINGS,COS_PSI);
      /* THEORY AND ALGORITHM BY STANLEY W. SHEPPERD */
9960 4 0 DCL NRINGS FIXED BINARY;
9970 4 0 DCL COS_PSI(*) FLOAT BINARY(53);
10000 4 0 DCL CASE1,J) FIXED BINARY;
10010 4 0 DCL (A,DA,DB,COS_PSI) FLOAT BINARY(53);
10020 4 0 DCL (LN,M,S,T,MD,HT) FLOAT BINARY(53);
10030 4 0 DCL (NN1,NN2,NN3,NN4,NN5) FIXED BINARY;
10040 4 0 DCL T1 FLOAT BINARY(53) INITIAL(0.3334948490820);
10050 4 0 DCL T2 FLOAT BINARY(53) INITIAL(0.64766528844245);
10060 4 0 DCL T3 FLOAT BINARY(53) INITIAL(0.8556428774926);
10070 4 0 DCL A1 FLOAT BINARY(53) INITIAL(1.1225269012385);
10080 4 0 DCL A2 FLOAT BINARY(53) INITIAL(1.9111831089355);
10090 4 0 DCL A3 FLOAT BINARY(53) INITIAL(0.7886562079703);
10100 4 0 IF MOD(NRINGS,2)=0 THEN SIGNAL CONDITION(NOMINAL_COS_PSI_NOT_KNOWN);
10110 4 0 N2=NRINGS/2;
10120 4 0 N2=N2/2; A2=A2/2;
10130 4 0 N1=TRUNC((N2*A1-A2)/A+0.5);
10140 4 0 N3=TRUNC((N2*A3-A2)/A+0.5);
10150 4 0 DA=A1-N1*A3/(N3+1);
10160 4 0 DB=A3-N3*A1/(N1+1);
10170 4 0 IF DB<DA THEN DO; DA=0; CASE=0; N1=N1+1; END;
10180 4 0 ELSE DO; DB=0; CASE=1; N3=N3+1; END;
10190 4 0 NN1=N1;
10200 4 0 NN2=N1+N2;
10210 4 0 NN3=N1+N2+N3;
10220 4 0 HT=(A-2*(DA+DB))/N;
10230 4 0 COS_PSI(0)=+1;
10240 4 0 COS_PSI(N)=-1;
10250 4 0 COS_PSI(2*NN1)=1-2*T2**2;
10260 4 0 IF CASE=0 THEN COS_PSI(NN1)=1-2*T1**2;
10270 4 0 IF CASE=1 THEN COS_PSI(NN2)=1-2*T3**2;

10290 4 0 T=HT/4;
10300 4 0 DO I=1 TO NN1+CASE-1;
10310 4 1 MD=I*HT;
10320 4 1 DO J=1 TO 10;
10330 4 2 CALL VALUES;
10340 4 2 T=T-(M-MD)/S;
10350 4 2 END;
10360 4 1 COS_PSI(I)=1-2*T**2;
10370 4 1 END;
10380 4 0 IF CASE=1 THEN COS_PSI(COS_PSI(NN1));

10400 4 0 T=T2;
10410 4 0 DO I=(2*NN1-1) TO (NN1+CASE+1) BY -1;
10420 4 1 MD=(2*NN1-I)*HT;

```

PL/I OPTIMIZING COMPILER FITFILT: PROCEDURE(PARAMEters) OPTIONS(MAIN) REORDER;

NUMBER LEV NT

```

10430 4 1 DO J=1 TO 10;
10440 4 2 CALL VALUES;
10450 4 2 T=T-(M-WD)/S;
10460 4 2 END;
10470 4 1 COS_PSI(I)=1-2*T**2;
10480 4 1 END;

10500 4 0 T=T2;
10510 4 0 DO I=(2*N1+1) TO (N2-CASE);
10520 4 1 M0=(2*N1-I)*MT;
10530 4 1 DO J=1 TO 10;
10540 4 2 CALL VALUES;
10550 4 2 T=T-(M-WD)/S;
10560 4 2 END;
10570 4 1 COS_PSI(I)=1-2*T**2;
10580 4 1 END;
10590 4 0 IF CASE=0 THEN COS_PSI(COS_PSI(N2));

10610 4 0 T=1;
10620 4 0 DO I=(N-1) TO (N2-CASE) BY -1;
10630 4 1 M0=(I-N)*MT;
10640 4 1 DO J=1 TO 10;
10650 4 2 CALL VALUES;
10660 4 2 T=T-(M-WD)/S;
10670 4 2 END;
10680 4 1 COS_PSI(I)=1-2*T**2;
10690 4 1 END;

10710 4 0 IF CASE=0 THEN COS_PSI(N2)=COS_PSI(COS_PSI(N2));
10720 4 0 IF CASE=1 THEN COS_PSI(N1)=COS_PSI(COS_PSI(N1));

10740 4 0 RETURN;

10770 4 0 VALUES: PROCEDURE;
10780 5 0 LN=LOG(T+T**2);
10790 5 0 N=4*T-5*T**2-6*T**3+7*T**4-6*T**5+2*T**6-1*T**7)MLN;
10800 5 0 S=4-16*T-24*T**2+40*T**3-12*T**4)MLN;
10810 5 0 END VALUES;

10830 4 0 END EQUI_INTEGRAL_PSI_CALC_STOKES;

```

PL/I OPTIMIZING COMPILER FITFLT: PROCEDURE(PARAMEters) OPTIONS(MAIN) REORDER;

NUMBER LEV NT

```

10850 3 0 EQUI INTEGRAL PSI_CALC_VM_DEN:PROC(PSIZEZERO,NRINGS,COS_PSI);
10860 4 0 DCL PSIZEZERO FLOAT BINARY(53);
10870 4 0 DCL NRINGS FIXED BINARY;
10880 4 0 DCL COS_PSI(*) FLOAT BINARY(53);
10890 4 0 DCL PSI(0:NRINGS) FLOAT BINARY(53) CONTROLLED;
10900 4 0 DCL (I,ITERATION) FIXED BINARY;
10910 4 0 DCL D_PSI FLOAT BINARY(53);
10920 4 0 DCL INT FLOAT BINARY(53);
10930 4 0 DCL TOTAL_INT FLOAT BINARY(53);
10940 4 0 DCL CONST FLOAT BINARY(53);
10950 4 0 DCL FACTOR FLOAT BINARY(53) INITIAL(1.2);
10960 4 0 ALLOCATE PSI;
10970 4 0 PSI(0)=PSIZEZERO*DEGTORAD;
10980 4 0 COS_PSI(0)=COS(PSI(0));
10990 4 0 TOTAL_INT=2*LOG(TAN(PSI(0)/4))+2*COS(PSI(0)/2);
11000 4 0 INT=TOTAL_INT/NRINGS;
11010 4 0 DO I=0 TO NRINGS-2;
11020 4 1 CONST=EXP(INT)*FCN(PSI(I));
11030 4 1 PSI(I+1)=FACTOR*PSI(I);
11040 4 1 DO ITERATION=1 TO 25;
11050 4 2 D_PSI=-(FCN(PSI(I+1))-CONST)/FCN_DERIV(PSI(I+1));
11060 4 2 PSI(I+1)=PSI(I+1)+D_PSI;
11070 4 2 IF ABS(D_PSI/PSI(I+1))<1E-15 THEN LEAVE;
11080 4 2 END;
11090 4 1 COS_PSI(I+1)=COS(PSI(I+1));
11100 4 1 END;
11110 4 0 COS_PSI(NRINGS)=-1;
11120 4 0 RETURN;

11140 4 0 FCN: PROC(PSI) RETURNS(FLOAT BINARY(53));
11150 5 0 DCL PSI FLOAT BINARY(53);
11160 5 0 RETURN(1/TAN(PSI/4))*2*EXP(-2*COS(PSI/2));
11170 5 0 END FCN;

11190 4 0 FCN_DERIV: PROC(PSI) RETURNS(FLOAT BINARY(53));
11200 5 0 DCL PSI FLOAT BINARY(53);
11210 5 0 RETURN(FCN(PSI)*(SIN(PSI/2)-1/SIN(PSI/2)));
11220 5 0 END FCN_DERIV;

11240 4 0 END EQUI INTEGRAL_PSI_CALC_VM_DEN;

11270 3 0 END KERNEL_NOMINAL_COS_PSI_SURFACE;

```

PL/I OPTIMIZING COMPILER FITFLT: PROCEDURE(PARAMETERS) OPTIONS(MAIN) REORDER;

NUMBER LEV NT

11290	2	0	KERNEL_NOMINAL_COS_PSI_ALTITUDE;	00011290
			PROC(KERNEL_NAME,PSI_TEMPLATE_NAME,RADIUS_RATIO,IMAX,COS_PSI);	00011300
11310	3	0	DCL KERNEL_NAME CHAR(31) VARYING;	00011310
11320	3	0	DCL PSI_TEMPLATE_NAME CHAR(31) VARYING;	00011320
11330	3	0	DCL RADIUS_RATIO FLOAT BINARY(53);	00011330
11340	3	0	DCL IMAX FIXED BINARY;	00011340
11350	3	0	DCL COS_PSI(*) FLOAT BINARY(53);	00011350
11360	3	0	END KERNEL_NOMINAL_COS_PSI_ALTITUDE;	00011360

PL/I OPTIMIZING COMPILER FITFLT: PROCEDURE(PARAMEters) OPTIONS(MAIN) REORDER;

```

NUMBER  LEV  NT
11380   2   0  KERNEL_NOMINAL_ALPHA;
          PROC(ALPHA_TEMPLATE_TYPE_NAME,IMAX,JMAX,ALPHA);
11400   3   0  DCL ALPHA_TEMPLATE_TYPE_NAME CHAR(31) VARYING;
11410   3   0  DCL IMAX FIXED BINARY;
11420   3   0  DCL JMAX(*) FIXED BINARY;
11430   3   0  DCL ALPHA(*,*) BINARY FLOAT(53);
11440   3   0  DCL JR BINARY FIXED;
11450   3   0  DCL ITERMIN BINARY FIXED;
11460   3   0  ITERMIN=LBOUND(ALPHA,1);

11480   3   0  SELECT(ALPHA_TEMPLATE_TYPE_NAME);
11490   3   1  WHEN('CONTINUOUS')
          GO TO CONTINUOUS;
11510   3   1  WHEN('EQUI_SINE_DIFF')
          GO TO EQUI_SINE_DIFF;
11530   3   1  WHEN('EQUI_ALPHA')
          GO TO EQUI_ALPHA;
11550   3   1  END;

11580   3   0  EQUI_SINE_DIFF;
          DO I=1 TO IMAX;
11600   3   1  DO J=0 TO JMAX(I)/4;
11610   3   2  JR=JMAX(I)-J;
11620   3   2  ALPHA(ITERMIN,I,J)=ASIN(4*FLOAT(J,53)/FLOAT(JMAX(I),53));
11630   3   2  ALPHA(ITERMIN,I,JR)=2*PI-ALPHA(ITERMIN,I,J);
11640   3   2  END;
11650   3   1  DO J=JMAX(I)/4+1 TO JMAX(I)/2;
11660   3   2  JR=JMAX(I)-J;
11670   3   2  ALPHA(ITERMIN,I,J)=PI-ASIN(2-4*FLOAT(J,53)/FLOAT(JMAX(I),53));
11680   3   2  ALPHA(ITERMIN,I,JR)=2*PI-ALPHA(ITERMIN,I,J);
11690   3   2  END; RETURN;

11710   3   0  EQUI_ALPHA:DO I=1 TO IMAX;
11720   3   1  DO J=0 TO JMAX(I);
11730   3   2  ALPHA(ITERMIN,I,J)=2*PI*FLOAT(J,53)/FLOAT(JMAX(I),53);
11740   3   2  END;
11750   3   1  END; RETURN;

11770   3   0  CONTINUOUS: DO I=1 TO IMAX;
11780   3   1  DO J=0 TO JMAX(I);
11790   3   2  ALPHA(ITERMIN,I,J)=0;
11800   3   2  END;
11810   3   1  END; RETURN;

11830   3   0  END KERNEL_NOMINAL_ALPHA;

```


PL/1 OPTIMIZING COMPILER FITFILT: PROCEDURE(PARAMETERS) OPTIONS(MAIN) REORDER;

NUMBER LEV NT

11850 2 0 END ALLOCATE_CORE; 00011850

PL/I OPTIMIZING COMPILER FITFLT: PROCEDURE(PARAMETERS) OPTIONS(MAIN) REORDER;

NUMBER LEV NT

```

11870 1 0 MAXIMUM: PROCEDURE(ARRAY) RETURNS(FIXED BINARY);
/* FINDS THE MAXIMUM ELEMENT IN AN ARRAY */
11890 2 0 DCL ARRAY(*) FIXED BINARY;
11900 2 0 DCL MAX_ELEMENT FIXED BINARY;
11910 2 0 DCL N BINARY FIXED;
11920 2 0 MAX_ELEMENT=ARRAY(LBOUND(ARRAY,1));
11930 2 0 DO N=LBOUND(ARRAY,1)+1 TO HBOUND(ARRAY,1);
11940 2 1 IF ARRAY(N)>MAX_ELEMENT THEN MAX_ELEMENT=ARRAY(N);
11950 2 1 END;
11960 2 0 RETURN(MAX_ELEMENT);
11970 2 0 END MAXIMUM;
00011870
00011890
00011890
00011900
00011910
00011920
00011930
00011940
00011950
00011960
00011970

```

PL/I OPTIMIZING COMPILER FITFLT: PROCEDURE(PARAMEters) OPTIONS(MAIN) REORDER;

NUMBER LEV NT

```

11900 1 0 KERNEL_ORDER_SET: PROC(KERNEL_NAME) RETURNS(FIXED BINARY);
12000 2 0 DCL KERNEL_NAME CHAR(31) VARYING;
12020 2 0 SELECT(KERNEL_NAME);
12030 2 1 WHEN('STOKES','HEIGHT_FROM_ANOMALY')
      GO TO STOKES;
12050 2 1 WHEN('HEIGHT_FROM_VARIATION')
      GO TO HEIGHT_FROM_VARIATION;
12070 2 1 WHEN('HEIGHT_FROM_DENSITY')
      GO TO HEIGHT_FROM_DENSITY;
12090 2 1 WHEN('HEIGHT_FROM_DISTURBANCE')
      GO TO HEIGHT_FROM_DISTURBANCE;
12110 2 1 WHEN('MALKIN','HEIGHT_FROM_OUT_PARTIAL')
      GO TO HEIGHT_FROM_OUT_PARTIAL;
12130 2 1 WHEN('VENING_MEINSEZ','DEFLECTION_FROM_ANOMALY')
      GO TO VENING_MEINSEZ;
12150 2 1 WHEN('DEFLECTION_FROM_VARIATION')
      GO TO DEFLECTION_FROM_VARIATION;
12170 2 1 WHEN('DEFLECTION_FROM_DENSITY')
      GO TO DEFLECTION_FROM_DENSITY;
12190 2 1 WHEN('HILBERT','DEFLECTION_FROM_DISTURBANCE')
      GO TO DEFLECTION_FROM_DISTURBANCE;
12210 2 1 WHEN('DISTURBANCE_FROM_ANOMALY')
      GO TO DISTURBANCE_FROM_ANOMALY;
12230 2 1 WHEN('DISTURBANCE_FROM_VARIATION')
      GO TO DISTURBANCE_FROM_VARIATION;
12250 2 1 WHEN('DISTURBANCE_FROM_DENSITY')
      GO TO DISTURBANCE_FROM_DENSITY;
12270 2 1 END;

12290 2 0 STOKES:HEIGHT_FROM_ANOMALY:
      HEIGHT_FROM_VARIATION:
      HEIGHT_FROM_DENSITY:
      HEIGHT_FROM_DISTURBANCE:
      MALKIN:HEIGHT_FROM_OUT_PARTIAL:
      RETURN(0);

12350 2 0 DISTURBANCE_FROM_ANOMALY:
      DISTURBANCE_FROM_VARIATION:
      DISTURBANCE_FROM_DENSITY:
      RETURN(0);

12400 2 0 VENING_MEINSEZ:DEFLECTION_FROM_ANOMALY:
      DEFLECTION_FROM_VARIATION:
      DEFLECTION_FROM_DENSITY:
      HILBERT:
      DEFLECTION_FROM_DISTURBANCE:
      RETURN(1);

12450 2 0 END KERNEL_ORDER_SET;

```

NUMBER LEV NT

```

12470 1 0 IMAX_SET: PROC(KERNEL_NAME, PSI_TEMPLATE_NAME)
      RETURNS(FIXED BINARY);
      /* ESTABLISHES THE NUMBER OF RINGS FOR SPECIFIED TEMPLATE */
12500 2 0 DCL KERNEL_NAME CHAR(31) VARYING;
12510 2 0 DCL PSI_TEMPLATE_NAME CHAR(31) VARYING;
12530 2 0 SELECT(KERNEL_NAME);
12540 2 1 WHEN('STOKES', 'HEIGHT_FROM_ANOMALY')
      GO TO STOKES;
12560 2 1 WHEN('HEIGHT_FROM_VARIATION')
      GO TO HEIGHT_FROM_VARIATION;
12580 2 1 WHEN('HEIGHT_FROM_DENSITY')
      GO TO HEIGHT_FROM_DENSITY;
12600 2 1 WHEN('HEIGHT_FROM_DISTURBANCE')
      GO TO HEIGHT_FROM_DISTURBANCE;
12620 2 1 WHEN('VENING_MEINESZ', 'DEFLECTION_FROM_ANOMALY')
      GO TO VENING_MEINESZ;
12640 2 1 WHEN('DEFLECTION_FROM_VARIATION')
      GO TO DEFLECTION_FROM_VARIATION;
12660 2 1 WHEN('DEFLECTION_FROM_DENSITY')
      GO TO DEFLECTION_FROM_DENSITY;
12680 2 1 WHEN('HILBERT', 'DEFLECTION_FROM_DISTURBANCE')
      GO TO DEFLECTION_FROM_DISTURBANCE;
12700 2 1 END;

12720 2 0 STOKES: HEIGHT_FROM_ANOMALY:
      HEIGHT_FROM_VARIATION:
      HEIGHT_FROM_DENSITY:
      HEIGHT_FROM_DISTURBANCE:
      SELECT(PSI_TEMPLATE_NAME);
12770 2 1 WHEN('PICK_PICHA_VYSKOCIL') RETURN(34);
12780 2 1 WHEN('DMAAC') RETURN(101);
12790 2 1 WHEN('EQUI_INTEGRAL') RETURN(MRINGS);
12800 2 1 END;

12820 2 0 VENING_MEINESZ: DEFLECTION_FROM_ANOMALY:
      DEFLECTION_FROM_VARIATION:
      DEFLECTION_FROM_DENSITY:
      DEFLECTION_FROM_DISTURBANCE:
      SELECT(PSI_TEMPLATE_NAME);
12870 2 1 WHEN('PICK_PICHA_VYSKOCIL') RETURN(23);
12880 2 1 WHEN('DMAAC') RETURN(101);
12890 2 1 WHEN('RICE_DMAAC') RETURN(125);
12900 2 1 WHEN('EQUI_INTEGRAL') RETURN(MRINGS);
12910 2 1 END;

12930 2 0 END IMAX_SET;

```

PL/I OPTIMIZING COMPILER FITFLT: PROCEDURE(PARAMETERS) OPTIONS(MAIN) REORDER;

```

NUMBER  LEV  NT
12950   1   0   JMAX_SET: PROC(KERNEL_NAME, ALPHA_TEMPLATE_NAME,
/* ESTABLISHES THE NUMBER OF COMPARTMENTS IN EACH RING */
12980   2   0   DCL KERNEL_NAME CHAR(31) VARYING;
12990   2   0   DCL ALPHA_TEMPLATE_NAME CHAR(31) VARYING;
13000   2   0   DCL JMAX_FIXED_BINARY;
13010   2   0   DCL JMAX(* ) FIXED BINARY;
13020   2   0   DCL I FIXED BINARY;
13030   2   0   DCL I FIXED BINARY;

13050   2   0   SELECT(KERNEL_NAME);
13060   2   1   WHEN('VENING_MEINSEZ', 'DEFLECTION_FROM_ANOMALY')
GO TO VENING_MEINSEZ;
13080   2   1   WHEN('DEFLECTION_FROM_VARIATION')
GO TO DEFLECTION_FROM_VARIATION;
13100   2   1   WHEN('DEFLECTION_FROM_DENSITY')
GO TO DEFLECTION_FROM_DENSITY;
13120   2   1   WHEN('HILBERT', 'DEFLECTION_FROM_DISTURBANCE')
GO TO DEFLECTION_FROM_DISTURBANCE;
13140   2   1   END;

13160   2   0   VENING_MEINSEZ: DEFLECTION_FROM_ANOMALY:
DEFLECTION_FROM_VARIATION:
DEFLECTION_FROM_DENSITY:
DEFLECTION_FROM_DISTURBANCE:
HILBERT:
SELECT(ALPHA_TEMPLATE_NAME);
WHEN('PICK_PICHA_VYSKOCIL') DO I=1 TO IMAX;
IF I>=1 & I<=10 THEN JMAX(I)=16;
IF I>=11 & I<=15 THEN JMAX(I)=24;
IF I>=16 & I<=19 THEN JMAX(I)=33;
IF I>=20 & I<=23 THEN JMAX(I)=23;
END;
WHEN('DMAAC') DO I=1 TO IMAX;
JMAX(I)=24;
END;
WHEN('EQUI_SECTOR') DO I=1 TO IMAX;
JMAX(I)=NSECTORS;
END;
END;

13360   2   0   END JMAX_SET;
13380   1   0   END FITFLT;

```

ATTRIBUTE AND CROSS-REFERENCE TABLE (SHORT)

DCL NO.	IDENTIFIER	ATTRIBUTES AND REFERENCES
10010	A	AUTOMATIC ALIGNED BINARY /* DOUBLE */ FLOAT (53) 10120.2,10130 10140,10220
*****	ABS	BUILTIN 11070
*****	ACOS	BUILTIN 1840,2180
1160	ALPHA	(*,*,*) CONTROLLED ALIGNED BINARY /* DOUBLE */ FLOAT (53) 1650,1650,1780,1850,1970,2400,2530,2530,2540,2540,3720,3720
11430	ALPHA	(*,*,*) /* PARAMETER */ ALIGNED BINARY /* DOUBLE */ FLOAT (53) 11460,11620,11630,11630,11670,11680,11680,11730,11790
1280	ALPHA_DIFF2	AUTOMATIC ALIGNED BINARY /* DOUBLE */ FLOAT (53) 2540,2550,2550
1280	ALPHA_SUM2	AUTOMATIC ALIGNED BINARY /* DOUBLE */ FLOAT (53) 2530,2550
130	ALPHA_TEMPLATE_NAME	AUTOMATIC UNALIGNED INITIAL CHARACTER (31) VARYING 10,310,580,890
12990	ALPHA_TEMPLATE_NAME	/* PARAMETER */ UNALIGNED CHARACTER (31) VARYING 13160
150	ALPHA_TEMPLATE_TYPE_NAME	AUTOMATIC UNALIGNED INITIAL CHARACTER (31) VARYING 10,310,580,890,1780,2360,2450
11400	ALPHA_TEMPLATE_TYPE_NAME	/* PARAMETER */ UNALIGNED CHARACTER (31) VARYING 11480
180	ALTITUDE	AUTOMATIC ALIGNED INITIAL BINARY /* DOUBLE */ FLOAT (53) 10,310,580,1690
3850	ALTITUDE	/* PARAMETER */ ALIGNED BINARY /* DOUBLE */ FLOAT (53) 3660
11890	ARRAY	(*) /* PARAMETER */ ALIGNED BINARY FIXED (15,0) 11920,11920,11930,11930,11940,11940
*****	ASIN	BUILTIN

PL/I OPTIMIZING COMPILER		FI/FILT: PROCEDURE(PARAMEters) OPTIONS(MAIN) REORDER:	PAGE 41
DCL NO.	IDENTIFIER	ATTRIBUTES AND REFERENCES	
10070	A1	4240,11620,11670 AUTOMATIC ALIGNED INITIAL BINARY /* DOUBLE */ FLOAT (53) 9950,10130,10150,10160	
10080	A2	AUTOMATIC ALIGNED INITIAL BINARY /* DOUBLE */ FLOAT (53) 9950,10120,2,10130,10140	
10090	A3	AUTOMATIC ALIGNED INITIAL BINARY /* DOUBLE */ FLOAT (53) 9950,10140,10150,10160	
10000	CASE	AUTOMATIC ALIGNED BINARY FIXED (15,0) 10170,3,10180,3,10260,10270,10300,10360,10410,10510,10590,10620,10710,10720	
10940	CONST	AUTOMATIC ALIGNED BINARY /* DOUBLE */ FLOAT (53) 11020,11050	
11770	CONTINUOUS	/* STATEMENT LABEL CONSTANT */ 11490	
*****	COS	BUILTIN 1880,2550,9610,9630,9790,9810,9860,9870,10980,10990,11090,11160	
5810	COS_HALF_PSI	AUTOMATIC ALIGNED INITIAL BINARY /* DOUBLE */ FLOAT (53) 5760,6200,6280,6280,6280,6280,6280,6340,6380,6400	
7140	COS_HALF_PSI	AUTOMATIC ALIGNED INITIAL BINARY /* DOUBLE */ FLOAT (53) 7090,7640,7640,7640	
8990	COS_PSI	(*) /* PARAMETER */ ALIGNED BINARY /* DOUBLE */ FLOAT (53) 9610,9630,9650,9790,9810,9860,9870,9890	
7120	COS_PSI	/* PARAMETER */ ALIGNED BINARY /* DOUBLE */ FLOAT (53) 7090,7090,7430,7430	
9990	COS_PSI	(*) /* PARAMETER */ ALIGNED BINARY /* DOUBLE */ FLOAT (53) 10230,10240,10250,10260,10270,10360,10380,10470,10570,10590,10680,10710,10720	
5790	COS_PSI	/* PARAMETER */ ALIGNED BINARY /* DOUBLE */ FLOAT (53) 5760,5760,5930,6110,6110,6140	
6460	COS_PSI	/* PARAMETER */ ALIGNED BINARY /* DOUBLE */ FLOAT (53) 6450,6790,6790,6850,6850,6910,6950,6950,6970,6970,7010,7010	
10880	COS_PSI	(*) /* PARAMETER */ ALIGNED BINARY /* DOUBLE */ FLOAT (53) 10980,11090,11110	
1050	COS_PSI	(*) AUTOMATIC ALIGNED BINARY /* DOUBLE */ FLOAT (53)	

PL/I OPTIMIZING COMPILER FITFLT: PROCEDURE(PARAMETERS) OPTIONS(MAIN) REORDER;

DCL NO.	IDENTIFIER	ATTRIBUTES AND REFERENCES
10010	COS_PSIX	1730,1760,1830,1840,1880,1970,2050,2050,2060,2080,2130,2130,2150,2150,2160,2230,3620,3670,3670,3960,3960,4000,3,4030,4140,4140,4160,4200,4240,4240 AUTOMATIC ALIGNED BINARY /* DOUBLE */ FLOAT (53) 10380,10590,10710,10720
6510	D	AUTOMATIC ALIGNED INITIAL BINARY /* DOUBLE */ FLOAT (53) 6450,6790,6790,6830,6850,6850,6850,6850,6910,6970,6970,6970,6970,6970,7030
1180	D_ALPHA	(*,*) CONTROLLED ALIGNED BINARY /* DOUBLE */ FLOAT (53) 1650,1650
10910	D_PSI	AUTOMATIC ALIGNED BINARY /* DOUBLE */ FLOAT (53) 11050,11060,11070
10010	DA	AUTOMATIC ALIGNED BINARY /* DOUBLE */ FLOAT (53) 10150,10170,10170,2,10220
470	DAMPING_POWER	AUTOMATIC ALIGNED INITIAL BINARY /* SINGLE */ FLOAT (21) 10,310,510,530,580,3060,3080
10010	DB	AUTOMATIC ALIGNED BINARY /* DOUBLE */ FLOAT (53) 10160,10170,10180,2,10220
5680	DEFLECTION_COMMON	/* STATEMENT LABEL CONSTANT */ 5620,5640,5660,5670,2
9740	DEFLECTION_FROM_DENSITY	/* STATEMENT LABEL CONSTANT */ 9430
12820	DEFLECTION_FROM_DENSITY	/* STATEMENT LABEL CONSTANT */ 12660
12400	DEFLECTION_FROM_DENSITY	/* STATEMENT LABEL CONSTANT */ 12170
8770	DEFLECTION_FROM_DENSITY	/* STATEMENT LABEL CONSTANT */ 8650
6380	DEFLECTION_FROM_DENSITY	/* STATEMENT LABEL CONSTANT */ 5990
5650	DEFLECTION_FROM_DENSITY	/* STATEMENT LABEL CONSTANT */ 5380
7640	DEFLECTION_FROM_DENSITY	/* STATEMENT LABEL CONSTANT */ 7310

PL/I OPTIMIZING COMPILER FITFLT: PROCEDURE(PARAMETERS) OPTIONS(MAIN) REORDER;

DCL NO.	IDENTIFIER	ATTRIBUTES AND REFERENCES
8240	DEFLECTION_FROM_DENSITY	/* STATEMENT LABEL CONSTANT */ 7920
7010	DEFLECTION_FROM_DENSITY	/* STATEMENT LABEL CONSTANT */ 6670
13160	DEFLECTION_FROM_DENSITY	/* STATEMENT LABEL CONSTANT */ 13100
9740	DEFLECTION_FROM_DISTURBANCE	/* STATEMENT LABEL CONSTANT */ 9450
12400	DEFLECTION_FROM_DISTURBANCE	/* STATEMENT LABEL CONSTANT */ 12190
7040	DEFLECTION_FROM_DISTURBANCE	/* STATEMENT LABEL CONSTANT */ 6690
13160	DEFLECTION_FROM_DISTURBANCE	/* STATEMENT LABEL CONSTANT */ 13120
6400	DEFLECTION_FROM_DISTURBANCE	/* STATEMENT LABEL CONSTANT */ 6010
8260	DEFLECTION_FROM_DISTURBANCE	/* STATEMENT LABEL CONSTANT */ 7940
5670	DEFLECTION_FROM_DISTURBANCE	/* STATEMENT LABEL CONSTANT */ 5400
8770	DEFLECTION_FROM_DISTURBANCE	/* STATEMENT LABEL CONSTANT */ 8670
7660	DEFLECTION_FROM_DISTURBANCE	/* STATEMENT LABEL CONSTANT */ 7330
12820	DEFLECTION_FROM_DISTURBANCE	/* STATEMENT LABEL CONSTANT */ 12680
8770	DEFLECTION_FROM_VARIATION	/* STATEMENT LABEL CONSTANT */ 8630
9740	DEFLECTION_FROM_VARIATION	/* STATEMENT LABEL CONSTANT */ 9410
8210	DEFLECTION_FROM_VARIATION	/* STATEMENT LABEL CONSTANT */ 7900
12400	DEFLECTION_FROM_VARIATION	/* STATEMENT LABEL CONSTANT */

PL/I OPTIMIZING COMPILER FITFLT: PROCEDURE(PARAMETERS) OPTIONS(MAIN) REORDER:

DCL NO.	IDENTIFIER	ATTRIBUTES AND REFERENCES
13160	DEFLECTION_FROM_VARIATION	12150 /* STATEMENT LABEL CONSTANT */ 13080
7620	DEFLECTION_FROM_VARIATION	/* STATEMENT LABEL CONSTANT */ 7290
7000	DEFLECTION_FROM_VARIATION	/* STATEMENT LABEL CONSTANT */ 6650
12820	DEFLECTION_FROM_VARIATION	/* STATEMENT LABEL CONSTANT */ 12640
5630	DEFLECTION_FROM_VARIATION	/* STATEMENT LABEL CONSTANT */ 5360
6340	DEFLECTION_FROM_VARIATION	/* STATEMENT LABEL CONSTANT */ 5970
1410	DEG_SIG_OUTPUT_RESID	AUTOMATIC ALIGNED BINARY /* DOUBLE */ FLOAT (53) 3310,3330
1410	DEG_SIG_OUTPUT_RESID_CUM	AUTOMATIC ALIGNED BINARY /* DOUBLE */ FLOAT (53) 3320,3330,3500,3510
5160	DEG_VAR_INPUT	ENTRY RETURNS(BINARY /* DOUBLE */ FLOAT (53)) 3210,3240,3330
1420	DEG_VAR_OUTPUT_RESID	AUTOMATIC ALIGNED BINARY /* DOUBLE */ FLOAT (53) 3210,3260,3290,3310
1420	DEG_VAR_OUTPUT_RESID_CUM	AUTOMATIC ALIGNED BINARY /* DOUBLE */ FLOAT (53) 2700,3290,3290,3320
40	DEGTORAD	AUTOMATIC ALIGNED INITIAL BINARY /* DOUBLE */ FLOAT (53) 10,10,8320,8320,9610,9630,9790,9810,9870,10970
6230	DISTURBANCE_FROM_ANOMALY	/* STATEMENT LABEL CONSTANT */ 6030
6870	DISTURBANCE_FROM_ANOMALY	/* STATEMENT LABEL CONSTANT */ 8690
5610	DISTURBANCE_FROM_ANOMALY	/* STATEMENT LABEL CONSTANT */ 5420
7550	DISTURBANCE_FROM_ANOMALY	/* STATEMENT LABEL CONSTANT */ 7350

PL/I OPTIMIZING COMPILER FITFLT: PROCEDURE(PARAMETERS) OPTIONS(MAIN) REORDER;

DCL NO.	IDENTIFIER	ATTRIBUTES AND REFERENCES
8110	DISTURBANCE_FROM_ANOMALY	/* STATEMENT LABEL CONSTANT */ 7960
9690	DISTURBANCE_FROM_ANOMALY	/* STATEMENT LABEL CONSTANT */ 9478
6850	DISTURBANCE_FROM_ANOMALY	/* STATEMENT LABEL CONSTANT */ 6710
12350	DISTURBANCE_FROM_ANOMALY	/* STATEMENT LABEL CONSTANT */ 12210
12350	DISTURBANCE_FROM_DENSITY	/* STATEMENT LABEL CONSTANT */ 12250
7550	DISTURBANCE_FROM_DENSITY	/* STATEMENT LABEL CONSTANT */ 7390
6230	DISTURBANCE_FROM_DENSITY	/* STATEMENT LABEL CONSTANT */ 6070
6910	DISTURBANCE_FROM_DENSITY	/* STATEMENT LABEL CONSTANT */ 6750
5650	DISTURBANCE_FROM_DENSITY	/* STATEMENT LABEL CONSTANT */ 5460
8870	DISTURBANCE_FROM_DENSITY	/* STATEMENT LABEL CONSTANT */ 8730
9690	DISTURBANCE_FROM_DENSITY	/* STATEMENT LABEL CONSTANT */ 9510
8150	DISTURBANCE_FROM_DENSITY	/* STATEMENT LABEL CONSTANT */ 8000
5630	DISTURBANCE_FROM_VARIATION	/* STATEMENT LABEL CONSTANT */ 5440
6230	DISTURBANCE_FROM_VARIATION	/* STATEMENT LABEL CONSTANT */ 6050
7550	DISTURBANCE_FROM_VARIATION	/* STATEMENT LABEL CONSTANT */ 7370
8130	DISTURBANCE_FROM_VARIATION	/* STATEMENT LABEL CONSTANT */ 7980
12350	DISTURBANCE_FROM_VARIATION	/* STATEMENT LABEL CONSTANT */

PL/I OPTIMIZING COMPILER FITFLT: PROCEDURE(PARAMEters) OPTIONS(MAIN) REORDER;

DCL NO.	IDENTIFIER	ATTRIBUTES AND REFERENCES
		12230
8870	DISTURBANCE_FROM_VARIATION	/* STATEMENT LABEL CONSTANT */ 8710
6890	DISTURBANCE_FROM_VARIATION	/* STATEMENT LABEL CONSTANT */ 6730
9690	DISTURBANCE_FROM_VARIATION	/* STATEMENT LABEL CONSTANT */ 9490
1400	DX	(*) CONTROLLED ALIGNED BINARY /* DOUBLE */ FLOAT (53) 1920,1920,3670,4610,2,4650,4710,4710,4720,4720,4730,4770,4770,4810,4810, 4820,4820,4870,4870,4880,4880,4890,4890,4910,4910,4940
11710	EQUI_ALPHA	/* STATEMENT LABEL CONSTANT */ 11530
9950	EQUI_INTEGRAL_PSI_CALC_STOKES	ENTRY RETURNS(DECIMAL /* SINGLE */ FLOAT (6)) 9650
10850	EQUI_INTEGRAL_PSI_CALC_VM_DEN	ENTRY RETURNS(DECIMAL /* SINGLE */ FLOAT (6)) 9890
11580	EQUI_SINE_DIFF	/* STATEMENT LABEL CONSTANT */ 11510
1220	EVEN	(*) /* IN PREV IN INTEGRAL_PN1_INDEF /* CONTROLLED ALIGNED BINARY /* DOUBLE */ FLOAT (53) 4230,4290,4310
1220	EVEN	(*) /* IN NEXT IN INTEGRAL_PN1_INDEF /* CONTROLLED ALIGNED BINARY /* DOUBLE */ FLOAT (53) 4260,4290,4310,4380,4440
*****	EXP	BUILTIN 11020,11160
10950	FACTOR	AUTOMATIC ALIGNED INITIAL BINARY /* DOUBLE */ FLOAT (53) 10850,11030
11140	FCN	ENTRY RETURNS(BINARY /* DOUBLE */ FLOAT (53)) 11020,11050,11210
11190	FCN_DERIV	ENTRY RETURNS(BINARY /* DOUBLE */ FLOAT (53)) 11050
1430	FIGURE_OF_MERIT	(*) AUTOMATIC ALIGNED BINARY /* SINGLE */ FLOAT (21) 3500,5050

FITFLT: PROCEDURE(PARAMETERS) OPTIONS(MAIN) REORDER;

PL/I OPTIMIZING COMPILER

DCL NO.	IDENTIFIER	ATTRIBUTES AND REFERENCES
1600	FIXED_FORMAT	/* STATEMENT LABEL CONSTANT */ 2210,2230,2400,2600
4540	FIXED_FORMAT	/* STATEMENT LABEL CONSTANT */ 4650,4940
*****	Float	BUILTIN 2760,11620,11670,11670,11730,11730
1610	Float_FORMAT	/* STATEMENT LABEL CONSTANT */ 2250,2270,2290
*****	HBOUND	BUILTIN 11930
5540	HEIGHT_COMMON	/* STATEMENT LABEL CONSTANT */ 5500,2,5510,2,5520,2,5530,2
5520	HEIGHT_FROM_DENSITY	/* STATEMENT LABEL CONSTANT */ 5300
12290	HEIGHT_FROM_DENSITY	/* STATEMENT LABEL CONSTANT */ 12070
6830	HEIGHT_FROM_DENSITY	/* STATEMENT LABEL CONSTANT */ 6590
7500	HEIGHT_FROM_DENSITY	/* STATEMENT LABEL CONSTANT */ 7210
9550	HEIGHT_FROM_DENSITY	/* STATEMENT LABEL CONSTANT */ 9330
8770	HEIGHT_FROM_DENSITY	/* STATEMENT LABEL CONSTANT */ 8570
8070	HEIGHT_FROM_DENSITY	/* STATEMENT LABEL CONSTANT */ 7820
12720	HEIGHT_FROM_DENSITY	/* STATEMENT LABEL CONSTANT */ 12580
6160	HEIGHT_FROM_DENSITY	/* STATEMENT LABEL CONSTANT */ 5890
6840	HEIGHT_FROM_DISTURBANCE	/* STATEMENT LABEL CONSTANT */ 6610
7510	HEIGHT_FROM_DISTURBANCE	/* STATEMENT LABEL CONSTANT */

PL/I OPTIMIZING COMPILER FITFLT: PROCEDURE(PARAMETERS) OPTIONS(MAIN) REORDER;

DCL NO.	IDENTIFIER	ATTRIBUTES AND REFERENCES
		7230
9550	HEIGHT_FROM_DISTURBANCE	/* STATEMENT LABEL CONSTANT */ 9350
8080	HEIGHT_FROM_DISTURBANCE	/* STATEMENT LABEL CONSTANT */ 7840
8770	HEIGHT_FROM_DISTURBANCE	/* STATEMENT LABEL CONSTANT */ 8590
12290	HEIGHT_FROM_DISTURBANCE	/* STATEMENT LABEL CONSTANT */ 12090
6180	HEIGHT_FROM_DISTURBANCE	/* STATEMENT LABEL CONSTANT */ 5910
12720	HEIGHT_FROM_DISTURBANCE	/* STATEMENT LABEL CONSTANT */ 12600
5530	HEIGHT_FROM_DISTURBANCE	/* STATEMENT LABEL CONSTANT */ 5320
7520	HEIGHT_FROM_OUT_PARTIAL	/* STATEMENT LABEL CONSTANT */ 7250
8090	HEIGHT_FROM_OUT_PARTIAL	/* STATEMENT LABEL CONSTANT */ 7860
9550	HEIGHT_FROM_OUT_PARTIAL	/* STATEMENT LABEL CONSTANT */ 9370
6200	HEIGHT_FROM_OUT_PARTIAL	/* STATEMENT LABEL CONSTANT */ 5930
12290	HEIGHT_FROM_OUT_PARTIAL	/* STATEMENT LABEL CONSTANT */ 12110
9550	HEIGHT_FROM_VARIATION	/* STATEMENT LABEL CONSTANT */ 9310
12720	HEIGHT_FROM_VARIATION	/* STATEMENT LABEL CONSTANT */ 12560
7490	HEIGHT_FROM_VARIATION	/* STATEMENT LABEL CONSTANT */ 7190
12290	HEIGHT_FROM_VARIATION	/* STATEMENT LABEL CONSTANT */ 12050

FITFILT: PROCEDURE(PARAMETERS) OPTIONS(MAIN) REORDER;

PL/I OPTIMIZING COMPILER

DCL NO.	IDENTIFIER	ATTRIBUTES AND REFERENCES
70	IMAX	11580,11710,11770 AUTOMATIC ALIGNED BINARY FIXED (15,0) 850,880,890,970,970,1650,1650,1650,1650,1650,1650,1650,1650,1650,1730, 1760,1780,1880,1910,2040,2120,2390,2450,2490,2810,2850,2990,3600,3660,3690, 5090
13010	IMAX	/* PARAMETER */ ALIGNED BINARY FIXED (15,0) 13210,13270,13300
12470	IMAX_SET	ENTRY RETURNS(BINARY FIXED (15,0)) 850
70	IMIN	AUTOMATIC ALIGNED BINARY FIXED (15,0) 1690,1910,2850,2850,2990,3000,3060,3060,3080,3080,3600,3620,3660,3670
4520	INCREMENT_CALC	ENTRY RETURNS(BINARY FIXED (15,0)) 3640
10920	INT	AUTOMATIC ALIGNED BINARY /* DOUBLE */ FLOAT (53) 11000,11020
1090	INTEGRAL_KERNEL	(*) AUTOMATIC ALIGNED BINARY /* DOUBLE */ FLOAT (53) 2130,2150,2290
1120	INTEGRAL_PN	(*) AUTOMATIC ALIGNED BINARY /* DOUBLE */ FLOAT (53) 2840,3940,3960
3890	INTEGRAL_PN_CALC	ENTRY RETURNS(BINARY FIXED (15,0)) 2830
1210	INTEGRAL_PN1	(*) CONTROLLED ALIGNED BINARY /* DOUBLE */ FLOAT (53) 1650,1650,2960,4120,4140
4070	INTEGRAL_PN1_CALC	ENTRY RETURNS(BINARY FIXED (15,0)) 2950
1220	INTEGRAL_PN1_INDEF	(*) CONTROLLED /* STRUCTURE */ 1650,1650
4160	INTEGRAL_PN1_INDEF_CALC	ENTRY RETURNS(BINARY FIXED (15,0)) 4090,4110
1010	ITER	AUTOMATIC ALIGNED BINARY FIXED (15,0) 1950,1950,1970,2180,2200,2210,2400,2530,2530,2540,2540,3500,3550,3720,3720, 5020,5020,5020,5050,5050,5050,5100,5100,5100
10900	ITERATION	AUTOMATIC ALIGNED BINARY FIXED (15,0) 11040,11040

FITFILT: PROCEDURE(PARAMETERS) OPTIONS(MAIN) REORDER;

PL/I OPTIMIZING COMPILER

DCL NO.	IDENTIFIER	ATTRIBUTES AND REFERENCES
90	ITERMAX	AUTOMATIC ALIGNED INITIAL BINARY FIXED (15,0) 10,310,580,970,970,1650,1950,3550,5020,5050,5100
11450	ITERMIN	AUTOMATIC ALIGNED BINARY FIXED (15,0) 11460,11620,11630,11670,11680,11690,11730,11790
90	ITERMIN	AUTOMATIC ALIGNED INITIAL BINARY FIXED (15,0) 10,310,580,970,970,1650,1720,1950,5020,5050,5100
10000	J	AUTOMATIC ALIGNED BINARY FIXED (15,0) 10320,10320,10430,10430,10530,10530,10640,10640
1010	J	AUTOMATIC ALIGNED BINARY FIXED (15,0) 2400,2400,2400,2520,2520,2530,2530,2540,2540,2540,3710,3710,3720,3720,11600, 11600,11610,11620,11620,11630,11650,11650,11660,11670,11670,11680,11720, 11720,11730,11730,11780,11780,11790
11420	JMAX	(*) /* PARAMETER /*/ ALIGNED BINARY FIXED (15,0) 11600,11610,11620,11650,11650,11660,11670,11720,11730,11780
13020	JMAX	(*) /* PARAMETER /*/ ALIGNED BINARY FIXED (15,0) 13220,13230,13240,13250,13280,13310
860	JMAX	(*) CONTROLLED ALIGNED BINARY FIXED (15,0) 880,880,890,920,1780,2400,2520,3710
12950	JMAX_SET	ENTRY RETURNS(BINARY FIXED (15,0)) 890
910	JMAXMAX	AUTOMATIC ALIGNED BINARY FIXED (15,0) 920,1650,1650
11440	JR	AUTOMATIC ALIGNED BINARY FIXED (15,0) 11610,11630,11660,11680
5210	K	AUTOMATIC ALIGNED BINARY /* DOUBLE /*/ FLOAT (53) 5500,5510,5520,5530,5560,5570,5610,5630,5650,5670,5690,5700,5710
1080	KERNEL	(*) AUTOMATIC ALIGNED BINARY /* DOUBLE /*/ FLOAT (53) 2060,2080,2250,2850,3000
1480	KERNEL_FUNCTION	GENERIC 2060,2080
6450	KERNEL_FUNCTION_AT_ALTITUDE	ENTRY RETURNS(BINARY /* DOUBLE /*/ FLOAT (53)) 2080
5760	KERNEL_FUNCTION_AT_SURFACE	ENTRY RETURNS(BINARY /* DOUBLE /*/ FLOAT (53)) 2060

PL/I OPTIMIZING COMPILER FITFILT: PROCEDURE(PARAMEters) OPTIONS(MAIN) REORDER;

DCL NO.	IDENTIFIER	ATTRIBUTES AND REFERENCES
730	KERNEL_FUNCTION_NOT_KNOWN	CONDITION 780,6230,6820,6840,6890,7000,7040
7090	KERNEL_INTEGRAL_INDEF	ENTRY RETURNS(BINARY /* DOUBLE /* FLOAT (53)) 2130,2130
730	KERNEL_INTEGRAL_NOT_KNOWN	CONDITION 790,7490,7510,7520,7550,7600,7620,7660
5780	KERNEL_NAME	/* PARAMETER /* UNALIGNED CHARACTER (31) VARYING 5830,2
8470	KERNEL_NAME	/* PARAMETER /* UNALIGNED CHARACTER (31) VARYING 8520,8770,8870
8960	KERNEL_NAME	/* PARAMETER /* UNALIGNED CHARACTER (31) VARYING 9280
110	KERNEL_NAME	AUTOMATIC UNALIGNED INITIAL CHARACTER (31) VARYING 10,310,580,840,850,890,1730,1760,2060,2080,2130,2130,3170,3180,3180,3210, 3240,3330,3330
7110	KERNEL_NAME	/* PARAMETER /* UNALIGNED CHARACTER (31) VARYING 7160
12980	KERNEL_NAME	/* PARAMETER /* UNALIGNED CHARACTER (31) VARYING 13050
7730	KERNEL_NAME	/* PARAMETER /* UNALIGNED CHARACTER (31) VARYING 7770
12000	KERNEL_NAME	/* PARAMETER /* UNALIGNED CHARACTER (31) VARYING 12020
6470	KERNEL_NAME	/* PARAMETER /* UNALIGNED CHARACTER (31) VARYING 6540
5180	KERNEL_NAME	/* PARAMETER /* UNALIGNED CHARACTER (31) VARYING 5250
12500	KERNEL_NAME	/* PARAMETER /* UNALIGNED CHARACTER (31) VARYING 12530
11380	KERNEL_NOMINAL_ALPHA	ENTRY RETURNS(BINARY FIXED (15,0)) 1780
1520	KERNEL_NOMINAL_COS_PSI	GENERIC 1730,1760

PL/I OPTIMIZING COMPILER FITFILT: PROCEDURE(PARAMETERS) OPTIONS(MAIN) REORDER:

DCL NO.	IDENTIFIER	ATTRIBUTES AND REFERENCES
11290	KERNEL_NOMINAL_COS_PSI_ALTITUDE	ENTRY RETURNS(BINARY FIXED (15,0)) 1760
8940	KERNEL_NOMINAL_COS_PSI_SURFACE	ENTRY RETURNS(BINARY FIXED (15,0)) 1730
830	KERNEL_ORDER	AUTOMATIC ALIGNED BINARY FIXED (15,0) 840,870,1630,1650,1780,1850,2350,2820,2940,3690
11990	KERNEL_ORDER_SET	ENTRY RETURNS(BINARY FIXED (15,0)) 840
1500	KERNEL_SPECTRUM	GENERIC 3170,3180,3180,3330
7710	KERNEL_SPECTRUM_AT_SURFACE	ENTRY RETURNS(BINARY /* DOUBLE /*/ FLOAT (53)) 3170,3180,3180,3330,8770,8870
730	KERNEL_SPECTRUM_NOT_KNOWN	CONDITION 800
*****	LBOUND	BUILTIN 11460,11920,11930
*****	LENGTH	BUILTIN 500
10020	LN	AUTOMATIC ALIGNED BINARY /* DOUBLE /*/ FLOAT (53) 10780,10790,10800
*****	LOG	BUILTIN 6110,6140,6180,6280,6790,6850,6970,7430,7640,10780,10990
11900	MAX_ELEMENT	AUTOMATIC ALIGNED BINARY FIXED (15,0) 11920,11940,11940,11960
11870	MAXIMUM	ENTRY RETURNS(BINARY FIXED (15,0)) 920
1090	MEAN_KERNEL	(*) AUTOMATIC ALIGNED BINARY /* DOUBLE /*/ FLOAT (53) 2150,2270,2840,2850,2850,2850,2960,3000,3000,3000
1120	MEAN_PN	(*) AUTOMATIC ALIGNED BINARY /* DOUBLE /*/ FLOAT (53) 2850,2850,2850,2850,3960
1210	MEAN_PN1	(*) CONTROLLED ALIGNED BINARY /* DOUBLE /*/ FLOAT (53) 1650,1650,3000,3000,3000,3000,4140
1550	MLSQ	EXTERNAL ENTRY((*,*) ALIGNED BINARY /* SINGLE /*/ FLOAT (21),(*,*) ALIGNED

PL/I OPTIMIZING COMPILER FITFILT: PROCEDURE(PARAMETERS) OPTIONS(MAIN) REORDER;

DCL NO.	IDENTIFIER	ATTRIBUTES AND REFERENCES
7750	NN	AUTOMATIC ALIGNED INITIAL BINARY /* DOUBLE */ FLOAT (53) 7710,8050,8060,2,8070,8080,8120,8140,8140,8150,8150,8200,8200, 8230,8230,8230,8240,8240,8240,8260,8260,8260
8500	NN	AUTOMATIC ALIGNED INITIAL BINARY /* DOUBLE */ FLOAT (53) 8440
8390	NN	AUTOMATIC ALIGNED INITIAL BINARY /* DOUBLE */ FLOAT (53) 8370
10030	NN1	AUTOMATIC ALIGNED BINARY FIXED (15,0) 10190,10260,10300,10380,10410,10720
10030	NN2	AUTOMATIC ALIGNED BINARY FIXED (15,0) 10200,10270,10510,10590,10620,10710
10030	NN3	AUTOMATIC ALIGNED BINARY FIXED (15,0) 10210
760	NOMINAL_COS_PSI_NOT_KNOWN	CONDITION 810,9690,10100
210	NRINGS	AUTOMATIC ALIGNED INITIAL BINARY FIXED (15,0) 10,310,580,9650,9690,12790,12900
10870	NRINGS	/* PARAMETER */ ALIGNED BINARY FIXED (15,0) 10960,11000,11010,11110
9980	NRINGS	/* PARAMETER */ ALIGNED BINARY FIXED (15,0) 10100,10110
220	NSECTORS	AUTOMATIC ALIGNED INITIAL BINARY FIXED (15,0) 10,310,580,13310
10030	N1	AUTOMATIC ALIGNED BINARY FIXED (15,0) 10130,10150,10160,10170,4,10170,4,10190,10200,10210,10250,10410,10420,10510, 10520
10030	N2	AUTOMATIC ALIGNED BINARY FIXED (15,0) 10110,10120,10200,10210
10030	N3	AUTOMATIC ALIGNED BINARY FIXED (15,0) 10140,10150,10160,10180,4,10180,4,10210
1220	OOD	(*) /* IN NEXT IN INTEGRAL_PNI_INDEF /* CONTROLLED ALIGNED BINARY /* DOUBLE */ FLOAT (53) 4300,4390,4430,4450
1220	OOD	(*) /* IN PREV IN INTEGRAL_PNI_INDEF /* CONTROLLED ALIGNED BINARY

ATTRIBUTES AND REFERENCES

8770,8870
/* PARAMETER */ ALIGNED BINARY /* DOUBLE */ FLOAT (53)

AUTOMATIC ALIGNED INITIAL BINARY /* DOUBLE */ FLOAT (53)
10,1690,1730,1760,2060,2080

```
ENTRY RETURNS(BINARY /* DOUBLE */ FLOAT (53))
1690
```

AUTOMATIC ALIGNED INITIAL BINARY /* DOUBLE */ FLOAT (53)
10,1840,2180,2400,9840

AUTOMATIC ALIGNED BINARY /* DOUBLE */ FLOAT (53)
3180,3200,3330

(*) CONTROLLED ALIGNED BINARY /* SINGLE */ FLOAT (21)
1640,1640,3170,3180,3210,3330,4590

(*) CONTROLLED ALIGNED BINARY /* DOUBLE */ FLOAT (53)
1650,1650,2470,2510,2550,2550,2580,2580,2600,2600,2960,3000,3000,3000,3000,3000,
3000

AUTOMATIC ALIGNED INITIAL BINARY /* DOUBLE */ FLOAT (53)
5160,5560,5570

AUTOMATIC ALIGNED BINARY /* DOUBLE */ FLOAT (53)
10340,10450,10550,10660,10800

AUTOMATIC ALIGNED INITIAL BINARY FIXED (15,0)
10,310,580,1970

BULTIN
4870.4870,4910

BUILT IN
2550, 11210, 11210

AUTOMATIC ALIGNED INITIAL BINARY /* DOUBLE #/ FLOAT (53)

AUTOMATIC ALIGNED INITIAL BINARY /* DOUBLE */ FLOAT (53)
7090,7430,7430,7430,7430,7430,7430,7430,7500

AUTOMATIC ALIGNED BINARY /* DOUBLE */ FLOAT (53)
6950,6970,6970,7010,7030

```
(* ) AUTOMATIC ALIGNED BINARY /* DOUBLE */ FLOAT (53)
2050,4170.3,4240,4260,4310,4390,4450
```


FITFLT: PROCEDURE(PARAMETERS) OPTIONS(MAIN) REORDER;

PL/I OPTIMIZING COMPILER

DCL NO.	IDENTIFIER	ATTRIBUTES AND REFERENCES
8290	SHALL_CAP_SPECTRUM	ENTRY RETURNS(BINARY /* DOUBLE */ FLOAT (53)) 8200,8230,8240,8260
1320	SPECTRUM	AUTOMATIC ALIGNED BINARY /* DOUBLE */ FLOAT (53) 2770,2840,2840,2960,2960,3170,3330
*****	SQRT	BUILTIN 2050,2050,2960,3060,3310,3320,6950,6950,7010,7010,8200,8230,8240,8260,8320 5800,5810,6510,7130,7140
6110	STOKES	/* STATEMENT LABEL CONSTANT */ 5850
5500	STOKES	/* STATEMENT LABEL CONSTANT */ 5260
8770	STOKES	/* STATEMENT LABEL CONSTANT */ 8530
12720	STOKES	/* STATEMENT LABEL CONSTANT */ 12540
7430	STOKES	/* STATEMENT LABEL CONSTANT */ 7170
12290	STOKES	/* STATEMENT LABEL CONSTANT */ 12030
8040	STOKES	/* STATEMENT LABEL CONSTANT */ 7780
9550	STOKES	/* STATEMENT LABEL CONSTANT */ 9290
6790	STOKES	/* STATEMENT LABEL CONSTANT */ 6550
4990	SUMMARY	ENTRY RETURNS(DECIMAL /* SINGLE */ FLOAT (6)) 3800
*****	SYSIN	EXTERNAL FILE 310,1030,1850
*****	SYSPRINT	EXTERNAL FILE PRINT 300,300,2,310,530,570,580,2200,2210,2230,2250,2270,2290,2380,2400,2600,2650, 3330,3510,4640,4650,4670,4740,4830,4940,5010,5020,5040,5050,5070,5080,5100
10020	T	AUTOMATIC ALIGNED BINARY /* DOUBLE */ FLOAT (53) 10290,10340,10340,10360,10400,10450,10450,10470,10500,10550,10550,10570,

FITFLT: PROCEDURE(PARAMETERS) OPTIONS(MAIN) REORDER;

PL/I OPTIMIZING COMPILER

DCL NO.	IDENTIFIER	ATTRIBUTES AND REFERENCES
		12130
9740	VENING_MEINESZ	/* STATEMENT LABEL CONSTANT */ 9390
8770	VENING_MEINESZ	/* STATEMENT LABEL CONSTANT */ 8610
6950	VENING_MEINESZ	/* STATEMENT LABEL CONSTANT */ 6630
13160	VENING_MEINESZ	/* STATEMENT LABEL CONSTANT */ 13060
8180	VENING_MEINESZ	/* STATEMENT LABEL CONSTANT */ 7880
5610	VENING_MEINESZ	/* STATEMENT LABEL CONSTANT */ 5340
10020	W	AUTOMATIC ALIGNED BINARY /* DOUBLE */ FLOAT (53) 10340,10450,10550,10660,10790
A370	WALLIS	ENTRY RETURNS(BINARY /* DOUBLE */ FLOAT (53)) 8090
10020	WD	AUTOMATIC ALIGNED BINARY /* DOUBLE */ FLOAT (53) 10310,10340,10420,10450,10520,10550,10630,10660
1340	WEIGHT	(*) AUTOMATIC ALIGNED BINARY /* SINGLE */ FLOAT (21) 3240,3260,3330,4380,4590
480	WEIGHT_POWER	AUTOMATIC ALIGNED INITIAL BINARY /* SINGLE */ FLOAT (21) 10,310,510,530,580,3240,3260
490	WEIGHT_TYPE	AUTOMATIC UNALIGNED INITIAL CHARACTER (6) VARYING 10,310,510,530,580,3230
1380	WEIGHTED_RESIDUAL	(*,1) AUTOMATIC ALIGNED BINARY /* SINGLE */ FLOAT (21) 4590,4600,4610.2
10020	WT	AUTOMATIC ALIGNED BINARY /* DOUBLE */ FLOAT (53) 10220,10290,10310,10420,10520,10630
1390	X	(*) CONTROLLED ALIGNED BINARY /* DOUBLE */ FLOAT (53) 1920,1920,3620,4710,4710,4710,4720,4720,4730,4810,4810,4820,4820, 4910,4910

AGGREGATE LENGTH TABLE						
DCL NO.	IDENTIFIER	LVL	DIMS	OFFSET	ELEMENT LENGTH.	TOTAL LENGTH.
1160	ALPHA		3		ADJ	ADJ
11430	ALPHA		3		8	PARAM
11890	ARRAY		1		2	PARAM
1050	COS_PSI		1		ADJ	ADJ
8990	COS_PSI		1		8	PARAM
9990	COS_PSI		1		8	PARAM
10880	COS_PSI		1		8	PARAM
11350	COS_PSI		1		8	PARAM
1180	D_ALPHA		2		ADJ	ADJ
1400	DX		1		ADJ	ADJ
1430	FIGURE_OF_MERIT		1		ADJ	ADJ
1090	INTEGRAL_KERNEL		1		ADJ	ADJ
1120	INTEGRAL_PN		1		ADJ	ADJ
1210	INTEGRAL_PNI		1		ADJ	ADJ
1220	INTEGRAL_PNI_INDEF		1		ADJ	ADJ
	PREV	1	1		ADJ	ADJ
	ODD	2	1		16	16
	EVEN	3	1		8	
	HERE	3	1		ADJ	ADJ
	NEXT	2	1		ADJ	ADJ
	ODD	2	1		16	16
	EVEN	3	1		ADJ	ADJ
		3	1		8	
860	JMAX		1		ADJ	ADJ
11420	JMAX		1		2	PARAM
13020	JMAX		1		2	PARAM
1080	KERNEL		1		ADJ	ADJ
1090	MEAN_KERNEL		1		ADJ	ADJ

PL/I OPTIMIZING COMPILER		FITFIL: PROCEDURE(PARAMETERS) OPTIONS(MAIN) REORDER;				
DCL NO.	IDENTIFIER	LVL	DIMS	OFFSET	ELEMENT LENGTH.	TOTAL LENGTH.
1120	MEAN_PN		1		ADJ	ADJ
1210	MEAN_PN1		1		ADJ	ADJ
4530	OVERRATIO		1		ADJ	ADJ
4530	OVERRATIO_FIGHT		1		ADJ	ADJ
1350	PARTIAL		2		ADJ	ADJ
1110	PN		1		ADJ	ADJ
1110	PN_NEXT		1		ADJ	ADJ
1110	PN_PREV		1		ADJ	ADJ
1200	PN1		1		ADJ	ADJ
1200	PN1_NEXT		1		ADJ	ADJ
1200	PN1_PREV		1		ADJ	ADJ
1040	PSI		2		ADJ	ADJ
10890	PSI		1		ADJ	ADJ
9220	PSIRICE		1		4	144
9100	PSI101		1		4	408
9010	PSI23		1		4	96
9050	PSI34		1		4	140
1360	RESID_SPECTRUM		1		ADJ	ADJ
1270	RING_FACTOR		1		ADJ	ADJ
1060	SIN_PSI		1		ADJ	ADJ
1340	WEIGHT		1		ADJ	ADJ
1380	WEIGHTED_RESIDUAL		2		ADJ	ADJ
1390	X		1		ADJ	ADJ
					SUM OF CONSTANT LENGTHS	788

PL/I OPTIMIZING COMPILER FITFILT: PROCEDURE(PARAMETERS) OPTIONS(MAIN) REORDER;

STORAGE REQUIREMENTS

BLOCK, SECTION OR STATEMENT	TYPE	LENGTH	(HEX)	DSA SIZE	(HEX)
FITFILT1	PROGRAM CSECT	44776	AEEB		
FITFILT2	STATIC CSECT	12864	3240		
FITFILT	PROCEDURE BLOCK	1434	59A	904	308
780	ON UNIT	120	78	208	D0
790	ON UNIT	120	78	208	D0
800	ON UNIT	120	78	208	D0
810	ON UNIT	120	78	208	D0
BLOCK.06	BEGIN BLOCK	10590	295E	1072	430
RADIUS_RATIO_CALC	PROCEDURE BLOCK	176	B0	224	E0
INTEGRAL_PN_CALC	PROCEDURE BLOCK	374	176	232	E0
PN_CALC	PROCEDURE BLOCK	306	132	224	E0
INTEGRAL_PN1_CALC	PROCEDURE BLOCK	404	194	232	E0
INTEGRAL_PN1_INDEF_CALC	PROCEDURE BLOCK	1718	6B6	280	118
INCREMENT_CALC	PROCEDURE BLOCK	2942	87E	432	180
SUMMARY	PROCEDURE BLOCK	1100	44C	304	130
DEG_VAR_INPUT	PROCEDURE BLOCK	1076	434	304	130
KERNEL_FUNCTION_AT_SURFACE	PROCEDURE BLOCK	1612	64C	328	148
KERNEL_FUNCTION_AT_ALTITUDE	PROCEDURE BLOCK	1610	64A	360	168
KERNEL_INTEGRAL_INDEF	PROCEDURE BLOCK	1164	48C	320	140
KERNEL_SPECTRUM_AT_SURFACE	PROCEDURE BLOCK	1828	724	296	128
SMALL_CAP_SPECTRUM	PROCEDURE BLOCK	320	140	264	108
HALLIS	PROCEDURE BLOCK	172	AC	224	E0
KERNEL_SPECTRUM_AT_ALTITUDE	PROCEDURE BLOCK	924	39C	328	148
KERNEL_NOMINAL_COS_PSI_SURFACE	PROCEDURE BLOCK	7310	1C8E	1536	600
EQU1_INTEGRAL_PSI_CALC_STOKES	PROCEDURE BLOCK	2034	7F2	512	200
VALUES	PROCEDURE BLOCK	316	13C	240	F0
EQU1_INTEGRAL_PSI_CALC_VN_DEN	PROCEDURE BLOCK	1178	49A	348	170
FCN_DERIV	PROCEDURE BLOCK	302	12E	248	F8
KERNEL_NOMINAL_COS_PSI_ALTITUDE	PROCEDURE BLOCK	300	12C	264	108
KERNEL_NOMINAL_ALPHA	PROCEDURE BLOCK	156	9C	248	F8
MAXIMUM	PROCEDURE BLOCK	1992	7C8	488	1E8
KERNEL_ORDER_SET	PROCEDURE BLOCK	298	12A	248	F8
INAX_SET	PROCEDURE BLOCK	734	2DE	264	108
JMAX_SET	PROCEDURE BLOCK	1010	3F2	352	160
	PROCEDURE BLOCK	888	378	376	178

FITFILT: PROCEDURE(PARAMETERS) OPTIONS(MAIN) REORDER;

PL/I OPTIMIZING COMPILER

VARIABLE STORAGE MAP

IDENTIFIER	LEVEL	OFFSET	(HEX)	CLASS	BLOCK
JMAXMAX	1	284	11C	AUTO	FITFILT
KERNEL_ORDER	1	286	11E	AUTO	FITFILT
WEIGHT_TYPE	1	288	120	AUTO	FITFILT
WEIGHT_POWER	1	272	110	AUTO	FITFILT
DAMPING_POWER	1	276	114	AUTO	FITFILT
SAVE_RESULTS_SWITCH	1	296	128	AUTO	FITFILT
PLOT_SWITCH	1	298	12A	AUTO	FITFILT
PRINT_LEVEL	1	300	12C	AUTO	FITFILT
NSECTORS	1	302	12E	AUTO	FITFILT
NRINGS	1	304	130	AUTO	FITFILT
PSIZERO	1	280	118	AUTO	FITFILT
RADIUS_RATIO	1	192	C0	AUTO	FITFILT
ALTITUDE	1	200	C8	AUTO	FITFILT
VARIABLES	1	320	140	AUTO	FITFILT
ALPHA_TEMPLATE_TYPE_NAME	1	332	14C	AUTO	FITFILT
ALPHA_TEMPLATE_NAME	1	366	16E	AUTO	FITFILT
PSI_TEMPLATE_NAME	1	400	190	AUTO	FITFILT
KERNEL_NAME	1	434	1B2	AUTO	FITFILT
ITERMIN	1	306	132	AUTO	FITFILT
ITERMAX	1	308	134	AUTO	FITFILT
NMIN	1	310	136	AUTO	FITFILT
NMAX	1	312	138	AUTO	FITFILT
IMIN	1	314	13A	AUTO	FITFILT
IMAX	1	316	13C	AUTO	FITFILT
RADTODEG	1	248	F8	AUTO	FITFILT
DEGTORAD	1	256	100	AUTO	FITFILT
PI	1	264	109	AUTO	FITFILT
DEG_VAR_OUTPUT_RESID	2	192	C0	AUTO	BLOCK.06
DEG_VAR_OUTPUT_RESID_CUM	2	200	C8	AUTO	BLOCK.06
DEG_SIG_OUTPUT_RESID	2	208	D0	AUTO	BLOCK.06
DEG_SIG_OUTPUT_RESID_CUM	2	216	D8	AUTO	BLOCK.06
RELATIVE_RESIDUAL	2	232	E8	AUTO	BLOCK.06
VARMAX	2	456	1C8	AUTO	BLOCK.06
SPECTRUM	2	248	F8	AUTO	BLOCK.06
ALPHA_SUM2	2	256	100	AUTO	BLOCK.06
ALPHA_DIFF2	2	264	108	AUTO	BLOCK.06
NN	2	360	168	AUTO	BLOCK.06
I	2	458	1CA	AUTO	BLOCK.06
J	2	460	1CC	AUTO	BLOCK.06
N	2	462	1CE	AUTO	BLOCK.06
ITER	2	464	1D0	AUTO	BLOCK.06
VAR	2	466	1D2	AUTO	BLOCK.06
ROVERGSQ	3	184	B8	AUTO	DEG_VAR_INPUT
K	3	192	C0	AUTO	DEG_VAR_INPUT
NN	3	200	C8	AUTO	DEG_VAR_INPUT
COS_HALF_PSI	3	184	B8	AUTO	KERNEL_FUNCTION_AT_SURFACE
SIN_HALF_PSI	3	192	C0	AUTO	KERNEL_FUNCTION_AT_SURFACE

FITFLT: PROCEDURE(PARAMEters) OPTIONS(MAIN) REORDER;

PL/I OPTIMIZING COMPILER

0		3	184	B8	AUTO	KERNEL_FUNCTION_AT_ALTITUDE
SIN_PSI		3	192	C0	AUTO	KERNEL_FUNCTION_AT_ALTITUDE
COS_HALF_PSI		3	184	B8	AUTO	KERNEL_INTEGRAL_INDEF
SIN_HALF_PSI		3	192	C0	AUTO	KERNEL_INTEGRAL_INDEF
NN		3	184	B8	AUTO	KERNEL_SPECTRUM_AT_SURFACE
NN		4	184	B8	AUTO	SMALL_CAP_SPECTRUM
NN		4	184	B8	AUTO	WALLIS
NN		3	184	B8	AUTO	KERNEL_SPECTRUM_AT_ALTITUDE
PSIRICE		3	5128	1408	STATIC	KERNEL_NOMINAL_COS_PSI_SURFACE
PSI101		3	184	B8	AUTO	KERNEL_NOMINAL_COS_PSI_SURFACE
PSI34		3	592	250	AUTO	KERNEL_NOMINAL_COS_PSI_SURFACE
PSI23		3	732	20C	AUTO	KERNEL_NOMINAL_COS_PSI_SURFACE
A3		4	184	B8	AUTO	EQUI_INTEGRAL_PSI_CALC_STOKES
A2		4	192	C0	AUTO	EQUI_INTEGRAL_PSI_CALC_STOKES
A1		4	200	C8	AUTO	EQUI_INTEGRAL_PSI_CALC_STOKES
T3		4	208	D0	AUTO	EQUI_INTEGRAL_PSI_CALC_STOKES
T2		4	216	D8	AUTO	EQUI_INTEGRAL_PSI_CALC_STOKES
T1		4	224	E0	AUTO	EQUI_INTEGRAL_PSI_CALC_STOKES
N		4	312	130	AUTO	EQUI_INTEGRAL_PSI_CALC_STOKES
N1		4	314	13A	AUTO	EQUI_INTEGRAL_PSI_CALC_STOKES
N2		4	316	13C	AUTO	EQUI_INTEGRAL_PSI_CALC_STOKES
N3		4	318	13E	AUTO	EQUI_INTEGRAL_PSI_CALC_STOKES
NN1		4	320	140	AUTO	EQUI_INTEGRAL_PSI_CALC_STOKES
NN2		4	322	142	AUTO	EQUI_INTEGRAL_PSI_CALC_STOKES
NN3		4	324	144	AUTO	EQUI_INTEGRAL_PSI_CALC_STOKES
LN		4	232	E8	AUTO	EQUI_INTEGRAL_PSI_CALC_STOKES
H		4	240	F0	AUTO	EQUI_INTEGRAL_PSI_CALC_STOKES
S		4	248	F8	AUTO	EQUI_INTEGRAL_PSI_CALC_STOKES
T		4	256	100	AUTO	EQUI_INTEGRAL_PSI_CALC_STOKES
HD		4	264	108	AUTO	EQUI_INTEGRAL_PSI_CALC_STOKES
HT		4	272	110	AUTO	EQUI_INTEGRAL_PSI_CALC_STOKES
A		4	280	118	AUTO	EQUI_INTEGRAL_PSI_CALC_STOKES
DA		4	288	120	AUTO	EQUI_INTEGRAL_PSI_CALC_STOKES
DB		4	296	128	AUTO	EQUI_INTEGRAL_PSI_CALC_STOKES
COS_PSIX		4	304	130	AUTO	EQUI_INTEGRAL_PSI_CALC_STOKES
CASE		4	326	146	AUTO	EQUI_INTEGRAL_PSI_CALC_STOKES
I		4	328	148	AUTO	EQUI_INTEGRAL_PSI_CALC_STOKES
J		4	330	14A	AUTO	EQUI_INTEGRAL_PSI_CALC_STOKES
FACTOR		4	184	B8	AUTO	EQUI_INTEGRAL_PSI_CALC_VH_DEN
CONST		4	192	C0	AUTO	EQUI_INTEGRAL_PSI_CALC_VH_DEN
TOTAL_INT		4	200	C8	AUTO	EQUI_INTEGRAL_PSI_CALC_VH_DEN
INT		4	208	D0	AUTO	EQUI_INTEGRAL_PSI_CALC_VH_DEN
D_PSI		4	216	D8	AUTO	EQUI_INTEGRAL_PSI_CALC_VH_DEN
I		4	224	E0	AUTO	EQUI_INTEGRAL_PSI_CALC_VH_DEN
ITERATION		4	226	E2	AUTO	EQUI_INTEGRAL_PSI_CALC_VH_DEN
ITERMIN		3	184	B8	AUTO	KERNEL_NOMINAL_ALPHA
JR		3	186	BA	AUTO	KERNEL_NOMINAL_ALPHA
N		2	184	B8	AUTO	MAXIMUM
MAX_ELEMENT		2	186	BA	AUTO	MAXIMUM
I		2	184	B8	AUTO	JMAX_SET

PL/I OPTIMIZING COMPILER FITFILT: PROCEDURE(PARAMETERS) OPTIONS(MAIN) REORDER;

'NOLIST' OPTION HAS CAUSED STATIC MAP LISTING TO BE SUPPRESSED

PL/I OPTIMIZING COMPILER FITFILT: PROCEDURE(PARAMETERS) OPTIONS(MAIN) REORDER;

COMPILER DIAGNOSTIC MESSAGES

ERROR ID L NUMBER MESSAGE DESCRIPTION

WARNING DIAGNOSTIC MESSAGES

IEL0916I W 10 ITEM(S) 'JMAX', 'JMIN', 'JMAX' MAY BE UNINITIALIZED WHEN USED IN THIS BLOCK.

IEL0916I W 970 ITEM(S) 'INTEGRAL_PNI', 'PNI', 'PNI_PREV', 'INTEGRAL_PNI_INDEF_PREV_EVEN', 'INTEGRAL_PNI_INDEF_HERE', 'INTEGRAL_PNI_INDEF_NEXT_ODD', 'INTEGRAL_PNI_INDEF_NEXT_EVEN', 'PNI_PREV', 'MEAN_PNI', 'INTEGRAL_KERNEL', 'MEAN_KERNEL', 'KERNEL', 'COS_PSI', 'PSI', 'I', 'J', 'VAR', 'PNI_NEXT', 'ALPHA', 'INTEGRAL_PNI', 'PNI', 'VARNAX', 'PNI_NEXT', 'INTEGRAL_PNI_INDEF_PREV_ODD', 'FIGURE OF MERIT', 'DE G SIG OUTPUT RESID_CUM', 'WEIGHTED_RESIDUAL', 'WEIGHT', 'RING_FACTOR' MAY BE UNINITIALIZED WHEN USED IN THIS BLOCK.

IEL0640I W 1730 ARGUMENT NUMBER 4 TO GENERIC FUNCTION IS ASSUMED TO MATCH ITS CORRESPONDING AGGREGATE PARAMETER.

IEL0640I W 1760 ARGUMENT NUMBER 5 TO GENERIC FUNCTION IS ASSUMED TO MATCH ITS CORRESPONDING AGGREGATE PARAMETER.

IEL0916I W 5590 5720 STATEMENT MAY NEVER BE EXECUTED.

IEL0671I W 9890 ARGUMENT NUMBER 1 TO ENTRY 'EQUI INTEGRAL_PSI_CALC_VM_DEN' DOES NOT MATCH ITS CORRESPONDING PARAMETER OR IS AN ISUB-DEFINED ARRAY. A DUMMY ARGUMENT HAS BEEN CREATED.

IEL0916I W 9950 ITEM(S) 'LN', 'COS_PSI' MAY BE UNINITIALIZED WHEN USED IN THIS BLOCK.

COMPILER INFORMATORY MESSAGES

IEL0533I I NO 'DECLARE' STATEMENT(S) FOR 'LENGTH', 'SYSPRINT', 'SYSIN', 'EXP', 'ABS', 'LBOUND', 'HBOUND', 'ACOS', 'COS', 'SORT', 'SIN', 'FLOAT', 'MOD', 'ASIN', 'SIGN', 'LOG', 'TRUNC', 'TAN'.

END OF COMPILER DIAGNOSTIC MESSAGES

COMPILE TIME 0.29 MINS SPILL FILE: 101 RECORDS, SIZE 4051

APPENDIX D

EXPLANATION OF THE COMPREHENSIVE FILTER DESIGN COMPUTER PROGRAM

FITFILT is the name of the comprehensive spherical filter design program for determining optimal template parameters of discrete summation geodetic transformations. Its major inputs are listed in Table D-1 with short explanations of the possible choices. All inputs to the program have default values, so that at run-time the user only needs to specify those inputs which are special to the run.

The main portion of FITFILT consists of only nine pages of code (lines 10-3800). The remaining twenty-nine pages of code are listings of subprocedures (lines 3840-13380) nested within FITFILT.

After reading the inputs (line 310), printing them (line 580), and calculating a few preliminary parameters (lines 840-920), the program enters a BEGIN block in which storage is automatically allocated for a large number of arrays whose size depends upon the inputs and the preliminary parameters. Establishment of the initial template parameters begins at line 1720.

The outermost loop in the program is on the iteration number ITER, beginning at line 1950 and concluding at line 3760. At the beginning of this loop a large number of variables which depend upon the current template parameter values (at this iteration) are initialized, between lines 2030 and 2710.

The second outermost loop is on the spherical harmonic degree N, beginning at line 2750 and concluding at line 3460. At each pass through this loop the theoretical, actual, and residual spectrum of the transformation is calculated, as well as its partial derivatives.

The third outermost loop is on the ring or ring boundary index I, beginning at line 2810 and concluding at line 3130. At each pass the contribution of the respective ring to the spectral values is evaluated. The recursions on the integrals of the associated Legendre functions are

performed here (one for each ring). The partial derivative of the spectrum with respect to each ring radius is also calculated.

After the loop over all spherical harmonic degrees has been accomplished (line 3460) during each iteration, the program calls the INCREMENT_CALC subprocedure (line 3640) to determine the increments which are added to the current values of the template parameters (lines 3660-3750) for use in the next iteration.

After all iterations have been completed (line 3760), the program prints a summary of the intermediate results of all iterations including the values of the figure-of-merit and of the template parameters.

The functions of the subprocedures should be fairly obvious from their (rather long) names.

- **KERNEL_NAME**

(Name of the Spherical Geodetic Transformation)

'STOKES', 'HEIGHT_FROM_ANOMALY' (Default)

'HEIGHT_FROM_DENSITY'

'DEFLECTION_FROM_DENSITY'

Coding has been provided to recognize the following names, but certain subroutines, calculating their kernel values, integrals, or spectra are incomplete:

'HEIGHT_FROM_VARIATION'

'HEIGHT_FROM_DISTURBANCE'

'MALKIN', 'HEIGHT_FROM_OUT_PARTIAL'

'VENING_MEINESZ', 'DEFLECTION_FROM_ANOMALY'

'DEFLECTION_FROM_VARIATION'

'HILBERT', 'DEFLECTION_FROM_DISTURBANCE'

'DISTURBANCE_FROM_ANOMALY'

'DISTURBANCE_FROM_VARIATION'

'DISTURBANCE_FROM_DENSITY'

- **PSI_TEMPLATE_NAME**

(Name of the initial spherical ring template)

'PICK_PICHA_VYSKOCIL' (Default)

Either the 34-ring template for zeroth-order transformations, or the 23-ring template for first-order transformations. (Requires PSIZEO)

'DMAAC'

The 101-ring Circularized AGEMIT template. (Requires PSIZEO)

'RICE_DMAAC'

The 125-ring "Rice-DMAAC" Template

'EQUI_INTEGRAL'

The Equal-Ring-Contribution template. (Requires PSIZEO and NRINGS to specify truncation radius and number of rings.)

Table D-1. Major Inputs to FITFILT.

- ALPHA_TEMPLATE_NAME

(Establishes number of compartments in each ring for non-zeroth order transformations.)

'PICK_PICHA_VYSKOCIL' (Default)

Pick-Picha-Vyskocil distribution (16, 24, 33, 23)

'DMAAC'

24 compartments in each ring*

'EQUI_SECTOR'

Equal number of compartments in each ring. (Requires NSECTORS to specify the number.)

- ALPHA_TEMPLATE_TYPE_NAME

(Name of the type of initial compartment template)

'CONTINUOUS' (Default)

No compartmental discretization is to be considered.

'EQUI_SINE_DIFF'

Compartment boundary azimuths are to be selected by the equal-sector-contribution method.

'EQUI_ALPHA'

Compartment boundary azimuths are to be equally (uniformly) distributed.

- PSIZERO

(The spherical truncation radius ψ_0 expressed in degrees)

Default = 0.03°

- NRINGS

(The number of rings for an equal-ring-contribution template.)

- NSECTORS

(The number of sectors for an equal-sector-contribution template or a uniform azimuth template.)

* A more elaborate scheme was originally planned for the 'DMAAC' distribution, but it has not yet been implemented.

Table D-1. (continued)

APPENDIX E

DISCUSSION OF THE EXCLUSION OF SMALL RING RADII FROM THE DIFFERENTIAL ADJUSTMENT PROCEDURE

The reasons for the exclusion of the smaller ring boundary radii parameters from differential adjustment during the optimization process have been described in Section 6.3.3. This Appendix gives seven examples of numerical computations which illustrate the necessity for this exclusion. They also show the dependence of the spherical radius separating reasonable from unreasonable increments upon the maximum spherical harmonic degree considered and the number of rings in the template.

Each of the seven examples (Figures E-1 through E-7) is presented in an identical format consisting of three blocks of numbers. The first block gives the values of the spherical ring radii ψ_i of the template in degrees. The second block gives the cosines x_i of the radii ψ_i . The third block gives the raw increments Δx_i in the cosines which have been computed by the Gauss-Newton algorithm, before any constraint checking.

As seen in the figures, the raw increments corresponding to the smaller ring radii are generally so large* that if they were to be added to the values of the independent variables, the results would not only overlap but they would also exceed the theoretical bound of $x = +1$ or $\psi = 0$. Consequently, in order to exclude most of these cases, the increments corresponding to values of the spherical ring boundary radii which are less than ψ_{LIMIT} are zeroed before they are submitted to the inequality constraint satisfaction algorithm.

A summary of the examples is presented in Figure E-8. In the last column of this figure, the ratio of the observed spherical radius corresponding the first reasonable increment to the "estimated" spherical radius given by the rule-of-thumb is listed.

*excluding the first increment which is always zero.

Naturally, a value of one would mean that the rule-of-thumb is ideal. It is seen that for a small number of rings in the template, the rule-of-thumb is too large by about a factor of two, while for a large number of rings the rule-of-thumb is too small by a factor of one third or one fourth. Certainly there are other factors which influence these results, such as the kernel itself* and the initial values of the spherical ring radii parameters.

SPHERICAL RADII PSI (DEGREES)					
0.000009997722	0.043999999761	0.062999963760	0.088999986648	0.127999961376	0.182999968529
0.260999977509	0.371999979019	0.529999971390	0.752999961376	1.068999290466	1.793999671936
2.965999603271	4.820999145508	7.590999603271	11.469999313354	18.549987792969	28.299987792969
40.799987792969	65.299987792969	98.599990844727	114.399993896484	130.500000000000	180.000000000000
INDEPENDENT VARIABLE VALUES X					
1.000000000000	0.999999705130	0.999999395487	0.999998793563	0.999997504577	0.999994899340
0.999999624598	0.999978922988	0.999957216793	0.999913640843	0.999825952826	0.999509844392
0.998660416065	0.996462124040	0.991236303723	0.980028961480	0.946046461376	0.880477454515
0.756995194865	0.417867267361	-0.149535185451	-0.413104332813	-0.649448048330	-1.000000000000
RAW INCREMENTS IN INDEPENDENT VARIABLES					
0.000000000000	0.000796638662	-0.131530463696	-0.067849397659	-0.153551518917	-0.099590241909
0.341211974621	-0.350839265537	-3.826305389404	2.078421592712	7.648271369934	3.694955825806
-9.600479888916	4.303641319275	-0.836096882820	0.075040996075	-0.011155508459	0.001902790740
-0.001500146929	-0.002837406239	-0.003046664875	-0.015168551356	-0.026527497917	0.000000000000

Figure E-1. Example of Large Increments (Vening-Meinesz, 23 rings, Maximum degree 30).

*The frequency domain explanation in Section 6.3.3 implies that the separation radius for the Vening-Meinesz' kernel should be twice that for the Stokes' kernel in the mean.

SPHERICAL RADII PSI (DEGREES)					
0.00000000000	0.06840000000	0.17530000000	0.30780000000	0.44740000000	0.71160000000
0.97500000000	1.23480000000	1.48830000000	1.98600000000	2.47800000000	2.96100000000
4.14800000000	5.88400000000	8.18000000000	10.48800000000	12.85000000000	15.99000000000
20.17000000000	25.30000000000	33.90000000000	52.00000000000	61.00000000000	72.00000000000
82.00000000000	94.20000000000	106.30000000000	126.30000000000	135.90000000000	142.70000000000
149.00000000000	155.40000000000	162.90000000000	176.40000000000	180.00000000000	

INDEPENDENT VARIABLE VALUES X					
1.00000000000	0.99999287415	0.999995319543	0.999985570180	0.999969513014	0.999922875735
0.999954977339	0.999767779171	0.999662649558	0.999399324740	0.999064896577	0.998664927363
0.997330535358	0.994731483424	0.989825957496	0.983293053318	0.974955645484	0.961309789091
0.933673691819	0.904082549661	0.830012285095	0.615661475326	0.484809620246	0.309016994375
0.139173100960	-0.073238197128	-0.280666708921	-0.592013178799	-0.718126297763	-0.795473480855
-0.857167300702	-0.909236109047	-0.955793014798	-0.998026728428	-1.000000000000	

INCREMENTS IN INDEPENDENT VARIABLES					
0.00000000000	133933.530920723130	9897064.994782713000	2032938.510839480000	1894403.314123990000	0100943.640946900000
3668737.558594300000	7338697.256554000000	7154874.726231030000	5222606.736206200000	2678117.970351000000	6624614.933013230000
7514196.708851765000	437472.244078556670	-65551.386001849720	10867.283470125945	-639.173537034833	26.416047457364
-1.529124001736	0.184269505353	0.059554322357	-0.007943673599	-0.029115926541	-0.010655791156
-0.031823224478	-0.035355481130	0.030403237578	-0.098648960543	0.077801117446	0.612819008185
0.712835033028	0.531043223691	0.137234852777	0.014910309473	0.000000000000	

Figure E-2. Example of Large Increments (Stokes, 34 rings, Maximum degree 50).

SPHERICAL RADII PSI (DEGREES)					
0.00000000000	0.06840000000	0.17530000000	0.30780000000	0.44740000000	0.71160000000
0.97500000000	1.23480000000	1.48830000000	1.98600000000	2.47800000000	2.96100000000
4.14800000000	5.88400000000	8.18000000000	10.48800000000	12.85000000000	15.99000000000
20.17000000000	25.30000000000	33.90000000000	52.00000000000	61.00000000000	72.00000000000
82.00000000000	94.20000000000	106.30000000000	126.30000000000	135.90000000000	142.70000000000
149.00000000000	155.40000000000	162.90000000000	176.40000000000	180.00000000000	

INDEPENDENT VARIABLE VALUES X					
1.00000000000	0.99999287415	0.999995319543	0.999985570180	0.999969513014	0.999922875735
0.999954977339	0.999767779171	0.999662649558	0.999399324740	0.999064896577	0.998664927363
0.997330535358	0.994731483424	0.989825957496	0.983293053318	0.974955645484	0.961309789091
0.933673691819	0.904082549661	0.830012285095	0.615661475326	0.484809620246	0.309016994375
0.139173100960	-0.073238197128	-0.280666708921	-0.592013178799	-0.718126297763	-0.795473480855
-0.857167300702	-0.909236109047	-0.955793014798	-0.998026728428	-1.000000000000	

INCREMENTS IN INDEPENDENT VARIABLES					
0.00000000000	1.172499656677	-2.375228881836	6.992014884949	-0.676611027241	0.344479382038
-0.165163516973	0.084941506356	-0.002380404389	0.001437092200	0.000175711146	0.001105129020
0.00146154347	0.001522401348	0.000674712704	0.001339778296	0.008145853877	0.012606538832
0.016223310375	0.028527390212	0.026670992374	-0.050538759679	-0.030925475061	-0.032637000084
-0.012455124403	0.013382936188	0.031220365316	-0.019832070917	-0.004077050835	0.004928622395
0.002559453249	-0.00068353038	-0.007685072720	-0.017202876509	0.000000.000000000000	

Figure E-3. Example of Large Increments (Stokes, 34 rings, Maximum degree 500).

SPHERICAL RADII PSI (DEGREES)

0.000000000000	0.083333313465	0.166666626930	0.250000000000	0.333333313465	0.416666626930
0.500000000000	0.583333313465	0.666666626930	0.750000000000	0.833333313465	0.916666626930
1.000000000000	1.083333315442	1.166666630884	1.250000000000	1.333333315442	1.416666630884
1.500000000000	1.583333315442	1.666666630884	1.750000000000	1.833333315442	1.916666630884
2.000000000000	2.083333315442	2.166666630884	2.250000000000	2.333333315442	2.416666630884
2.500000000000	2.583333315442	2.666666630884	2.750000000000	2.833333315442	2.916666630884
3.000000000000	3.250000000000	3.500000000000	3.750000000000	4.000000000000	4.250000000000
4.500000000000	4.750000000000	5.000000000000	5.250000000000	5.500000000000	5.750000000000
6.000000000000	6.250000000000	6.500000000000	6.750000000000	7.000000000000	8.000000000000
9.000000000000	10.000000000000	11.000000000000	12.000000000000	13.000000000000	14.000000000000
15.000000000000	16.000000000000	17.000000000000	18.000000000000	19.000000000000	20.000000000000
21.000000000000	22.000000000000	23.000000000000	24.000000000000	25.000000000000	30.000000000000
35.000000000000	40.000000000000	45.000000000000	50.000000000000	55.000000000000	60.000000000000
65.000000000000	70.000000000000	75.000000000000	80.000000000000	85.000000000000	90.000000000000
95.000000000000	100.000000000000	105.000000000000	110.000000000000	115.000000000000	120.000000000000
125.000000000000	130.000000000000	135.000000000000	140.000000000000	145.000000000000	150.000000000000
155.000000000000	160.000000000000	165.000000000000	170.000000000000	175.000000000000	180.000000000000

INDEPENDENT VARIABLE VALUES X

1.000000000000	0.999998942301	0.999995769208	0.999990480721	0.999983076860	0.999973557637
0.999961923064	0.999948173182	0.999932308012	0.999914327574	0.999894231932	0.999872021117
0.999847695156	0.999821254236	0.999792698311	0.999762027080	0.999729241309	0.999694340728
0.999657324976	0.999618194978	0.999576950405	0.999533590837	0.999488117357	0.999440529578
0.999390827019	0.999339010923	0.999285080844	0.999229036241	0.999170878516	0.999110607162
0.999048221582	0.998983723335	0.998917111855	0.998848386485	0.998777548943	0.998704598606
0.998629534755	0.998591670557	0.998513479842	0.998458923239	0.998364050260	0.998250185099
0.998491733373	0.998455024298	0.998394698092	0.998304927575	0.998196198367	0.998068518251
0.99821895368	0.998056338222	0.997971855677	0.997868456955	0.997746151641	0.997606060742
0.997688340595	0.9974807753012	0.99731627183448	0.997147600734	0.996970064785	0.996795726276
0.99745826289	0.997261695938	0.997056304755963	0.99685105616295	0.9966518575599	0.99642620786
0.9973580426497	0.997183854567	0.9970504853452	0.99691354547643	0.9967307787037	0.9965025403784
0.99719152044289	0.996944443119	0.996770106781187	0.99662787609687	0.9964576436351	0.99626000000000
0.99692618261741	0.996720143326	0.9965819045103	0.99643648177667	0.99627155742748	0.99600000000000
-0.087155742748	-0.173648177667	-0.258819045103	-0.342020143326	-0.422618261741	-0.500000000000
-0.573576436351	-0.642767609687	-0.707106781187	-0.76604443119	-0.819152044289	-0.866025403784
-0.906307787037	-0.939692620786	-0.965925826289	-0.984807753012	-0.996194698092	-1.000000000000

RAW INCREMENTS IN INDEPENDENT VARIABLES

0.000000000000	-47.988937377930	-35.035934448242	161.058624267578	221.881027221680	-625.382812500000
-48.251251220703	735.539550781250	1033.012207031250	-4312.964843750000	4465.839843750000	-273.512939453125
-2760.917480468750	21.843505859375	4736.457031250000	-4724.328125000000	323.026123046875	2017.893066406250
-186.815216064453	-1067.657714843750	-1013.688720703125	2075.136474609375	2173.812255659375	-8390.417968750000
9645.582031250000	-4834.175781250000	-506.852539062500	1851.751953125000	-503.969970703125	64.457672119141
-1451.775634765625	2766.857421875000	-2614.054199218750	1460.519042968750	-472.537646484375	55.998321533203
0.295540630817	-0.062968969345	0.013691093773	-0.008642513305	0.001882606652	-0.003748088144
0.001587662147	-0.003705637995	0.002750977874	0.002967894543	-0.000358792255	0.001581556397
-0.000903337240	-0.000292437384	-0.000339779770	0.000671830960	-0.001016347436	-0.000573679379
-0.000181866730	0.000256956728	0.000429115258	0.000780167757	0.001158984145	0.001294402406
0.001335446024	0.000368253794	0.002032726770	0.001091106096	0.001525897766	0.000627075555
0.002139975782	0.002682601800	0.002922888380	0.001625886187	-0.009800467640	-0.001700285124
0.003126074793	0.005856927484	0.007720775902	0.009225686875	0.009603582323	0.006275434047
-0.005059327930	-0.081308424473	-0.072332680225	-0.034014228731	-0.010626845927	-0.004778709263
-0.002958768047	0.001939212663	0.003289061598	0.003510709386	0.003603029763	0.003190943738
0.003201898653	0.002296169754	0.000262974994	-0.000745280879	-0.001098564593	-0.002601768123
-0.003783527762	-0.004327781498	-0.004046395421	-0.002617008286	-0.006218768656	0.000000000000

Figure E-4. Example of Large Increments (Stokes, 101 rings, Maximum degree 1000).

SPHERICAL RADII PSI (DEGREES)

0.0440003	0.0611177	0.0848950	0.1179225	0.1637990	0.2275235	0.3160396	0.4389928	0.6097818	0.8470203
1.1765695	1.6343682	2.2703009	3.1541283	4.3824956	6.0909150	8.4698169	11.7900031	16.4449830	23.0306519
32.5229409	46.7795915	70.6387639	179.9323089						

INDEPENDENT VARIABLE VALUES X

0.9999997	0.9999994	0.9999989	0.9999979	0.9999959	0.9999921	0.9999848	0.9999706	0.9999434	0.9998907
0.9997892	0.9995932	0.9992150	0.9984851	0.9970761	0.9943548	0.9890936	0.9789031	0.9590920	0.9202957
0.8431762	0.6848068	0.3315229	-0.9999993						

RAW INCREMENTS IN INDEPENDENT VARIABLES

0.0000000	0.0000059	-0.0000180	0.0000194	-0.0000101	0.0000029	-0.0000007	-0.0000001	-0.0000003	-0.0000003
-0.0000002	-0.0000001	-0.0000001	-0.0000002	-0.0000006	-0.0000014	-0.0000034	-0.0000064	-0.0000013	0.0000082
0.0006832	0.0032048	-0.0654269	0.0000000						

Figure E-5. Example of Large Increments (Vening-Meinesz, 23 rings, Maximum degree 1440).

SPHERICAL RADII PSI (DEGREES)

0.0021134	0.0023003	0.0025038	0.0027252	0.0029663	0.0032286	0.0035142	0.0038250	0.0041633	0.0045315
0.0049323	0.0053686	0.0058434	0.0063603	0.0069228	0.0075351	0.0082016	0.0089270	0.0097165	0.0105759
0.0115113	0.0125295	0.0136377	0.0148439	0.0161568	0.0175858	0.0191412	0.0208342	0.0226769	0.0246826
0.0268657	0.0292419	0.0318283	0.0346434	0.0377075	0.0410426	0.0446727	0.0486238	0.0529245	0.0576055
0.0627005	0.0682462	0.0742024	0.0808524	0.0880036	0.0957872	0.1042593	0.1134807	0.1235177	0.1344425
0.1463336	0.1592763	0.1733639	0.1886974	0.2053872	0.2235531	0.2433257	0.2648472	0.2882723	0.3137692
0.3415214	0.3717281	0.4046067	0.4403933	0.4793453	0.5217426	0.5678901	0.6181194	0.6727916	0.7322999
0.7970721	0.8675739	0.9443124	1.0278393	1.1187554	1.2177148	1.3254295	1.4426745	1.5702938	1.7092062
1.8604121	2.0253009	2.2041590	2.3991785	2.6114666	2.8425565	3.0941185	3.3679728	3.6661036	3.9906738
4.3440425	4.7237833	5.1477052	5.6038755	6.1006459	6.6416810	7.2309914	7.8729700	8.5724348	9.3346769
10.1655167	11.0713686	12.0593185	13.1372143	14.3137754	15.5987254	17.0029546	18.5387227	20.2199128	22.0623575
24.0842603	26.3067526	28.7546418	31.4574364	34.4507856	37.7785549	41.4959114	45.6740870	50.4080698	55.8297394
62.1319763	69.6173616	78.8107683	90.7798135	108.4698034	179.9999989				

INDEPENDENT VARIABLE VALUES X

1.0000000	1.0000000	1.0000000	1.0000000	1.0000000	1.0000000	1.0000000	1.0000000	1.0000000	1.0000000
1.0000000	1.0000000	1.0000000	1.0000000	1.0000000	1.0000000	1.0000000	1.0000000	1.0000000	1.0000000
1.0000000	1.0000000	1.0000000	1.0000000	1.0000000	1.0000000	0.9999999	0.9999999	0.9999999	0.9999999
0.9999999	0.9999999	0.9999998	0.9999998	0.9999998	0.9999997	0.9999997	0.9999996	0.9999996	0.9999995
0.9999994	0.9999993	0.9999992	0.9999990	0.9999988	0.9999986	0.9999983	0.9999980	0.9999977	0.9999972
0.9999967	0.9999961	0.9999954	0.9999946	0.9999936	0.9999924	0.9999910	0.9999893	0.9999873	0.9999850
0.9999822	0.9999790	0.9999751	0.9999705	0.9999650	0.9999585	0.9999509	0.9999418	0.9999311	0.9999183
0.9999832	0.9999854	0.9999864	0.9999839	0.9999804	0.9999742	0.9999734	0.99996830	0.99996245	0.9999551
0.99994729	0.99993755	0.99992601	0.99991234	0.9989615	0.9987696	0.9985422	0.9982728	0.9979536	0.9975754
0.9971272	0.9965961	0.9959667	0.9952208	0.9943367	0.9932889	0.9920468	0.9905742	0.9888232	0.9867577
0.9843320	0.9813887	0.9779318	0.9738285	0.9689563	0.9631685	0.9562897	0.9481090	0.9383730	0.9267756
0.9129463	0.8964342	0.8766878	0.8530281	0.8246124	0.7903844	0.7490030	0.6987389	0.6373155	0.5616540
0.4674365	0.3482000	0.1940500	-0.0136099	-0.3168048	-1.0000000				

Figure E-6. Example of Large Increments (Vening-Meinesz, 125 rings, Maximum Degree 1440).

RAW INCREMENTS IN INDEPENDENT VARIABLES

0.0000000	-0.0004304	0.0016415	-0.0010854	-0.0015195	-0.0016560	-0.0070365	-0.0070622	0.0030737	0.0075004
-0.0025599	0.0302498	-0.0036651	0.0070101	0.0156274	0.0004103	0.0044232	-0.0007154	0.0097669	0.0080344
-0.0026708	-0.0066335	0.0068252	-0.0015491	0.0036352	0.0021265	-0.0212513	0.0290662	0.0129250	0.0268354
0.0013693	-0.0480833	-0.0251793	-0.0305502	-0.0771326	-0.1898146	0.0145926	-0.0086407	0.0468956	0.0239837
0.0735098	-0.0237839	-0.0720922	-0.0462631	0.0240415	-0.0168706	0.1179152	0.1037630	0.0313040	0.1623265
-0.0325536	-0.1051043	-0.2245467	0.0478108	0.0104654	0.0332987	-0.0188410	0.0260864	0.1274729	0.0396429
-0.3397384	0.1422613	0.1412255	-0.0031571	-0.2247467	0.1406184	0.1242039	-0.2695050	0.2313055	-0.1247967
0.0452842	-0.0098222	-0.0000629	0.0011810	-0.0006359	0.0002514	-0.0000662	0.0000314	0.0000043	0.0000121
0.0000101	0.0000103	0.0000090	0.0000075	0.0000052	0.0000030	0.0000017	0.0000003	-0.0000002	-0.0000003
-0.0000006	0.0000003	-0.0000001	-0.0000007	0.0000002	-0.0000001	-0.0000003	-0.0000000	0.0000000	0.0000010
0.0000009	-0.0000002	-0.0000009	0.0000004	-0.0000023	-0.0000014	-0.0000007	0.0000005	-0.0000031	-0.0000074
-0.0000008	-0.0000035	-0.0000228	-0.0000402	-0.0000324	0.0000097	-0.0000212	-0.0001076	0.0000497	0.0002271
0.0003606	0.0000466	0.0004042	0.0009345	-0.0101685	0.0000000				

Figure E-6 (continued).

SPHERICAL RADII PSI (DEGREES)

0.0021134	0.0023003	0.0025038	0.0027252	0.0029663	0.0032286	0.0035142	0.0038250	0.0041633	0.0045315
0.0049323	0.0053686	0.0053434	0.0063603	0.0069228	0.0075351	0.0082016	0.0089270	0.0097165	0.0105759
0.0115113	0.0125295	0.0136377	0.0148439	0.0161568	0.0175858	0.0191412	0.0208342	0.0226769	0.0246826
0.0268557	0.0292419	0.0318283	0.0346434	0.0377075	0.0410426	0.0446727	0.0486238	0.0529245	0.0576055
0.0627005	0.0682462	0.0742824	0.0808524	0.0880036	0.0957872	0.1042593	0.1134807	0.1235177	0.1344425
0.1463336	0.1592763	0.1733639	0.1886974	0.2053872	0.2235531	0.2433257	0.2648472	0.2882723	0.3137692
0.3415214	0.3717281	0.4046067	0.4403933	0.4793453	0.5217426	0.5678901	0.6181194	0.6727916	0.7322999
0.7970721	0.8675739	0.9443124	1.0278393	1.1187554	1.2177148	1.3254295	1.4426745	1.5702938	1.7092062
1.8604121	2.0250009	2.2041590	2.3991785	2.6114666	2.8425565	3.0941185	3.3679728	3.6661036	3.9906738
4.3440425	4.7287833	5.1477052	5.6038755	6.1006459	6.6416810	7.2309914	7.8729700	8.5724348	9.3346769
10.1655167	11.0713686	12.0593185	13.1372143	14.3137754	15.5987254	17.0029546	18.5307227	20.2199128	22.0623575
24.0342603	26.3067526	28.7546418	31.4574364	34.4507856	37.7785549	41.4959114	45.6740870	50.4080698	55.8297394
62.1319763	69.6173616	78.8107683	90.7798135	108.4698034	179.9999989				

INDEPENDENT VARIABLE VALUES X

1.0000000	1.0000000	1.0000000	1.0000000	1.0000000	1.0000000	1.0000000	1.0000000	1.0000000	1.0000000
1.0000000	1.0000000	1.0000000	1.0000000	1.0000000	1.0000000	1.0000000	1.0000000	1.0000000	1.0000000
1.0000000	1.0000000	1.0000000	1.0000000	1.0000000	1.0000000	0.9999999	0.9999999	0.9999999	0.9999999
0.9999999	0.9999999	0.9999998	0.9999998	0.9999998	0.9999997	0.9999997	0.9999996	0.9999996	0.9999995
0.9999994	0.9999993	0.9999992	0.9999990	0.9999988	0.9999986	0.9999983	0.9999980	0.9999977	0.9999972
0.9999967	0.9999961	0.9999954	0.9999946	0.9999936	0.9999924	0.9999910	0.9999893	0.9999873	0.9999850
0.9999822	0.9999790	0.9999751	0.9999705	0.9999650	0.9999585	0.9999509	0.9999418	0.9999311	0.9999183
0.9999032	0.9998854	0.9998642	0.9998391	0.9998094	0.9997742	0.9997324	0.9996830	0.9996245	0.9995551
0.9994729	0.9993755	0.9992601	0.9991234	0.9989615	0.9987696	0.9985422	0.9982728	0.9979536	0.9975754
0.9971272	0.9965961	0.9959567	0.9952208	0.9943367	0.9932889	0.9920468	0.9905742	0.9888282	0.9867577
0.9843020	0.9813687	0.9779318	0.9738285	0.9689563	0.9631685	0.9562897	0.9481090	0.9383730	0.9267756
0.9129463	0.8964342	0.8766878	0.8530281	0.8246124	0.7903844	0.7490030	0.6987389	0.6373155	0.5616540
0.4674365	0.3482880	0.1940500	-0.0136099	-0.3168048	-1.0000000				

RAW INCREMENTS IN INDEPENDENT VARIABLES

0.0000000	-0.0022603	0.0066820	-0.0034697	0.0137664	-0.0111803	0.0016873	-0.0048678	-0.0006720	0.0086754
0.0064956	0.2422671	-0.0120976	0.2425094	0.1451166	-0.2636296	-0.0033999	-0.0020788	0.0516678	-0.2004985
-0.2937074	-0.2115872	0.0339952	-0.0960920	0.2033689	0.0400312	-0.4014489	0.2797658	0.4782538	-0.0282543
-0.1633011	0.1220964	0.1279842	0.0680982	-0.4573958	-0.3217300	-1.4391899	0.2029956	-0.6481801	-0.2833292
-1.1850624	-0.4698355	0.4411848	-0.1523405	0.0112345	0.3256243	0.6326106	0.6523260	-0.1341362	1.5530758
1.9512291	0.5210494	-0.6982923	-1.0705042	-2.4142294	-0.5616150	-0.6616700	1.1790876	1.7386065	1.2865305
-0.2449353	-3.0364563	-0.0774422	2.1904888	0.0297359	-0.3386355	-2.2155590	3.9365053	-3.5778694	2.3199310
-1.2194118	0.5516934	-0.2197874	0.0779063	-0.0246346	0.0071920	-0.0018397	0.0005654	-0.0000493	0.0001170
0.0000746	0.0000932	0.0000894	0.0000823	0.0000632	0.0000413	0.0000256	0.0000079	0.0000002	-0.0000047
-0.0000019	-0.0000004	0.0000028	0.0000092	0.0000007	-0.0000065	-0.0000079	-0.0000038	-0.0000056	-0.0000002
-0.0000073	0.0000069	-0.0000006	-0.0000044	-0.0000139	-0.0000128	0.00000245	-0.0000203	-0.0000398	-0.0000590
-0.0000807	-0.0000911	-0.0001676	-0.0002336	-0.0002287	0.0000615	0.0000101	-0.0003312	0.0007015	0.0032009
0.0031733	-0.0042512	-0.0003486	-0.0130000	-0.0810918	0.0000000				

Figure E-7. Example of Large Increments (Vening-Meinesz, 125 rings, Maximum degree 1440).

Fig.	MAX DEGREE	# RINGS	FIRST REASONABLE INCREMENT AT	ψ LIMIT	RATIO
E-1	30	23	18.54°	30°	0.62
E-2	50	34	33.9°	18°	1.83
E-3	500	34	2.478°	1.8°	1.37
E-4	1000	101	4.00°	0.9°	4.44
E-5	1440	23	0.228°	0.53°	0.43
E-6	1440	125	1.325°	0.53°	2.50
E-7	1440	125	1.570°	0.53°	2.96

$$\psi_{\text{LIMIT}} = 900^\circ / N_{\text{MAX}}$$

Figure E-8. Summary of Cases for Small Ring Radii Exclusion.

APPENDIX F

DERIVATION OF ALGORITHM FOR CALCULATING THE STOKES' EQUAL RING CONTRIBUTION TEMPLATE

by

Stanley W. Shepperd

It is desired* to find values ψ_i of the spherical ring boundary radii such that

$$\left| \int_{\psi_i}^{\psi_{i+1}} S(\psi) \sin \psi \, d\psi \right| = \begin{array}{l} \text{the same constant} \\ \text{value for all } i \end{array}$$

It is well known that the Stokes' function $S(\psi)$ has two distinct zeros, and thus so does the integrand $S(\psi) \sin \psi$. Consequently, the total area A lying under the curve of the integrand may be divided into three sub-areas, A_1 , A_2 , and A_3 , as shown in Figure F-1. Since the total integral between 0 and π is zero, the three areas must satisfy the relationship

$$A_2 = A_1 + A_3$$

where A_2 is considered positive by convention.

In a partition of the sphere into n spherical rings in which each ring has the same "weight" (i.e. the area under the $S(\psi) \sin \psi$ curve is constant in magnitude), a ring containing a zero of the integrand will suffer some cancellation. In other words, there will exist a "deadband" around each of the zeros having no overall contribution, unless a boundary radius happens to lie exactly on the zero. These deadbands are illustrated in Figure F-2. It is assumed that the remaining "active" sub-areas \bar{A}_1 , \bar{A}_2 , \bar{A}_3 are to be partitioned into n_1 , n_2 , and n_3 rings respectively. There are two possible locations for each of the radii ψ_{n1} and ψ_{n1+n2} because the shaded deadbands yield no net contribution.

* See Section 5.1.2.1 of this document.

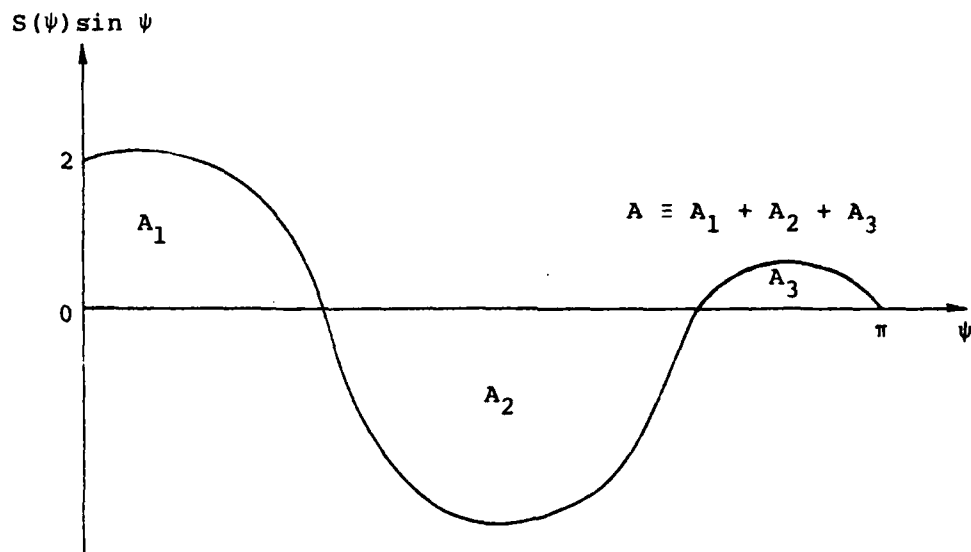


Figure F-1. Sub-areas under the curve $S(\psi) \sin \psi$.

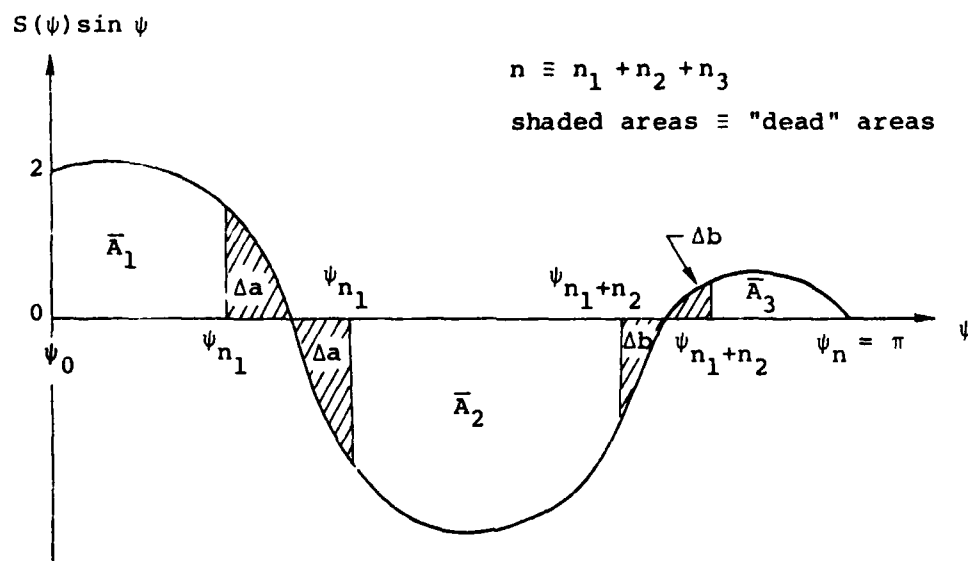


Figure F-2. Dead-bands around the zeros of $S(\psi) \sin \psi$.

It is important to note that since each deadband is symmetric in terms of area about its zero, the area relationship is preserved

$$\bar{A}_2 = \bar{A}_1 + \bar{A}_3$$

And since the number of rings must be proportional to the area for equal-ring contribution, it must be true that

$$n_2 = n_1 + n_3$$

This in turn implies that the total number of rings must be even, specifically half in the positive areas and half in the negative area. Thus, the original problem reduces to a problem of choosing n_1 and n_3 subject to the following constraints.

n_1, n_3 are integers

$n_1 + n_3$ is a known constant

$n_1 \bar{A}_3 = n_3 \bar{A}_1$ for equal contribution

One final assumption is necessary to make the solution unique, namely that the total amount of "dead" area ($2\Delta a + 2\Delta b$) is to be minimized.

The equal-ring contribution constraint may be rewritten as

$$n_3 \Delta a - n_1 \Delta b = n_3 A_1 - n_1 A_3$$

In $(\Delta a, \Delta b)$ space, this constraint is a straight line with positive slope having either a positive or negative intercept on the Δb axis, as shown in Figure F-3.

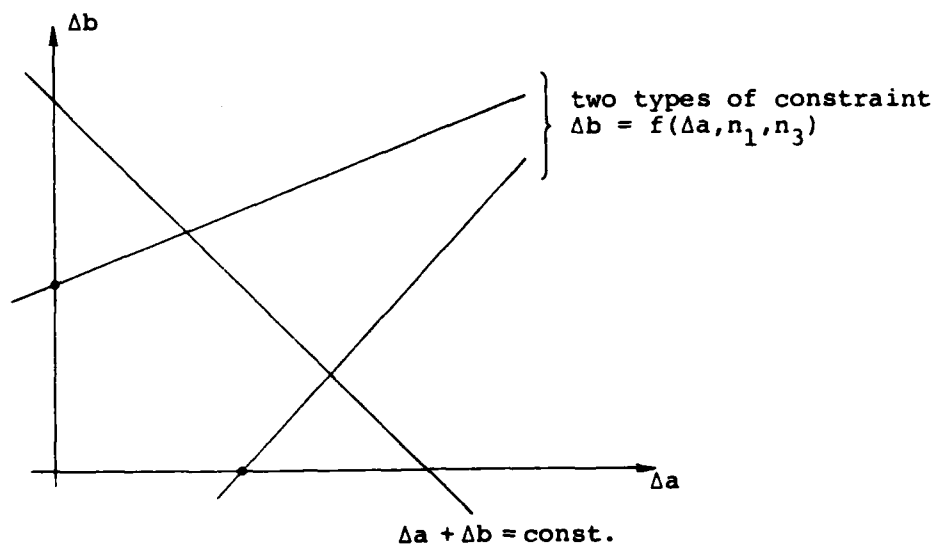


Figure F-3. Nature of Solution.

Since the areas Δa and Δb must be non-negative, there are two types of solutions to the problem of minimizing the total dead area ($2\Delta a + 2\Delta b$). Specifically $\Delta a = 0$ or $\Delta b = 0$. The details of these solutions are given in the following paragraphs. The correct solution will then be the one with the smaller dead area Δa or Δb .

Once Δa and Δb are determined, the "weight" per ring is known

$$[A_1 + A_2 + A_3 - 2(\Delta a + \Delta b)]/n$$

and the ring boundary radii ψ_i may be calculated iteratively from knowledge of this constant ring area.

Case 1

$$\Delta b = 0$$

$$\Delta a = A_1 \left(1 - \frac{n_1}{n_3} \frac{A_3}{A_1} \right) = A_1 \left(1 - \frac{n_1}{n_2} \frac{A_2}{A_1} \frac{n_2}{n_3} \frac{A_3}{A_2} \right)$$

The minimum positive Δa is determined by choosing

$$n_1 = \text{floor} \left(\frac{n_2 A_1}{A_2} \right) = \text{round} \left(\frac{n_2 A_1}{A_2} - \frac{1}{2} \right)$$

$$n_3 = \text{ceiling} \left(\frac{n_2 A_3}{A_2} \right) = \text{round} \left(\frac{n_2 A_3}{A_2} + \frac{1}{2} \right)$$

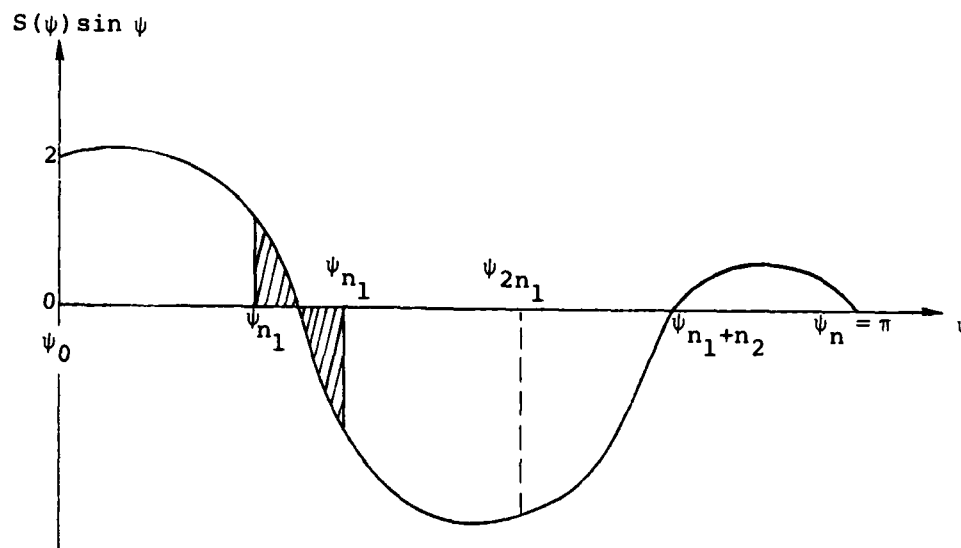


Figure F-4. Solution for $\Delta b = 0$.

Case 2

$$\Delta a = 0$$

$$\Delta b = A_3 \left(1 - \frac{n_3}{n_1} \frac{A_1}{A_3} \right) = A_3 \left(1 - \frac{n_2}{n_1} \frac{A_1}{A_2} \frac{n_3}{n_2} \frac{A_2}{A_3} \right)$$

The minimum positive Δb is determined by choosing

$$n_1 = \text{ceiling} \left(\frac{n_2 A_1}{A_2} \right) = \text{round} \left(\frac{n_2 A_1}{A_2} + \frac{1}{2} \right)$$

$$n_3 = \text{floor} \left(\frac{n_2 A_3}{A_2} \right) = \text{round} \left(\frac{n_2 A_3}{A_2} - \frac{1}{2} \right)$$

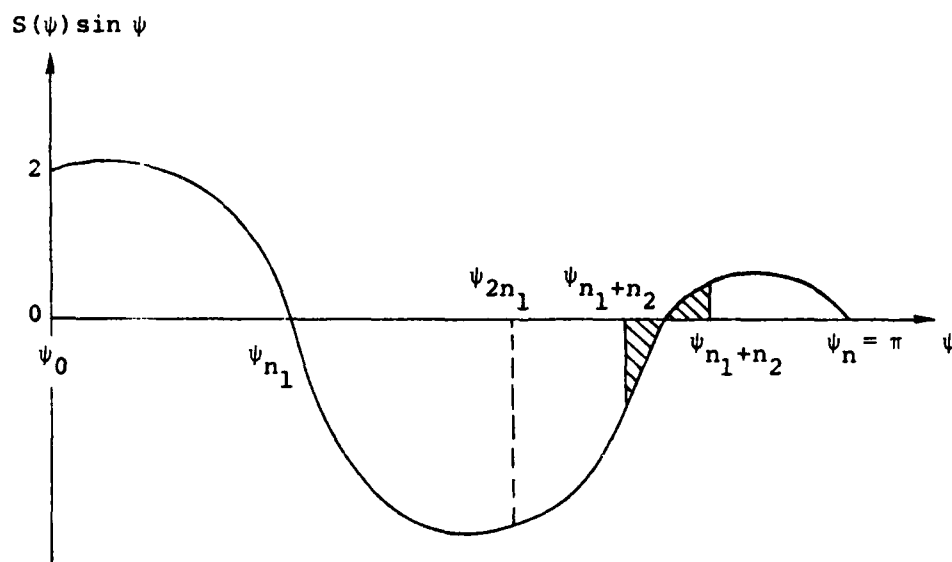


Figure F-5. Solution for $\Delta a = 0$.

LIST OF REFERENCES

- Abramowitz, Milton, and I.A. Stegun (editors), (1964), Handbook of Mathematical Functions, National Bureau of Standards, Applied Mathematics Series No. 55, U.S. Government Printing Office. Also reprinted by Dover, 1965, 1968.
- Adams, M.B., and G. Prado, (1978) The Design of Two Dimensional Digital Filters for Geodetic Applications, CSDL Report R-1154, March 1978.
- Avriel, M. (1976), Nonlinear Programming, Analysis and Methods, Prentice-Hall, Inc., New Jersey.
- Bracewell, Ron, (1965), The Fourier Transform and Its Applications, McGraw-Hill, New York.
- Buglia, James J., (1976), The Effect of Remote Zones on the Accuracy of Evaluating the Molodensky Integral, NASA TMX-72798, January 1976, National Technical Information Service Accession No. N-76-17681.
- Calvez, L.C., and R. Genin, (1977), "An Algorithm for Summing Series and Their Derivatives", Proceedings of the IEEE, 65, pp. 163-165, (January 1977).
- Churchill, R.V., (1954), "The Operational Calculus of Legendre Transforms", Journal of Mathematics and Physics, 33 (1954), pp. 165-178.
- Churchill, R.V., and C.L. Dolph, (1954), "Inverse Transforms of Products of Legendre Transforms", Proc. Amer. Math. Soc., 5 (1954), pp. 93-100.
- Clenshaw, C.W., (1955), "A Note on the Summation of Chebyshev Series", Mathematical Tables and Other Aids to Computation, 9 (1955), pp. 118-120.

- Colombo, O.L., (1977), "Optimal Kernels for Band-Limited Data", Unisurv G27 (1977), pp. 77-87, University of New South Wales, Sidney, Australia. Presented as paper G6 at the AGU Fall Meeting 1977 in San Francisco (EOS, Vol. 58, page 1117). Available from: O.L. Colombo, Dept. of Geodesy, University of New South Wales, P.O. Box 1, 2033 New South Wales, Australia.
- Cook, A.H., (1951), "The Calculation of Deflexions of the Vertical from Gravity Anomalies", Proceedings of the Royal Society of London, Series A: Mathematical and Physical Sciences, 204 (1951), pp. 374-395.
- Courant, Richard and David Hilbert, (1953), Methods of Mathematical Physics, Volume I, Interscience Publishers, New York.
- Dahlquist, Germund and Åke Björk, (1974), Numerical Methods, Prentice-Hall, Inc., New Jersey.
- deWitte, L., (1967), "Truncation Errors in the Stokes and Vening-Meinesz Formulae for Different Order Spherical Harmonic Gravity Terms," Geophysical Journal of the Royal Astronomical Society, 12 (1967), pp. 449-464.
- deWitte, L., (1969), "Altitude Extensions of the Three Anomalous Gravity Components", Bulletin Géodésique, No. 93 (1969), pp. 287-305.
- Dennis, J.E., Jr., (1977), "Non-Linear Least Squares and Equations", pp. 269-312 of The State of the Art in Numerical Analysis, Jacobs, ed., Academic Press, New York.
- DiDonato, A.R., (1977), Recurrence Relations for the Indefinite Integrals of the Associated Legendre Functions, NSWC/DL TN-DK-5/77, July 1977, Naval Surface Weapons Center, Dahlgren Laboratory, Dahlgren, VA, 22448.
- Dorny, C.N., (1975), A Vector Space Approach to Models and Optimization, John Wiley and Sons, New York.
- Dunford, N., and J.T. Schwartz, (1958, 1963), Linear Operators, Part I: General Theory, 1958; Part II: Spectral Theory, 1963, Interscience Publishers, New York.
- Dwight, H.B., (1961), Tables of Integrals and Other Mathematical Data, Fourth Edition, Macmillan Co., New York.
- Edmonds, A.R., (1957), Angular Momentum in Quantum Mechanics, Princeton University Press, New Jersey.

- Erdélyi, A. (ed.), (1953), Higher Transcendental Functions, Volumes I, II, III, McGraw-Hill, New York.
- Erdélyi, A. (ed.), (1954), Tables of Integral Transforms, Volumes I, II, McGraw-Hill, New York.
- Flinn, E.A., (1967), "Foreword" to the Special Issue on the M.I.T. Geophysical Analysis Group Reports, Geophysics 32 (1967), Issue No. 3 (June), pp. 411-413.
- Frank, Philipp, and Richard von Mises, (1930, 1961), Die Differential- und Integralgleichungen der Mechanik und Physik, Volume I (Mathematical Part), Vieweg and Son, 1930; Reprinted by Dover, 1961.
- Gill, P.E., and W. Murray, (1978), "Algorithms for the Solution of the Non-Linear Least-Squares Problem", SIAM Journal of Numerical Analysis, 15 (1978), pp. 977-992.
- Gradshteyn, I.S., and I.M. Ryzhik, (1965), Tables of Integrals, Series, and Products, Academic Press, New York.
- Heiskanen, W.A., and H. Moritz, (1967), Physical Geodesy, Freeman, San Francisco.
- IBM, (1968), System/360 Scientific Subroutine Package (PL/I), Program Description and Operation Manual, International Business Machines Corporation, Document GH20-0586-0, First Edition, January 1968.
- Jacobs, D., (ed.), (1977), The State of the Art in Numerical Analysis, Academic Press, New York.
- Jahnke, Eugene, and Fritz Emde, (1945), Tables of Functions with Formulae and Curves, Dover, New York.
- Kahng, S.W., (1972), "Best L_p Approximation", Mathematics of Computation, 26 (1972), pp. 505-508.
- Kato, Tosio, (1966), Perturbation Theory for Linear Operators, Springer-Verlag, New York.
- Kaula, W.M., (1967), "Theory of Statistical Analysis of Data Distributed over a Sphere", Reviews of Geophysics 5 (1967), pp. 83-107.
- Kazansky, I., (1935), "Ein praktischer Versuch der gravimetrischen Bestimmung der Lotabweichungen", Verh. Balt. geod. Komm., Tag. VII, Bd. 2, Helsinki 1935, p. 388.

- Lawson, C.L., and R.J. Hanson, (1974), Solving Least Squares Problems, Prentice-Hall, New Jersey.
- Liusternik, L.A., and V.J. Sobolev, (1961), Elements of Functional Analysis, Fredrick Ungar Publishing Co., New York.
- Luenberger, David G., (1973), Introduction to Linear and Nonlinear Programming, Addison-Wesley, Reading, MA.
- Luke, Y.L., (1975), Mathematical Functions and Their Approximations, Academic Press, New York.
- Magnus, Wilhelm, and Fritz Obergettinger, (1949), Formulas and Theorems for the Functions of Mathematical Physics, Chelsea, New York.
- Malkin, N., (1933), "Über die Formeln von Vening-Meinesz, Calandreaud und einige andere Formlen der höheren Geodäsie", Gerlands Beiträge der Geophysik, 38 (1933), pp. 53-63.
- Meissl, Peter, (1971), A Study of Covariance Functions Related to the Earth's Disturbing Potential, Report No. 151, Department of Geodetic Science, Ohio State University, April 1971, AFCRL-TR-71-0240.
- Molodenskii, M.S., Eremeev, V.F., and M.I. Yurkina, (1962), Methods for Study of the External Gravitational Field and Figure of the Earth, Israel Program for Scientific Translations, Jerusalem, 1962. (Available from the National Technical Information Service as document #TT-61-31207.)
- Morse, P.M., and H. Feshbach, (1953), Methods of Theoretical Physics, Volumes I and II, McGraw-Hill, New York.
- Nettleton, L.L., (1976), Gravity and Magnetism in Oil Prospecting, McGraw-Hill, Inc., New York.
- Neyman, Y.M., (1974), "Computation for Some Integral Transform in Physical Geodesy", Geodesy, Mapping, and Photogrammetry, 16 (1974), pp. 9-12. Originally published in Russian in: Izvestiya vuzov. Geodeziya i aerofotos' yemka, No. 4, 1974, pp. 49-54.
- Paul, M.K., (1978), "Recurrence Relations for Integrals of Associated Legendre Functions", Bulletin Géodésique, 52 (1978), pp. 177-190.
- Peasley, Q.D., (1976), Coefficients of Associated Legendre Functions, NASA Technical Note D-8200, Marshall Space Flight Center, Alabama, April 1976.

- Pick, M., Picha, J., and V. Vyskocil, (1973), Theory of the Earth's Gravity Field, Elsevier Scientific, Amsterdam.
- Potter, J.E., and E.J. Frey, (1967), Rotation Invariant Probability Distributions on the Surface of a Sphere, with Applications to Geodesy, Report RE-27, Experimental Astronomy Laboratory, Massachusetts Institute of Technology, May 1967. Presented at the International Colloquium on Dynamic Methods in Satellite Geodesy, Paris, May 1967.
- Prado, G., (1977a), "The Role of the Hilbert Transform on Potential Theory Problems", CSDL Internal Memo #AGS-4300-77-01, January 1977.
- Prado, G., (1977b), "Calculating the External Gravity Field, A Signal Processing Approach", Proceedings of the National Aerospace and Electronics Conference (NAECON), Dayton, Ohio, May 1977.
- Reed, G.B., (1973), Application of Kinematical Geodesy for Determining the Short Wave Length Components of the Gravity Field by Satellite Geodesy, Report No. 201, Department of Geodetic Science, Ohio State University, March 1973, AFCRL-TR-73-0535, AD768973.
- Rektorys, Karel (ed.), (1969), Survey of Applicable Mathematics, M.I.T. Press, Cambridge, MA.
- Robertson, William M., (1977a), Spectral Theory of the Integral Transformations of Geodesy, CSDL Report P-406, January 1977.
- Robertson, William M., (1977b), Spectral Theory of the Discrete Summation Transformations of Geodesy, Part I: Stokes' Transformation, CSDL Report P-455 (Part I), March 1977.
- Robertson, William M., (1978), Spectral Theory of the Discrete Summation Transformations of Geodesy, Part II: Vening-Meinesz' Transformation, CSDL Report P-455 (Part II), April 1978.
- Robin, Louis, (1957), Fonctions Sphériques de Legendre et Fonctions Sphéroïdales, Volumes I, II, III, Gauthier-Villars, Paris.
- Robinson, E.A., (1954), "Predictive Decomposition of Time Series with Application to Seismic Exploration", M.I.T. Geophysical Analysis Group Report No. 7, July 1954; reprinted in Geophysics, 32 (1967), Issue No. 3 (June), pp. 418-484; also reprinted in Deconvolution, Geophysics Reprint Series No. 1, Society of Exploration Geophysicists, 1978, pp. 52-118.

- Titchmarsh, E.C., (1948), Theory of Fourier Integrals, 2nd Edition, Oxford University Press, Oxford.
- Tranter, C.J., (1950), "Legendre Transforms", Quart. J. Math. Oxford (2), 1 (1950), pp. 1-8.
- Tscherning, C.C., (1977), Introduction to Functional Analysis with a View to Its Applications in Approximation Theory, Lecture Notes (38 pages), Second International Summer School in the Mountains, Ramsau, Austria, 23 August to 2 September 1977. Available from: C.C. Tscherning, Geodaetisk Institut, Gamlehave Allé 22, DK-2920 Charlottenlund, Denmark.
- Tscherning, C.C., and R.H. Rapp, (1974), Closed Covariance Expressions for Gravity Anomalies, Geoid Undulations, and Deflections of the Vertical Implied by Anomaly Degree Variance Models, Report No. 208, Department of Geodetic Science, Ohio State University, AFCRL-TR-74-0231, May 1974.
- Vogel, Théodore, (1953), Les Fonctions Orthogonales dans les Problèmes aux Limites de la Physique Mathématique, Centre National de la Recherche Scientifique, Paris.
- Whittaker, E.T., and G.N. Watson, (1927), A Course of Modern Analysis, Fourth Edition, Cambridge University Press, Cambridge.
- Wigner, E.P., (1959), Group Theory and Its Application to the Quantum Mechanics of Atomic Spectra, Academic Press, New York.
- Zondek, B., (1977), Aggregation Errors of Cell-Averaged Geoid Height, Technical Report TR-3608, Naval Surface Weapons Center, Dahlgren Laboratory, Dahlgren, Virginia, 22448, May 1977.